FUNDAMENTAL INVESTIGATIONS OF THE QUADRUPOLE ION STORAGE TRAP OPERATING IN NOVEL MODES.

Peter Jan Lodewijk Heesterman

A thesis submitted in fulfilment of the requirements of the Council for National Academic Awards for the degree of Doctor of Philosophy.

April 1990

The Polytechnic of Wales in collaboration with Leisk Engineering Ltd.

ABSTRACT

The Quadrupole Ion Store (Quistor) is a device which traps charged particles in an electric field composed only of radio - frequency (RF) and DC voltage components. The Quistor therefore operates on very similar principles to the Quadrupole Mass Filter, but has not been developed to the same extent.

This thesis presents a novel approach to the construction, operation and use of a Quistor as a mass spectrometer. It is felt that the method used offers significant advantages over other methods employed in previous work.

The research undertaken includes a substantial amount of computer simulation work which has been used to predict in detail the performance of the Quistor and thus the benefit, if any, of modifications in its design. Naturally this is closely linked to experimental verification of predicted improvements in the quality of spectra obtained.

In addition to its use as a simple mass spectrometer, the Quistor can be operated so as to produce Chemical Ionisation spectra, and can also perform multiple stages of mass analysis so as to monitor ion reactions. These capabilities, however, have yet to be developed upon this system.

It is intended that a Quistor system based on this work will enter commercial production in the near future.

Acknowledgements.

I would like thank my supervisor, Dr. Iwan Griffiths, for his invaluable support over the last three years. The project was his idea and his drive and determination got it off the ground. I would also like to thank Dr. Guto Roberts for his advice and encouragement.

The assistance of the technical staff of both the Department of Science and Chemical Engineering, and the Mechanical and Production Engineering Unit has been of great value, and is much appreciated.

Essential help has been received from Mr. Alan Baxendine and Leisk Engineering Ltd., both in terms of equipment and technical vacuum knowhow. This has been a very important part of the project and I would like to record my thanks.

I would also like to thank my parents for the use of their computer and printer in producing this thesis.

Finally the receipt of funding from the British Technology Group is very gratefully acknowledged.

Contents

Contents

Contents

Table of figures.

TABLE OF FIGURES.

Table of figures.

Table of figures.

Table of figures.

Table of figures.

Table of figures.

INTRODUCTION

1) Theory of operation of Quadrupole devices.

Consider the ideal Quadrupole electric field given by (in rectangular co-ordinates) :

$$\phi_{xyz} = \phi_0(\lambda x^2 + \gamma y^2 + \alpha z^2) \qquad (I.1.1)$$

where λ, γ, α are constants defining the shape and dimensions of the electric field and the electrode configuration required to produce it. In the absence of electric charge (such as that of stored ions), Laplace's equation gives

$$\nabla^2\phi_{xyz} = \phi\,(2\lambda + 2\gamma + 2\alpha) = 0. \qquad (I.1.2)$$

So for any ideal Quadrupole field,

$$\lambda + \gamma + \alpha = 0. \qquad (I.1.3)$$

Two cases with symmetrical geometries are of special interest :

a) The Quadrupole mass filter.

IF $\alpha = 0$ then $\lambda = -\gamma$, and $\phi = \phi_0\lambda(x^2-y^2)$. If $\lambda = 1 / r_0^2$ (where r_0 is the minimum distance of the electrodes from the centre of the filter) then :

$$\phi = \phi_0 \frac{(x^2 - y^2)}{r_0^2}. \qquad (I.1.4)$$

On the electrode surfaces, given by

$$x^2 - y^2 = r_0^2 \qquad (I.1.5)$$

and

$$x^2 - y^2 = -r_0^2 \qquad (I.1.6)$$

the potentials are $\phi = \phi_0$, and $\phi = -\phi_0$ respectively.

This geometry implies that the electrodes used are four, infinitely long, rods with hyperbolic cross sections as described by the equations (I.1.5 and I.1.6) above. The rods extend to infinity in both the x and y directions. (naturally in any practical device the rods are not infinite in extent, and usually do not have hyperbolic surfaces since these are very difficult to machine). The shape required is shown below :

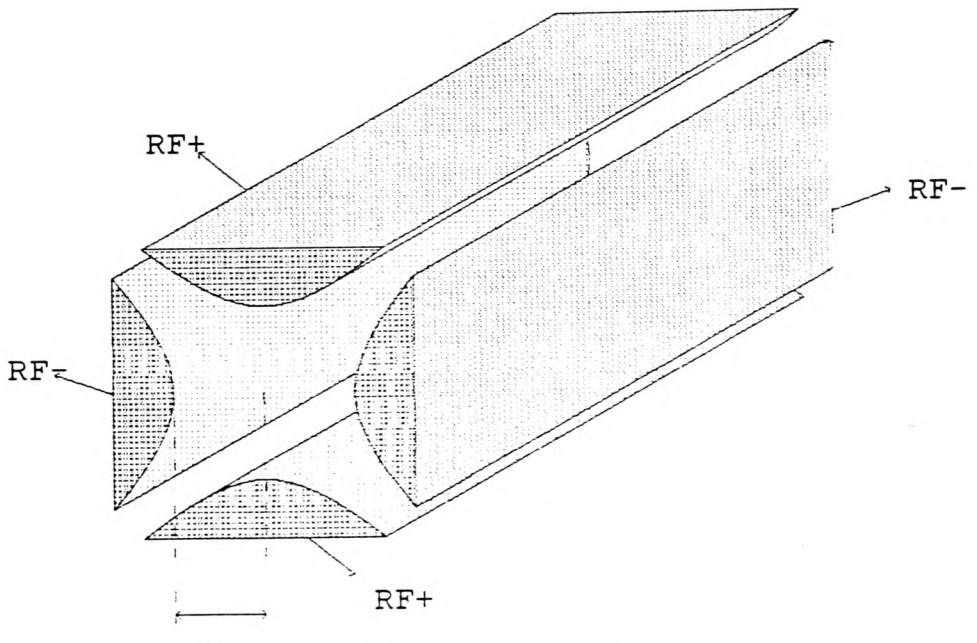

Fig. I.1.1 Quadrupole mass filter rods.

To alternate rods (in pairs) are applied the potentials ϕ_0 and $-\phi_0$. Generally,

$$\phi_0 = U_0 + V_0 \sin (t) \qquad (I.1.7)$$

so that the electric field is a mixture of DC and radio frequency (RF) voltage components. The latter will usually be at a frequency of 1 MHz or so.

b) The Quadrupole Ion trap (Quistor).

The Quistor operates on very similar principles. In this case, $\lambda = \gamma$, and $\alpha = -2\lambda$, where $\lambda = 1 / r_0^2$ (r_0 being the radial distance between the centre of the trap, and the nearest point on the electrode surface), so that

$$\phi = \phi_0 \frac{(2z^2 - x^2 - y^2)}{r_0^2} \qquad (I.1.8)$$

or if $r^2 = x^2 + y^2$, then

$$\phi = \phi_0 \frac{(2z^2 - r^2)}{r_0^2} \qquad (I.1.9)$$

At the electrode surfaces, given by :

$$2z^2 - r^2 = r_0^2 \qquad (I.1.10)$$

and

$$2z^2 - r^2 = -r_0^2 \qquad (I.1.11)$$

the potentials are ϕ_0 and $-\phi_0$ respectively.

The electrode geometry implied consists of three electrodes, each hyperboloids of revolution about the z - axis as defined by the equations (I.1.10 and I.1.11) above. The electrodes extend to infinity. (In practice, of course, the electrodes are not of infinite extent, but the electrodes will be hyperbolic in shape since,

because of the cylindrical symmetry, they may be machined on a suitable lathe). The shape of the electrodes required is shown below :

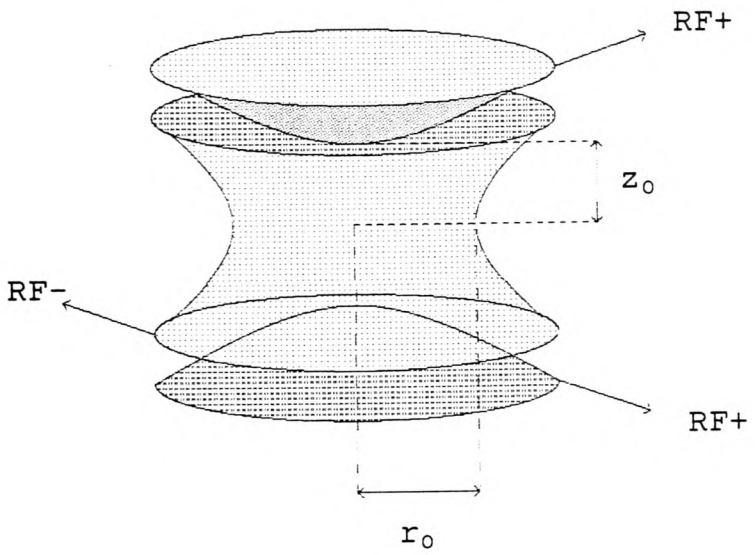

Fig. I.1.2 Quistor electrode surfaces

To the upper and lower electrodes (referred to as end caps) are applied the potential ϕ_0, and to the middle electrode (the ring), the potential $-\phi_0$. In general, once again, the potentials are a mixture of DC and radio frequency AC voltages.

ϕ_0 is given by :

$U + V \sin(\omega t)$.

so that

$$\phi = (U + V \sin(\omega t)) \frac{(2z^2 - r^2)}{r_0^2} \qquad (I.1.12)$$

2) Mathieu Equations

From the above equation (I.1.11), it is clear that the electric field

$$\underline{E} = - \underline{\nabla}\phi$$

$$= - (U + V \sin(\omega t)) \frac{(4z\hat{k} - 2r\hat{r})}{r_0^2} \qquad (I.2.1)$$

where $\hat{k}$ and $\hat{r}$ unit vectors in the z and r directions respectively.

Since (e and m being the particle charge and mass respectively), the components of the field in each direction (E_z and E_r) will equal to

$$eE_r = m \frac{d^2 r}{dt^2}$$

and

$$eE_z = m \frac{d^2 z}{dt^2}$$

then

$$\frac{d^2 r}{dt^2} - \frac{2e}{mr_0^2} (U + V \sin(\omega t)) r = 0 \qquad (I.2.2)$$

and

$$\frac{d^2 z}{dt^2} + \frac{4e}{mr_0^2} (U + V \sin(\omega t)) z = 0 \qquad (I.2.3)$$

By substituting :

$\omega t = 2\delta$

$$a_r = \frac{-8eU}{m\omega^2 r_0^2} \qquad (I.2.4)$$

$$q_r = \frac{-4eV}{m\omega^2 r_0^2} \qquad (I.2.5)$$

$$a_z = \frac{16eU}{m\omega^2 r_0^2} \qquad (I.2.6)$$

$$q_z = \frac{8eV}{m\omega^2 r_0^2} \qquad (I.2.7)$$

we have :

$$\frac{d^2u}{d\delta^2} + (a_u + 2q_u \sin(2\delta))\, u = 0 \qquad (I.2.8)$$

where u is either r or z. Equation (I.2.8) is known as the canonical form of the Mathieu Equation.

The quantities a_r, q_r, a_z and q_z (described by the equations I.2.4 to I.2.7 above) are used frequently. The behaviour of the Quistor may often be described in terms of a and q values only since it is then independent of the frequency used, the size of the Quistor, the mass and the charge of particles trapped.

Note that $a_z = -2a_r$ and $q_z = -2q_r$. (I.2.9)

Very similar equations may also be formed describing the behaviour of ions in a Quadrupole mass filter, although in this case

$$a_x = -a_y = \frac{2eU}{m\omega^2 r_0^2} \qquad (I.2.10)$$

and

$$q_x = -q_y = \frac{eU}{m\omega^2 r_0^2}. \qquad (I.2.11)$$

3) Stability diagrams

An analytical solution of Mathieu equations is beyond the scope of this document and the reader is referred to a suitable text on the subject. (Ref. 59) It is sufficient to say that it can be shown that two very different types of solutions can result, depending on the values of a and q; those which show stable oscillation with a constant amplitude, and those which have unstable oscillation with an exponentially increasing amplitude.

In either case, ions execute complex motions consisting of components at the following frequencies :

$\omega_n = (\beta / 2 + n)\,\omega$ for $n = 0, 1, \ldots, \infty$.

The parameter β arises from the solution of Mathieu's equation and is related only to the values of a and q. Values of β which lie between 0 and 1 lead to stable, bound motion, while other β values lead to unstable motion.

Motions in the r and z directions are completely independent of each other, (at least for an ideal, undistorted Quistor). It is therefore quite possible, depending on the β values in each direction, for an ions motion to be stable in one direction, but unstable in the other.

By plotting values of β against a and q values, we obtain lines of constant β (known as iso-beta lines). By emphasising the iso-beta lines β = 0 and β = 1, a diagram is produced showing those values of a and q (with β values between 0 and 1) which lead to stable solutions. This is known as the stability diagram.

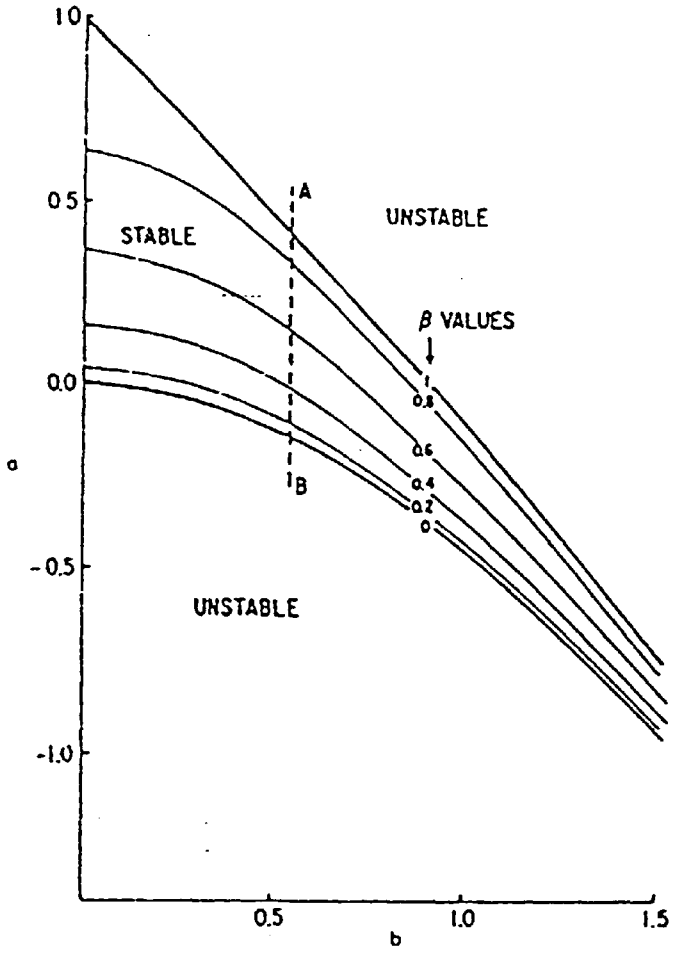

Fig. I.3.1 Plot of iso-β lines vs. a_z and q_z.

The diagram may be extended to show that there are a large (or infinite) number of areas on it which lead to stable solutions, in addition to that shown above. However it has generally been found to be impractical to operate a

quadrupole device using any of these higher order stable solution areas and all but the first (nearest to the origin) are generally ignored.

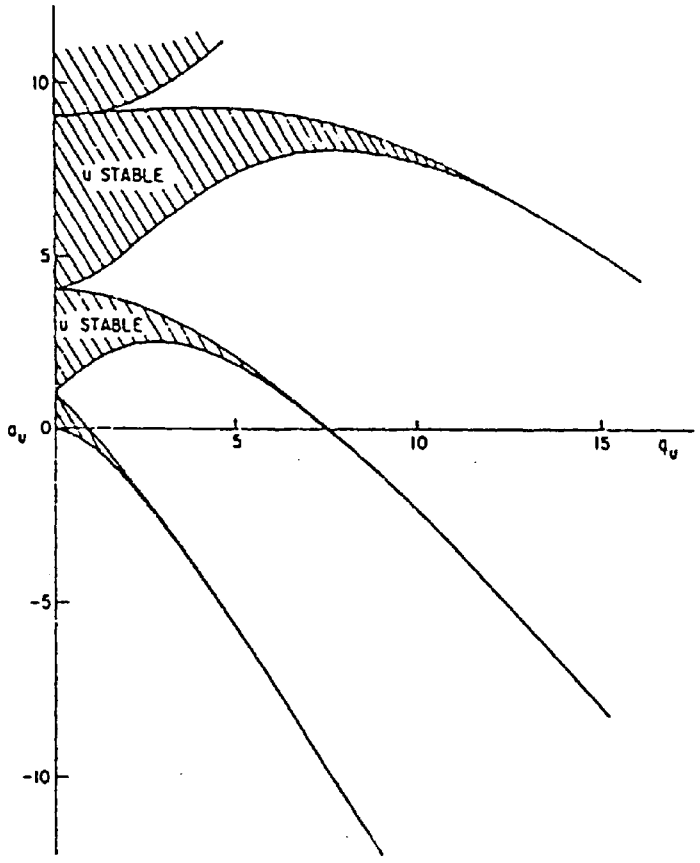

Fig. I.3.2 Extended stability diagram.

By superimposing these diagrams for stability in both the r and z directions (and allowing for a factor of -2 in the values of a_z and q_z (see I.2.9)), it becomes clear which values of a and q lead to ion motions which are stable in both the r and z directions simultaneously. Only ions with these a and q values can ever be trapped and held in the Quistor. Ions whose motions are not stable in one direction,

will be rapidly ejected from the trap in that direction.

Consequently, the region of the stability diagram, indicated below by shading, corresponds to values of a and q which lead to stable ion motion in both r and z directions, and therefore to ion trapping within the Quistor. The region is four-sided, being bound by the iso-beta lines $\beta_r = 0$, $\beta_r = 1$, $\beta_z = 0$ and $\beta_z = 1$.

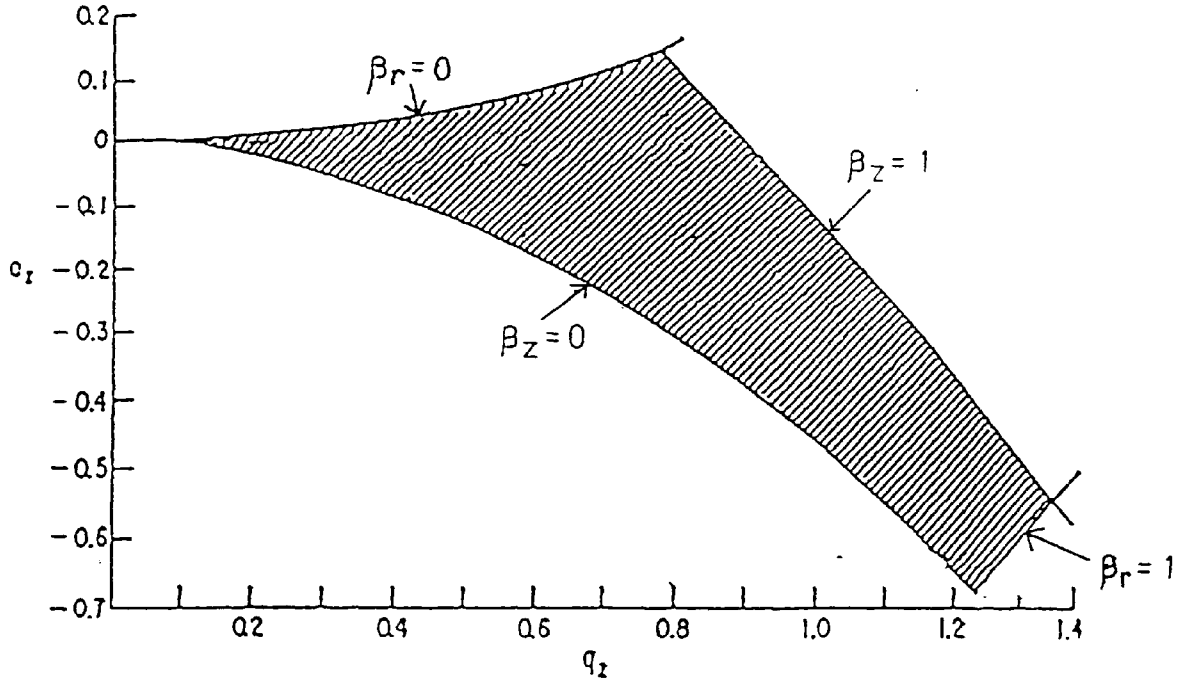

Fig. I.3.3 Quistor stability diagram.

The stability diagram for the Quadrupole mass filter is a little different from that of the Quistor because of the

difference in their geometry, which means that the factor of 2 found between a and q values in each direction (see I.2.9) is not present (see I.2.10 and I.2.11).

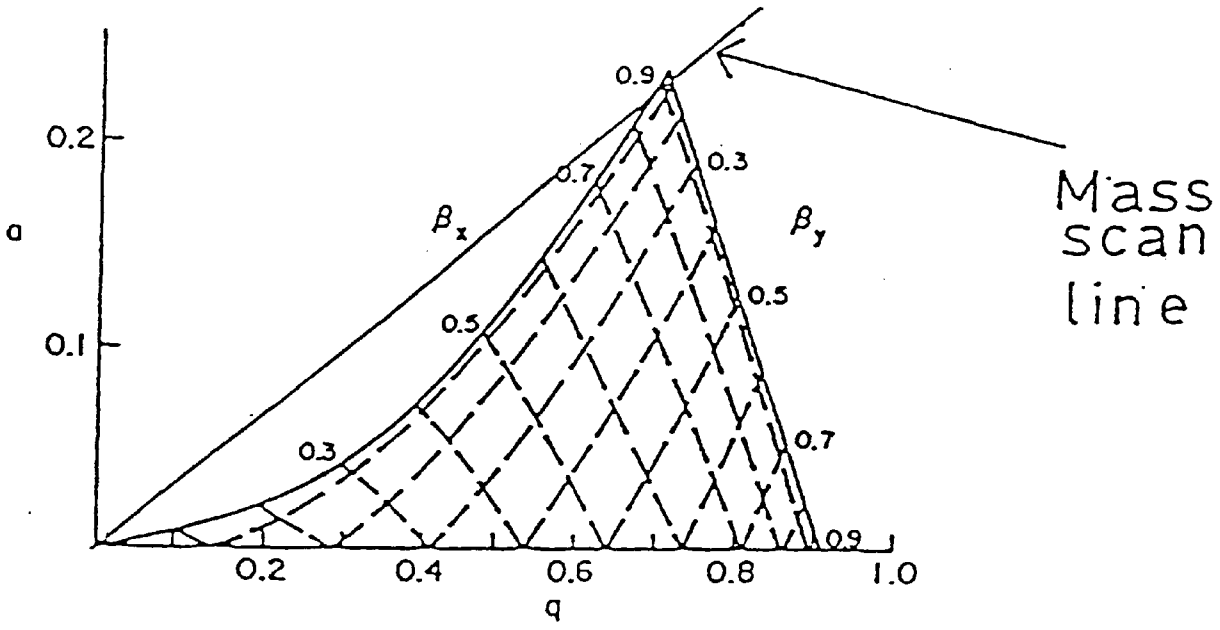

Fig. I.3.4 Quadrupole mass filter stability diagram.

Ions whose motions are stable are able to pass along the length of the device and so are detected, but ions which are not stable rapidly hit the rods. By choosing a ratio of a to q (that is, of DC to RF voltage) which passes close to the apex of the stability diagram, only ions with masses close to the selected mass are able to pass through. Lighter ions will be unstable in one direction, heavier ions in the other,

and either way will quickly strike the rods and be lost. The selected ions are detected at the end of the filter, either with a Faraday plate or by using an electron multiplier.

By scanning the amplitudes of the voltages applied to the rods, the selected mass is scanned and a mass spectrum is built up.

4) Pseudo - Potentials, Trapping efficiency and Trapping ability

Many publications (Refs. 30, 8, 33) in the Quistor field define a quantity referred to as pseudo - potential. Gauss's law makes it clear that it is mathematically impossible to produce a (static) electrical potential well which will trap ions in all three dimensions at once. However, within the Quistor's dynamic fields ions may be said to behave as if there were a potential well which traps the ions in all three directions.

Therefore the concept of pseudo - potential is introduced as being apparently responsible for the net force toward the centre of the trap which ions experience while trapped. The pseudo - potential at a point in the Quistor is the sum of three components; the DC potential due to the DC voltage on the Quistor electrodes, the DC potential due to the trapped ion cloud, and a component which is equivalent to the net inward force on ions due to the RF applied to the electrodes.

It is convenient to define the centre of the trap as being the point of zero pseudo - potential. Pseudo - potential increases (for stable ions) in all directions from the centre.

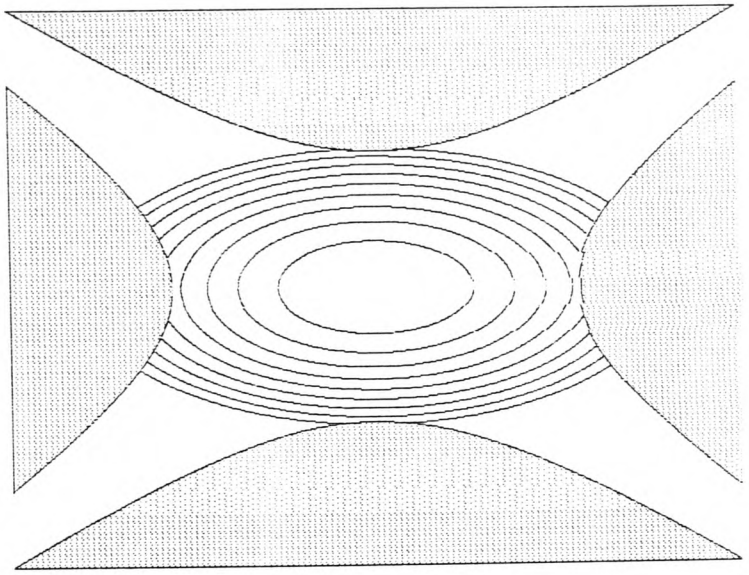

Fig I.4.1 Pseudo - potential distribution.

The trapping efficiency of the Quistor is defined for the purposes of this project as the the ratio of ion velocity amplitude, to ion position amplitude. In other words, it is the ability of the trap to contain high velocity ions within a small space.

It may be easily shown that the trapping efficiency, and pseudo - potential well depth are closely related. If an ion of mass M is just trapped in a Quistor of dimension u_0, and the trapping efficiency is T, then the velocity amplitude is :

$$V_{max} = Tu_0.$$

The maximum kinetic energy of the ion is :

$$E = \frac{MV_{max}^2}{2}.$$

The pseudo - potential energy at the position u_0 (u_0

being the trap size, where the ion velocity and energy are 0) can be equated to this kinetic energy by analogy with electrostatic potential so that :

$$P = E/e \text{ (where e is } 1.6 \times 10^{-19} \text{ C)}$$

$$= \frac{MV_{max}^2}{2e}$$

$$= \frac{M(Tu_0)^2}{2e} \qquad \text{(I.4.1)}$$

The trapping ability of the Quistor is defined here as the maximum number of ions which the trap can store at one time. This quantity is also related to the pseudo - potential well depth since it is the number of ions which results in the space charge related potential being equal and opposite to the sum of the other two components of the pseudo - potential (as discussed above).

The exact potential due to a cloud of charge will depend upon the geometrical arrangement of the charge density, but it is possible to form an estimate of the relationship as follows :

Consider a uniform spherical ball of charge, radius u_0. Gauss's law gives that E, the electric field at radius r, is equal to

$$E = \frac{Q_{enc}}{\epsilon_0 A_{surf}}.$$

Where the charge enclosed in a sphere of radius r, constant charge density ρ (the charge density being zero outside the sphere), is equal to

$$Q_{enc} = \frac{4\pi r^3 \rho}{3}$$

and the surface area of the sphere is

$$A_{surf} = 4\pi r^2 .$$

Therefore

$$E = \frac{\rho r}{3\ e_0}.$$

The potential difference between the centre and at a radius r is given by

$$V = -\int_0^r E.dr$$

$$= -\frac{\rho r^2}{6\epsilon_0}.$$

If the potential at the outer surface is to be 0, then the potential is

$$V = \frac{\rho(u_0^2 - r^2)}{6\epsilon_0}.$$

Thus the potential at the centre is

$$V_{max} = \frac{\rho u_0^2}{6\epsilon_0} \qquad (I.4.2)$$

The maximum charge density, ρ_{max}, which can be sustained (such that there is still a pseudo - potential well) is found when $V_{max} = P$, the depth of the potential

well without charge. In this case

$$\rho_{max} = \frac{6\epsilon_0 P}{u_0^2} \qquad (I.4.3)$$

The total charge is equal to

$$Q = \frac{4\pi u_0^3 \rho}{3}$$

so that the number of ions is given by

$$N = Q / e$$

$$= \frac{4\pi u_0^3 \rho}{3e}$$

Thus the maximum number of ions which can be trapped is given by

$$N_{max} = \frac{8\pi\epsilon_0 u_0 P}{e}. \qquad (I.4.4)$$

In terms of the trapping efficiency,

$$N_{max} = \frac{4\pi M\epsilon_0 T^2 u_0^3}{e^2}. \qquad (I.4.5)$$

For a Quistor operated at the upper apex of the stability diagram, with a 2 MHz RF frequency, it is found that T_z, the tapping efficiency in the z direction, is about 5 x 10^6, and T_r, the trapping efficiency in the r direction is about 2 x 10^6 (see chapter III). Since it is the latter which will limit the number of ions trapped, this value is used. If $u_0 = r_0 = 7.5$ mm, it follows that :

$N_{max} = 1.22 \times 10^7 \, m$

where m is the ion mass number in AMU.

It must be emphasised that the performance of the Quistor in terms of resolution will be affected by space charge, long before this number of ions has been trapped. In addition, it is found that the maximum number of ions which can be trapped at any time is also limited by the ion losses due to ion molecule collisions.

5) History of the Quadrupole mass filter and the Quadrupole ion trap.

Both the Quadrupole mass filter and the Quistor have their origins in a 1956 German patent by Paul (Ref. 64) which described the electric fields and electrode geometries required for these systems. For this reason the Quistor has sometimes been known as the Paul trap. Paul's work followed the discovery that charged particle beams could be focused using magnetic quadrupole fields, a technique which was used in particle accelerators.

Considerable development of the Quadrupole mass filter followed, mostly on the basis of trial and error experimentation, and the Quadrupole now dominates the routine low-cost, low-resolution market in commercially available mass spectrometer systems.

However until recently, no Quistor system has been commercially available since its operation was generally felt to more complex than the the Quadrupole and the design was insufficiently developed.

However a number of research groups had been experimenting with different aspects of its design and

applications. Fischer (Ref. 27), who used resonant circuits to detect the presence of trapped ions, built a Quistor spectrometer achieving a resolution level of 85, and a minimum detectable partial pressure of 10^{-8} Torr. Rettinghaus (Ref. 66), using a phase sensitive detection circuit, reported a resolution level of 300 and a minimum detectable partial pressure of the order of 10^{-13} Torr. Dawson and Whetton (Refs. 17, 20) constructed a Quistor device which detected ions by applying a pulse to one end cap, thereby drawing out all trapped ions in order to be detected by an electron multiplier.

Dawson and Whetton (Ref. 19) also investigated the so - called non - linear resonances which were found to give the Quistor (and Quadrupole) poor, split, peak shapes because of errors in the electric fields. They detailed a method whereby this drawback could be overcome (though at the expense of sensitivity) by applying a DC bias between the end caps.

More recently, work by Todd et al has led to the commercial production by the American company, Finnegan MAT, of a Quistor mass spectrometer system which forms a detector for a gas chromatograph. Ions are trapped without mass - selection and ejected from the trap mass selectively, by ramping the RF voltages applied, so as to be detected by an electron multiplier. (Refs. 26, 44, 75, 77)

A proposal by Griffiths (Refs. 36, 37, 38), which led to this project, explained a possible new method of scanning the Quistor by trapping ions with mass selection at the upper apex of the stability diagram, and ejecting them mass - selectively by digitally ramping the RF and DC voltages. This method would offer a larger mass range for given RF voltages than others; it was also especially convenient for electronic operation under computer control.

Several quite different applications for the ion trap have been investigated. These included its use as an ion source for another mass spectrometer, (Ref. 6) for which an increase in sensitivity of more than one order of magnitude was claimed.

Ion traps have also been used to trap small charged macroscopic particles instead of ions (Ref. 102). This makes an effective lab demonstration particularly because no expensive equipment is required. Instead of RF voltages, low frequency AC voltages (such as the mains) can be used, and operation at atmospheric pressure is practical. The particles are then visible with a simple microscope.

Considerable interest has been aimed at using the Quistor for the study of ion -molecule reactions (Refs. 11, 28, 43, 100, 104), generally with the help of a tandem spectrometer system.

This has led to Chemical ionisation (abbreviated C. I.) mass spectroscopy (Refs. 7, 54, 78) as a convenient technique to be used in connection with a Quistor system. In this case, a reagent gas (say, methane or ammonia) is ionised in the trap. The trapped ions ionise the molecules of a second gas (often by proton transfer) and a spectrum of these ions may be produced. Generally, the spectrum produced in this way contains far fewer fragmentation products than is normally the case and therefore easier to interpret.

This is extended to allow two stages of mass analysis, referred to as Mass Spectrometry - Mass Spectrometry (usually abbreviated MS - MS), (Refs. 45, 46). One ion mass is selected and this is permitted to undergo a reaction, such as decomposition, and the reaction products are scanned out as a spectrum.

This process can be repeated in the Quistor by selecting one of the products and allowing this to react to produce a new set of daughter products, and so on. This is referred to as MS^n where n is the number of stages of MS analysis.

Devices based on non quadrupolar geometries have been investigated. These include the Monopole mass filter (Ref. 14), which operates on the same principles as the Quadrupole, but has only one cylindrical rod, and an earthed 90 degree plate, as shown.

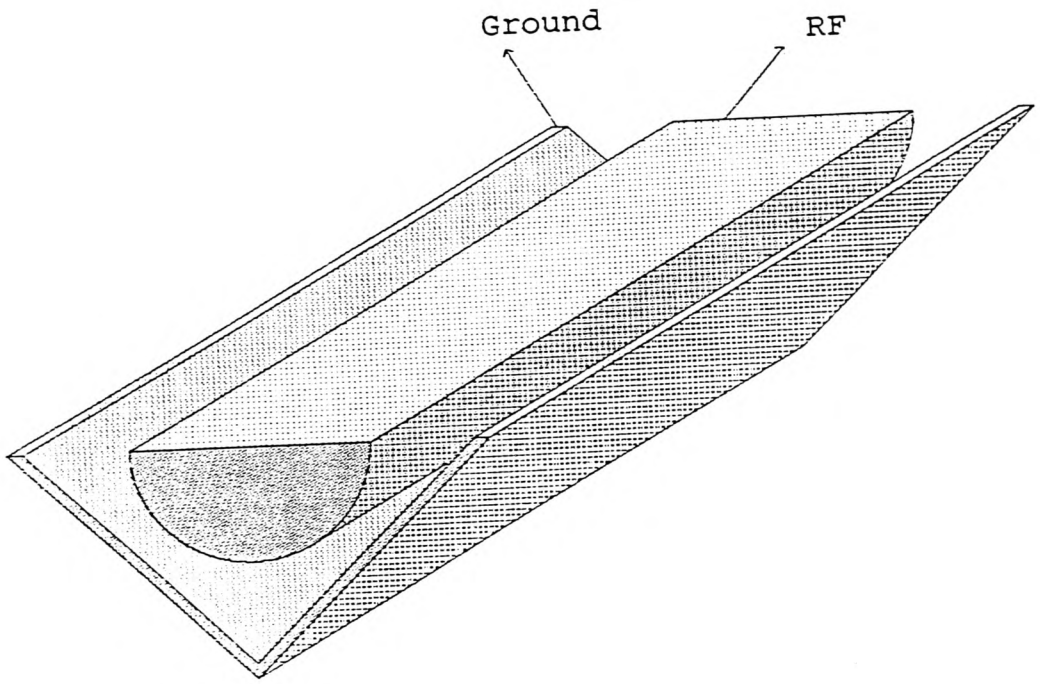

Fig. I.5.1 Monopole mass filter electrodes

Other unusual mass filter type devices have included the multiple mass filter (essentially four Monopoles in one) (Ref. 88) and a Quadrupole which was curved, so that the ion beam was led around a corner. This was extended to the

point where the the device formed a ring so that ions could be trapped by travelling around and around.

A number of non Quadrupolar ion traps have been investigated, such as the Cylindrical ion trap (Refs. 2, 10, 32, 48), basically a cylindrical ring electrode and two flat circular end caps (the simpler geometry makes this easier and cheaper to construct). The electric fields can be made approximately quadrupolar at the centre of the trap, but the mass resolution is still quite poor. A closer approximation to the correct Quistor shape (but still cheaper to manufacture) can be formed by using spherically shaped electrodes (Ref. 68).

The six - electrode trap is constructed on a cubic basis and opposite pairs of electrodes are connected to a three phase RF supply. Ideally the electrodes are hyperbolic in shape in which case this trap is capable of operating in a similar way to the Quistor, although practical devices built have used flat or annular electrodes. Naturally, the RF power supplies required to operate this device are more complex and expensive than for the Quistor, while no great practical advantage is found over the Quistor.

Quistors have also been operated by scanning the electrode voltages in unusual ways. For example, square wave excitation (or, probably, any other periodic waveform) can be applied to the Quistor instead of sine waves in order to provide ion storage and mass selection (Ref. 67). In addition, the Quistor has been scanned by Sheretov (Ref. 71) by maintaining the RF and DC voltages constant, and scanning the RF frequency.

Finally the Penning or static ion trap (Refs. 81, 105) is a three electrode device (such as a Quistor, or cylindrical trap), but with no RF voltages applied. There is a strong

axial magnetic field which traps ions in the radial direction, and a DC voltage between the ring and end cap electrodes traps ions in the axial direction. Ions are trapped in the z (axial) direction by the DC electric field, while ions are trapped in the r (radial) direction by the magnetic field which causes the ions to execute complex Lissajous figure motions around the axis of the trap.

Penning traps have been used to trap ions for ion molecule reaction studies, in a similar way to the Quistor. Penning traps are also heavily used as pressure sensors (Penning gauges) for operation at pressures of 10^{-4} to 10^{-11} torr. A continuous ion current is produced due to collisions with electrons which spiral around the trap until the walls of the trap are struck.

Considerable interest has been shown recently in the use of ion traps combined with tuned lasers (Refs. 41, 42, 53, 81, 82) in order to slow the motion of ions right down to near zero energies. This is done by tuning the laser to a frequency just below an excitation frequency of the ion species. What happens is that when an ion is moving towards the laser beam, the doppler shift produced by its motion means that the ion can absorb a photon. The photon's momentum is also absorbed, reducing the velocity of the ion. The photon will later be re-emitted, but in a random direction, resulting (on average) in no velocity change. Ions moving away from the laser beam do not absorb photons.

Consequently, over a period of time, all the ions lose energy, until their velocities are virtually zero. At this point, ions will be stationary near to the centre of the trap.

This has created a new field of ion trap research, opening up the unique possibility of studying single ions

and systems of ions at the near absolute zero temperatures where quantum effects begin to take an important role in ion behaviour.

An alternate means of reducing the ions' kinetic energy is found in the cooling (or "quenching") of the ion cloud by collisions with a buffer gas (Helium). The ions are cooled to the point where their kinetic energy is equivalent to the ambient temperature of the trap. This feature is an essential part of the Quistor system marketed by Finnegan MAT (Refs. 12, 26, 95)

Lasers have also been used to excite chemical reactions to produce reaction products for MS - MS experiments. An alternative to this approach has been to promote reactions by adding kinetic energy to selected ions by exiting the $w_0\beta_z$ frequency motion of the required ions.

6) Background and objectives of the project

The Quistor project is in the first instance a commercial venture aimed at creating a Quistor system which can be manufactured and sold as a mass spectrometer.

The project is funded by a grant from the British Technology Group. If the project is a commercial success it is the BTG who will hold the resulting patent, however this will be leased to Leisk Engineering Ltd. of Burgess Hill in Sussex, allowing them to manufacture and sell the device. The project is also assisted by Leisk Engineering.

It is hoped that the Quistor will offer significant advantages in performance and capabilities over existing similar Quadrupole Mass Filter instruments. In particular, it is believed that the Quistor will be :

i) Simpler and cheaper to manufacture than Quadrupole devices, firstly because the cylindrical symmetry of the electrodes allows them to be machined on a suitable lathe. (The hyperboloid rods of the Quadrupole Mass Filter are usually approximated by cylindrical rods for ease of manufacture, but this distorts the quadrupole field leading to a reduction in resolution.)

In addition, precise parallel alignment of the Quadrupole rods is extremely important. Any error would mean that a different ion mass would be selected at different points along the length of the filter - consequently it might not transmit ions in the required way at all. This makes the construction very vulnerable to errors so that a large number of Quadrupoles are rejected after manufacture due to imperfections. This does not apply to the assembly of the Quistor. For this reason, Quadrupole mass filters can never be

disassembled for cleaning or repair as the chances of re - assembling them in the correct alignment would be slim. The Quistor can be disassembled, have its electrodes cleaned, be reassembled - and still be expected to work.

ii) Capable of higher mass resolution. The performance of the Quadrupole is limited by the fact that, for convenient use, it's length may not be more than, say, 20 cms. In consequence the electric field within it is distorted, especially at the ends, which reduces its performance. Also the point mentioned above, that the rods used are often cylindrical, rather than hyperbolic, reduces the resolution of practical Quadrupole systems.

iii) Capable of operation at lower gas pressures, and capable of detecting very small concentrations of particular ionic species, in spite of a much larger background of other gases. Since the Quistor operates by storing ions, under these conditions a reasonable ionic output may still be obtained by using a long ionisation time.

iv) Capable of producing chemical ionisation mass spectra.

v) Capable of performing MS - MS and MS^n experiments.

vi) More compact than usual Quadrupole devices. Where space in a vacuum system is at a premium, this is naturally a helpful advantage.

Inevitably there is a degree of overlap between the purely commercial aspects of the investigation, and it's academic side leading to a second degree by thesis.

In this respect it is proposed to investigate several novel aspects of the Quistor's behaviour in the following ways :

a) Computer simulation of the motion of ions in the Quistor field, both in the case of an ideal, "perfect" Quistor, and in the more practical case of a Quistor whose electric fields are perturbed by various imperfections. The investigation will consider the effects of this on the motion of ions in the Quistor.

The results will give the information required to find out the consequences of these perturbations on the performance of the Quistor as regards its ability to trap ions, and eject them in the required way. The results will indicate the output pulse intensity and the resolution of the spectrum produced by the Quistor, and how this depends upon the design and operation of the device.

The perturbations which are to be considered will include :

i) The effect of single holes (of, say, 1 mm diameter) in the end cap electrodes.

ii) The effect of a larger number of small holes (of, say, 0.2 mm diameter) in the end cap electrodes.

iii) The effect of single, large holes (of, say, 8 mm diameter) in the end cap electrodes which are covered by a fine gauze preformed to the shape of the end cap.

In this case it may be possible to compensate for

the effects of distortion produced by the gauze by altering it's shape.

iv) The advantage, if any, in placing a gauze on the end caps, close to the hole(s) and outside the main body of the Quistor.

v) The consequences of imprecise assembly of the Quistor electrodes; both as a result of inaccurate lengths of the ceramic spacers between the electrodes, and of lateral displacements of the electrodes.

vi) The effects of the space charge of ions which are stored within the Quistor.

vii) The effect of collisions between trapped ions and neutral gas molecules.

b) In addition it is proposed to investigate the effect of combining an axial magnetic field with the electric fields produced by the Quistor electrodes. Once again, simulation by computer of the motion of ions in the combined fields can provide the required information.

Previous ion traps have been operated using a combination of DC electric fields and magnetic fields (the Penning trap), or using a combination of DC fields and RF fields (the Quistor); no ion trap system has ever been operated using all three field types at once. No publication refers to the possibility having been investigated, either theoretically, or experimentally.

It is thought that this may offer significant advantages over either system alone since it seems likely that ions may be more effectively trapped in the r

direction. Motion in the z direction would be unaffected by the magnetic field (assuming that it was purely axial) since no force components would exist in that direction.

c) The results of this theoretical computer simulation work will be verified by experimental work with the Quistor, especially where the simulation has indicated that the results will be beneficial. The results of this work will hopefully lead to a greatly improved Quistor performance.

This naturally requires more time to complete since each experiment in the design of the Quistor involves the delay involved in performing machining work on the electrode parts.

7) Possible modes of operation of the Quistor and the applications thereof.

The Quistor may be operated in several different ways in order to produce a mass spectrum, and may also be used for other purposes such as the study of ion molecule reactions. By combining these properties, the Quistor can also be used as a simple MS - MS device.

Each mode described below may be operated in one of two ways; each with a number of advantages over the other. Firstly, RF (and where appropriate, DC) voltages may be applied in opposite polarities to both sets of the Quistor's electrodes. Alternatively, unipolar voltages may be applied to one electrode only (usually the ring electrode), whilst the end caps are earthed.

The former approach gives the Quistor twice the mass range of the latter, for the same RF output voltage. This is naturally an important consideration. A second advantage is that the centre of the trap is at ground potential. This means that neither electrons nor ions will have an RF component in their energy at this point which would otherwise result in very unpredictable electron and ion energy values.

On the other hand, use of the latter approach may result in the use of a simpler RF power supply unit. Secondly, since the end caps are earthed, the construction of the Quistor itself may be simplified because high - voltage RF connections are not required to these electrodes. In addition this approach results in shielding of the RF from the adjacent electron gun electrodes and the multiplier and collector electrodes. This overcomes a number of pickup problems. Finally this approach allows the addition of an auxiliary AC. voltage to be applied to the end cap

electrodes (This will be discussed in chapter III.)

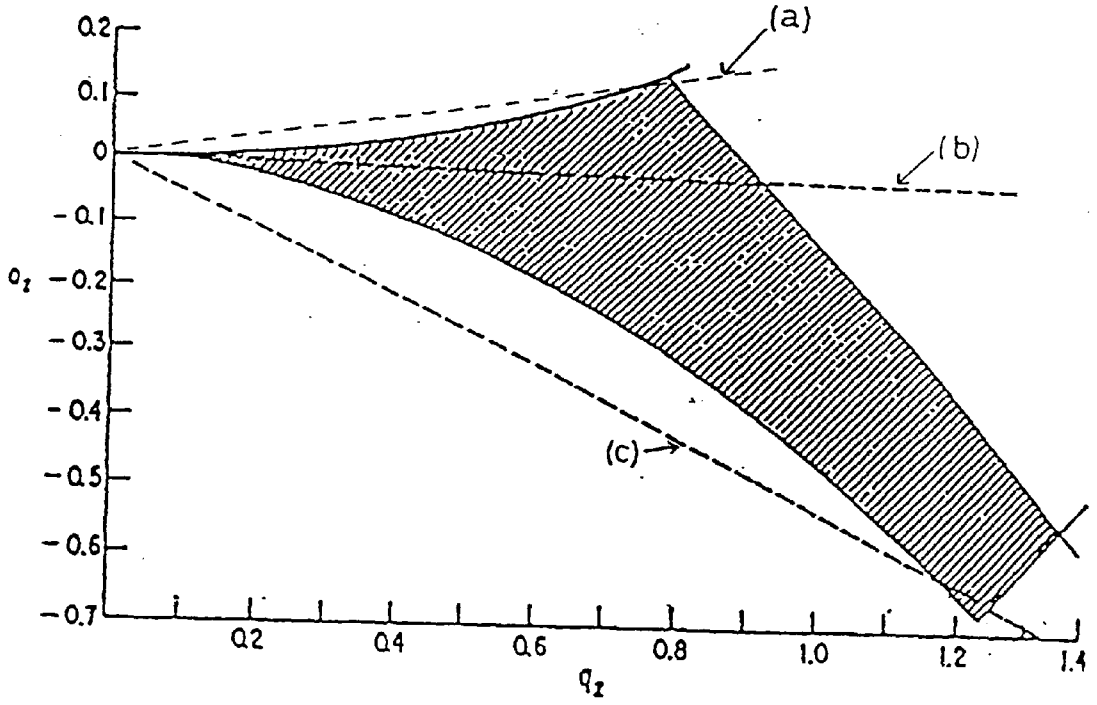

Fig. I.7.1 Quistor stability diagram showing possible scan lines.

The following are the alternative modes of Quistor operation :

a) Mass spectra may be obtained in the "Total Pressure" mode, by using only RF voltages and no DC on the Quistor electrodes. In terms of the stability diagram, a = 0 so that all ions with q values lower than the β_z = 1 boundary (q = 0.9) are stable at the same

time. This is shown as scan line (b) on the above stability diagram.

It is therefore possible to store a large range of ion masses simultaneously, by selecting a fairly low RF voltage and trapping all stable ions. Then the ionising electron beam is switched off and when the RF voltage is swept upwards, the stored ions successively cross the $\beta_z = 1$ boundary of the stability diagram, becoming unstable in the z direction so that they are ejected from the trap to both end caps. These ejected ions can therefore be detected, to form a mass spectrum with the lowest masses appearing first.

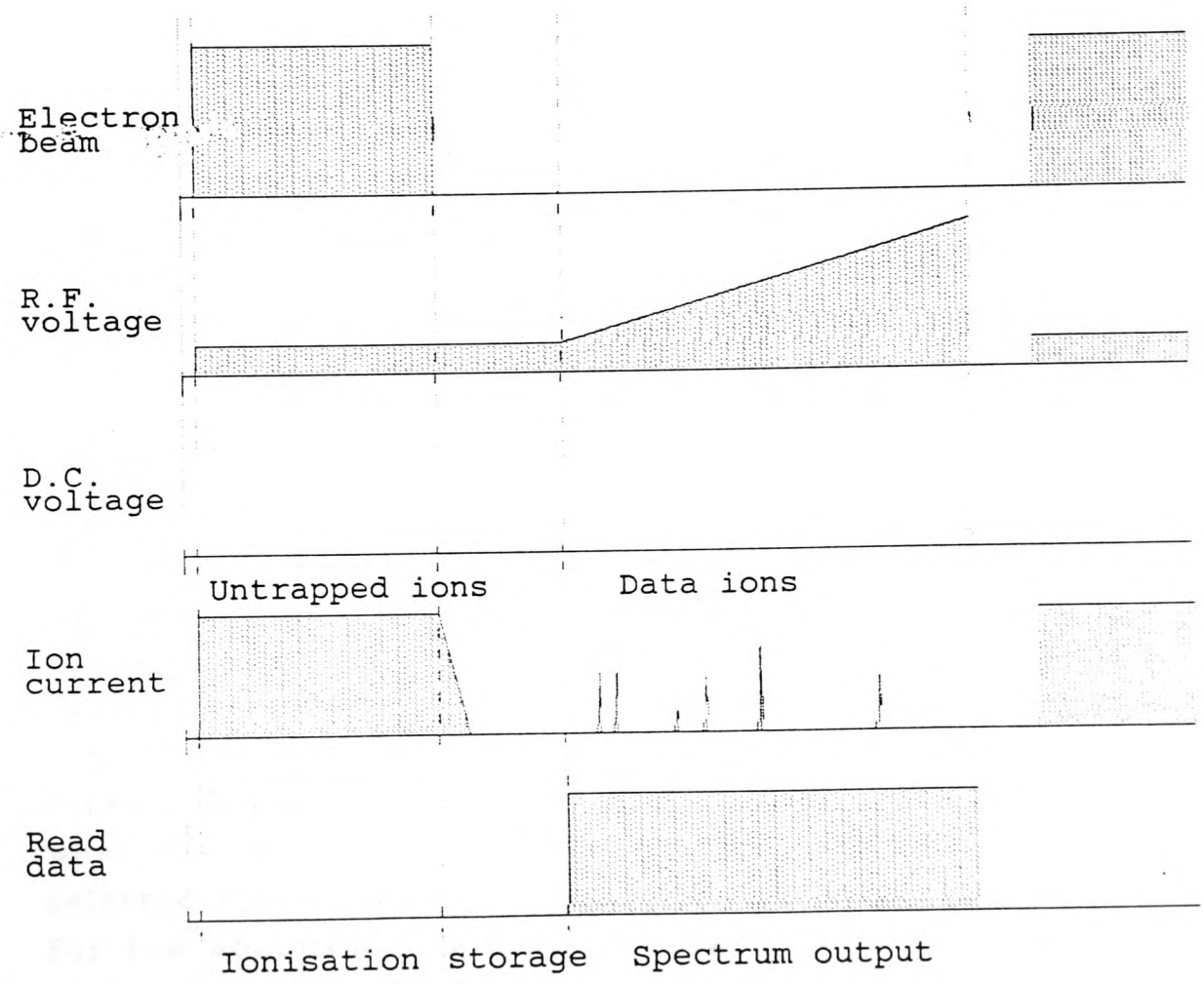

Fig. I.7.2 "Total pressure mode" scan timing diagram.

This method has the advantage that the spectrum data appears as a continuous stream, which makes it simpler to observe and to store. In addition it is possible to store many more ions in this mode (See section III.1) so it is easier to get a large signal output. It also seems probable that a greater resolution is achievable in this mode than in others.

However this mode of operation suffers from several disadvantages as follows :

i) Since a large range of ions can be stored at once, a singly ionised molecule and its doubly charged counterpart can be simultaneously trapped. There is a high probability that singly charged ions which are already trapped, will undergo electron impact collisions and be ionised again. The result is that a substantial proportion of multiply ionised species are present in the spectrum produced resulting in a confused spectrum with far too many peaks. This will be very hard to interpret.

If the Quistor is operated at either apex (as discussed below), ion - electron collisions can occur, resulting in reionisation just the same. However if this happens, the resulting ions will not be stable and so will be quickly lost from the trap, and in consequence are not seen in the spectrum.

ii) It is generally true that a larger number of ions can be trapped in the Quistor in this mode than in others. However, because there is no mass - selection in what is stored, it is probable that fewer ions of any one selected species will be stored. This is particularly true for low abundance ions which form part of a spectrum with much more abundant species. In this case it will not be possible to increase the ionisation time in order to

build up a greater number of the rare species without also storing the more numerous ions.

iii) The ion storage efficiency will generally be a function of the q value at the time of storage. Since a wide range of ion masses is stored before ramping the RF voltages to generate output, there will be a tendency for the spectrum peak amplitude sensitivity to vary depending on the q value selected for storage. In addition different ion masses will have to be scanned through different ranges of q, so that their ion storage times may not be the same. These effects will take place in fairly unpredictable ways and consequently it will be very hard to convert a peak intensity value into a gas partial - pressure value.

This mode of operation has been used in the Quistor system presently marketed by the American company, Finnegan MAT (Refs. 12, 44, 45, 75). That system also uses a single sided RF supply, the end caps being earthed, as described above.

b) The Quistor can be operated with an a to q ratio which lies close to the lower apex of the stability diagram (scan line (c) on the stability diagram shown above). This results in mass selection at the time of ion storage since only a small range of ion q values result in stable ion orbits. Subsequently, the stored ions can be ejected from the trap by applying a negative pulse to one end cap so that all trapped ions are ejected in that direction. This mode of operation has been employed in several previous Quistor systems. (Refs. 17, 21, 30)

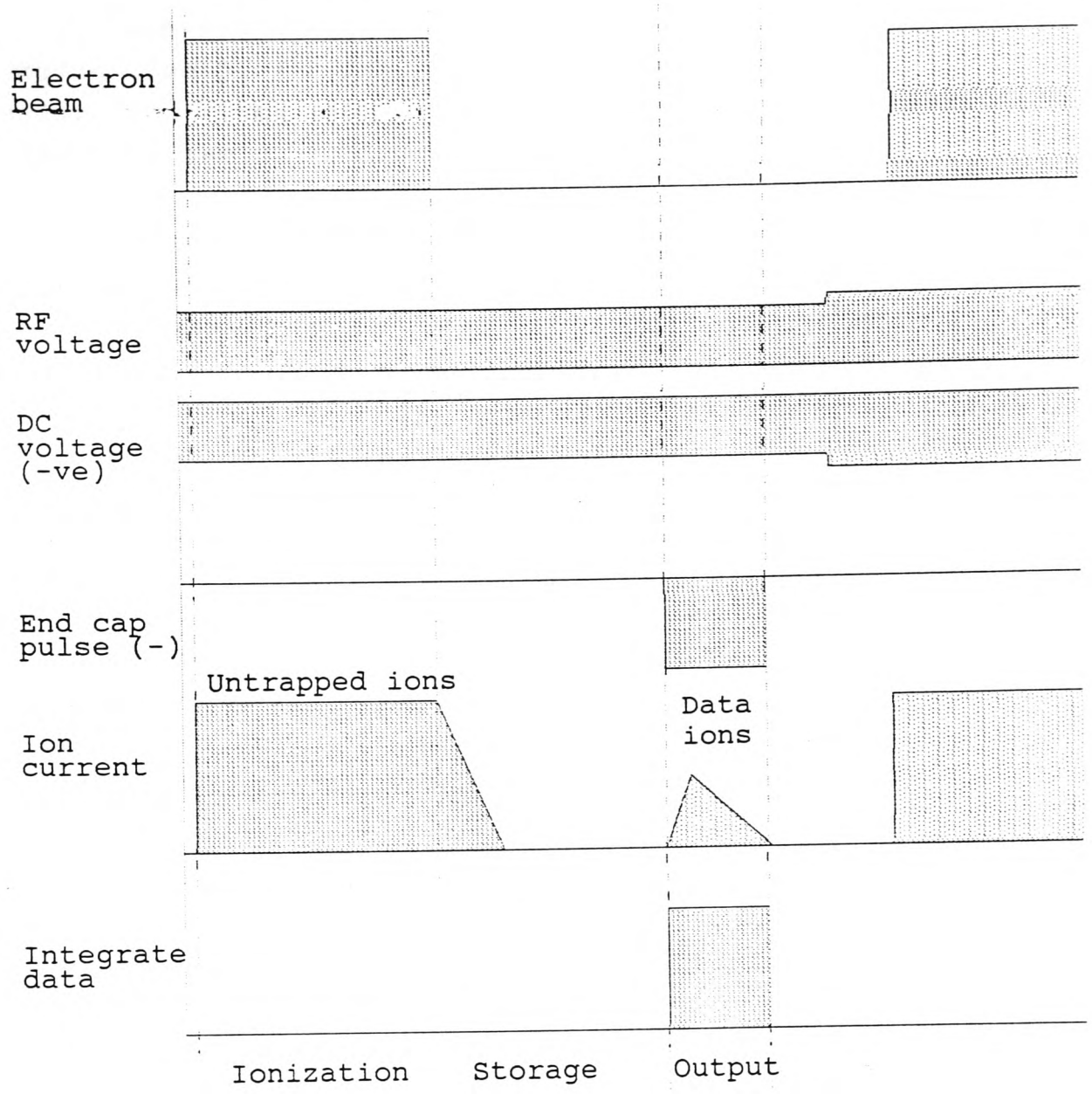

Fig. I.7.3 Lower apex scan type timing diagram.

It is not convenient to eject ions from the trap by ramping the RF and DC voltages in the way described for the total pressure mode. By ramping in the upward direction ions would be ejected from the trap (by crossing the $\beta_r = 1$ boundary), but in the r direction (towards the ring electrode) which is far from convenient for ion collection since ions would emerge at any point on the ring. By ramping the electrode voltages

in the downward direction ions are ejected axially by crossing the $\beta_z = 1$ boundary but (as shall be seen in chapter III) the resolution of this boundary is much poorer than the $\beta_z = 1$ boundary.

It is therefore necessary to select a value of the ratio of DC to RF which approaches very near to the apex of the stability diagram in order to achieve a high resolution level by allowing only a very small range of ion masses to be stored at once (1 AMU at most) so that peaks in the spectrum may be separated. The nearer to the apex the device is operated, the higher the resolution value, but also the fewer ions are able to be stored and therefore the lower the sensitivity of the device.

This is made more severe by the fact that several so called non-linear resonance lines are known to pass through the lower apex of the stability diagram. These lead to poor peak shapes, loss of resolution and loss of sensitivity.

In addition, the requirement that a pulse must be applied to one end cap in order to eject ions from the trap means that the electronic devices required to operate it are considerably more complex than is otherwise the case. The requirement also means that it is not practical to use a double - sided RF power supply; RF voltages can only applied to the ring electrode. This means an additional loss of achievable mass range of one half.

Another disadvantage of this mode is that the mass range of the spectrum which can be achieved for a given RF voltage range is substantially smaller than in any other mode of operation. This is because the q value required to trap ions is greater as a consequence of the stability diagrams' shape.

Ions can be removed from the trap by applying a negative pulse to one end cap so that all trapped ions are ejected in that direction. Subsequently they can be detected with an electron multiplier, as usual. This mode of operation has been employed in several previous Quistor systems, notably by Dawson and Whetton.

c) Ions can be stored in the trap with values of a and q which lie close to the upper apex of the stability diagram (Scan line (a) shown on the stability diagram above). This also leads to mass selection on storage of ions so that the device can be operated in a very similar fashion to that described above, with ions being ejected from the trap by a pulse applied to one end cap.

This mode of operation will have a much greater mass range than mode (b). The requirement of applying a pulse to one end cap, which results in complex electronics and prevents the use of a bipolar RF power supply, remains. It is also necessary (as before) to select an a to q ratio such that the scan line approaches very near to the apex in order to achieve a high resolution level, so that high resolution and sensitivity may not be achieved at the same time. However, there is only one non-linear resonance line which passes through the upper apex of the stability diagram; it is therefore to be expected that the resulting peak shapes are better than in mode (b).

d) The Quistor may also be operated near to the upper apex of the stability diagram (using scan line (a), as before), storing ions mass - selectively, as described above, but with one crucial difference.

Near to the upper apex (unlike the lower), ions may be ejected from the trap, mass selectively, in the axial direction by an increase in the voltages applied to the

electrodes. This results in ions passing the $\beta_z = 1$ boundary of the stability diagram so as to become unstable in the z - direction. This is very much more convenient than the application of a pulse to the end cap as described above. This approach to ion ejection is very much the same as that described for mode a) above.

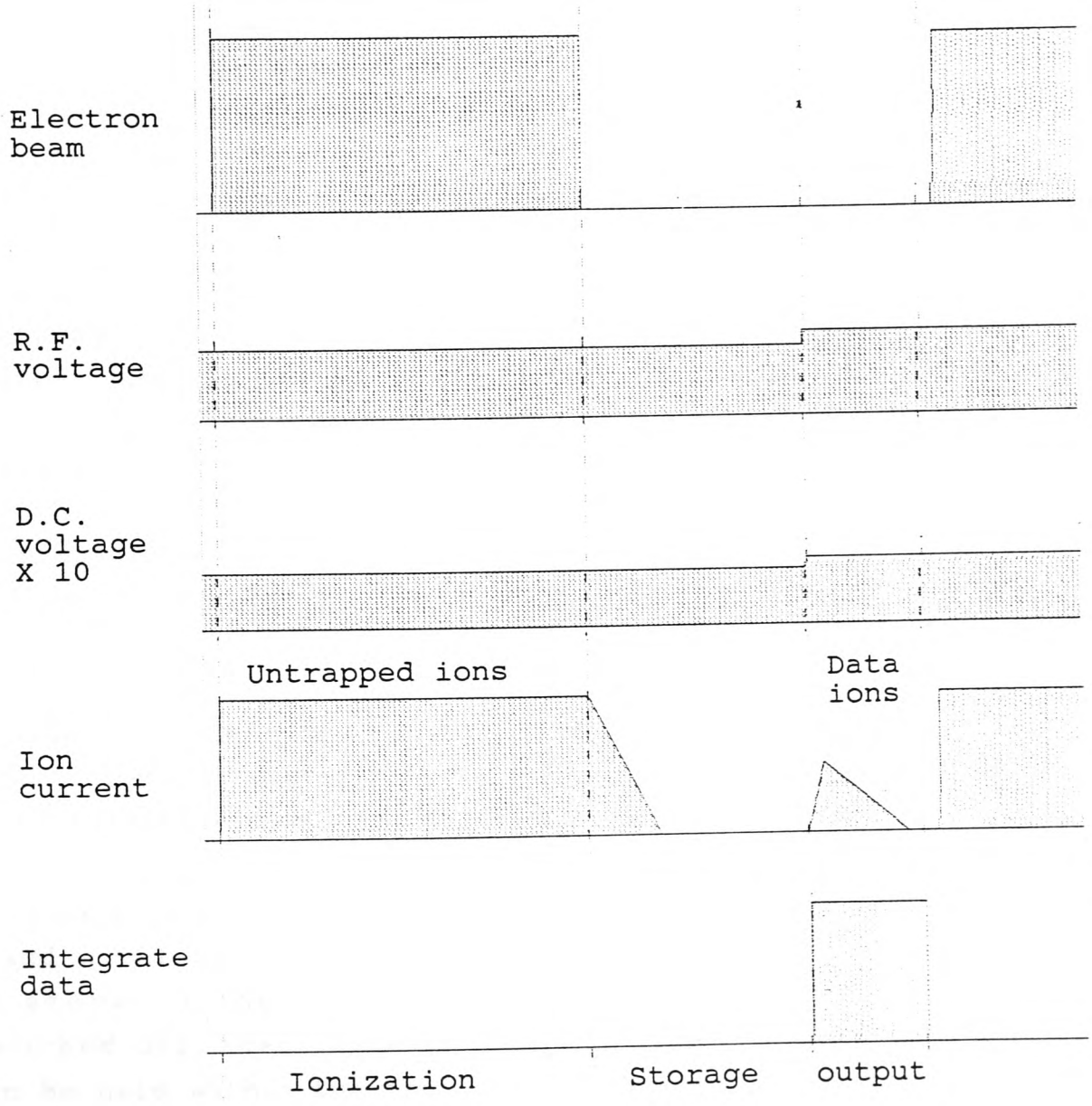

Fig. I.7.4 Upper apex scan type timing diagram

Ideally, the a to q ratio selected for ion storage should

correspond to a resolution level of 1 amu, so that only one ion mass will be trapped at once. However, the ion ejection resolution does not depend on the ion storage resolution. The spectrum's resolution depends on the former and will ideally be considerably better than this.

The mass range which can be achieved by the device for a given range of RF voltages in this mode is almost identical to that of the previous mode.

This mode of operation will only work well if the β_z boundary is sharp and clearly defined, in that all ions which cross it pass from being trapped to being ejected with only a small change in their q values. If this boundary is poorly defined (for example because of distortions in the electric field inside the Quistor), then ions with a and q values near to it will not be effectively stored, and ions which should be ejected by an increment in the electrode voltages will be ineffectively ejected. Only where an increase in these voltages results in well trapped ions being fully ejected does this method work.

This does mean that great effort needs to be taken to ensure that any distortions in the Quistor field are kept to an absolute minimum. (See section III.2)

e) Ions of a selected mass can be stored in the trap with a and q values at the upper apex of the stability diagram, as above. If the DC component of the Quistor field is switched off, then these ions will remain trapped, and so can be held within the trap for a period of time. Ions will collide with neutral molecules, or with other ions. This may result in ion losses from the trap, but chemical reactions can also take place between the colliding species. Many ions will also break down spontaneously into simpler groups of

atoms. In either case, the reaction products (if ionised) can remain trapped within the Quistor to be studied.

This allows investigation of ion - molecule collision processes and reactions (Refs. 4, 5, 7, 28, 100). In particular, reaction rates and reaction products can be studied in a very convenient fashion, without requiring any complex and expensive additional equipment.

By subsequently ramping the RF voltages, the trapped ion species can be ejected one by one and detected. If this is done without applying a DC voltage component, then the stored ions are ejected when they pass the β_z = 1 boundary with a q value of about 0.9. This means that the mass range is lower than that possible when scanning near to the upper apex.

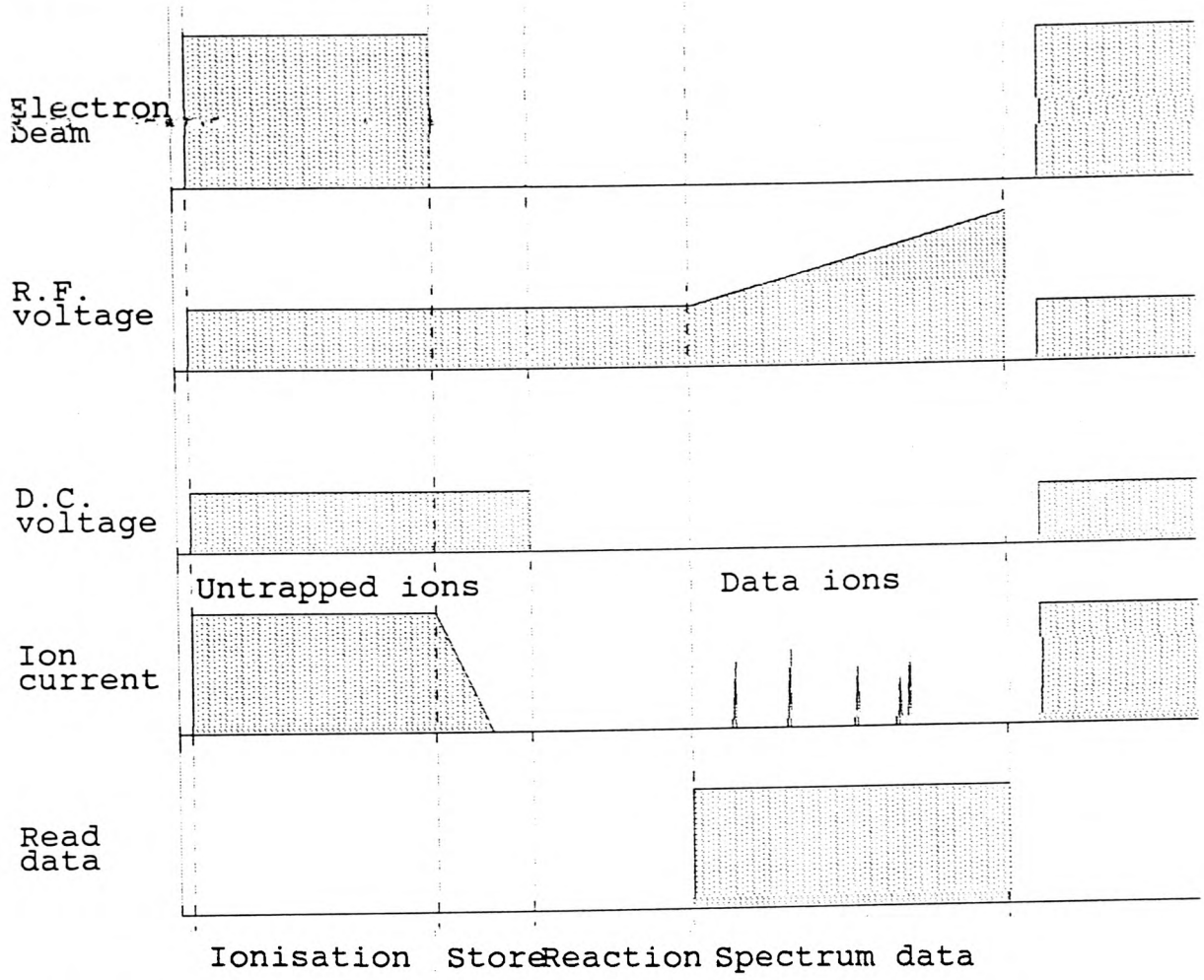

Fig. I.7.5 Chemical ionisation scan timing diagram

An alternate approach is to switch the DC component back on whilst altering the RF voltage so as to select the mass to be ejected at the upper apex of the stability diagram. This gives a greater mass range but does mean that a new set of ions must be generated for each final daughter ion mass scanned.

This method can be extended further still by performing multiple stages of MS analysis, by selecting, repeatedly, the breakdown products (or daughter ions) of previously selected ions. This process is referred to as MS^n, where n is the number of stages of ion mass selection. Using a Quistor, such experiments have been performed with large values of

n (Refs. 45, 46, 93). This allows the operator to gain considerable information about the structure of the compound with which the reactions began.

Multiple stages of mass analysis have been performed using tandem mass spectrometer instruments (in other words, more than one mass spectrometer in series). These instruments are, however, very expensive, and the same degree of flexibility is simply not available. Using a Quistor, in order to change the type of analysis, all that is required is to change the programming.

8) Proposed means of operating and controlling the Quistor

It is proposed that the Quistor will be operated in the mode described in part I.4.d above. Ions are stored mass selectively with a and q values just below the upper apex of the stability diagram, and are ejected from the trap mass selectively by incrementing the voltages applied to the electrodes.

This method has the advantages of a large mass range, combined with a high possible resolution and easy separation of ion species. It does mean however that great care must be taken to ensure that the electric fields within the Quistor are as undistorted as possible. It is also very desirable that a high proportion of trapped ions are detected since the number which can be trapped is quite limited.

Ions will be ejected from the trap in a pulse following the increment in the RF and DC voltages applied to the electrodes which causes their a and q values to pass the $\beta_z = 1$ boundary of the stability diagram. The ions in the pulse can be amplified and

detected.

The following are items of equipment will be required to operate the Quistor in the way described :

a) A programmable RF unit capable of producing, at a frequency of one or more MHz, large, opposite, voltages at the terminals. Superimposed on these should be DC components, at roughly 1/10 (adjustable) of the peak RF voltage. Both should respond to a programming input voltage change quickly - say within 40 μS.

b) A high gain, ultra low noise preamplifier circuit is required in order to detect and amplify the output signal current from the electron multiplier. The output response time of the amplifier must be good - certainly not as long as 100 μS or else the shape of the pulses will be substantially slurred. Some degree of slurring is however acceptable as this will not affect the overall area of the pulse - this being the quantity of main interest. An additional requirement is that the input impedance of the amplifier must be low - a virtual ground input type of amplifier would be ideal. The reason for this is that if the input voltage rises in response to an input current, this will impede the collection of electrons output from the channel plate, leading to a non-linear response.

c) Electronic circuits are required to interface the Quistor to the computer which controls it. This should incorporate a 12 bit digital to analogue converter to produce the programming voltage for the RF unit. Digital signals controlling a number of functions (such as the electron beam gateing) of the other equipment is included, and the signal returned from the Quistor is passed into a switchable integrating circuit in order to find the area of

the pulse. The result of this will be converted from analogue to digital and returned to the computer.

d) A computer is required to control the operation of the Quistor and to acquire, display and store the data produced. A suitable parallel digital I/O port is essential for interfacing with the Quistor's controlling electronics.

In addition suitable software is required for performing the tasks required. The control sections of this software will be have to be written in assembler in order to achieve the high speed interaction and control which is required.

e) Power supplies are required for :

1) To supply the RF unit.
2) Heating the filament.
3) Biasing the filament and accelerating electrodes.
4) To power the preamplifier circuit above.
5) To power the electronics which controls the Quistor.
6) A high voltage power supply is required to supply approximately -2kV to the electron multiplier.

It is also proposed to investigate what can be achieved in terms of operating the Quistor as a Chemical Ionisation instrument, extending this concept to examine its potential as a simple MS - MS device as described in section II.4.e above.

The only additional requirement for operation in this way is a facility for switching the DC component of the voltages applied to the Quistor electrodes on and off at high speed under software control. This is a fairly straightforward

matter; a FET switch shorting out the input to the DC component generator circuits is all that is required.

II PARAMETERS TO CONSIDER IN DESIGNING A QUISTOR SYSTEM.

1) The number of ions of a chosen species which can be stored in the trap at any one time.

The storage of ions within the Quistor is limited by the charge of those ions, which generally will repel each other from the trap. As more and more ions are trapped, the overall charge of those ions trapped in space results in a force which repels ions from the trap.

Another way of looking at this is to say that the depth of the pseudo - potential well which traps ions, (see section II.2) becomes progressively less deep. This means that there is a maximum number of ions which can possibly be stored (Refs. 33, 72, 85).

In whatever context the Quistor is used, this quantity is naturally of great concern.

In addition, as the space charge of ions builds up, the resulting electric field distorts the Quistor' s own field so as to alter the shape of the stability diagram and reduce the sharpness of it's boundaries. This results in peak broadening and loss of sensitivity well before the maximum number of ions is reached (Refs. 70, 72).

The maximum number of ions trapped is a function of several factors :

a) The size of the trap. In general, a large trap (With a large value of r_0) is able to store more ions within it.

b) The frequency of the applied RF voltages. The higher this frequency, the larger the trapping ability of

the trap.

c) The greater the mass of the ions, the more can be stored in the trap.

It should be noted that each of the above factors is also related to the DC and RF voltages which are required to trap ions with a given value of a and q. The larger the trap, the frequency, or the mass of the ions, the larger the voltages required to give certain a and q values.

The above points can therefore be summarised by saying that the greater the RF voltage required to store ions with given a and q values, the more of them may be trapped. This is because the depth of the pseudo - potential well is greater.

They are also underlined by the approximate relationship (I.4.5) derived in section 1, which indicates that the maximum number of ions which can be trapped is equal to

$$N_{max} = \frac{4\pi M \epsilon_0 T^2 u_0^3}{e^2}.$$

where M is the ion mass, T the trapping efficiency (which is proportional to the RF frequency used, amongst other factors), u_0 the trap dimension, and e the ion charge.

d) The number of ions trapped will also depend upon the a and q values used for ion storage. It is found that the trapping efficiency in each direction increases with the q value used (provided the ions remain within the stable region of the stability diagram), but also increases with the β value for a given q value (and thus depends on a).

Secondly, ions which are stored near to the boundaries of the stability diagram are liable to be trapped less effectively than ions which are trapped in the middle of the stability diagram (see chapter III). More ions can therefore be stored in the centre of the stability diagram. However, there will be no mass selection in what is stored. This means that it may not be possible to store so many ions of a given mass, since the total ion charge will be greater.

To store ions with mass selection, they must be stored at one of the apexes of the stability diagram. This necessarily means storage near to the boundaries. The resolution of mass storage selection depends on how near to the apex ions are stored; this in turn depends on the ratio of DC to RF voltages used. As the ratio increases (positive or negative), to approach the apex, the resolution increases but the number of ions stored falls.

The trapping efficiency close to the $\beta = 0$ boundaries is somewhat lower than that at the $\beta = 1$ boundaries (see chapter III). Ion storage at either apex necessarily implies that the a and q values are close to the $\beta = 0$ boundary on one direction, and to the $\beta = 1$ boundary in the other. This means that the number of ions which can be trapped, the trapping ability, will be limited by the behaviour of the trap in the former direction (at the upper apex, r). As the trap becomes full of ions, the depth of the pseudo - potential well in that direction will become zero even though the well remains in the other direction. Therefore ions will be lost in the first direction at the same rate as they are created.

e) Distortions in the electric field within the Quistor will probably reduce the storage ability of the trap, as ions may be prematurely ejected from the trap. This is known to occur at so - called multipole

resonance lines; lines on the stability diagram where the β values add up in such a way as to cause undesirable resonant ejection of ions from the trap. (ref.). This is considered in more detail in chapter III.

f) Collisions of stored ions with other ions, or with neutral gas molecules, or with electrons cause ions to be lost from the trap. Of the three, ion - neutral collisions are the most probable. Over a period of time, trapped ions will be lost from the trap in a random way. This will reduce the maximum number of ions which can be stored for any length of time, especially at high gas pressures. (Ref. 34)

This can be illustrated by calculating the mean free time of ion - molecule collisions in the Quistor at a given pressure. An ion storage time equal to this would mean a loss of 50% of the ions. The mean free time is given by:

$$\tau = \frac{1}{nvs}$$

where s is the collision cross sectional area, n is the number of gas molecules per unit volume, given by the equation

$$P = nkt$$

(where k is Boltzmann's constant, and t is the ambient temperature) and v is the ion speed which can be estimated as half the maximum ion velocity given by:

$2v = Tu_0$ (where T is the trapping efficiency, and u_0 the trap dimension). Immediately after ionisation has taken place, presumably ions can have all amplitudes up to the maximum. After a period of time, however, those with the

greatest amplitudes will have been lost since they undergo more collisions. More realistic estimates of the ion velocity (or kinetic energy) could perhaps be formed (Refs. 73, 83, 98), but this is adequate here.

Therefore:

$$\tau = \frac{2kt}{PTu_0 s}$$

Taking the following values as typical:

$t = 300$ K

$T = 2 \times 10^6$ (see chapter III)

$u_0 = r_0 = 7.5$ mm

$s = 7.04 \times 10^{-19}$ m^2 (collision cross section for nitrogen molecules)

we get:

$$\tau = \frac{7.84 \times 10^{-7}}{P}$$

where P is in Pascals. Converting to mBars,

$$\tau = \frac{7.84 \times 10^{-9}}{P}.$$

At the following pressures, we have mean free time values as follows (See also refs. 31, 95) :

Total Pressure	Mean free time
10^{-5} mBar	0.78 ms
10^{-6} mBar	7.84 ms
10^{-7} mBar	78.40 ms
10^{-8} mBar	784.00 ms.

Fig. II.1.1 Calculated mean free times between ion molecule collisions.

It is not true that every ion - molecule collision necessarily results in loss of the ion - this will depend on the ion and molecule velocities, and the type of interaction that takes place. A purely physical collision with a non-reactive molecule could result only in a change in the ions orbit in the Quistor, and perhaps kinetic energy loss by the ion (see below). In addition, it is even possible that the collision could result in ionisation of the neutral - thus generating more ions as time goes on. It must also be stressed that the collision cross section of molecules can vary considerably. Nonetheless, the above times are a good guide to the maximum ion storage times permitted in the Quistor.

The above values can be compared with approximate results established by experiment (see chapter IV) for argon in an equal mixture with helium. The results turn out to be about 10 times longer than the calculated values above. As stated, not every collision will necessarily cause ion loss and this can easily account for the discrepancy. Collisions with Helium atoms, in particular, are much less likely to cause ion loss (see below).

Total Pressure	Mean storage time
10^{-5}	6.7 ms
10^{-6}	80.0 ms
10^{-7}	668.7 ms.

Fig. II.1.2 Experimental mean ion storage times for Argon ions in an equal mixture of Helium and Argon.

Clearly very long ionisation and storage times are permitted provided the overall pressure is very low. However, the ability of the Quistor to store and detect low abundance ions against a high background pressure is limited by the number of ions which can be formed within the relatively short time interval allowed.

In complete contrast to the above points, it has been shown (Refs. 44, 76, 80, 97) that the inclusion of a high (say 10^{-3} mBar) pressure of a light collision gas such as Helium in the Quistor reduces the amplitude of motion of heavier ions until they have only thermal energies. This occurs because ions with greater energies lose it in mechanical collisions with the lighter helium atoms. Because helium is a very unreactive gas, any form of chemical interaction between it and other ions is unlikely to occur.

Ions will then be held in a dense cloud near the centre of the trap. Since the ion velocities are substantially lower, the frequency of collisions with non - helium molecules is proportionately lower. Consequently longer ionisation and storage times are permissible.

Many more ions can be stored as a result and the performance of the device is improved. Since the ions are stored near the centre of the trap the influence of distortions in the Quistor field is minimised. In addition,

since all ions will have much the same velocity and amplitude, they are more likely to be ejected from the trap with the same RF voltage applied to the electrodes (see below). This leads to improved resolution.

This does mean that the trap must be differentially pumped because a diffusion pump would not be able to operate at this pressure. This effect is used in the Quistor system built by Finnegan Mat, but in this case the device is often used in connection with a gas chromatograph, and the helium is included anyway.

2) The rate at which ions can be generated in the trap

The speed with ions can be created in the trap is naturally an important parameter. A low ion creation rate will mean that a long ionisation time will be required in order to build up a reasonable number of ions in the trap, leading to a long scan time, and (especially at high gas pressures) a lot of ion losses from the trap.

The most important quantity in determining this is the electron beam current which enters the trap in order to produce ions.

This quantity clearly depends on the filament temperature; but naturally a very hot filament has a drastically reduced lifetime. It has been found that a 1 mA emission current is consistent with reliable filament operation. A hot filament also produces much more light than a cooler one; this is unwelcome since it can lead to increased noise in the signal output; see section 6 of this chapter.

The material of which the filament is made can also

affect the emission current at a given temperature. The simplest and cheapest filaments are made of Tungsten wire, while they may also be made of Rhenium because this metal is less chemically reactive at high temperatures. However both of these metals have fairly high electron emission work functions; 4.4 eV and 4.9 eV respectively.

There are materials with much lower work functions than this; for example Thorium Oxide has a work function of 3.4 eV, and Lanthanum Hexaboride has a work function of 2.9 eV. Filaments which are made of Tungsten or Rhenium, but are coated with either Thorium Oxide or Lanthanum Hexaboride, will therefore be able to give the same emission current at a much lower temperature.

The emission of electrons per unit area from a hot metal surface is given by Richardson's equation:

$$N = AT^2 e^{-E / kT}$$

where A is a constant with a theoretical value of 12×10^5 Amp m^{-2} K^{-2}, E is the work function, T the absolute temperature and k the Boltzmann constant. It is clear that a reduction in the work function can lead to a substantial increase in the emission current, or a large reduction in the temperature required to achieve the same current.

The other important factor determining the ionising current is the way in which the electron beam enters the trap. This requires a hole in the end cap adjacent to the electron gun, but to minimise the effects of field distortions in the Quistor, it must be a small hole. This means that only a small current can enter the trap unless the beam is focused.

Focusing the electron beam is possible, but would add considerably to the complexity of the construction of the Quistor. This could however lead to a large ionising current being able to pass through a small hole, as is required.

An alternate approach is to use a large number of small holes spread over an area in the end cap through which a reasonable percentage of an unfocused beam will pass. Since the holes are small, the distortion level produced remains low. This can be done either by placing a formed gauze over a large hole in the end cap, or by drilling a large number of small holes in the end cap using an industrial laser. In either case, the object would be to achieve as high a transparency as possible, whilst maintaining the integrity and precision of the end cap surface.

The ion creation rate can be estimated by saying that the mean free path between electron ionising collisions will be:

$$D = \frac{1}{ns}$$

where n is the number of neutrals of the selected species present per unit volume, given by $P_p = nkt$ (P_p being the partial pressure of the selected species), and s the electron ionisation cross sectional area. Thus:

$$D = \frac{kT}{P_p s}.$$

Since the ion must be created within the a distance equal to the trap dimension u_0, the probability of an electron ionising is:

$$c = u_0 \; / \; D$$

$$= \frac{u_0 P_p s}{kT}.$$

It follows that the number of ionisations per second will be given by:

$$N = \frac{Ic}{e}$$

where I is the electron beam current in the trap.

$$= \frac{I u_0 P_p s}{ekT}$$

Assuming the following values as typical for the Quistor :

$I = 10\mu A$
$u_0 = z_0 = 5.3$ mm
$s = 2.904 \times 10^{-20}$ m² (nitrogen with 100eV electrons)
$T = 300$ K

we obtain

$$N = 2.324 \times 10^{12} P_p$$

where P_p is in pascals. Converting this to mbars, gives :

$$N = 2.324 \times 10^{14} P_p.$$

Of these ions, some will not be trapped due to excessive ion velocities. The exact proportion will depend upon the ion mass and velocity distribution of the ions produced. Note that ions will be created with fairly low velocities since electron collisions with molecules will not impart

large kinetic energies to the molecules (because of the great difference between their masses). The ion velocity will be the result of the action of the electric field upon the ion after creation. This will depend upon the ion creation point, and the RF phase at the moment of creation. If we assume that about half are lost, then

$$N_{trapped} = 1.096 \times 10^{14} P_p \tau_{ionisation}$$

where $\tau_{ionisation}$ is the ionisation time allowed (with a maximum useful value equal to roughly the ion loss time constant).

If for example we wish to detect a species with a partial pressure of 10^{-10} mbar, against a background of 10^{-5} mbar, with an ionisation time of 0.78 ms, we can only hope to trap about 9 ions. This would seem to represent about the limit of detectability. This therefore means that the Quistor can be expected to detect 1 part of a trace gas in 10^5 of the background.

At the other extreme, if we consider the sensitivity of the Quistor in the case of a pure gas, say nitrogen at 10^{-7} mbar, we get that the number trapped of ions trapped in 78.4 ms is 8.59×10^5. This is actually much less than the maximum number of ions which the trap can hold due to its space charge limitations (see the previous section). The implication is that it is important to ensure that the ionising current in the trap is large as great as possible in order to get the best sensitivity.

Again, it must be stressed that the electron impact ionisation cross section can vary considerably from one molecule to the next, depending on the molecular size, and ionisation energy. On the other hand, (other factors being equal) the larger a molecule is, the greater its ionisation

cross-section but also the greater the ion collision cross section. Consequently the effects are likely to oppose each other in the overall sensitivity.

An additional effect which may affect the ionisation efficiency is the energy with electrons enter the trap. This may have an effect on two important quantities :

i) The efficiency of ionisation. Low energy electrons clearly cannot ionise gas molecules; but very energetic electrons are not very good at doing so either. It is generally recognised that electrons with about 70 eV energy are ideal for the purpose.

ii) The kinetic energy of the resulting ions. High energy electrons are going to produce fast ions, which will be harder for the Quistor to trap. This point is illustrated by the calculations above.

Since the electrons will be heavily influenced by the electric fields within the Quistor, the electron energy in most parts of the Quistor will be much greater than that with which they enter the trap.

However, (at least if the ring and the end caps have equal and opposite potentials applied to them) the potential at the centre of the trap is always zero. This being the place where ions created are most likely to be trapped, ideally electrons should should have energies of roughly 70 eV when they reach the centre of the trap. In other words, the filament should be biased at -70 V.

Some Quistor systems (notably the Finnegan MAT system) have been constructed in which RF and DC voltages are applied only to the ring electrode, while the end caps are earthed. This does have a number of advantages in terms of

construction but aside from a 50% reduction in the mass range for a given output voltage, also results in the centre of the trap being at half the trap RF and DC potential. In consequence electrons in the centre of the trap probably have high kinetic energies during the positive phase of the ring's RF, whilst being unable to reach the centre of the trap during the negative phase.

This is a strong argument supporting the use of bipolar RF supplies, in which case the centre of the trap is always at ground potential. During the negative phase of the end caps' RF, electrons will be unable to pass the end caps and enter the trap. However during the positive phase, electrons can pass through the end caps, and will actually be focused into the centre of the trap since they will be repelled from the negative ring.

3) The efficiency with which ions will be ejected following a small increment in the voltages applied to the electrodes.

Following a small increment in the voltages applied to the electrodes, ideally all stable ions which are sufficiently close to the $\beta_z = 1$ boundary should pass from being completely stable and trapped, to being fully unstable and so be detected.

However in practice this is not quite so; as the $\beta_z = 1$ boundary is approached, the amplitude of motion of stable ions increases. This means that "stable" ions with large amplitudes will be ejected from the trap before the boundary is actually reached. Consequently, ions which are created near to the boundary will probably only be stored in small numbers, and following an increment in the RF and DC voltages, only a few will be detected. In addition, ions which are stored further from the boundary, and should remain in the trap following the increment, will not do so - most will be ejected and detected prematurely.

This effect is present in the case of an ideal Quistor without distortions, but any distortion in the Quistor field is likely to increase this "blurring" of the boundary of the stability diagram.

Since this effect reduces both the ion output pulse strength and the mass resolution of the device in the mode of operation employed for this project, it is vital that it be minimised if the Quistor is to work at all well.

It is important that the correct step size (or voltage increment) is used in the Quistor. Ideally, one would wish to 'step over' the blurred edge of the

stability diagram so that all ions pass from being stable to being unstable in one step. If the step chosen is smaller than the inherent resolution of the $\beta_z = 1$ boundary then the output intensity is correspondingly reduced. On the other hand, if the step size is larger than the resolution of the boundary, the resolution of the spectrum will be limited by the step size.

Another, rather similar effect is that there is a random variation in the time of ion ejection from the trap following an increment in the voltages applied to the electrodes. Since it is not possible to wait forever for ions to be emitted, it is never certain that all output signal ions will be detected. However in a reasonable time period (say 0.5 ms), the vast majority will be detected and this problem may reasonably be discounted.

These effects are discussed in much more detail in chapter III.

4) The proportion of the ions stored and ejected from the trap which can be detected.

Ions which have been successfully stored and correctly ejected from the trap after an increment in the RF voltage must still be received by a detector in order to be of any value. There are two reasons why this will not be so for most ions.

i) Following a voltage increment, ions will be ejected along the Z axis of the trap in both directions. This means that on average half of the ions will be ejected in the wrong direction; towards the electron gun, rather than the detector.

ii) Those ions which are ejected in the correct direction must still pass through the end cap. This requires one or more holes in the end cap, but in order to minimise the effects of distortion in the Quistor field, such holes must be small. The ideal end cap would be made of a fine gauze; in practice it may prove to be difficult to shape a gauze into the curved surface of an end cap with any accuracy. A possible alternative to this which would be almost as good is the drilling of a large number of very small holes in the solid steel end caps using a powerful laser. These alternative approaches apply also to the other end cap, as discussed in the previous section.

5) The intensity of the resulting output signal current

The output signal from the Quistor will be a small ion current at best, and it is necessary to take special steps in order to detect it.

Generally an electron multiplier is used as a detector in quadrupole systems in order to amplify the signal current to a detectable level. A proper choice of multiplier (Ref. 61) is very important to the Quistor and the following factors need to be taken into consideration in making this selection

i) The gain of the amplifier. This generally depends on the EHT voltage applied to the multiplier, but there is a limit to the voltage used and the gain achieved consistent with normal operation. Ideally the multiplier chosen should be capable of operating at a gain of about 10^6.

ii) Ease of mounting in the Quistor system. Some types of multipliers are awkwardly shaped and would increase the complexity of the Quistor's construction.

iii) The proportion of ions emitted from the trap to which the multiplier actually responds. Ions may not always strike the sensitive surfaces of the detector, and so some may not be detected.

iv) The dark current (i.e. the output current produced by the multiplier when no signal input is present) should be very low. Any such current would appear as noise in the output and so would tend to obscure the signal.

v) Generally it is necessary to ensure that there is a potential difference between the output side of the

multiplier and and the Faraday plate receiving the output signal. This ensures that electrons are efficiently drawn from the multiplier and collected by the Faraday plate. Between 10 and 15 volts is generally found to be adequate.

This needs to be borne in mind when designing a Quistor system since it means that either the output side of the multiplier must be at a negative potential w.r.t. ground, or the Faraday plate must be at a positive potential w.r.t. ground.

If the Faraday plate is at ground potential, this is somewhat simpler in terms of the electronic preamplifier required (see section VII.1). On the other hand if the output side of the multiplier is at ground potential, this is an advantage in terms of the construction of the Quistor itself (see chapter V).

vi) A wide dynamic range (i.e. a wide range of measurable signal current outputs) is an important requirement. Any multiplier will saturate it's output current, generally at 0.1 to 1 μA output current. At the other end of the scale, as the output current approaches the dark current mentioned above, any measurement becomes meaningless.

6) Any sources of noise obscuring the signal output.

The limit of sensitivity to ions of the detector is necessarily that current which can just be detected over the noise level. It is therefore very important that the noise level of the analog signal output from the Quistor be minimised.

This noise generally falls into three groups :

a) Electronic noise in the preamplifier detecting the signal output from electron multiplier. This is discussed in more detail in section VII.1.

b) Spurious output produced by the multiplier without ion input. This may be because the multiplier responds to particles other than ions - particularly photons. Where line-of-sight exists between the hot, bright filament, and the multiplier surface, this problem may not be trivial. Reflected light will also be present, but at a lower intensity

In addition, the multiplier will have a certain (very small) dark current even without light input. For one thing, radiation can never be excluded from it.

c) Ions may genuinely be emitted from the trap when they should not, in principle, do so. These would then be detected as noise. This could happen for the following reasons :

i) Collisions between stored ions and neutral gas molecules, or other stored ions, can throw ions from the trap when they should remain in it. These ions could be ejected in any direction, but those which are ejected along the axis and towards the multiplier will

be detected.

At low gas pressures, this is probably quite an improbable event since the mean free path of ions is quite long. However this effect may become significant at higher gas pressures.

ii) So - called non - linear resonances due to distortions in the Quistor field may give rise to spurious and unpredictable ion ejections from the trap. These ions would be seen as noise; on a mass spectrum the result would probably be a "clump" of random ion output appearing to the left of a peak.

iii) If any ions are created in the trap during the period when the electron beam is off, then these ions will probably be thrown out of the trap in either the r or z directions (depending on their mass and the electrode voltages at the time). Ions ejected in the z - direction would be received as noise by the detector.

This would happen if the electron beam were not fully switched off; if there was some leakage current. The most probable reason for this would be the photoemission of electrons from the gauze covering the filament. Naturally the gauze is brightly illuminated by the hot filament. The electrons so created could then easily be drawn down into the trap, where ions would be created. These ions would probably be ejected and so could be detected as noise.

This effect can only be overcome by restricting or eliminating the light output from the filament (whilst, of course, not restricting the normal electron beam

current from the filament). Possible means for doing this involve the application of electric and / or magnetic fields to the electron beam (which naturally would not affect the light).

Another step which can easily be taken to reduce substantially (though not eliminate) this problem is to use a filament coated, say, with Thorium or Lanthanum Hexaboride (see section III.3). The filament would then produce electron output at a lower filament temperature. Consequently far less light would be produced, especially light with high photon energy, as would be required to produce photoemission effects.

iv) If ions are entering the trap during the period when the electron beam is off then the effect will be very similar to that described above as these ions would probably be rapidly thrown out of the trap, and strike the multiplier.

This could take place if ions were created by electrons which leave the filament only to return to it, repelled by the gauze potential. These ions would not be repelled by the gauze and could easily pass down into the trap. This effect could be overcome by the use of a second gauze at a potential positive with respect to the filament, between the first gauze and the end cap. Ions would then be able to pass the first gauze, but would be blocked by the second.

In addition a very similar effect would be produced if ions, created during the interval when the electron beam is on, in the region between the gate and the end cap were stored there only to "leak" into the trap over a period of time while the electron beam is

off. It has been shown that a conical volume with RF fields applied can trap ions effectively.

v) Correctly trapped ions may collide with each other or with neutral gas molecules. In this case it is possible that the trapped ion may be scattered and leave the trap in the z - direction unexpectedly and so be detected. Alternatively, the neutral in a collision could be ionised by the collision and be ejected along the z axis depending on its mass. A third possibility is that a trapped ion could undergo a reaction (perhaps spontaneously) so that its mass is reduced. In this case it would also be ejected along the z axis.

It is very difficult to say which of the above processes takes place in the Quistor under given conditions. Very probably, several or all of these effects can take place and produce noise. As stated, steps can be taken to overcome these problems; this will be discussed in more detail in section V.

7) The mass range of the spectrum produced which the device can achieve.

The range of masses which can be achieved by the Quistor in a mass spectrum depends on a number of factors, most of which are in conflict with the need to be able to store a large number of ions (see above). These factors are :

a) The size of the Quistor. A small Quistor with low value of R0 will have a larger mass range.

b) The frequency of the RF which is used. The lower this frequency, the heavier the ions which can be stored. It is worth mentioning that small charged particles of aluminium metal (certainly the most massive objects ever so trapped) have been trapped in a Quistor using a frequency of only 50 Hz.

c) The ratio of DC to RF which is chosen. Depending on which point on the stability diagram is used for operating the Quistor, for any given RF voltage, different mass ranges will be stable since different ranges of a and q lie within the stability diagram. Consequently the mass range of the spectrum produced is different.

If the ratio is zero, a large range of ions can be trapped at once; in principle from a small mass depending on the RF voltage selected, to infinity. In practice, of course, the ability of the trap to store ions in this way depends heavily on the mass of the ion trapped; very heavy ions in with a low value of β_r (while stable in principle), will be poorly trapped. Light ions with a value of β_z of 1 or greater, of course, will not be stable. This mode of Quistor operation was employed by Finnegan Mat in

their system. (See section I.4). Since the spectrum depends on ion ejection at the right hand boundary of the stability diagram, this q_z value (about 0.9) determines the mass range of the spectrum.

The other regions of the stability diagram which can be usefully used are at the tips. Previous Quistor systems have been operated at the lower apex of the diagram. In this mode the mass which of the spectrum which can be produced is about 30% smaller for a given RF potential applied than in the Total pressure mode since the q value required to trap ions is greater (about 1.25).

At the upper apex of the stability diagram, which is the region of main concern to this project, ions are trapped and ejected from the trap with a q_z value of about 0.75. This means that the mass range is about 20% greater for any given range of RF voltages than in the total pressure mode.

III COMPUTER SIMULATION OF THE BEHAVIOUR OF THE QUISTOR

1) Introduction to the computer simulation programs

The computer simulation work undertaken for this project has proved invaluable as a means of understanding the way in which ions behave in the Quistor. Fairly realistic simulation is possible, while total control over the conditions under which ion motion takes place is retained. This makes the technique very powerful.

The simulation work has concentrated mainly upon ion motion near to the upper apex of the stability diagram, this being the region of main interest to the project.

The programs fall essentially into three parts; there is a program which computes the electric field distribution within the Quistor due to the arrangement of the electrodes, and a second group of programs which simulate ion motion within the Quistor upon the basis of the electric field data provided by the first. Finally there is a third program which analyses the electrical potentials around a gauze which has different electric fields incident on either side. The results from this program may be entered into the fields program in order to calculate the consequences of using a gauze instead of a solid electrode.

It must be stressed that these programs were built up over a period of time; for example, early results in the simulation work were based on simpler algorithms, and in particular were based on the assumption that the Quistor's electric field was perfect, without distortion.

a) The ion motion simulation program.

The present algorithm employed by the simulation work

operates on the basis of a 5'th order Lagrangian interpolation of the time varying acceleration an ion experiences. In other words, the acceleration at the present instant is calculated from the present position and time, while this and the acceleration at the previous 4 time steps are used to calculate the motion in the next time step. The time step employed in all simulations has been 10^{-8} s.

It is felt that this approach has resulted in extremely accurate plotting of ion motion, even over long time intervals. It was found that where the algorithm employed was inaccurate, the result was that the amplitude of stable ion motion increased very slowly with time as the errors accumulated.

This was very unfortunate because the program was set up so as to continue plotting the ion position until either :

i) The ion had escaped the confines of the trap, or

ii) The ion amplitudes had not increased for a period of 400 cycles or so, or

iii) The ion plot time had exceeded about 0.01 seconds.

In the case where the ion amplitude increased very slowly, as described above, the result was that the computer spent very large amounts of CPU time calculating the motion of stable ions. An accurate algorithm was therefore essential.

The results the program was mainly looking for were the ion position amplitudes, and the ion velocity amplitudes in both r and z directions. Dividing the velocity amplitude by the position amplitude gave the

trapping efficiency. Where the ion was unstable in either direction, the trapping efficiency in that direction was zero, of course.

The simulation programs are able to take account of the the following permutations in the Quistor's normal (or ideal) behaviour :

i) The presence of gas molecules, resulting in random collisions between ions and neutrals.

ii) A choice of sinusoidal RF voltages applied to the electrodes, or square wave RF. In the latter case, the mark : space ratio of the square wave can be selected.

iii) The presence of an additional exciting RF field along the Quistor's axis at a different frequency to the fundamental.

iv) The presence of an axial magnetic field in the Quistor.

v) The results from the fields program (see below) can be read into the ion plotting program in order to simulate the ion motion in the case where the electric field is distorted due to the limitations of its construction.

The electric fields at any arbitrary point are calculated from a quadratic interpolation of the electrical potential pixel values.

vi) The space charge of other ions present in the Quistor.

A number of different results can be obtained by the various simulating programs, including :

i) A simple plot of ion position under a given set of conditions. Output in the form of r vs. t, z vs. t and r vs. z can be obtained.

ii) The trajectories of a large number of ions under identical conditions, with a and q values close to the right hand boundary of the stability diagram, but with random initial positions and velocities, are plotted. Initially those ions with excessive amplitudes will be ejected, and after a period of time, an RF and DC voltage increment is applied, making the ions unstable. The number of ions ejected was plotted vs. ejection time, thus clearly showing the nature of the pulse which can be expected in the real Quistor, following a voltage increment.

iii) The trapping efficiency of the Quistor can be plotted vs. RF voltage on a selected scan line (i.e. for a selected DC to RF ratio). A number of other factors can be added to affect the Quistor's performance including :

iv) The trapping efficiency can be plotted at all points on the stability diagram. Essentially the same approach is taken as that above, and the user can control the same factors which may affect the Quistor's performance. Limitations upon memory and runtime mean that it is not practical to plot the trapping efficiency with the same level of detail as that above, but the approach gives an extremely valuable insight into the overall affect on the stability diagram of a modification.

v) The amplitude of ion motion can be plotted as a function of time. For a stable ion, this amplitude should be constant (although, as will be seen, the motion is inherently a pulsing one due to the superposition of components of motion a different frequencies). However for an unstable ion, the amplitude will increase exponentially; and, of greater interest, if a large pressure of helium gas is present in the Quistor, the amplitude will decrease with time.

b) The electric fields program.

The electric fields program mentioned above is able to calculate both the DC and RF components of potential at all points within the Quistor.

The algorithm used is a modified version of the mean value theorem. This theorem states that a good approximation to the potential at any point may be obtained by finding the mean value of the potentials at surrounding nearest - neighbour points. Thus the potential at each point is replaced by average value of its nearest - neighbour potentials. This process is repeated many times. The theorem is valid for data stored in one or more cartesian dimensions, and as long as no charge is present in the space considered.

The theorem can be proved as follows. Laplace's equation gives the divergence at a point located by the vector displacement $\underline{p}$ from the origin as

$$\nabla^2 \phi(\underline{p}) = 0. \qquad \text{(III.1.1)}$$

Taylor's theorem (in vector geometry) states that the potential at a point located by the vector $\underline{p} + \underline{h}$ is equal to

$$\phi(\underline{p} + \underline{h}) = \phi(\underline{p}) + \underline{h}.\underline{\nabla}\phi(\underline{p}) + \underline{h}.\underline{h}D^2\phi(\underline{p}) + \ldots \qquad \text{(III.1.2)}$$

Ignoring terms higher than second order, and combining (III.1.1) and (III.1.2), it is clear that (approximately):

$$\phi(\underline{p} + \underline{h}) = \phi(\underline{p}) + \underline{h}.\underline{\nabla}\phi(\underline{p}) \qquad \text{(III.1.3)}$$

In this case, the potentials at the nearest neighbour points are given by:

$$\phi(\underline{p} + \underline{i}) = \phi(\underline{p}) + \underline{i}.\underline{\nabla}\phi(\underline{p}) \qquad \text{(III.1.4)}$$

$$\phi(\underline{p} - \underline{i}) = \phi(\underline{p}) - \underline{i}.\underline{\nabla}\phi(\underline{p}) \qquad \text{(III.1.5)}$$

$$\phi(\underline{p} + \underline{j}) = \phi(\underline{p}) + \underline{j}.\underline{\nabla}\phi(\underline{p}) \qquad \text{(III.1.6)}$$

$$\phi(\underline{p} - \underline{j}) = \phi(\underline{p}) - \underline{j}.\underline{\nabla}\phi(\underline{p}) \qquad \text{(III.1.7)}$$

$$\phi(\underline{p} + \underline{k}) = \phi(\underline{p}) + \underline{k}.\underline{\nabla}\phi(\underline{p}) \qquad \text{(III.1.8)}$$

$$\phi(\underline{p} + \underline{k}) = \phi(\underline{p}) - \underline{k}.\underline{\nabla}\phi(\underline{p}) \qquad \text{(III.1.9)}$$

where $\underline{i}$, $\underline{j}$, $\underline{k}$, are array unit vectors along the cartesian axes. It follows from adding equations (III.1.4) to (III.1.9) together that:

$$\begin{aligned}\phi(\underline{p}) = (&\phi(\underline{p} + \underline{i}) + \phi(\underline{p} - \underline{i}) + \\ &\phi(\underline{p} + \underline{j}) + \phi(\underline{p} - \underline{j}) + \\ &\phi(\underline{p} + \underline{k}) + \phi(\underline{p} - \underline{k})) \,/\, 6\end{aligned} \qquad \text{(III.1.10)}$$

In other words, the average value of the nearest-neighbour points is a good guess at the correct potential at a point. However, in this case, given the Quistor's cylindrical symmetry, it is essential to use cylindrical

polar co-ordinates in the program so that a two dimensional array of points (in the r - z plane) only is required. This however leads to a problem because cylindrical polar co-ordinates are (obviously) not cartesian.

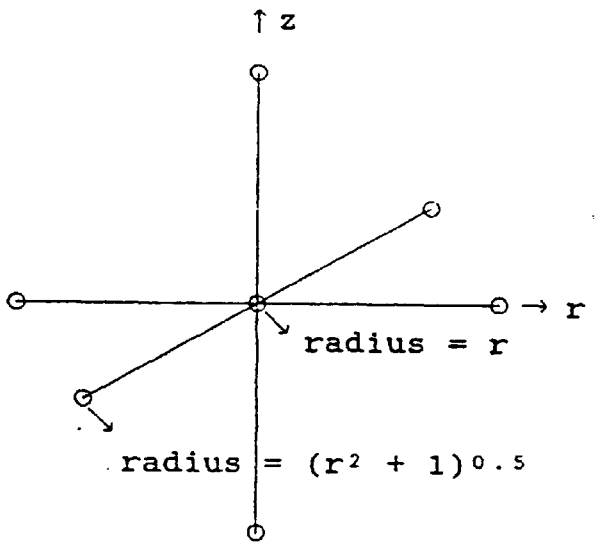

Fig. III.1.1 Nearest-neighbour points in cylindrical polar co-ordinates.

The r direction is equated with the x direction by saying that the y component of $\underline{p}$ is zero. This is an arbitrary but convenient assignment to make since the Quistor is cylindrically symmetrical. In other words,

$$\underline{p} = \underline{k}z + \underline{i}r\cos(\alpha) + \underline{j}r\sin(\alpha),$$

where α has been selected arbitrarily as 0 so that $\underline{p} = \underline{z} + \underline{i}r$. Consequently the nearest neighbour points at $\underline{p}$ +/- $\underline{i}$ and $\underline{p}$ +/- $\underline{k}$ remain at integer array locations in r - z space.

This is not true for the two points at $\underline{p}$ +/- $\underline{j}$. In order to calculate the potentials $\phi(\underline{p} + \underline{j})$ and $\phi(\underline{p} - \underline{j})$, we can say that

$$\underline{p} + \underline{j} = \underline{k}z + \underline{i}r + \underline{j}.$$

From Pythagoras's theorem, this point lies at a distance of $(r^2 + 1)^{0.5}$ from the axis of the Quistor. Applying the cylindrical symmetry of the Quistor, it is clear that the potential at this point is equal to $\phi(\underline{k}z + \underline{i}(r^2 + 1)^{0.5})$.

The above potential is interpolated quadratically from the potentials $\phi(\underline{p} - \underline{i})$, $\phi(\underline{p})$ and $\phi(\underline{p} + \underline{i})$. Subsequently, the average of all six potentials is found, and the old potential $\phi(\underline{p})$ is replaced by this new value. It should be mentioned that the potential distribution of the (undistorted) Quistor is quadratic so that in the case of a perfect Quistor, a quadratic interpolation is exact.

The potentials at electrode surfaces (whose locations are programmed into memory in advance) are fixed. In the case of curved electrode surfaces (i.e. the endcaps and ring) it was found to be necessary to set the potentials close to the surface to being the ideal Quistor potential:

$$\phi = \phi_0 \frac{(2z^2 - r^2)}{r_0^2}$$

instead of $+/-\phi_0$. The reason for this was that the surface was artificially "rough" and inaccurate due to the finite size and discrete nature of the potential array elements.

The program was set up so as to keep iterating the data until the value of no potential changed by more than one part in 10^7, this being roughly the limit of the numerical accuracy.

The program is able to take account of the geometrical layout of the Quistor, with only a small degree of simplification. The position of the (earthed) gate electrode gauze, the position and voltage of the channel plate and the presence (or otherwise) and position of any shielding gauzes on either side are all allowed for. The finite size of the Quistor electrodes is taken into account, the potential outside the Quistor being taken as ground. Finally the size of the holes in the end caps, and whether or not these are covered by a gauze, are taken into account.

The data produced by the electric fields program can be read into the simulation program in order to find the effect upon the performance of the distortions involved. When read into the simulation program, the data is normalised according to the following rules :

$$V_n = V / V_{ec}$$

$$U_n = U - U_{ec}V_n$$

where U and V are the DC and RF voltage values read in, U_n and V_n are the normalised data values, and U_{ec} and V_{ec} are the DC and peak RF voltage values applied to the end caps in the fields program.

This means that V_n represents a normalised value, ranging from -1 at the ring electrode to +1 at the end cap, of the RF and DC voltages which are related to the voltages applied to the Quistor. U_n is the DC voltage

which is present which is related to sources of voltage outside the Quistor (especially the channel plate at -2000 V).

When the simulation program is operating, the actual voltage at any pixel point is found from the following :

$$V_{act} = V_n V'_{ec} \sin(\omega t)$$

$$U_{act} = V_n U'_{ec} + U_n$$

where V'_{ec} and U'_{ec} are the peak RF voltage and DC voltage values applied to the end caps in the simulation program.

To find the potentials at any arbitrary point within the Quistor, a quadratic interpolation of the nearest pixel points is used. Note that for a perfect Quistor, this interpolation would be exact since the Quistor's potential fields vary quadratically.

In addition, the program was modified so as to allow it to generate the distortion produced by the presence of space charge in the form of stored ions. In this case, Laplace's equation gives:

$$\nabla^2 \phi = \frac{\rho}{\epsilon_0}$$

which means that

$$6\phi(\underline{p}) = (\phi(\underline{p} + \underline{i}) + \phi(\underline{p} - \underline{i}) + \phi(\underline{p} + \underline{j}) + \phi(\underline{p} - \underline{j}) + \phi(\underline{p} + \underline{k}) + \phi(\underline{p} - \underline{k})) + \frac{6\rho}{\epsilon_0} \qquad \text{(III.1.12)}$$

so that the potential value at a point is repeatedly replaced by the average of the nearest neighbour potentials, plus the divergence of electric field ρ/ϵ_0.

The charge distribution was assumed to be of the form:

$\rho = A\,(1 - r^2/r_0^2 - z^2/z_0^2)$, for $r^2/r_0^2 + z^2/z_0^2 < 1$ and $\rho = 0$ elsewhere.

This is a realistic assumption about the distribution of ion charge, one which means that the distribution has a broad maximum at the centre of the trap, decreases in all directions from there, and is zero at the trap boundaries. It is not claimed, however that this is precisely the distribution which will, in fact, be adopted by an ion cloud.

The total number of ions N in this distribution will be given by:

$$eN = \int \rho dV.$$

Making the substitution $a^2 = r^2/r_0^2 + z^2/z_0^2$ (where $r_0^2 = 2z_0^2$. Note that a is dimensionless) and splitting the distribution into spheroidal shells of thickness da, each with a volume equal to

$$dv = 8\pi z_0^3 a^2 da$$

we get that

$$eN = \int_{a=0}^{1} A(1 - a^2)\, 8\pi z_0^3 a^2 da$$

$$= 8\pi z_0^3 A\ (1/3 - 1/5)$$

$$= 3.351\ A z_0^3$$

Thus if $z_0 = 5.3$ mm,

$$A = 3.207 \times 10^{-13}\ N.$$

Therefore the charge distribution is given by

$$\rho = 3.207 \times 10^{-13}\ N\ (1 - r^2/r_0^2 - z^2/z_0^2).$$

This enables the program to calculate the distortion in the electric field due to a selected number of ions being trapped in the Quistor. In actual fact, it is only necessary to calculate this electric field for one level of charge. Subsequently, if the electric field due to a different number of trapped ions is required, this will be formed as the former field, multiplied by the ratio of the numbers of ions.

The resulting electric potential values can be entered into the ion motion simulation program in order to find out what the Quistor's behaviour will be when it is affected by a particular level of space charge.

c) The gauze field program.

There is one remaining program which sets up a three dimensional array of points around a single square hole in a gauze. On the upper side, an electric field of one volt per mm is assumed to be incident onto the gauze. On the lower side, no field is incident. The potential of the gauze itself is at 0V. By calculating the electric potential field using the nearest-neighbour method, as above, the potentials at points on the gauze surface

where the hole is, are found. The quantity of main interest is the average value across the gauze surface, of the voltage change (from 0V) due to an incident electric field.

The algorithm requires a small correction due to the fact that the Quistor end caps require gauzes which are curved. The program therefore is based on a slightly curved co-ordinate system.

The Quistor fields program is able to consider the consequences upon the Quistor's electric fields of the use of a gauze which may be regarded as electrically "permeable". The voltage change at the surface of the gauze due to this effect is equal to the result from the gauze program (in volts / (volts mm^{-1})), multiplied by the difference in electric field values on each side. This results in an overall distortion in the electric field throughout the Quistor spreading from the gauzes.

There is a problem which is that the Quistor's gauze is inherently curved; while the electrical potential points lie upon a cylindrically symmetrical raster. The consequence of this is that the gauze surface is artificially "rough", introducing an unacceptable error. In the case of the solid electrode surfaces, this problem was also found (see above), but was solved by modifying the electrode pixel values. In the case of the gauze, however, this solution will not work because the electric field on both sides of the gauze is required.

The solution was found to lie in keeping an accurate (non -discrete) record of the exact z co- ordinate required for the gauze surface. In effect the points are moved from their normal grid positions into the actual positions of the gauze. In consequence, the algorithm

requires to be able to consider a non-integer interval between nearest- neighbour points in that direction.

The fields program is able to consider one more aspect. The average potential at the gauze surface drops by a small amount because of the presence of the holes in it; it follows that the position of the gauze can be modified so that it occupies the point in space where the result would be the correct Quistor potential. In this is done, the field returns to its ideal value in spite of the presence of the gauze.

The fields program is able to do this, and return to the user the co-ordinate data required to machine the end cap electrodes which will produce this result. The program takes into account not only the correction described above, but corrects also the overall positional error introduced by the point-to- point approximation to the curved surface.

End cap electrodes machined on this basis, with an accurately shaped and positioned gauze, should provide good transparency end caps which also maintain a precise electric field within the Quistor.

2) Plots of the ion motion in the Quistor.

Plots can be obtained of the motion of ions in the Quistor, in the forms z vs. t, r vs. t and z vs. r. These plots are a useful illustration of the ways in which ions are likely to move and thus help to give an insight into the way in which the Quistor works. The amount of information which can be obtained from them about the Quistor's performance is, however, fairly limited. some examples follow.

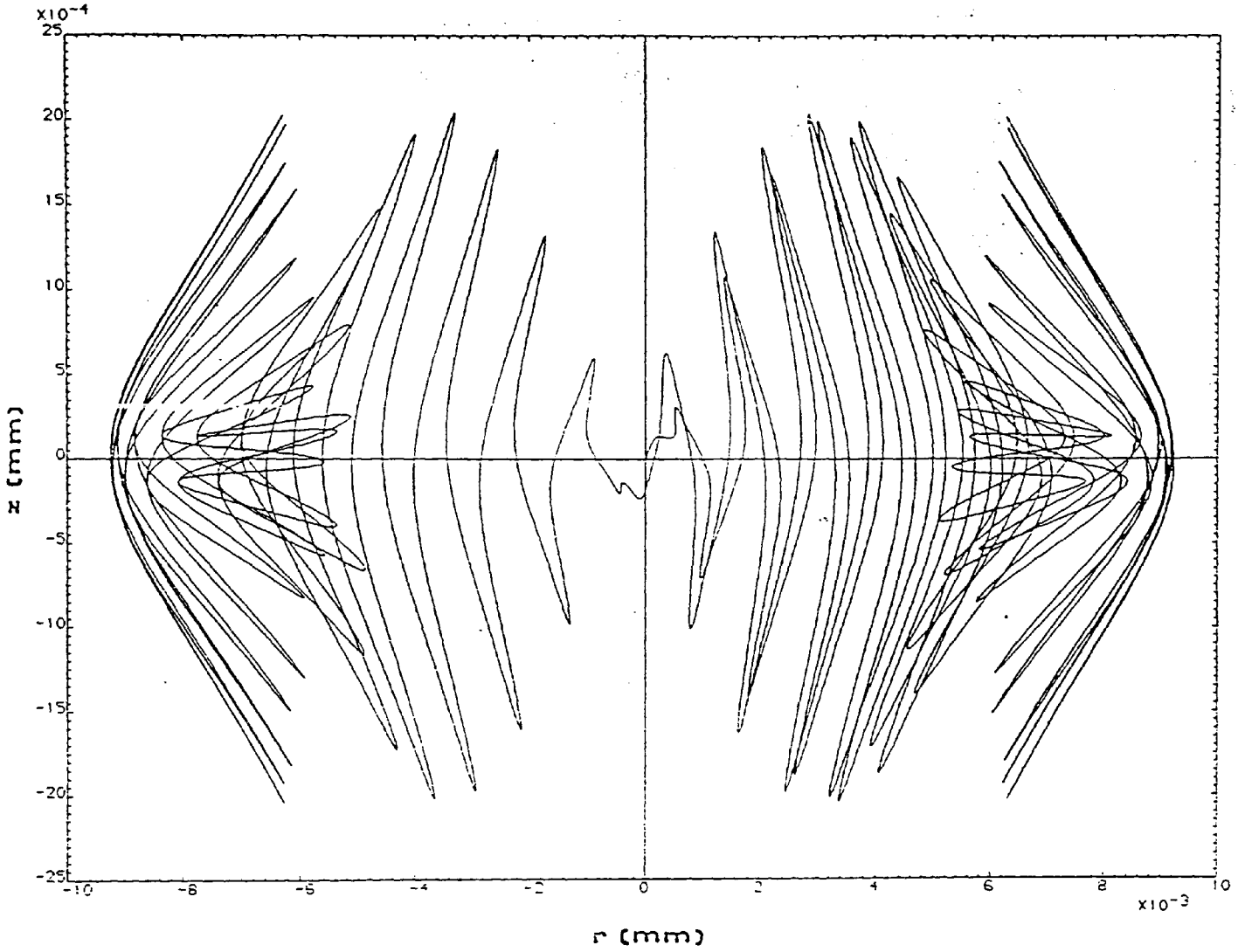

Fig. III.2.1 Plot of ion motion near to the upper apex of the stability diagram. R is plotted horizontally, z vertically.

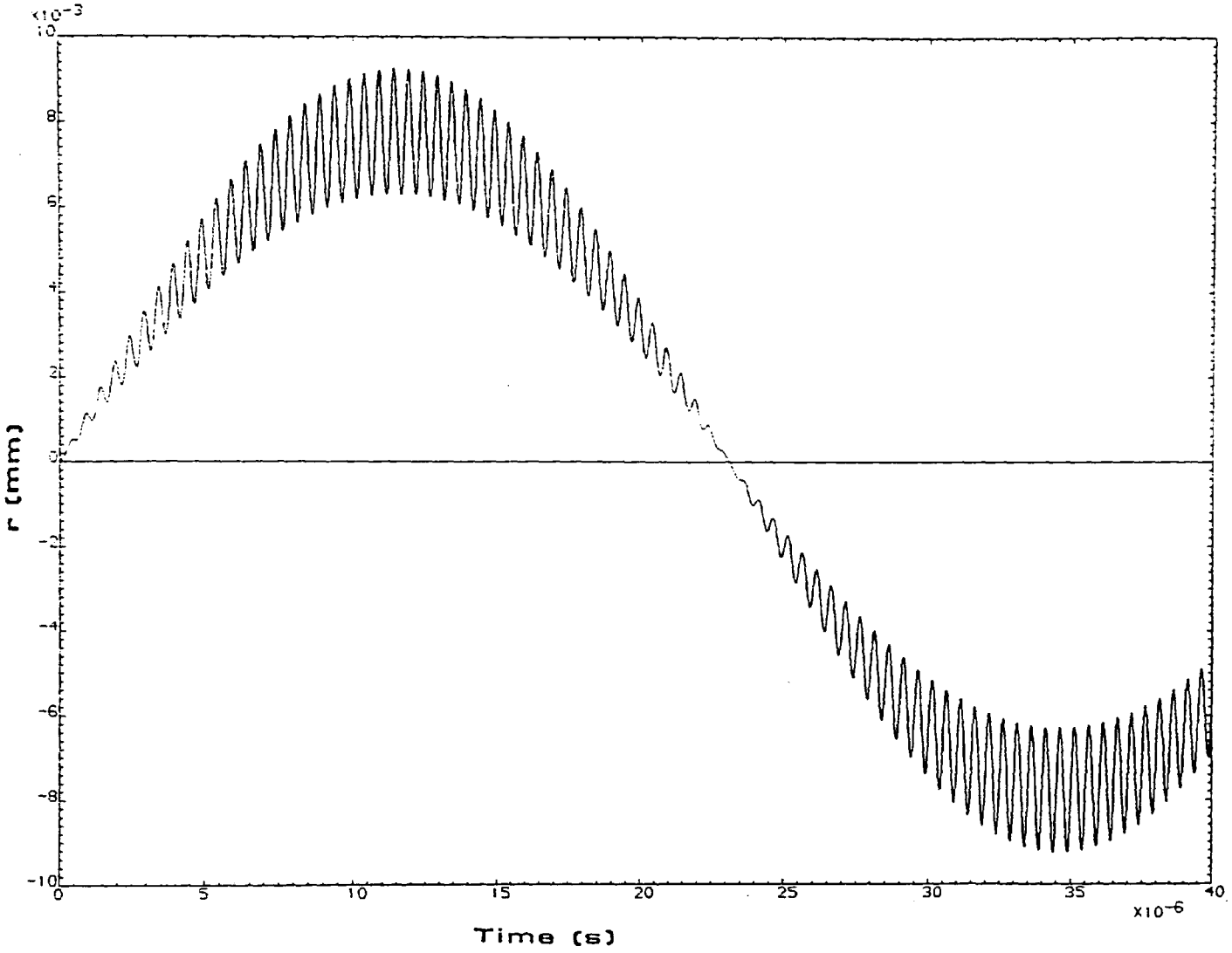

Fig. III.2.2 Plot of ion motion near to the upper apex of the stability diagram. Time (s) is plotted horizontally, r vertically.

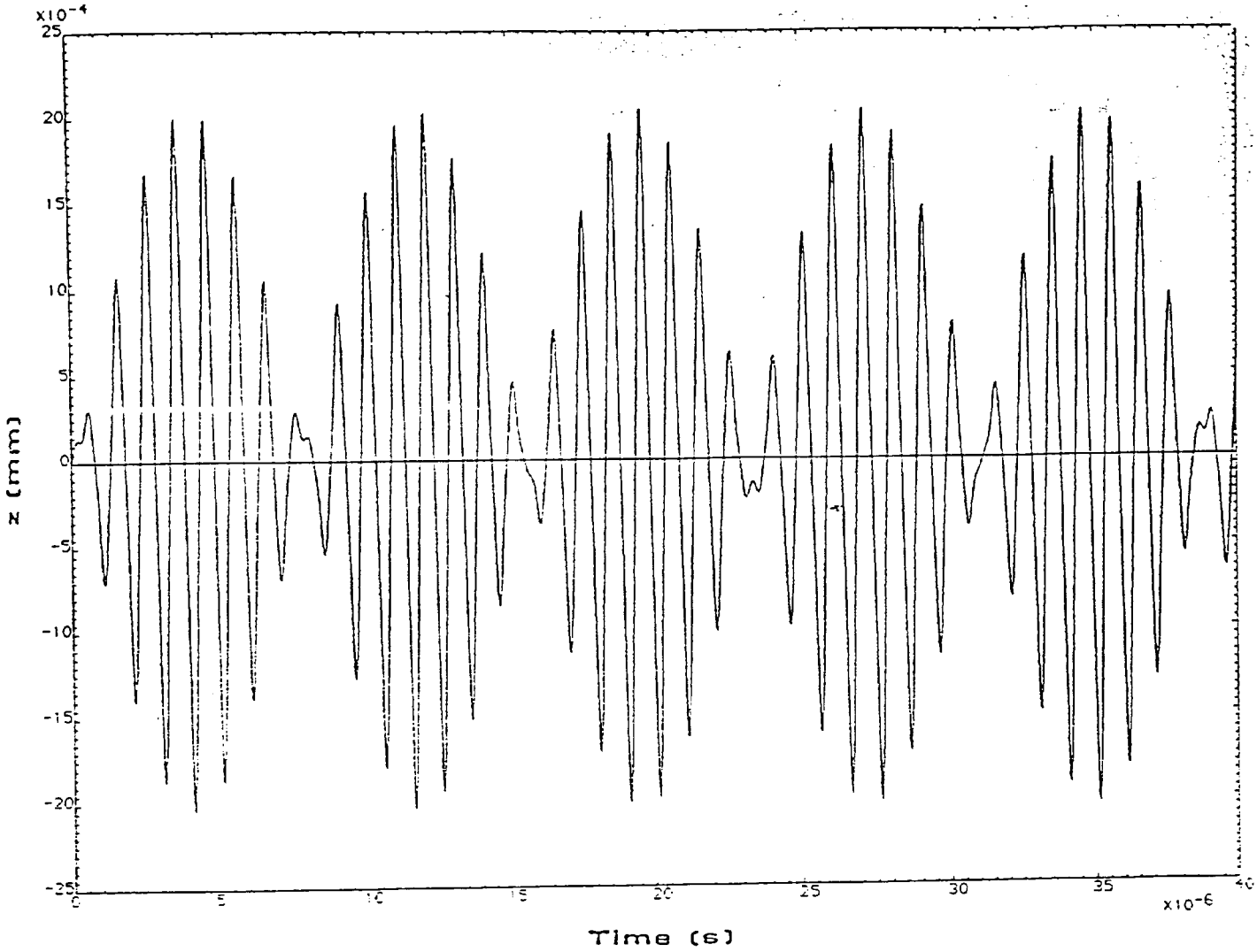

Fig. III.2.3 Plot of ion motion near to the upper apex of the stability diagram. Time (s) is plotted horizontally, z vertically.

3) Ion output data pulse simulation.

Ions are "created" in the Quistor with random initial position and velocity values, with a and q values which are within the stable portion of the stability diagram but close to the right hand boundary. Subsequently the motion of these ions may be plotted. Those with amplitudes in excess of the Quistor dimensions are lost from the trap but some will remain.

Subsequently the RF and DC voltages are incremented by a proportion selected by the user. Where this results in the ions becoming unstable, they are ejected in the z - direction and the ejection time is recorded as a count in an array.

If this process is repeated with a sufficiently large number of ions, then the data stored in the array is a representative indication of the ion output behaviour which can be expected from the Quistor.

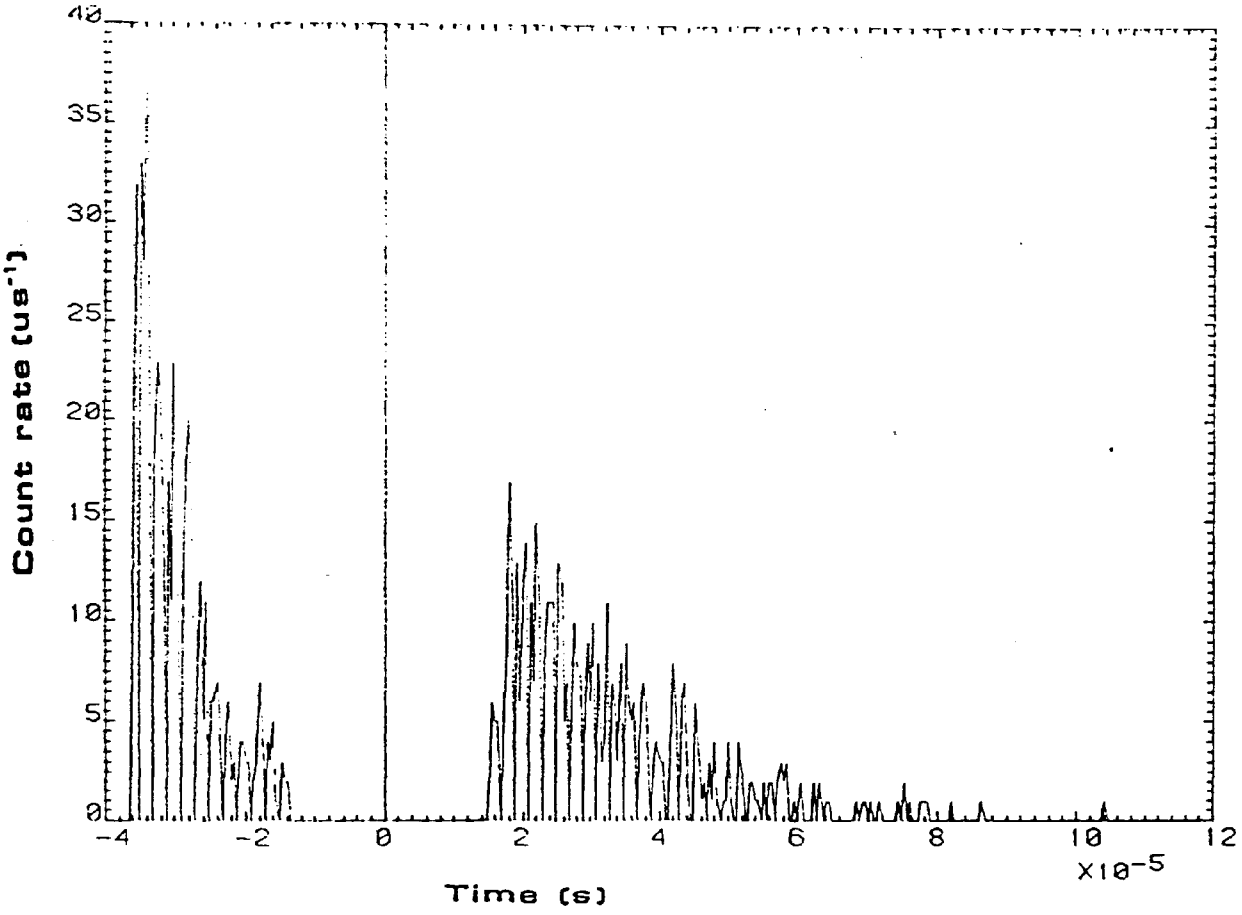

Fig. III.3.1 Ion ejection time plot for 1000 ions crossing the β_z = 1 boundary at time t = 0. The number of ions ejected in a given 10^{-6} s interval are plotted vertically, time (s) is plotted horizontally.

At time values preceding the voltage increment the ions recorded represent those ions whose amplitude in the z direction exceeded the trap dimension. The abundance of these ions will naturally depend upon the range of ion creation energy values permitted by the program, and the trapping efficiency (see section II.3). Ions which were ejected in the r direction are not shown here, since these would not be detected in the real Quistor.

Following an increment in the voltages, however, the intensity and distribution of ion ejection times will be representative of the intensity and shape of the ion output pulse which may be expected from the Quistor. The pulse rise time, pulse duration and height are items of particular interest.

4) Trapping efficiency plots.

The approach detailed above could be built up into a fairly rigorous method for investigation of Quistor performance on the basis of ion ejection pulse areas, and how these change as the RF and DC voltages are ramped. However the amount of computer runtime involved would be extremely large and so an alternate approach was developed.

The concept of trapping efficiency, defined as the ratio of ion velocity amplitude to ion position amplitude, has already been introduced.

If the Quistor has ions trapped in it at all amplitude values less than the trap dimensions, it follows that a reduction in trapping efficiency due to a voltage increment will result in those ions with large amplitudes being ejected from the trap and detected. If the ions become unstable, the trapping efficiency falls to zero and all ions are ejected.

We can make the assumption that all ion amplitudes are equally probable. This will not actually be the case but it is a convenient assumption to make in order to relate trapping efficiency with ion ejection output in a simple way.

If N_0 ions are trapped in the Quistor, and the trapping efficiency in the z direction drops from T_{z0} to T_{z1} upon a voltage increment, then the number of ions remaining in the

trap will fall from N_0 to

$$N = \frac{N_0 T_{z1}}{T_{z0}}. \qquad \text{(III.4.1)}$$

It follows that the number of ions ejected from the trap (a constant proportion of which will be detected) is given by

$$N_{ejected} = N_0 - N$$

$$= N_0 \frac{(T_{z0} - T_{z1})}{T_{z0}} \qquad \text{(III.4.2)}$$

If all ion creation velocities in x, y and z directions (up to a value greater than any which can be trapped) are assumed to be equally likely then the number of ions trapped as a proportion of those created is proportional to

$$N_0 = T_{r0}^2 T_{z0}. \qquad \text{(III.4.3)}$$

It must be stated that the above assumption is an over-simplification, but it is a convenient one to make and the result is still meaningful.

In this case the detected ion output is proportional to

$$N_{det} = T_{r0}^2 (T_{z0} - T_{z1}). \qquad \text{(III.4.4)}$$

It follows that a plot of trapping efficiency will be closely related to the number of ions which are stored in the trap and that the change in trapping efficiency from one point to another as the voltages are incremented is a good guide to the ion output which may be expected following a voltage increment. Naturally if the ions become unstable,

than the trapping efficiency falls to zero and all ions are ejected.

The main items of information which are of interest and relate to the Quistor's behaviour under a given set of conditions from these plots are as follows :

a) The maximum trapping efficiency in each direction, indicating the maximum possible sensitivity.

b) The locations of the $\beta = 0$ and $\beta = 1$ boundaries, indicating the ion storage resolution. This quantity is important to the way in which the Quistor is being operated for this project because it is desirable that only one, or at the most a few masses shall be stored in the Quistor at any one time.

c) The "sharpness" of the $\beta = 0$ and $\beta = 1$ boundaries, especially the $\beta_z = 1$ boundary which controls the ion ejection resolution. If this boundary is blurred, i.e. the trapping efficiency drops off gently as the boundary is approached, the result upon the Quistor in the mode of operation here employed, is a corresponding loss of both resolution and sensitivity. Consequently a lot a emphasis is placed upon this point.

d) The presence of any sharp "dips" in the trapping efficiency within the bounds of a supposedly stable region. These would indicate the presence of a so-called non-linear resonance line within the stability diagram. These result from the effect of non Quadrupolar electric field distortions within the Quistor and lead to unexpected ion ejection from the trap, giving poor (split) peak shapes and a loss of resolution and sensitivity.

The following diagram is the trapping efficiency plot for a perfect Quistor with a ratio of DC voltage to peak RF voltage of 0.095, which is found to be fairly close to the upper apex of the stability diagram. This ratio has been used for most of the plots which follow since changing it from one plot to another would be confusing. As the ratio increases, the $\beta_r = 0$ boundary will move to the right, while the $\beta_z = 1$ boundary moves to the left, in accordance with the shape of the stability diagram. The highest ratio of DC to peak RF voltage which has been found which still allows a stable region between the boundaries is about 0.0955.

What is plotted in this diagram is the product of T_z and T_r, the trapping efficiencies in each direction. They can also be plotted separately, of course. The peak RF voltage required per mass unit, V_1, is plotted along the horizontal axis. In each case, the frequency of RF selected has been 2 MHz, and the Quistor trap size, r_0, was 7.5 mm.

Since q_z is given by equation (I.2.7),

$$q_z = \frac{8eV}{m\omega^2 r_0^2}$$

(where e is the ion charge, V is the peak RF voltage applied to each electrode, m the ion mass, and r_0 is the Quistor dimension), it follows that the peak RF voltage per mass unit used here is related to the q_z value as :

$$q_z = 0.08683\ V_1 \qquad \text{(III.4.5)}$$

Also since, as stated, in most cases U = 0.095 V, and from equation (I.2.8);

$$a_z = \frac{16eU}{m\omega^2 r_0^2}$$

(where U is the DC bias applied to the end caps), it follows that the peak RF voltage V_1 as plotted is related to the a_z value as :

$$a_z = 0.01650\ V_1 . \qquad \text{(III.4.6)}$$

Thus V_1 = 9.00 V per mass unit corresponds to an a_z value of 0.1485, and a q_z value of 0.7815. This agrees with published stability diagrams as being approximately the location of the upper apex.

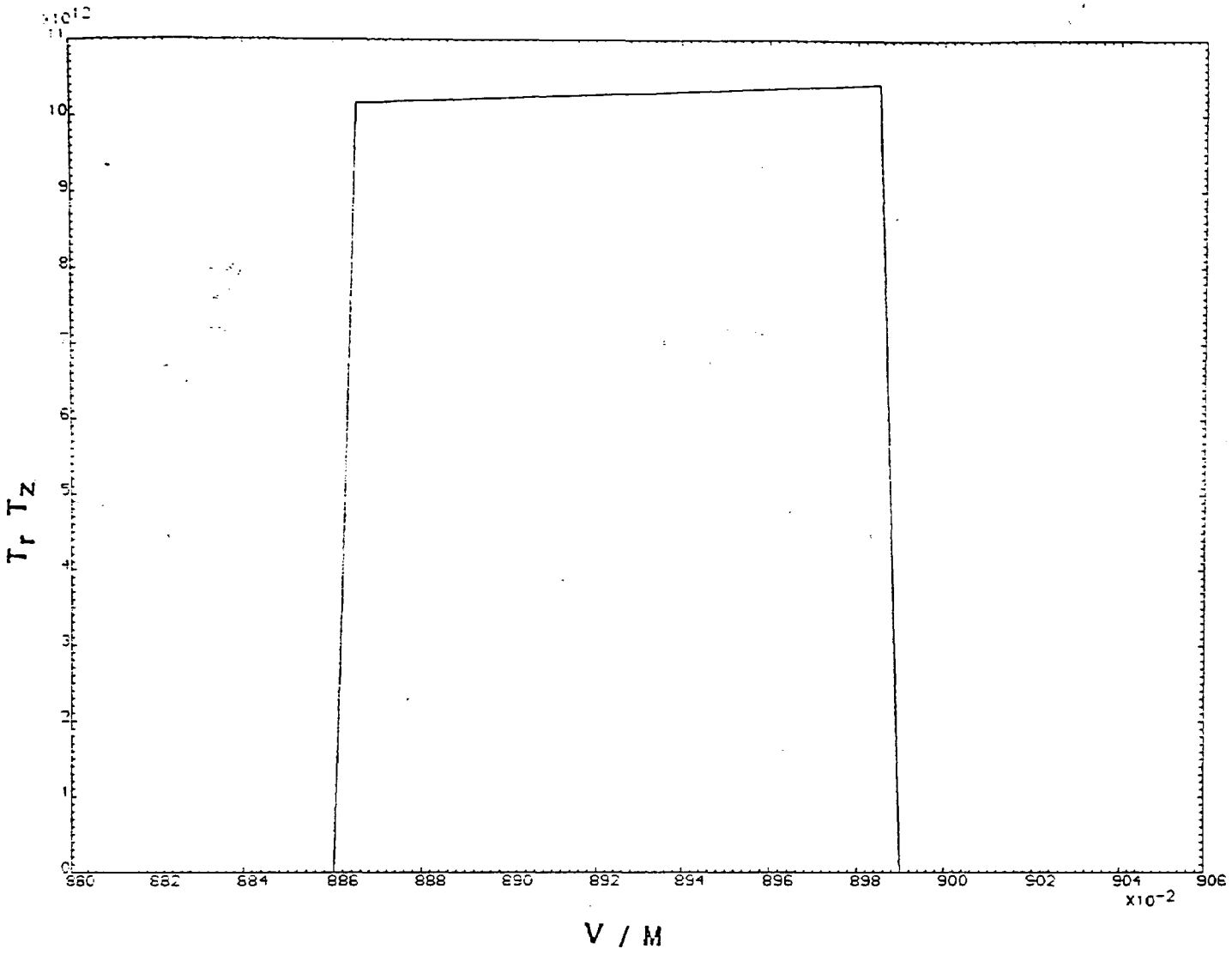

Fig. III.4.1 Plot of the product of the trapping efficiencies vs. peak RF voltage per mass unit, for an undistorted Quistor.

As can be seen, the plot is not far removed from the ideal expectation of what the plot should look like, that is to say, a rectangular box with vertical sides and a flat top. A plot like that would suggest infinite resolution at both boundaries, which is not quite the case.

The right hand ($\beta_z = 1$) boundary is located at $V_1 = 8.99$ V per mass unit, and the left hand ($\beta_r = 1$)

boundary is located at V_1 = 8.855 V / mass unit. When T_r and T_z are plotted separately (see below), we can see that (within the stable region), their values are roughly constant at about T_r = 2 x 10^6 and T_z = 5 x 10^6. (Both actually rise slightly with V_1) The product therefore is roughly constant at about $T_r T_z = 10^{13}$.

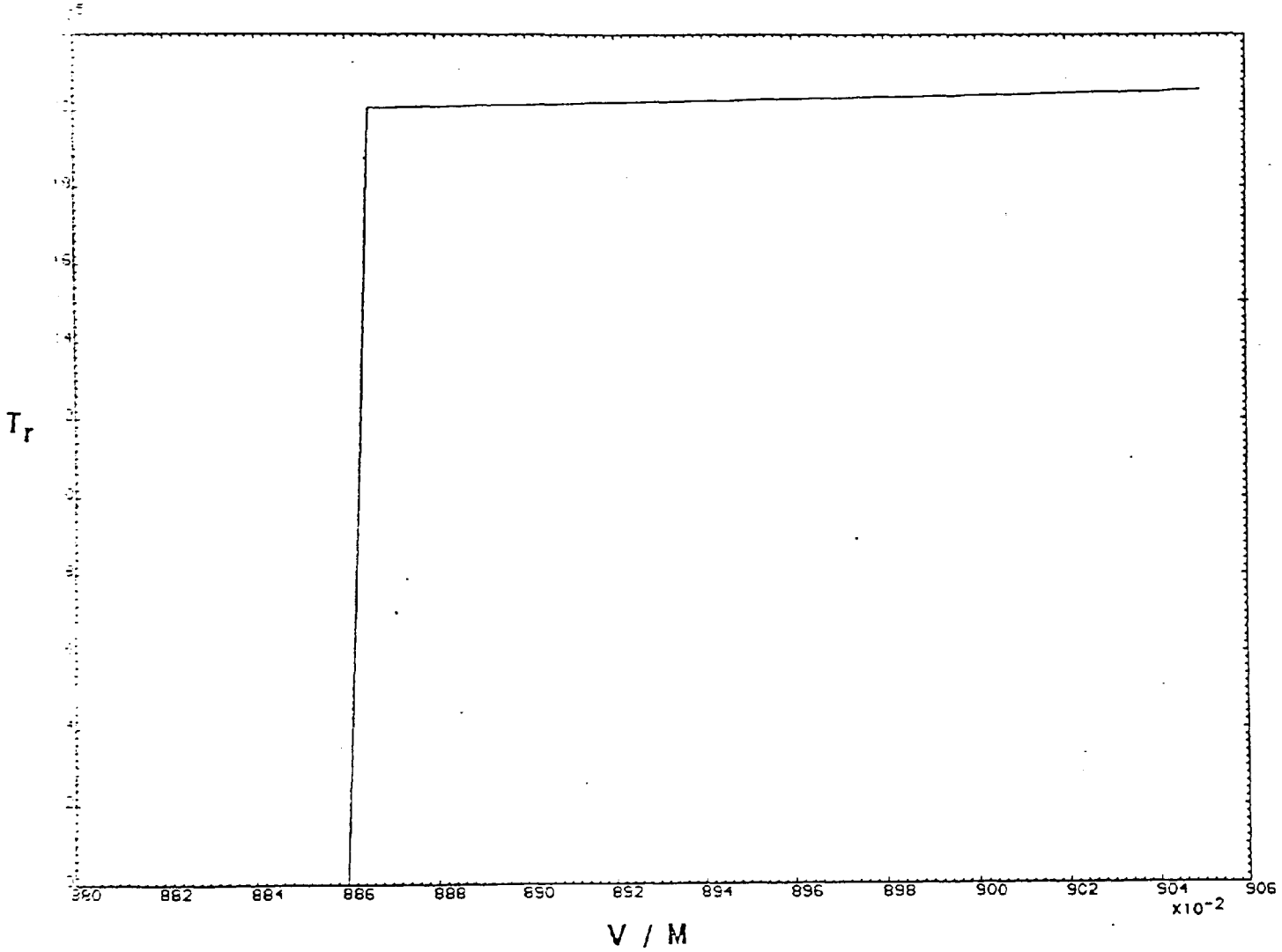

Fig. III.4.2 Plot of T_r vs. peak RF voltage per mass unit, for an undistorted Quistor.

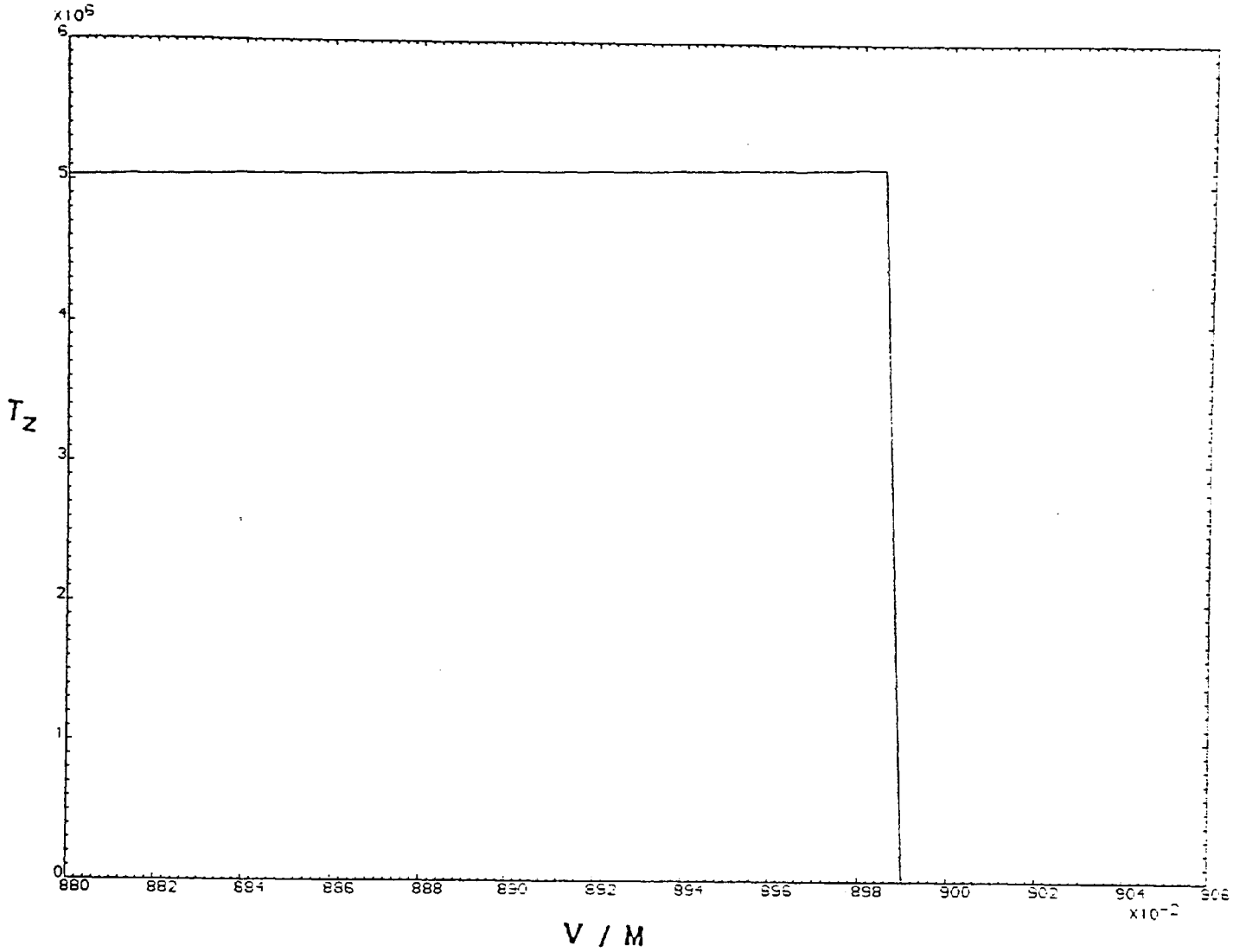

Fig. III.4.3 Plot of T_z vs. peak RF voltage per mass unit, for an undistorted Quistor.

The equation (III.4.4) derived above can be used to predict the ion output peak shape, resolution and intensity which can be expected from the Quistor. The values of trapping efficiency in each direction are known at each point on the plot, while the value of T_{z1}, the trapping efficiency at the RF voltage after an increment, is found by linear interpolation of the surrounding points.

Thus the peak shape and intensity can be found by plotting the value of (III.4.4) at all points. The user is

asked to enter the voltage increment value required. This is usually one part in 256, 512, 1024, 2048 or 4096 since the Quistor is inherently controlled by a binary D to A converter.

A sensible choice of step size is important for the Quistor's operation. A step size which is much smaller than the inherent resolution of the $\beta_z = 1$ boundary results in very poor sensitivity because (in terms of equation III.4.4) T_{z1} is not much smaller than T_{z0} and only a few ions are ejected. On the other hand, a step size which is much greater than the resolution of the boundary results in a spectrum which has a resolution limited by the step size.

This point is illustrated below by plotting the predicted peak shapes derived from the perfect Quistor trapping efficiency plot shown above, for some of the step sizes named.

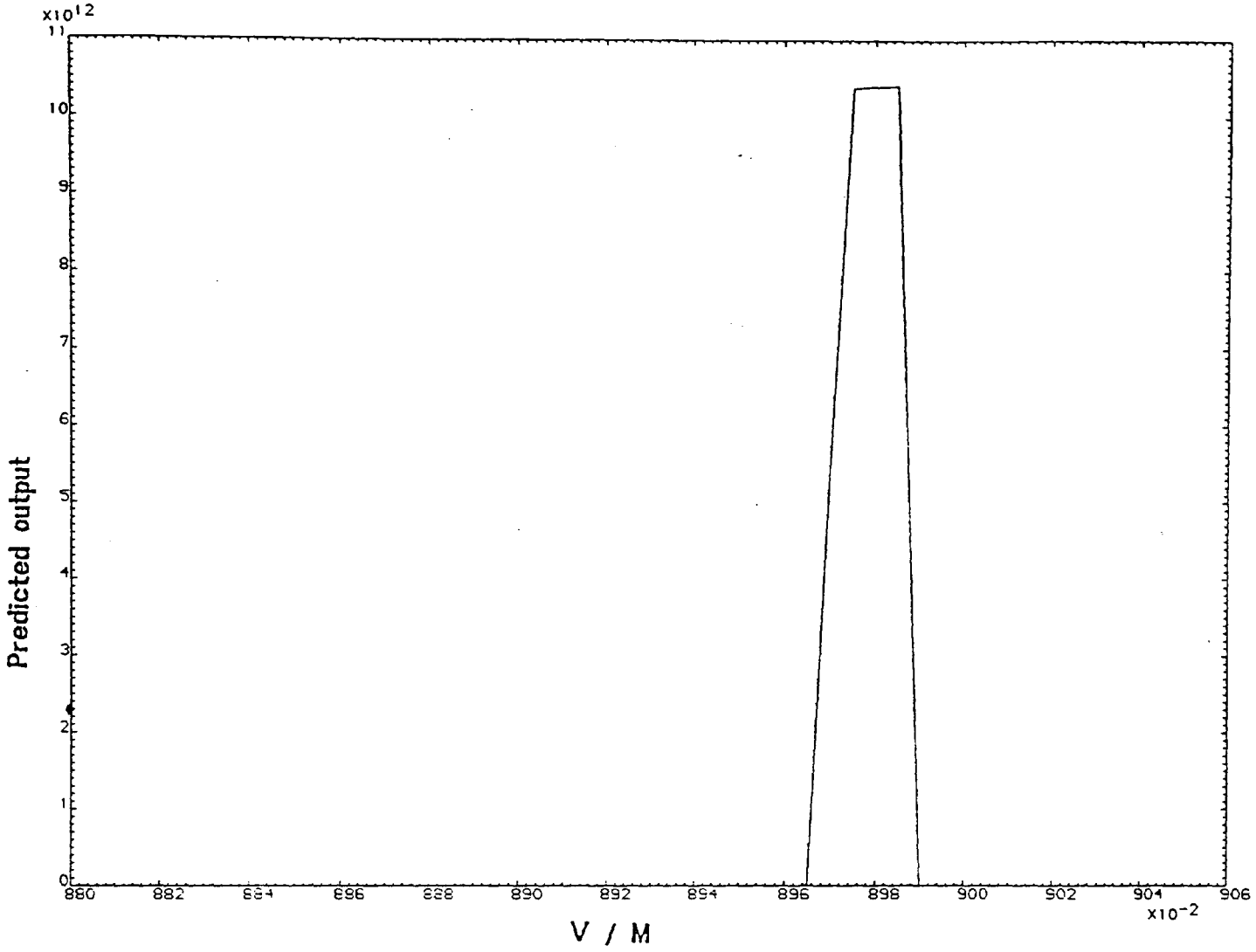

Fig. III.4.4 Plot of predicted peak shape vs. RF voltage per mass unit, for an undistorted Quistor with a step size of 1/512.

The resolution here is 375, much lower than the maximum which can be achieved from a perfect Quistor. The peak shape shows a flat top, indicating that any of the points in that region correspond to a jump from complete stability to instability.

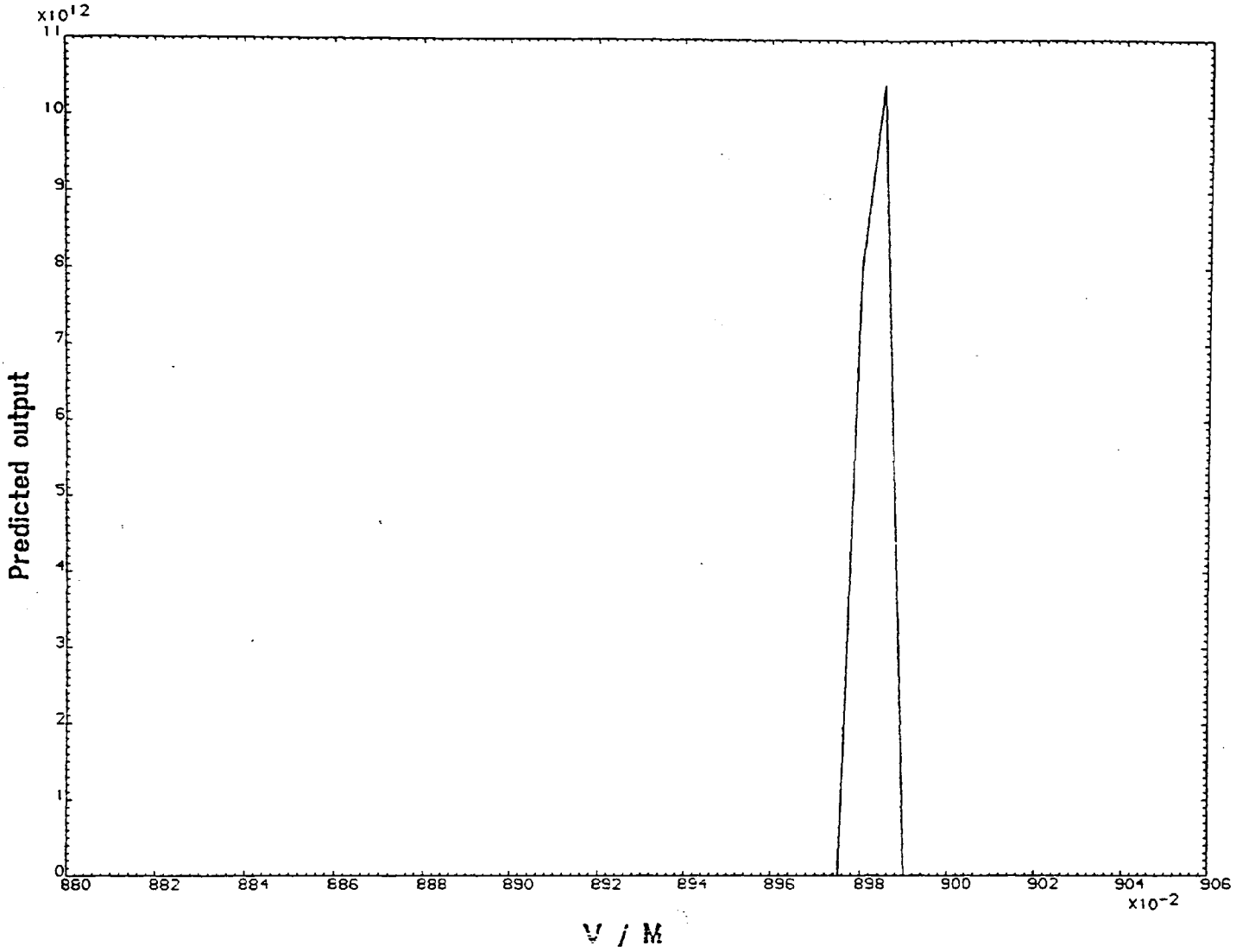

Fig. III.4.5 Plot of predicted peak shape vs. RF voltage per mass unit, for an undistorted Quistor with a step size of 1/1024.

The resolution here is 650. The peak shape no longer has a flat top, but the peak height is still the same as before.

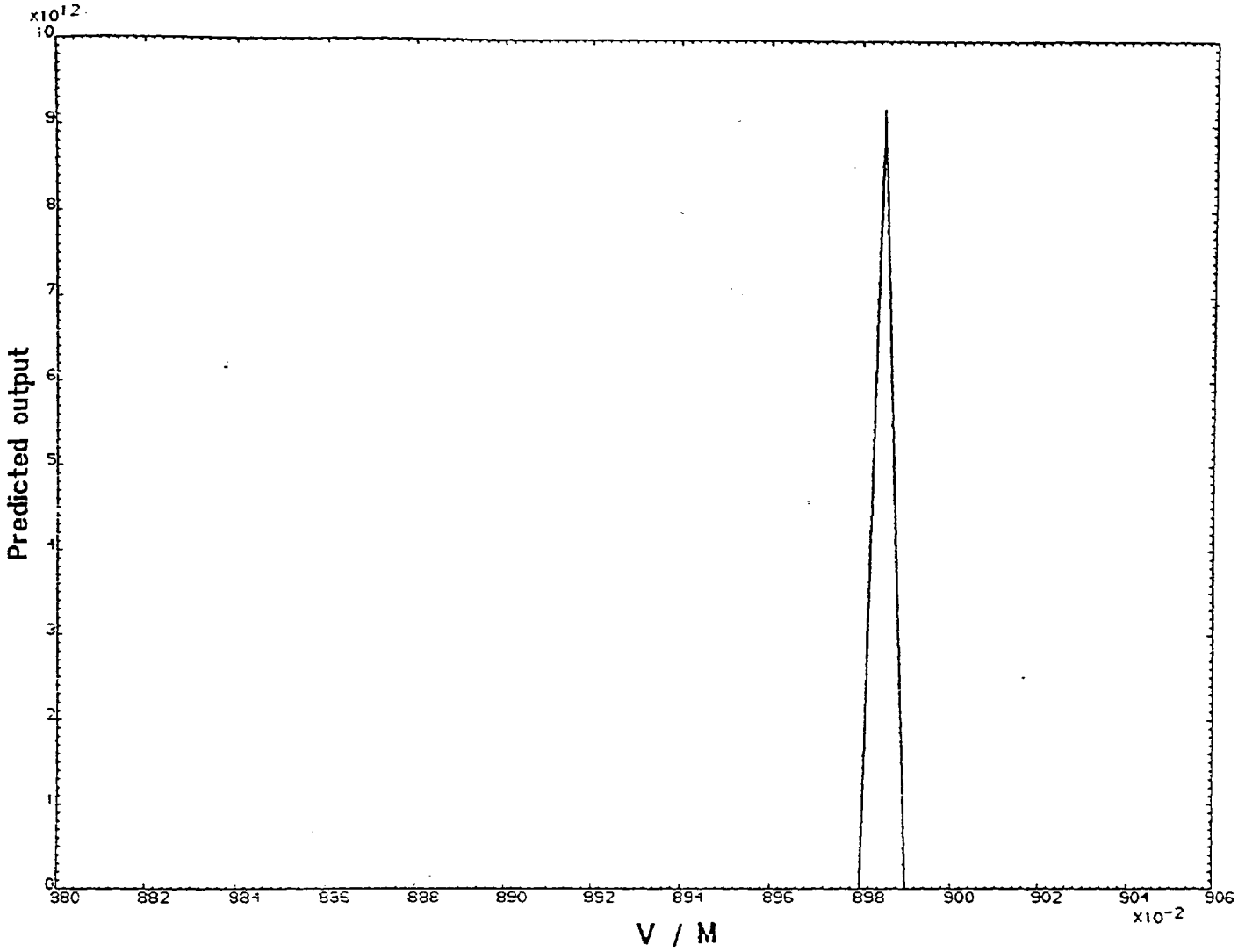

Fig. III.4.6 Plot of predicted peak shape vs. RF voltage per mass unit, for an undistorted Quistor with a step size of 1/2048.

The resolution is now about 800. The peak height has dropped slightly. (Note that since the number of points plotted is limited, the resolution may be higher than indicated. The fact that the peak height is still almost as great as before suggests that this is so, and that the resolution is more like 2000)

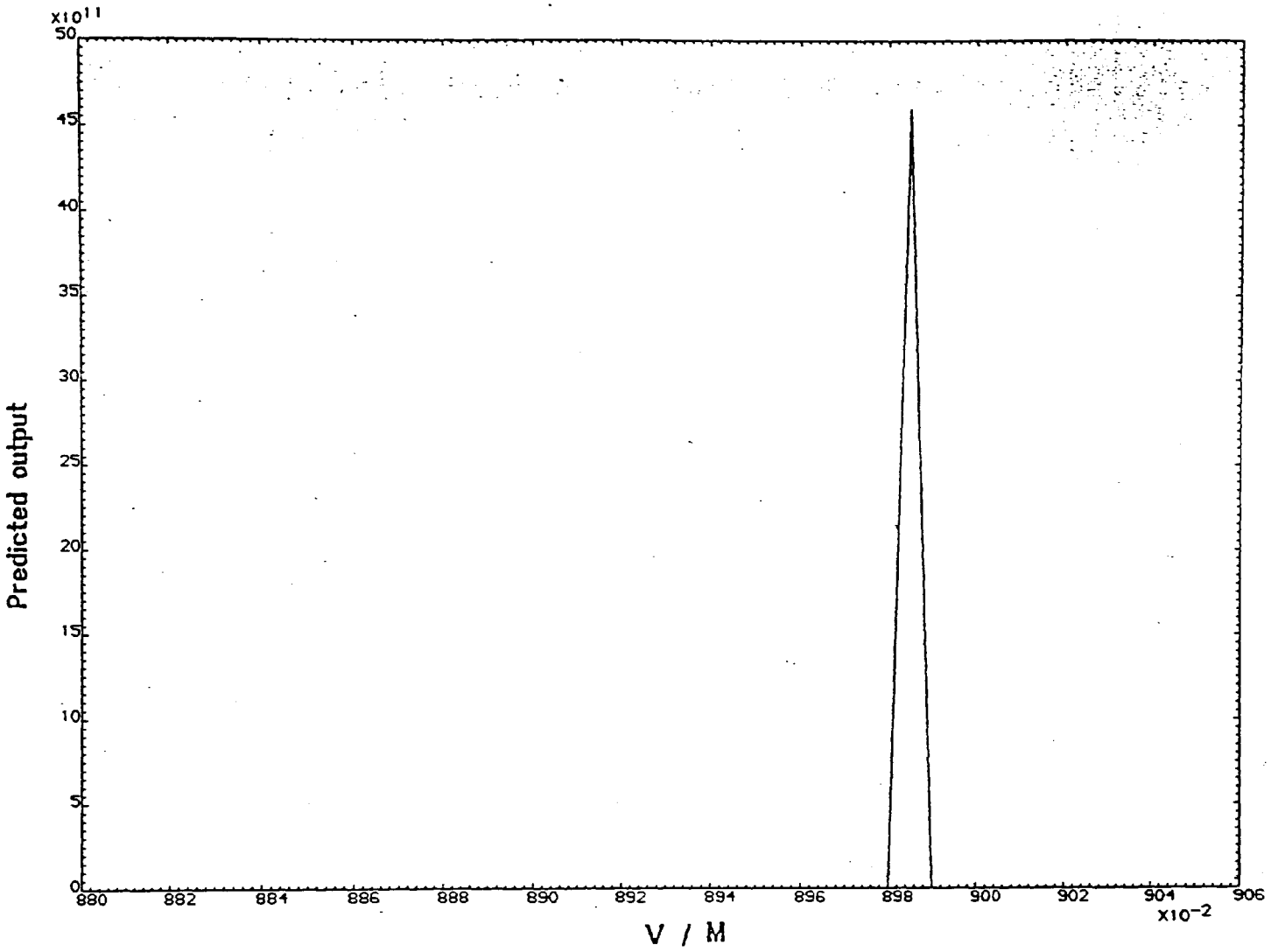

Fig. III.4.7 Plot of predicted peak shape vs. RF voltage per mass unit, for an undistorted Quistor with a step size of 1/4096.

This step size is too small since the peak height has clearly fallen to less than half its previous value. The resolution is still about the same as before, 850 (or 2000).

5) Trapping efficiency plotted across the entire stability diagram.

The simulation programs are able to plot the trapping efficiency at all points in a selected range across the stability diagram. This is essentially the same process as that described above for trapping efficiency plots along a selected scan line. However this approach supplies a more general overview of the Quistor's behaviour at all points on the stability diagram. However, due to limitations of program runtime, and data storage it is not practical to use this approach with the same level of detail and resolution.

The graphics plotting routine employed (combined with the limitation on the number of points plotted) to output the data has resulted in the appearance of a certain "fuzziness" around the edges of the stability diagram, which are, in fact, sharp.

Note that, as with the trapping efficiency plots, the product of the trapping efficiencies in each direction has generally been plotted. (Although they can be plotted separately, of course)

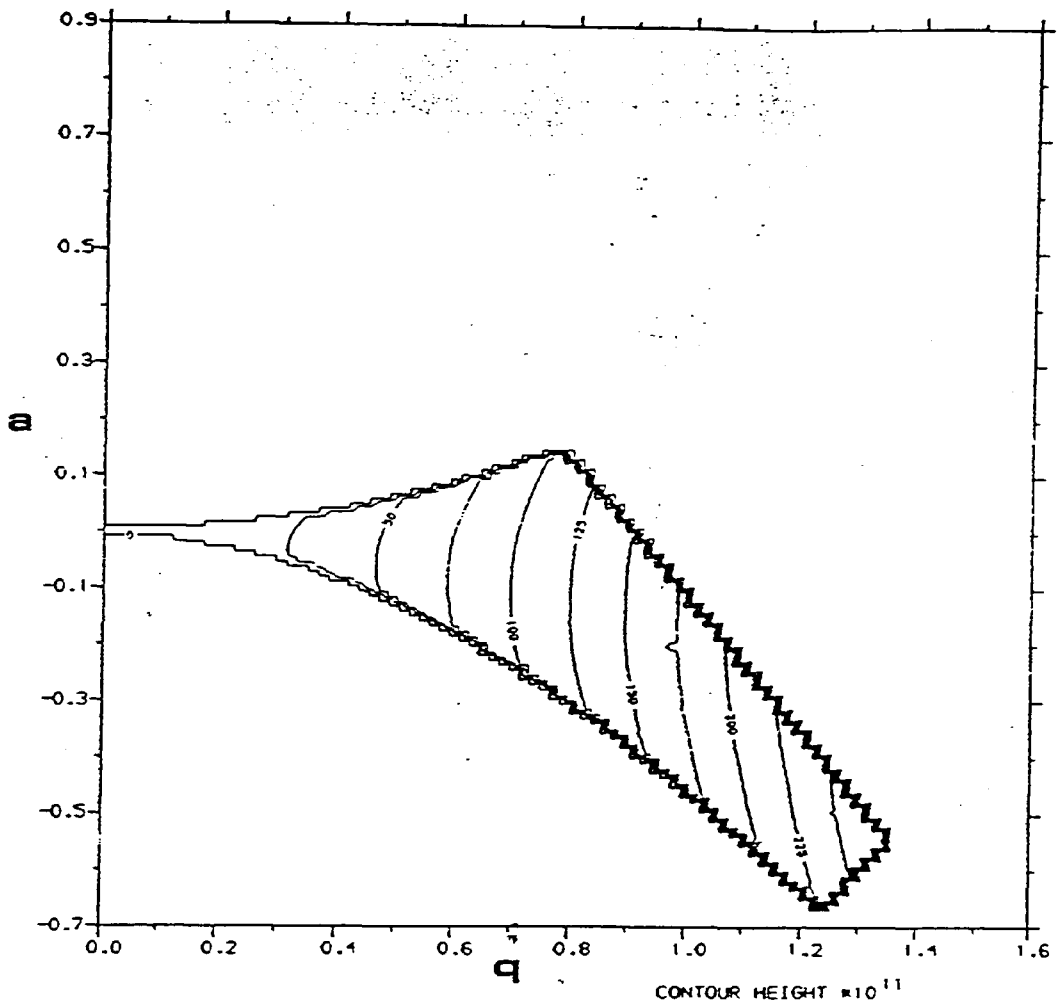

Fig. III.5.1 Normal Quistor stability diagram trapping efficiency plot.

6) Plots of ion amplitude against time.

As stated, the simulation program is able to plot the ion motion amplitude as a function of time. For example, this can clearly show the exponential increase in ion amplitude of a ion whose a and q values place it just to the right of $\beta_z = 1$ boundary.

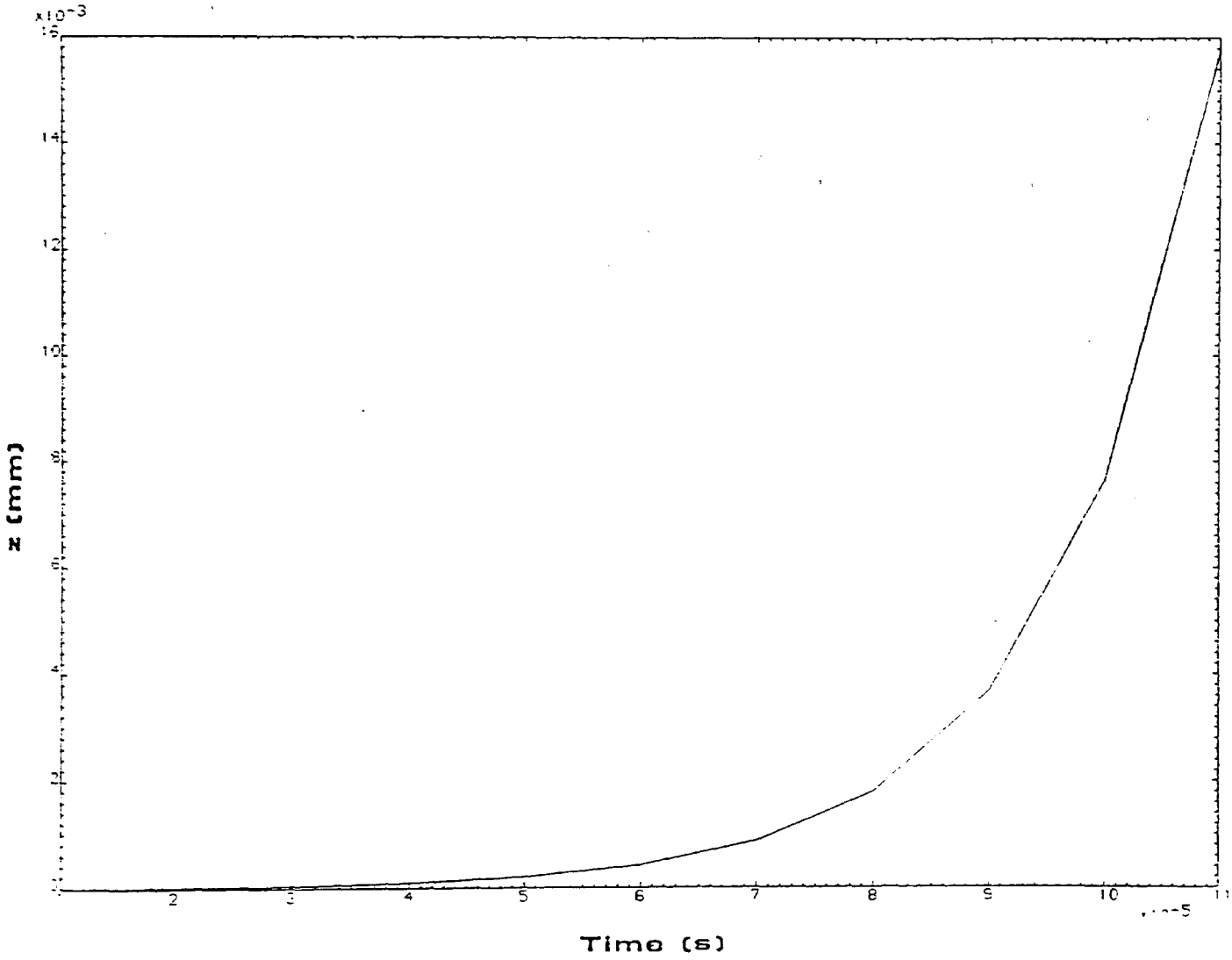

Fig. III.6.1 Amplitude of motion of an unstable ion

7) Results of the simulation programs.

a) The presence of a collision gas in the Quistor.

By considering the possibility of random (physical) collisions between an ion and a gas molecule the program is able to simulate the effects of the presence of a gas within the Quistor.

As has been previously discussed, one of the more probable results of this (unavoidable) process is to scatter the colliding ions which are lost from the trap because their new orbits are not confined to the trap. This is a detrimental effect because it reduces the sensitivity of the Quistor, limiting as it does the ion creation and storage time.

In addition this effect results in noise in the output because the scattered ions can be detected as noise.

On the other hand, it has been shown (Refs. 26, 97) that the presence of a high pressure of a light, non reactive, collision gas (Helium), can have the opposite effect on heavier stored ions. Since the helium atoms are light, the momentum change of the heavier ion upon a single collision is not so great that ion scattering is likely to take place. However, as a cumulative effect of many collisions, ions lose energy, gradually falling into orbits nearer to the centre of the trap. Finally the ions will have thermal energies only (say, 1/40 eV).

Hydrogen gas is not used for this purpose (in spite of its lighter mass) because it is reactive and is therefore much more likely to interact chemically with ions. In addition, of course, the hydrogen is likely to be much more corrosive to the filament, and the presence of large amounts of hydrogen

in the exhaust emissions from the vacuum system would be a safety hazard.

The reduced ion velocities mean that collisions between ions and other (non - helium) neutrals are much less frequent since (the mean free path being the same) the mean free time is proportionately increased. This permits longer ion creation and storage intervals and so a greater sensitivity and resolution can be achieved.

In addition since the ion orbits are confined to the centre, they remain well away from the Quistor electrodes. Where these electrodes have holes in them, leading to a localised distortion in the Quistor electric fields, this reduces the effect of that distortion upon the Quistor's resolution.

The collision probability per time step dt (10^{-8} s) is given by the collision frequency :

$$f = v\ n\ s,$$

where v is the velocity difference between the ion and the molecule, n the number of gas molecules per unit volume, and s the collision cross section. Thus the probability p is

$$p = v\ n\ s\ dt.$$

But

$$n = \frac{P}{kT}$$

where P is the gas pressure in Pascals, k the Boltzmann constant and T the absolute temperature (300K). The cross section s is assumed to be equal to 5.23×10^{-20} m^2, the

cross section of a helium atom. Thus

$$p = 12.6\ P\ v\ dt.$$

Converting this to mBars,

$$p = 1260\ P\ v\ dt. \qquad \text{(III.7.1)}$$

The ion velocity v'_{ion} after a "direct hit" collision with a molecule (assuming the collision is elastic) is given by :

$$v'_{ion} = v_{ion} + 2M_{gas}\ \frac{(v_{gas} - v_{ion})}{M_{gas} + M_{ion}} \qquad \text{(III.7.2)}$$

where v_{ion} is the ion velocity before collision, v_{gas} is the molecule velocity before collision and M_{ion} and M_{gas} are the ion and molecule masses respectively.

The program allows for a random variation in the velocity of the colliding molecule, up to a maximum limit (positive or negative) set by the user, in order to mimic the random behaviour of a real gas. It is assumed that all molecule velocities are equally probable, up to that limit. A more rigorous approach would have assumed a Maxwell - Boltzmann distribution of velocities, which would tend to make low velocity molecules proportionately more probable, but that is getting too complicated.

The program further assumes that if a collision takes place, it may not be a "direct hit". A random fraction between 0 and 1 of the maximum possible momentum is transferred between ion and molecule.

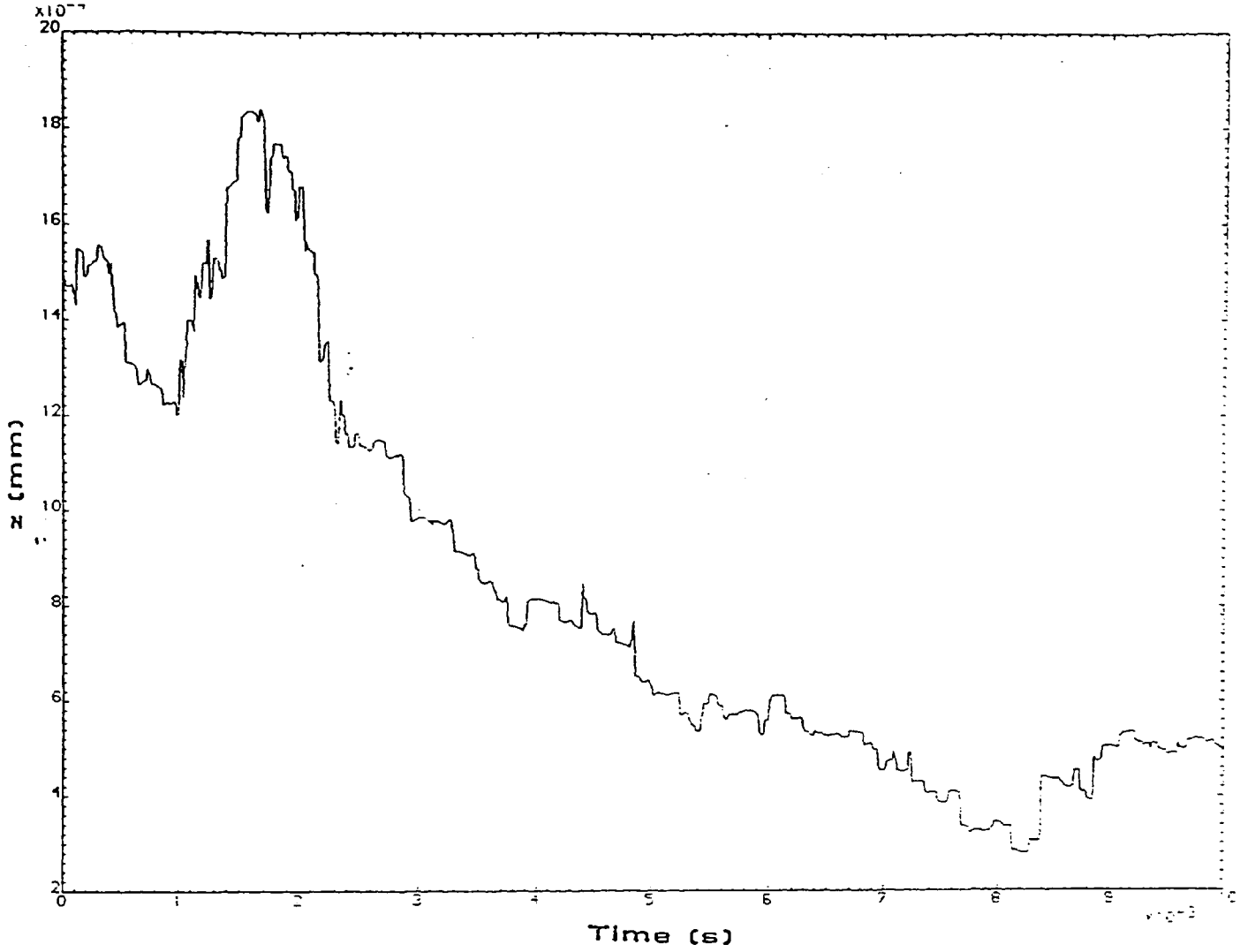

Fig. III.7.1 The variation in ion amplitude with time at 10^{-2} mBar of Helium.

The above plot is shows the way in which the ion amplitude in the z direction falls with time due to collisions with helium. It is produced assuming that that the ions have an initial velocity of 1000 ms^{-1} at the origin, and that the gas molecules have a maximum velocity of 2361 ms^{-1} (which corresponds to a temperature of 300 K for molecules of 4 AMU). The ion was assumed to have a mass of 400, while the gas molecules, a mass of 4.

As can be seen, it is quite possible for an ion - Helium

neutral collision to increase the ion amplitude - in which case, if the amplitude is already large, the ion may easily be lost from the trap. However, the overall trend of the amplitude is clearly downward.

The amount of the velocity change due to each collision depends upon the ratio of ion mass to molecule mass (see III.4.8), and so if the masses are roughly the same, large jumps in amplitude can be expected. This means that the probability is very high that the ion will be lost from the trap upon a collision which happens to increase the amplitude.

Using a light collision gas (Helium), however, means that each individual collision does not result in a big amplitude change so the ion is likely to remain trapped. On the other hand, however, a large number of collisions are required to have an appreciable effect, so that a high gas pressure is needed.

It must be noted that this effect does not necessarily increase the trapping efficiency, as defined, because the initial amplitude of the ions is the same as it would be without gas present. Consequently the trapping ability (maximum number of ions trapped) is about the same. It is simply that the ions have lower energies and amplitudes once they have been trapped for some time.

b) Square wave excitation as an alternative to sine wave.

It has been suggested (Ref. 67, 88) that square, or rectangular wave RF voltages applied to the Quistor would operate effectively as an alternative to the more usual sine wave RF.

This possibility has been allowed for within the simulation programs. It is known that the stability diagram for the Quistor under the influence of rectangular excitation has a somewhat different shape; although it is broadly similar.

The voltage applied to the end cap electrodes according to the definition chosen is given by :

$$V_{ec} = U_0 + V_0 \, \mathrm{squ}\,(\omega t)$$

where the function squ (ωt) has the values

$+2\,(1 - m)$, for $0 <= \omega t < 2\pi m$ and
$-2m$, for $2\pi m <= \omega t < 2\pi$,

where m:(1 - m) is the mark : space ratio. Defining the voltage in this way means that there is no average DC value associated with the RF component of the field, and also the peak to peak value of the RF is equal to $2\,V_0$, as for a normal sine wave.

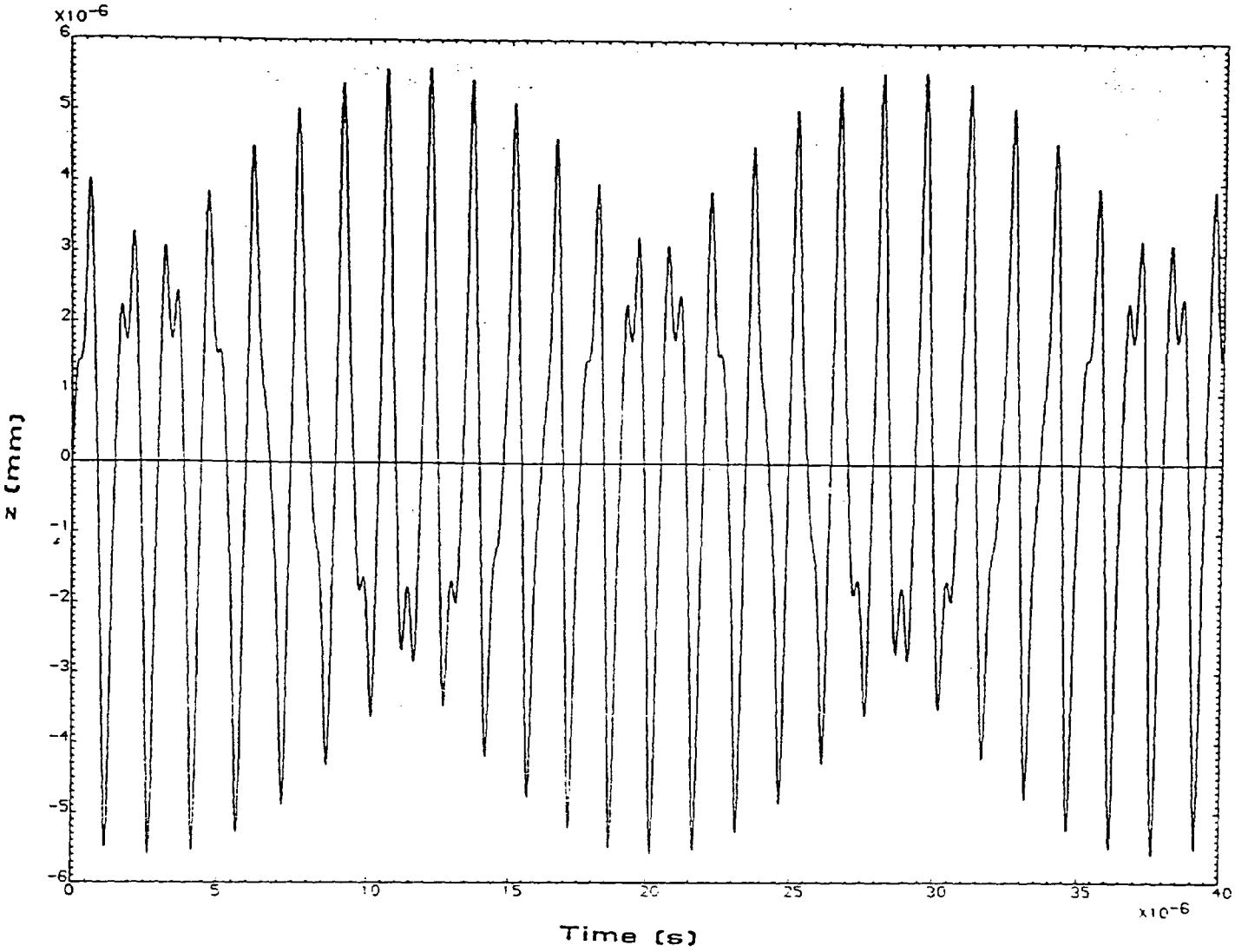

Fig. III.7.2 Motion of an ion in the z direction, vs. time, under the influence of square wave RF voltages in the Quistor.

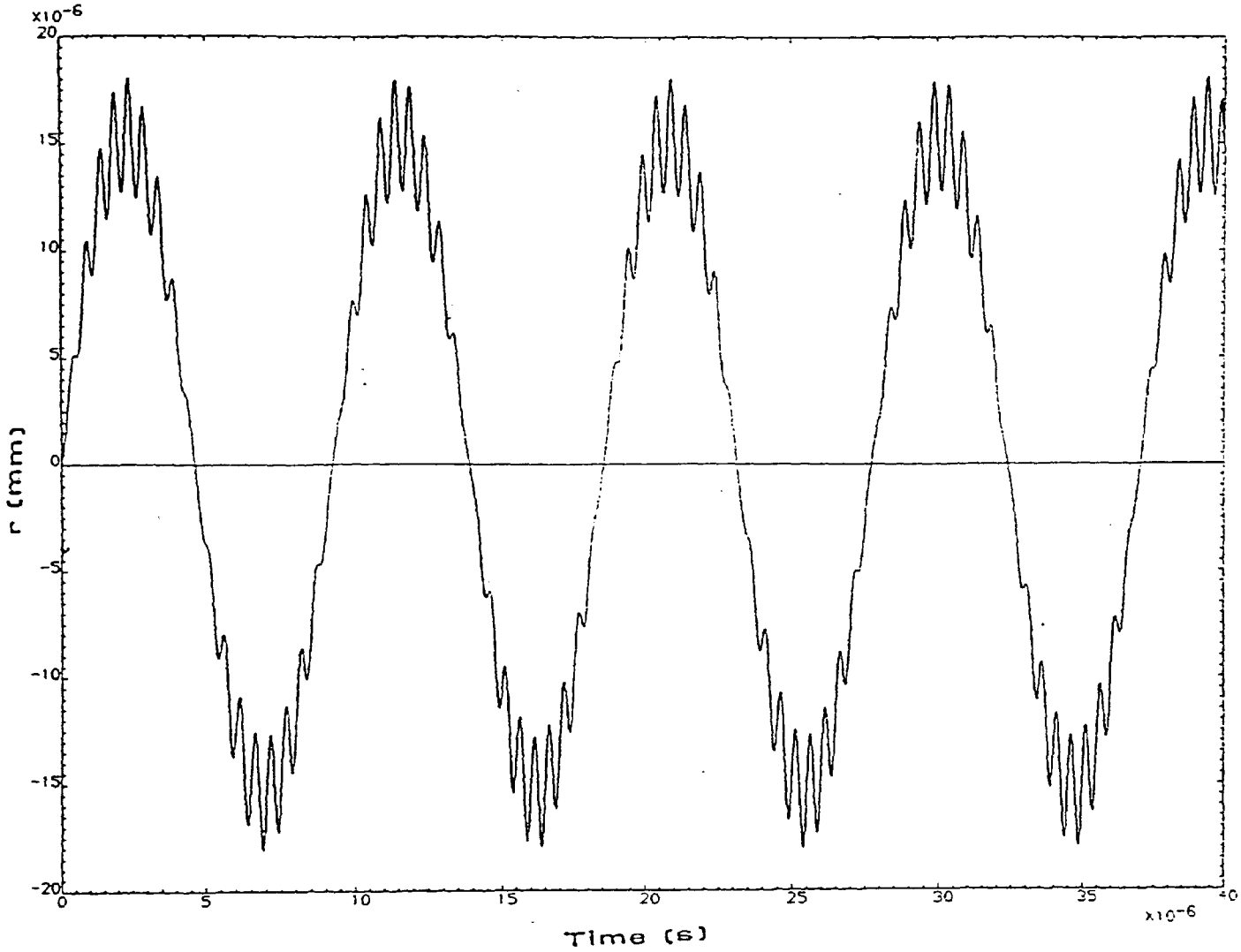

Fig. III.7.3 Motion of an ion in the r direction, vs. time, under the influence of square wave RF voltages in the Quistor.

The appearance of the motion is rather different from that for sine wave RF. Nonetheless ion trapping is clearly demonstrated.

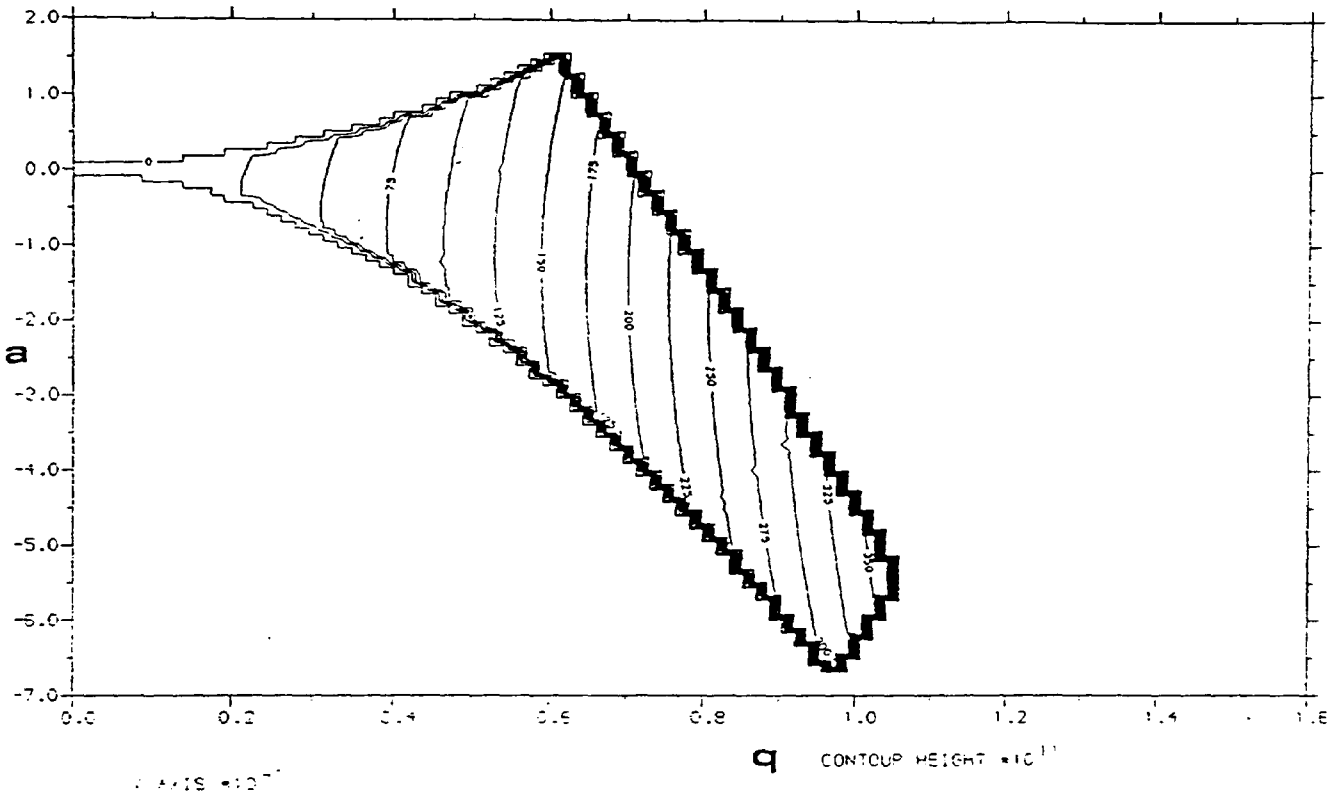

Fig. III.7.4 Quistor stability diagram with square wave RF. The mark : space ratio is 1:1.

The appearance of this stability diagram is very similar to that for sine wave RF voltages. The shape is slightly different however, it appears as if the square wave RF voltage required to produce a given q value is slightly lower. This might be because the mean voltage (disregarding sign) is greater for square waves than for sine waves.

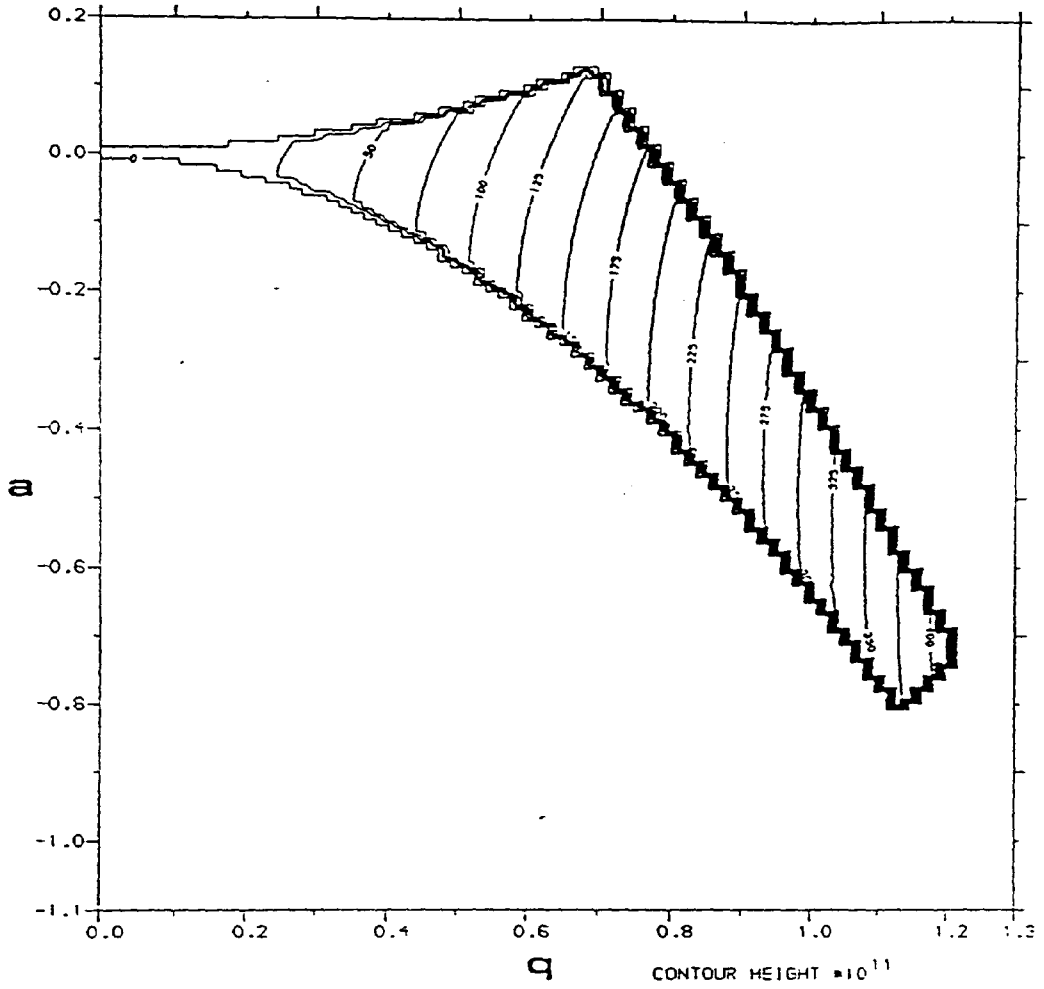

Fig. III.7.5 Quistor stability diagram with square wave RF. The mark : space ratio is 3:7.

If there were interest in it, the simulation program could be modified so as to consider the consequences of other waveforms than square and sine. It seems likely that these could also be used for ion trapping, and would also have sharp-edged stability diagrams.

The practical value of the use of square wave RF voltages, or any other waveform than sine, may be limited since these voltages cannot easily be passed through a step - up transformer. Generation of square waves of up to about

450 V pk-pk by the use of a transistor circuit is a straightforward matter, but suitable transistors with higher voltage ratings than this, combined with the required high speed ability required, are not available. In any case the pickup problems associated with square wave RF voltages of this magnitude (and especially the inherent harmonics), are likely to be severe. It has also not been shown that there is any advantage to be gained in using non - sinusoidal waveforms.

c) The effect of an axial magnetic field upon the Quistor.

The algorithm which calculates the motion of ions in two dimensions (r and z), was modified so that all three dimensions (x, y and z), could be considered. In normal operation, y = 0 and r = x. However when an axial magnetic field is applied to the Quistor, the motion becomes a little more complex in accordance with Maxwell's equations :

$$ma_x = -q\,(E_x + B_z v_y)$$

$$ma_y = -q\,(E_y - B_z v_x)$$

where m is the ion mass, q the ion charge, a_x and a_y are the accelerations in each direction, B_z is the axial magnetic field and v_x and v_y are the velocities in each direction. E_x and E_y are the electric field components in each direction, given by :

$$E_x = \frac{E_r x}{r}$$

and

$$E_y = \frac{E_r y}{r}.$$

It was chosen to produce output data on the basis of a magnetic field whose value was always proportional to the RF voltage applied to the end caps (in a similar way to the DC offset voltage applied). This means that the forces acting will always in in proportion to each other. It was also felt that the whole stability diagram trapping efficiency plots were the right form of approach to investigate the effect of magnetic fields upon the Quistor.

Firstly, an example of the ion motion which takes place has been included. As can be seen, it appears to be even more complex than before.

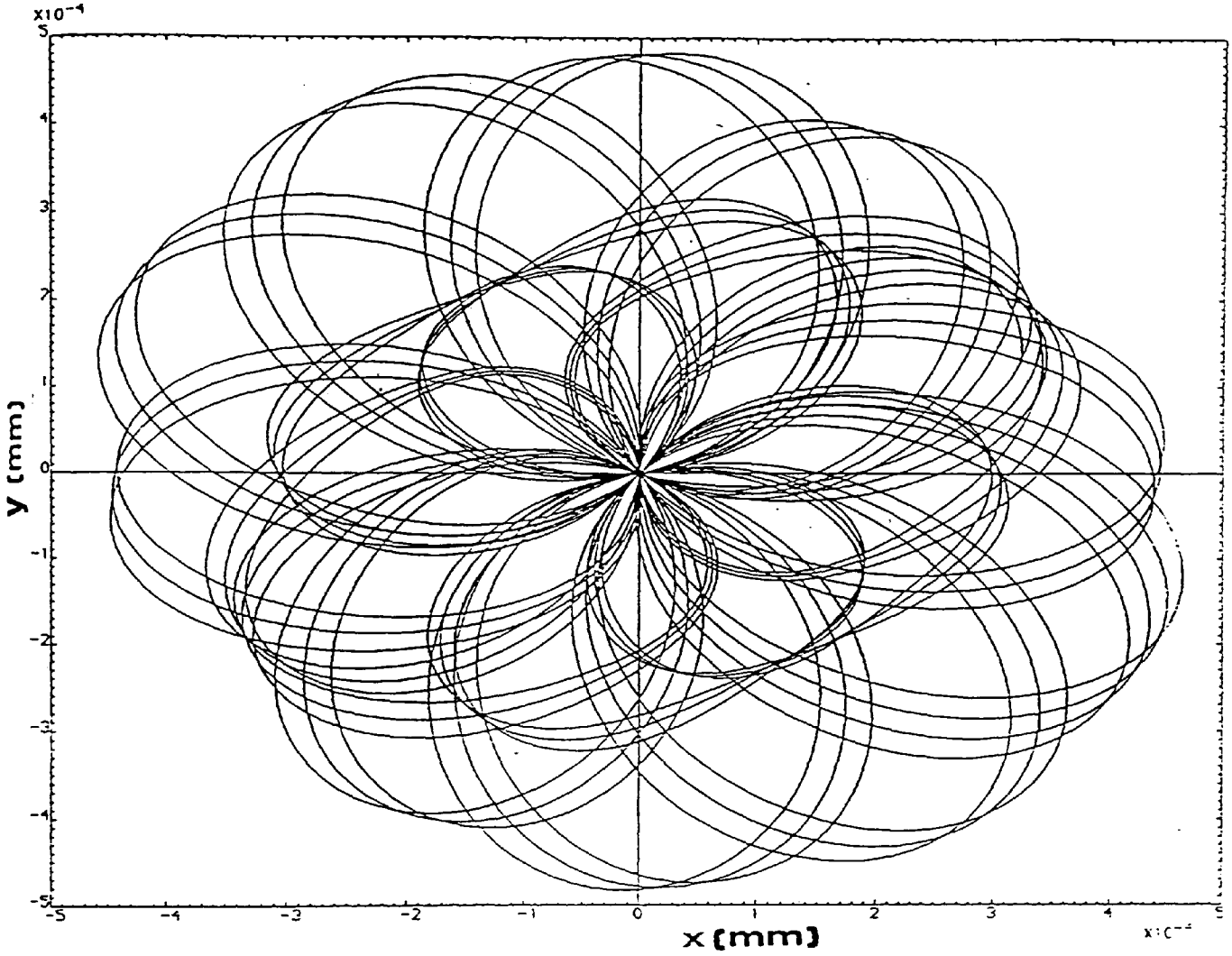

Fig. III.7.6 Plot of ion motion near to the upper apex of the stability diagram with a magnetic field / RF voltage ratio of 0.01. X is plotted horizontally, y vertically.

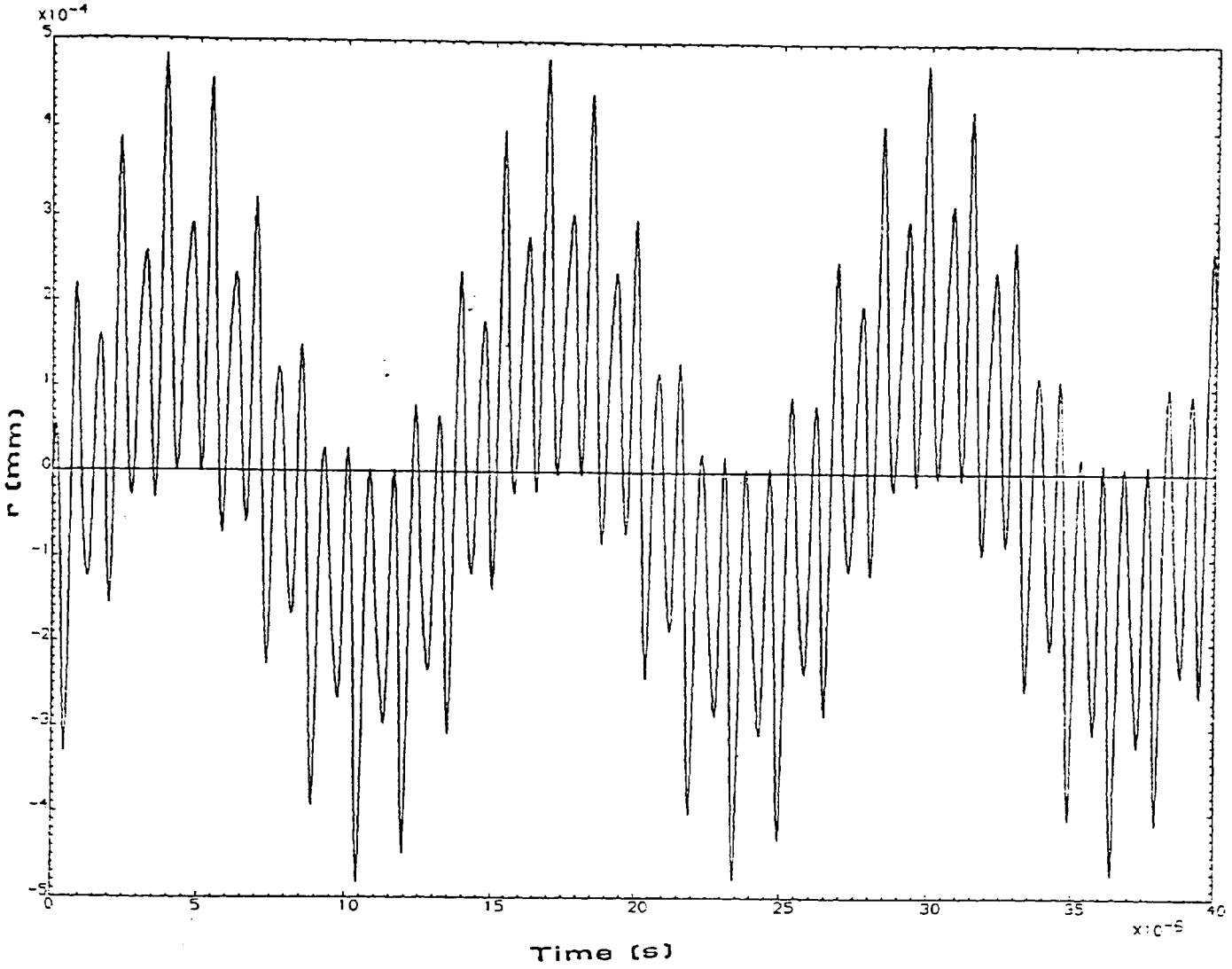

Fig. III.7.7 Plot of ion motion near to the upper apex of the stability diagram with a magnetic field / RF voltage ratio of 0.01. Time is plotted horizontally, r vertically.

The ion motion in the z direction is identical to that without a magnetic field applied, since there are no magnetic force components in that direction. It follows that the stability diagram for the the z direction is the same as that for a normal Quistor. The program was set up so as to calculate motion in the r direction only, relying upon data calculated for a normal Quistor for the z direction.

Stability diagrams for the Quistor with a number of different magnetic field strengths follow. Note that the axes are indicated in terms of a and q.

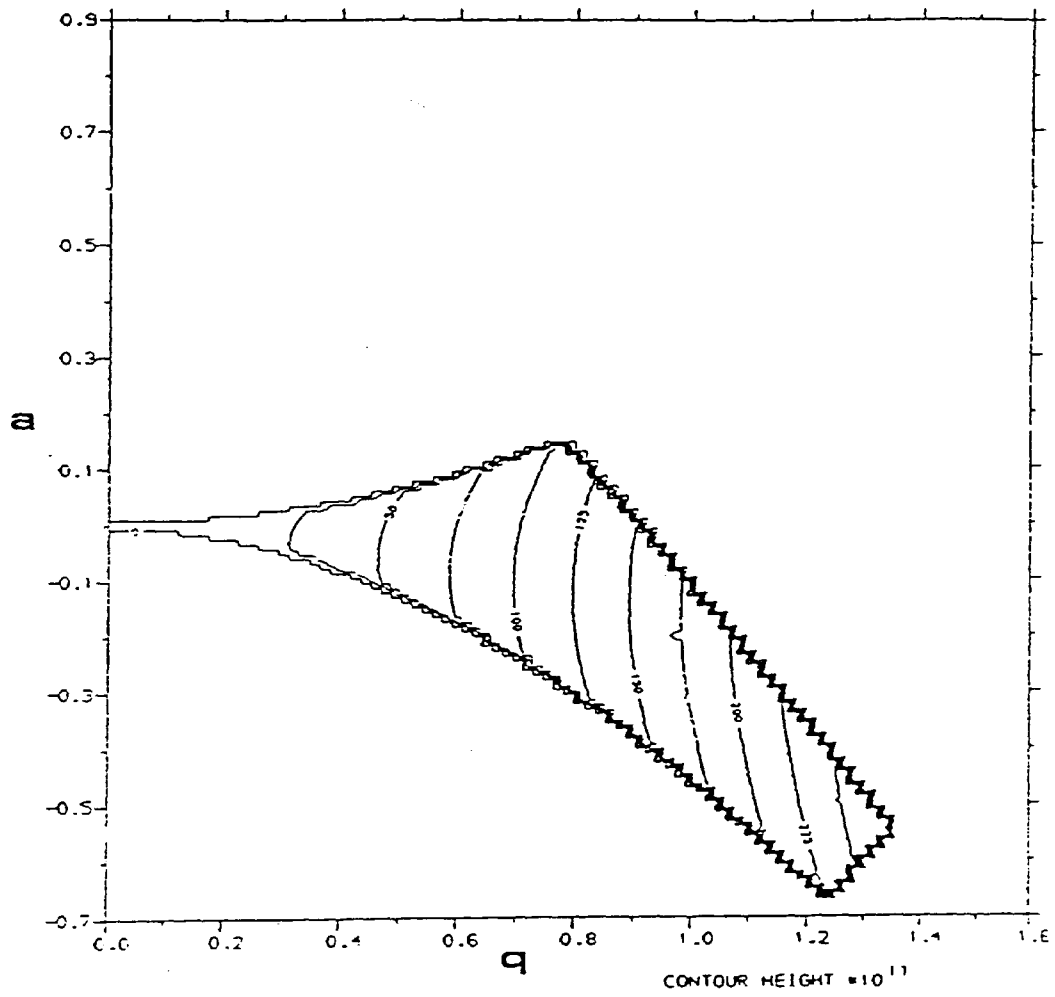

Fig. III.7.8 Normal Quistor stability diagram without magnetic field.

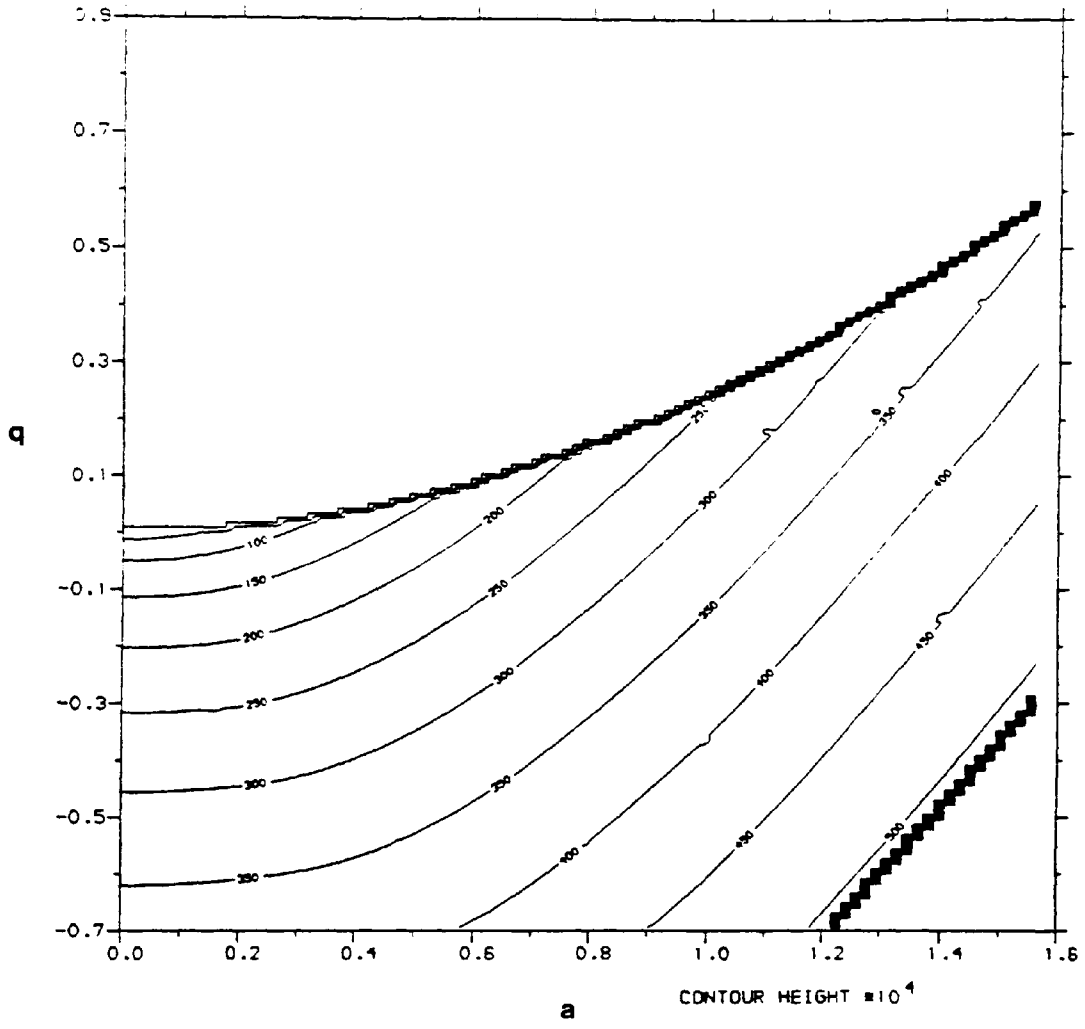

Fig. III.7.9 Trapping efficiency plot for motion in the r direction for a normal Quistor.

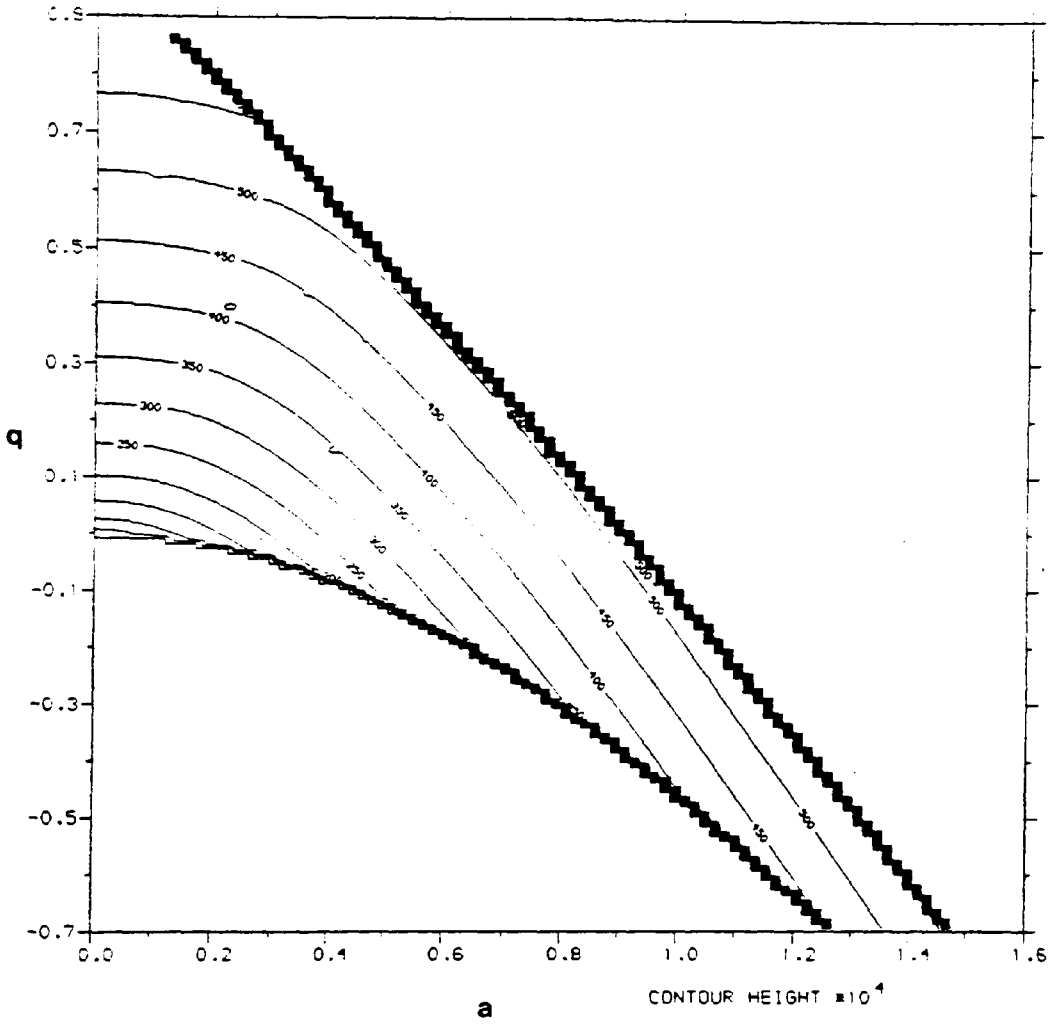

Fig. III.7.10 Trapping efficiency plot for motion in the z direction for a normal Quistor.

It is clear that the trapping efficiency values depend upon two things; the values increase with the voltage which is used for trapping, but also, they increase with the β values.

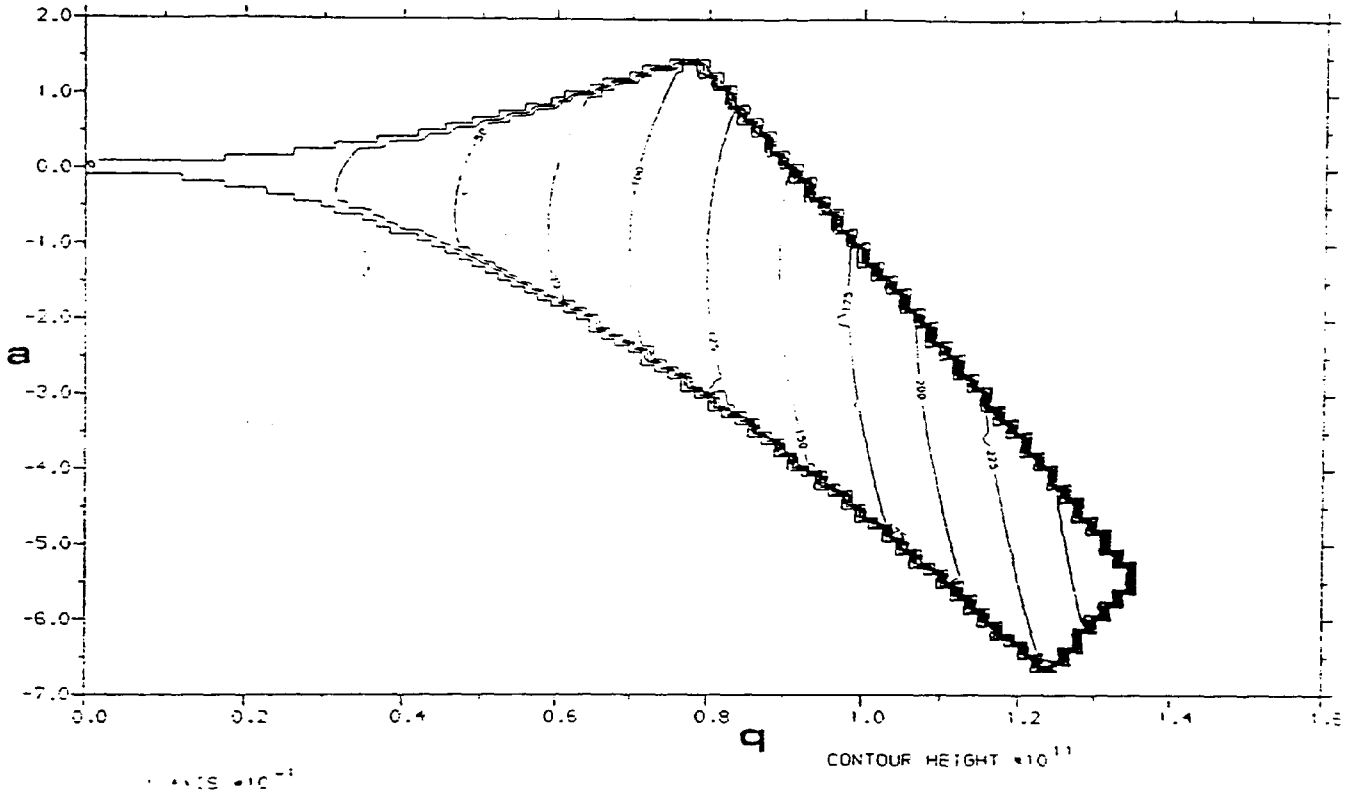

Fig. III.7.11 Stability diagram with a magnetic field ratio of 0.001.

This stability diagram is almost indistinguishable from that of a normal Quistor. (Other than the difference in plot scales)

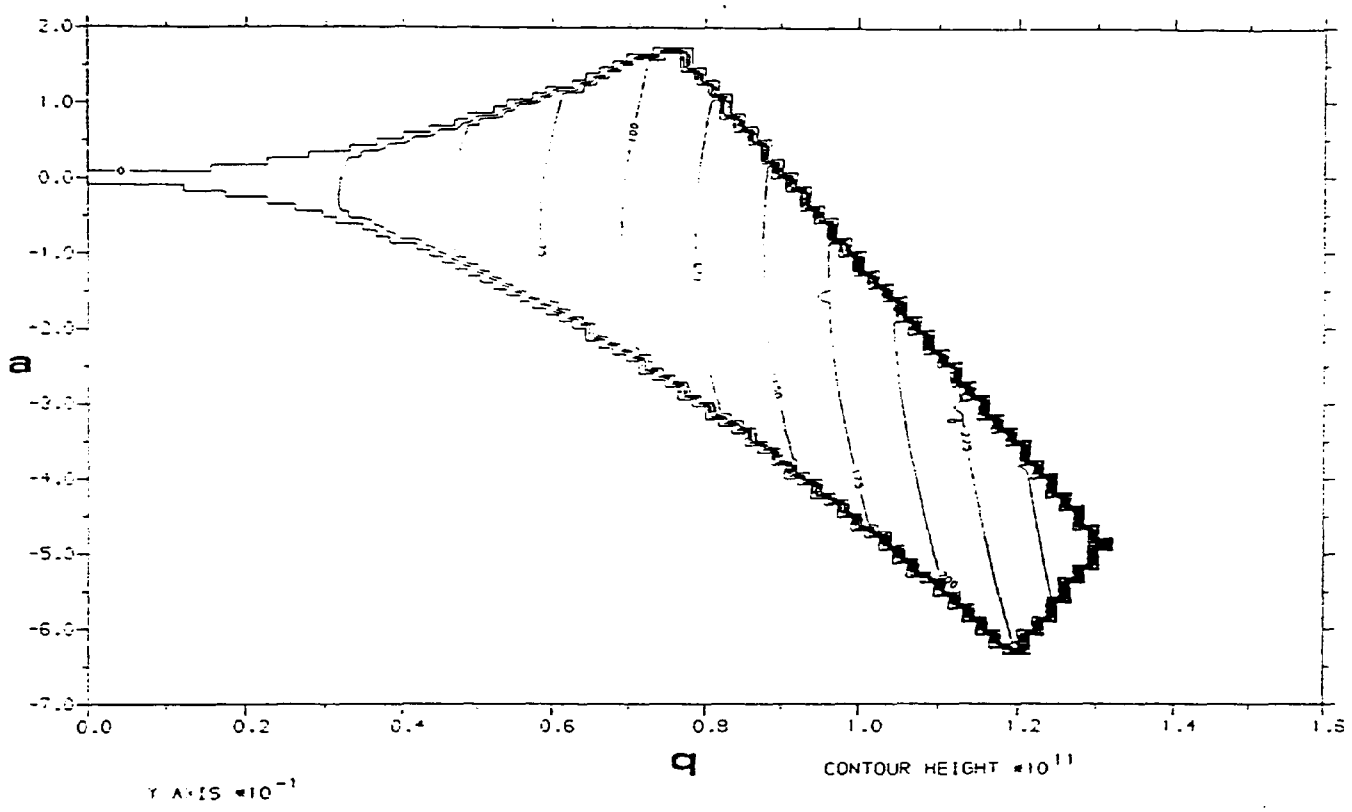

Fig. III.7.12 Stability diagram with a magnetic field ratio of 0.002.

Now on close inspection, some differences are seen. The $\beta_r = 0$ boundary rises a little more steeply, so that a higher ratio of a to q would be required to locate the upper apex of the stability diagram. The $\beta_r = 1$ boundary is somewhat closer to the origin, so that a less negative ratio of a to q would be required in order to locate the lower apex of the stability diagram.

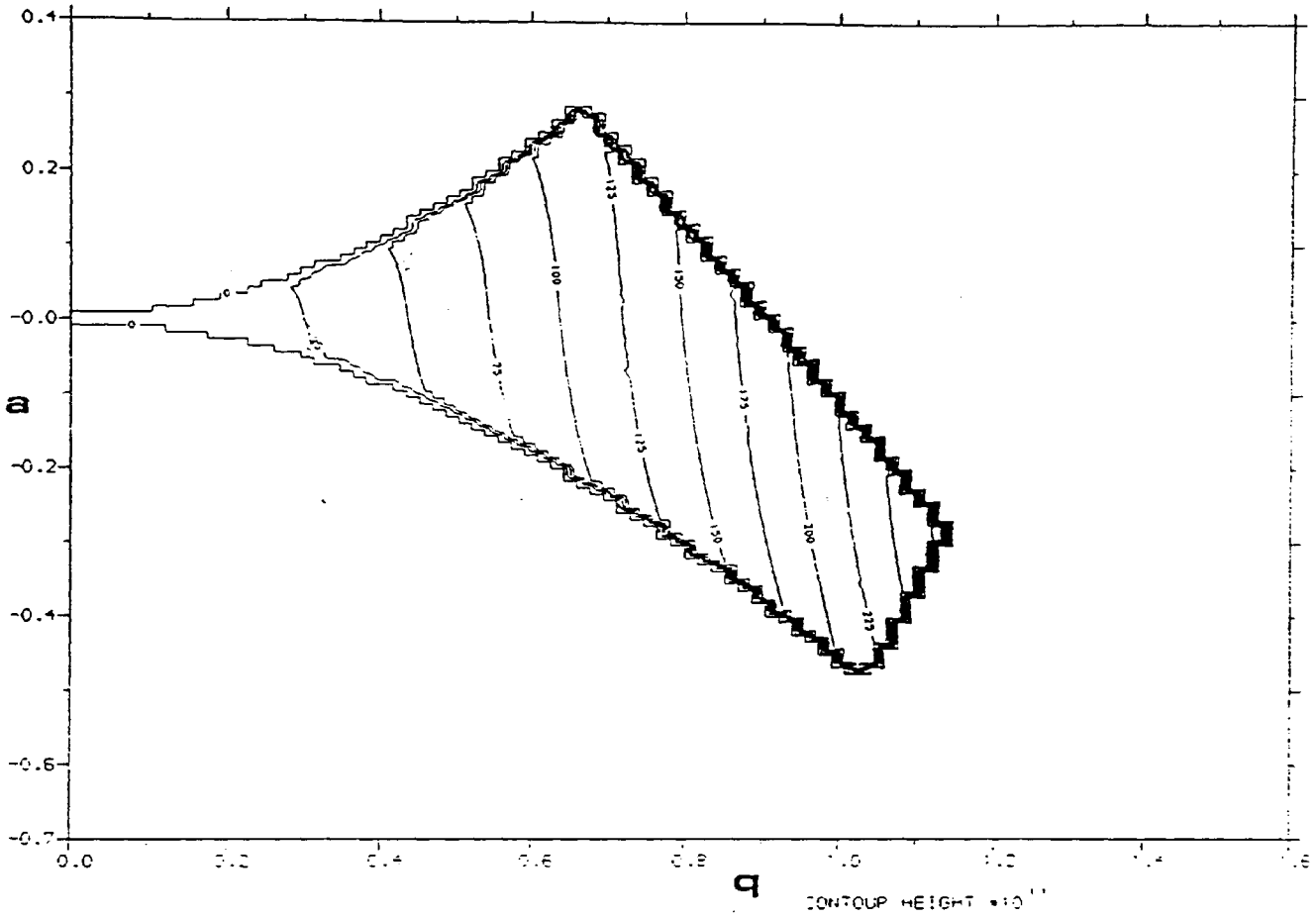

Fig. III.7.13 Stability diagram with a magnetic field ratio of 0.005.

The process described above has continued and become very noticeable. Crucially, however, it is clear that the stability diagram boundaries are remaining sharp so that there has not been a reduction in resolution.

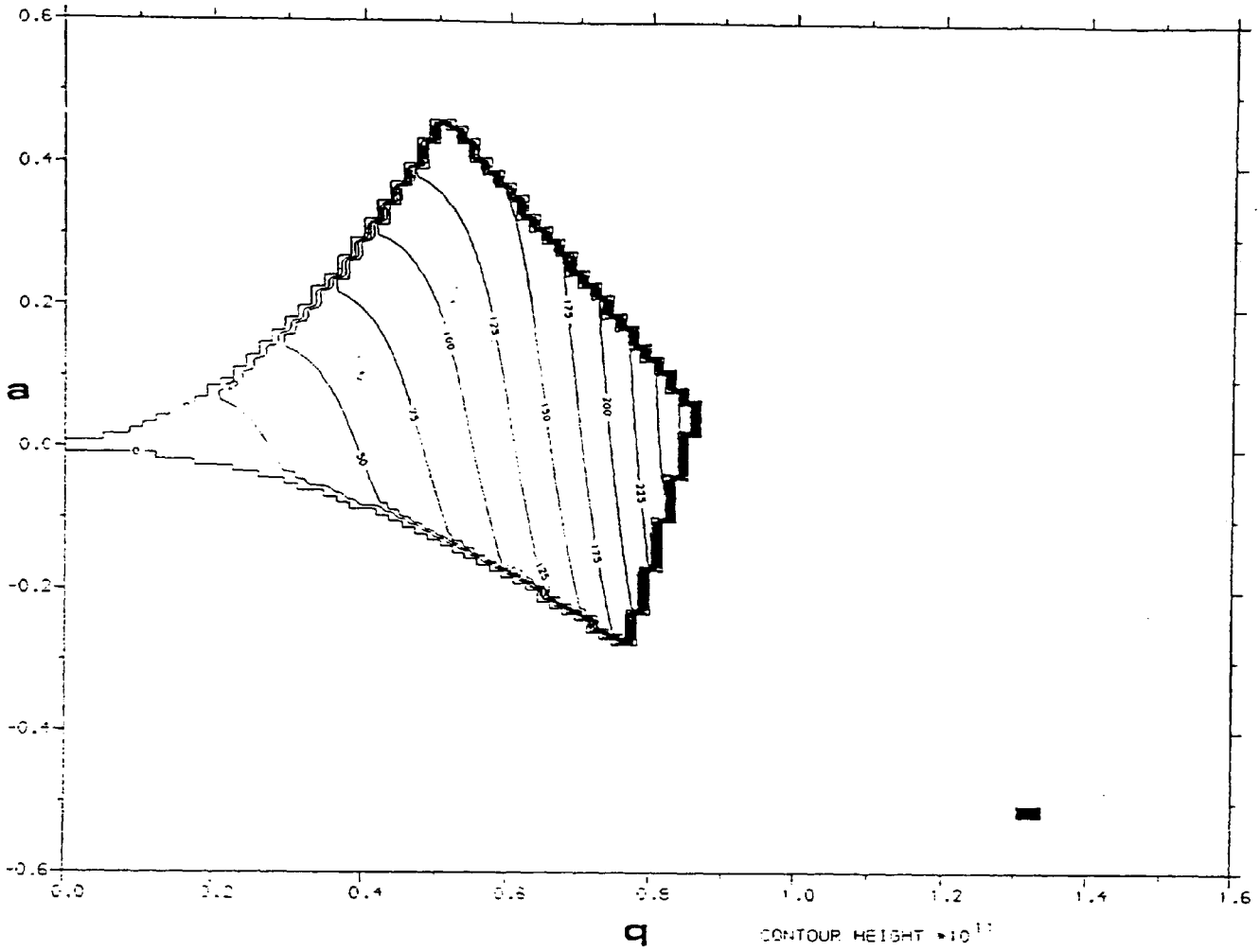

Fig. III.7.14 Stability diagram with a magnetic field ratio of 0.01.

Now the upper apex of the stability diagram lies at a greater ratio of a to q than the lower. There appears also to be a stable point at the lower right hand hand corner of the plotted region.

The trapping efficiency values have increased considerably. The product of the trapping efficiencies in each direction at the upper apex of the stability diagram is about 1.35×10^{15}, compared with about 1.00×10^{15} for a normal Quistor, while this is in fact achieved with a lower

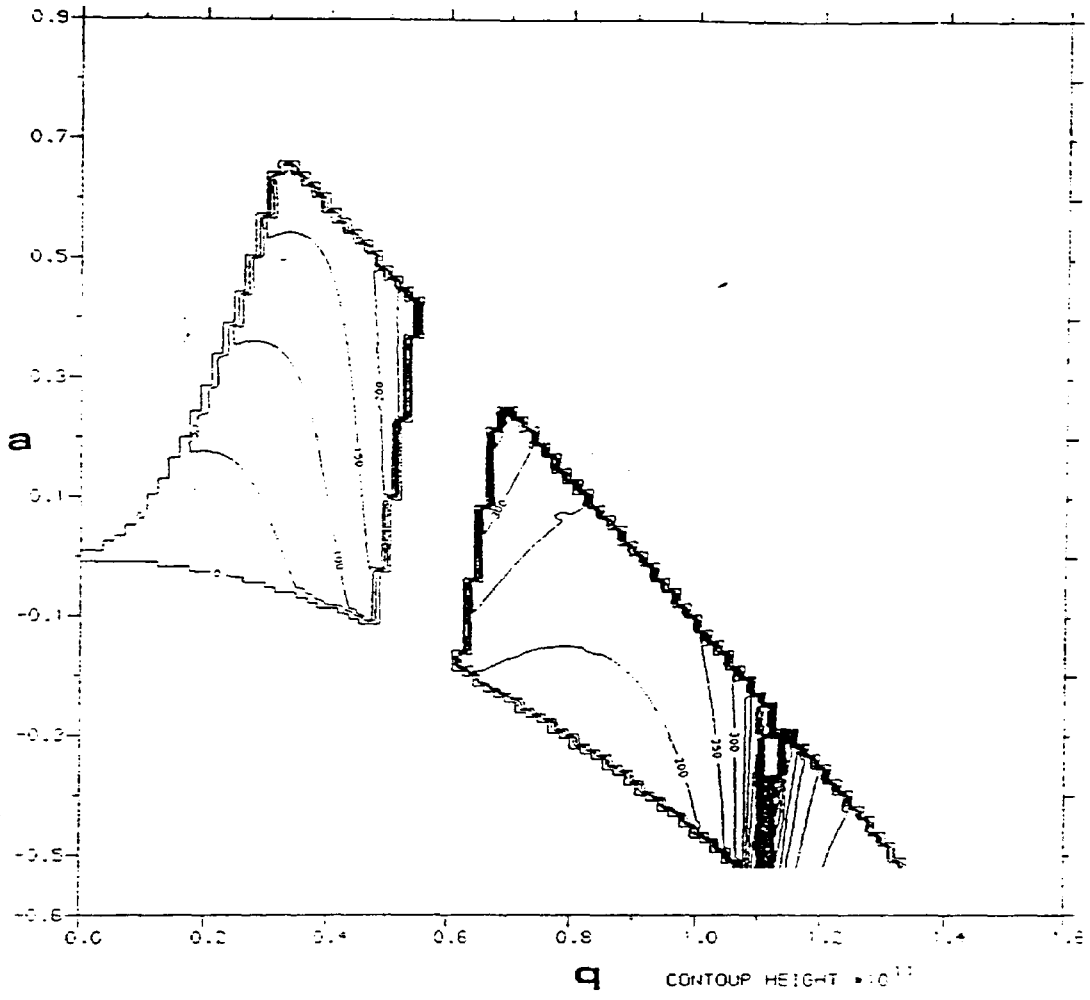

Fig. III.7.15 Stability diagram with a magnetic field ratio of 0.02.

The reason for the stable point referred to in the previous plot is now clear. What is happening is that the stable region boundaries have been bent around so far, that higher order stable regions have come into view (see Fig. I.3.2). These stable regions are superimposing upon the normal z - stability diagram in a way in which they would not usually do.

Again the trapping efficiency values for a given RF voltage are increasing considerably. The pattern formed by the values, however, is becoming much less straightforward.

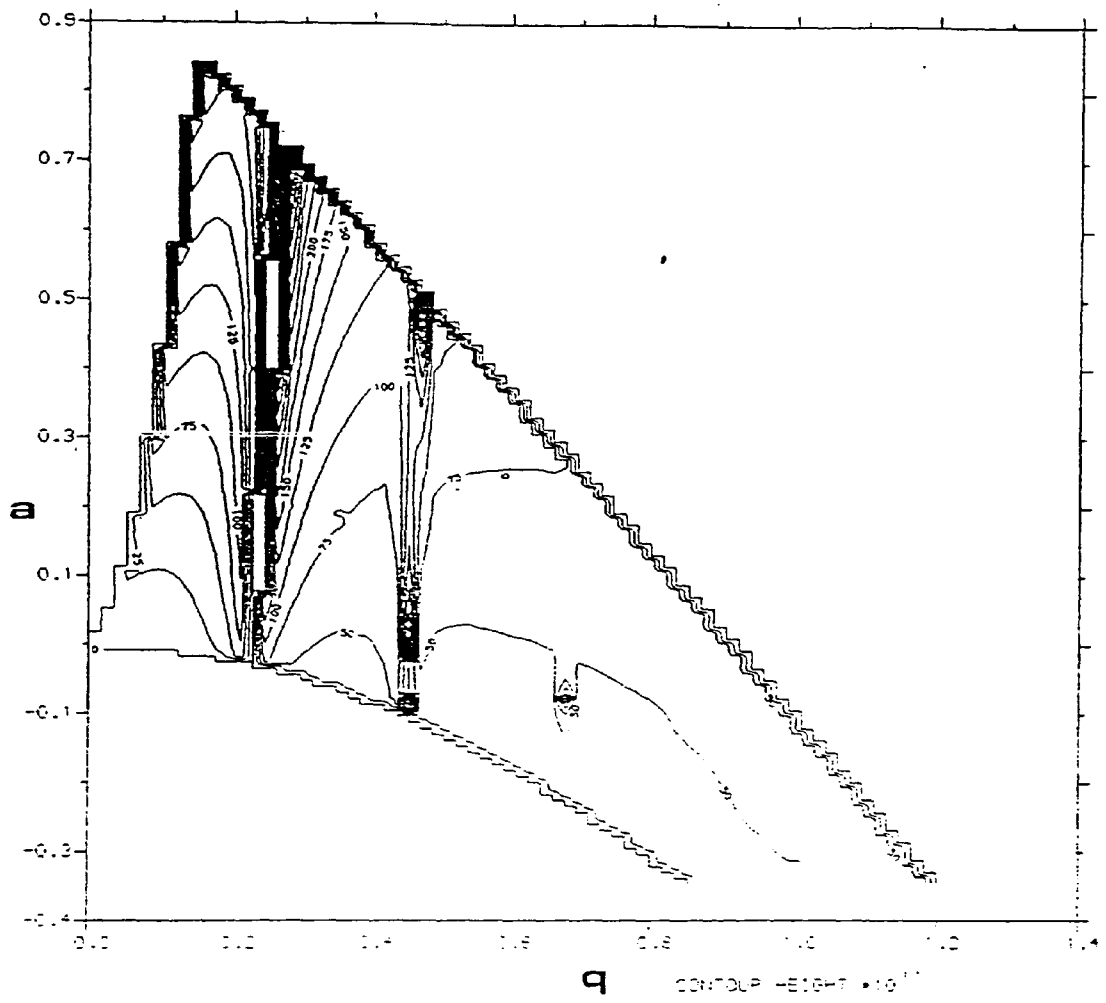

Fig. III.7.16 Stability diagram with a magnetic field ratio of 0.05.

Now this process has gone so far that the stable regions in the r direction are superimposing upon each other, in some cases without an intervening drop in trapping efficiency. The number of points plotted is not sufficient to interpret the detail of exactly what happens in the narrow bands between stable areas. Particularly at about q = 0.46

and a = 0, something interesting seems to be happening.

Accordingly, this area has been plotted linearly in order to investigate it in more detail. The following plot is taken across this region with a = 0.

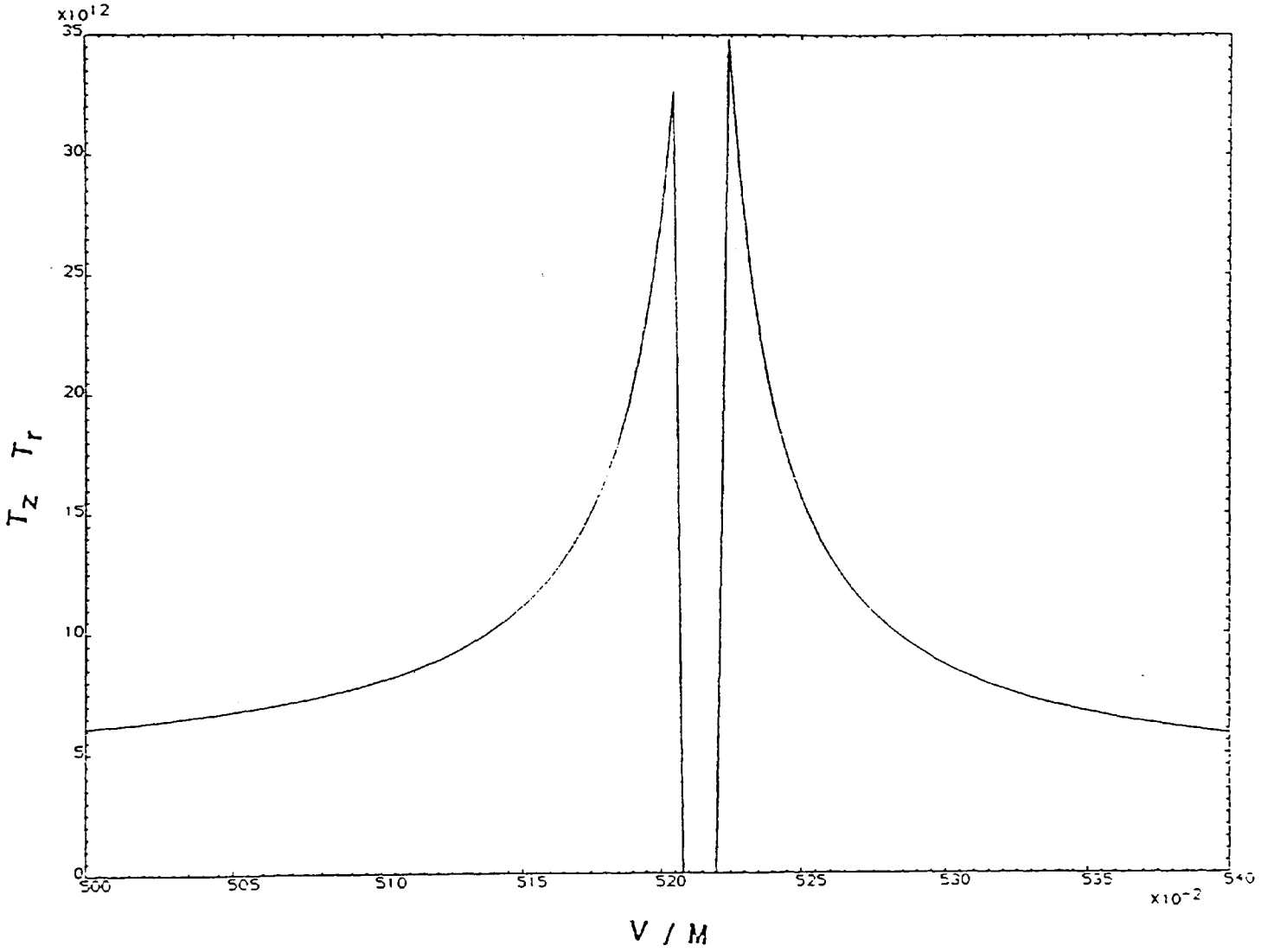

Fig. III.7.17 Trapping efficiency product plot with a magnetic field ratio of 0.05 and a = 0.

This result is most unexpected. The trapping efficiency falls to zero as ions become unstable, but bounding this region, there is an area of substantially greater trapping efficiency. What seems to be happening

here is that there is a resonance taking place, perhaps between the magnetic cyclotron frequency and the natural Quistor oscillation frequency $\beta\omega_0 / 2$.

It is clear that the application of an axial magnetic field to the Quistor would have a beneficial effect on its sensitivity. An appropriate selection of field strength is, however, important. A relatively weak magnetic field has little or no effect on the Quistor stability diagram. On the other hand, a very strong field has a dramatic effect, but the desirability of overlapping stability diagram regions, as seen in the last plot, would seem to be questionable.

The original intention has been to examine the value of the use of a magnetic field whose strength was in proportion to the electric fields used in the Quistor. This would suggest experimentally the use of a programmable current source coupled to a solenoid. However, it is clear that the magnetic field strengths involved far exceed the practical application of such an approach. For example, a magnetic field ratio of 0.01 Tesla / RF volt, combined with an RF unit capable of supplying 1000 V peak RF voltage, would mean a maximum magnetic field of 10 Tesla. That kind of field could not practically be generated without the use of superconducting electromagnet technology. Even with that technology, the power required to ramp the magnetic field strength at the scan speed required, would be ridiculous.

However, it would be practical to use a constant magnetic field strength of, say, 0.1 Tesla generated either by a permanent magnet or an electromagnet. Note that the stainless steel used in the construction of vacuum components, including the Quistor, is not ferromagnetic. Therefore there would be no inconvenient magnetic effects resulting.

The consequence of this approach would be that the stability diagram for the Quistor would change as the scan progressed. Within limits this is acceptable, although it might be necessary to increase the ratio of DC to RF voltages applied to the Quistor at low masses, in order to retain mass selection upon storage.

The sensitivity of the Quistor would be increased especially at low masses. In view of the fact that is just where the Quistor is at its least sensitive, that is a good thing. On the other hand, there would be a non - linear variation in the mass calibration which would be less welcome.

It is known that the rate of ionisation in an electron beam increases substantially when a magnetic field of this kind is applied. This is because the electrons are also contained by the magnetic field and so take very long spiralling paths. This could be a great advantage, quite separate from the effect of the magnetic field upon the ions. However, it may prove to be much more difficult to pass the electron beam through the gauzes which are used in the Quistor.

The spiralling paths taken up by electrons are likely to collide with the walls of the holes in the gauze and so be unable to enter the Quistor. This problem may be overcome by the use of single holes of a reasonably small diameter on the z axis, instead of each gauze. Since the electrons are contained by the magnetic field in spirals with a small radius (in a magnetic field of 0.1 Tesla, electrons with radial energy values equivalent to 10eV, would have a spiral path with a radius of only 0.107 mm), holes of 0.5 mm would be sufficient. Consequently the field penetration effects of this upon the Quistor would be small so that a reduction in resolution would not result.

Unfortunately, to date, it has not been possible to verify these predictions experimentally. This is seen as work which would usefully follow up this project. One publication (Ref. 62) does, however refer to this approach being used.

d) The effect of finite electrodes.

In theory, mathematically, the Quistor's electrodes extend to infinity in all directions. This is, of course, not the case in practice, and so, there is a distortion introduced at the edges of the Quistor.

The fields analysis program was used to determine the extent of this problem. The Quistor r_0 value used was 7.5 mm, while the the electrodes extended to 19 mm. This corresponded to the dimensions of the Quistor actually used experimentally. Outside the Quistor, the potential was assumed to be ground.

What has been plotted here, as in most of the field plots which follow, is not the absolute voltage in the Quistor, but a measure of the distortion, given by :

$$D = ((V - V_i)^2 + (U - U_i)^2)^{0.5}.$$

where U and V are the actual DC and RF voltages at each point, and U_i and V_i are the theoretical (ideal) Quistor values which would be there if the distortion was zero. Note that the distortion values outside the Quistor have been set to zero.

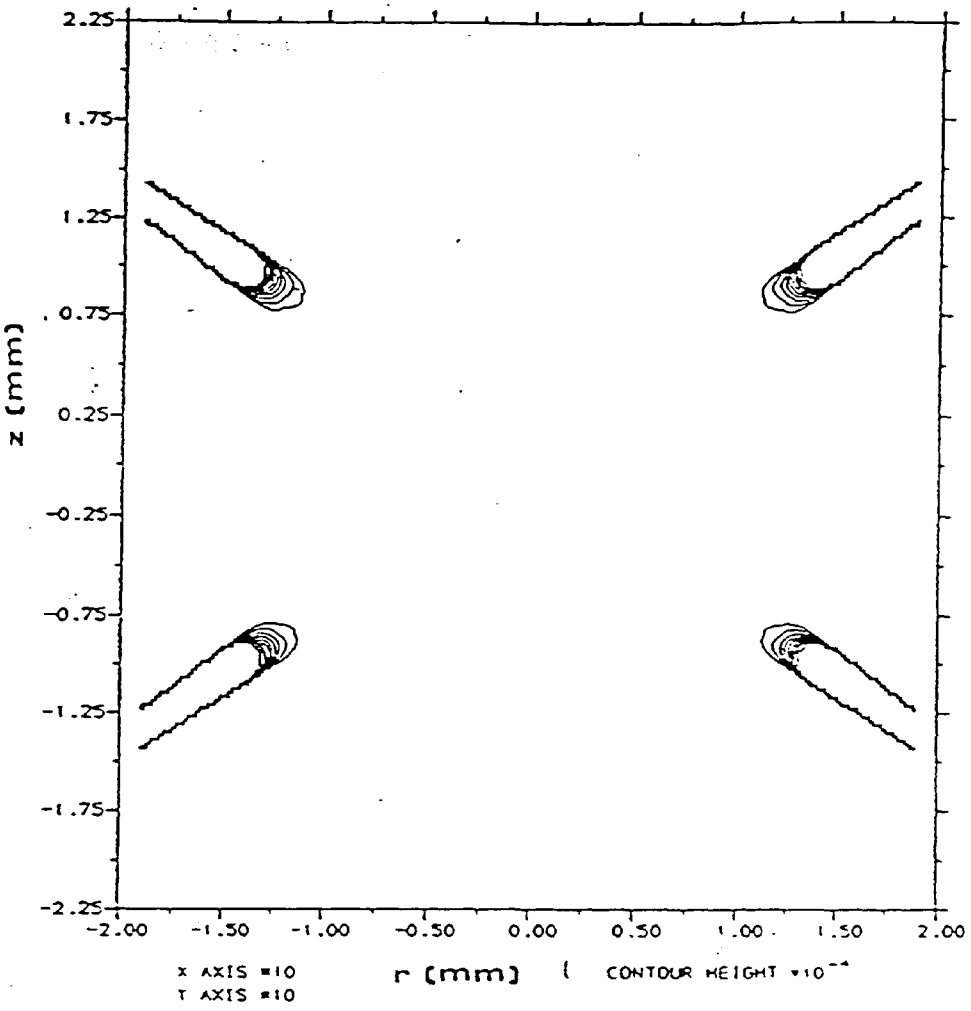

Fig. III.7.18 The electric field distortion due to the edge effect of the Quistor's electrodes.

The distortion near to the edges of the Quistor is very intense (indeed the software has here limited the distortion level displayed so that the data further into the Quistor can be successfully displayed). However it drops off quite quickly and the distortion level within the main body of the Quistor (where the ions will be) is virtually zero. The trapping efficiency plot shown below makes it clear that there is no effect due to the edges of the electrodes upon the resolution. This plot is indistinguishable from that for an ideal Quistor.

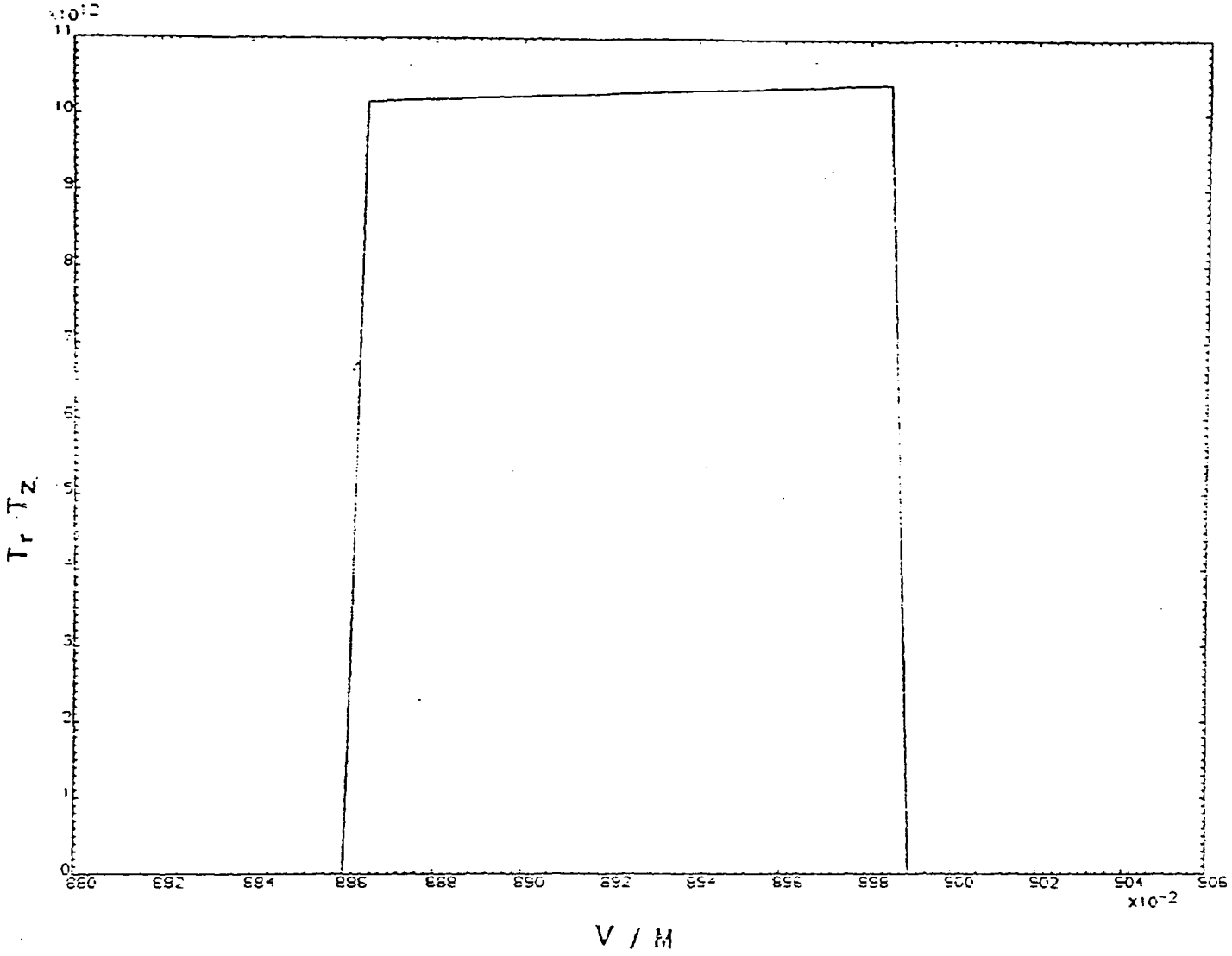

Fig. III.7.19 Trapping efficiency product plot for a Quistor whose electric fields are distorted only by the edge effect of finite electrodes.

It is felt that the Quistor's outer dimension can be reduced from this value of 19 mm, perhaps to about 17 mm, without any significant increase in the distortion level present within the main body of the Quistor, and thus without loss of resolution. This would have the advantage of making the Quistor more compact.

This is another advantage to the use of a bipolar RF

supply for the Quistor. If a single sided RF supply is applied to the ring electrode, as has been done in some cases, then the average voltage value between the Quistor's electrodes would not be zero (it would be half the ring voltage). This would mean that the voltage outside the Quistor (ground) would have a much greater effect.

e) The effect of a single hole in the Quistor's end cap electrodes.

The Quistor inherently requires some form of aperture in its electrodes through which an electron beam can enter the trap, and through which ions may leave it in order to be detected. This aperture will necessarily distort the electric fields within the Quistor, resulting in a loss of performance.

This effect has been investigated in detail and has been found to be of great importance. It is in relation to this point that this computer simulation work has proved to be of the greatest practical help.

The first, and simplest, configuration which has been researched has been that of a simple hole at the centre of each end cap. There is interpenetration of the electric fields inside, and outside, this hole. Since this results in a distortion in the electric fields inside the main body of the Quistor, it is of much greater importance than the edge effect detailed above.

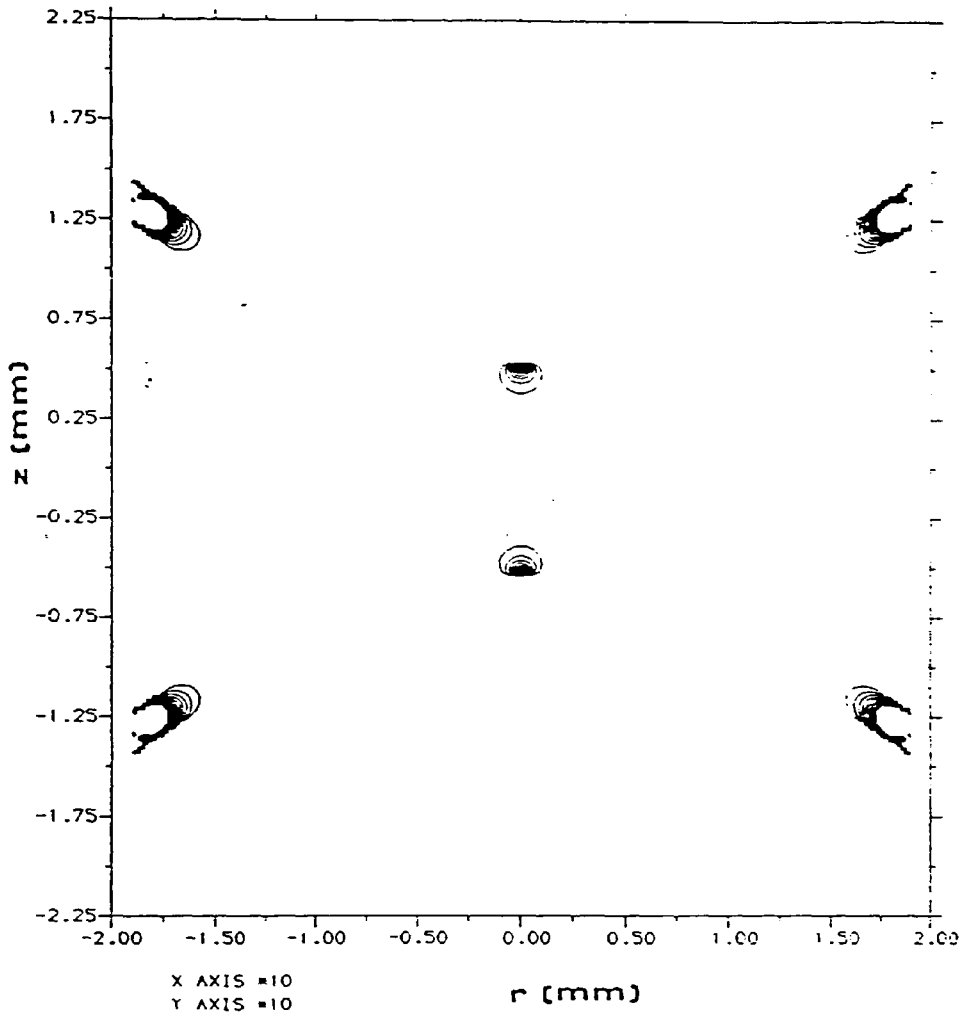

Fig. III.7.20 The electric field distortion due to a single hole of 1 mm diameter in the centre of each end cap.

The hole has clearly resulted in an intense level of distortion (with a maximum value equal to 28.0 volts, compared with 650 V of RF and 65 V of DC), localised close to the hole. This distortion also spreads throughout the main body of the Quistor at a much lower level.

The effect of this distortion upon the Quistor's performance is investigated by entering the data into the simulation program.

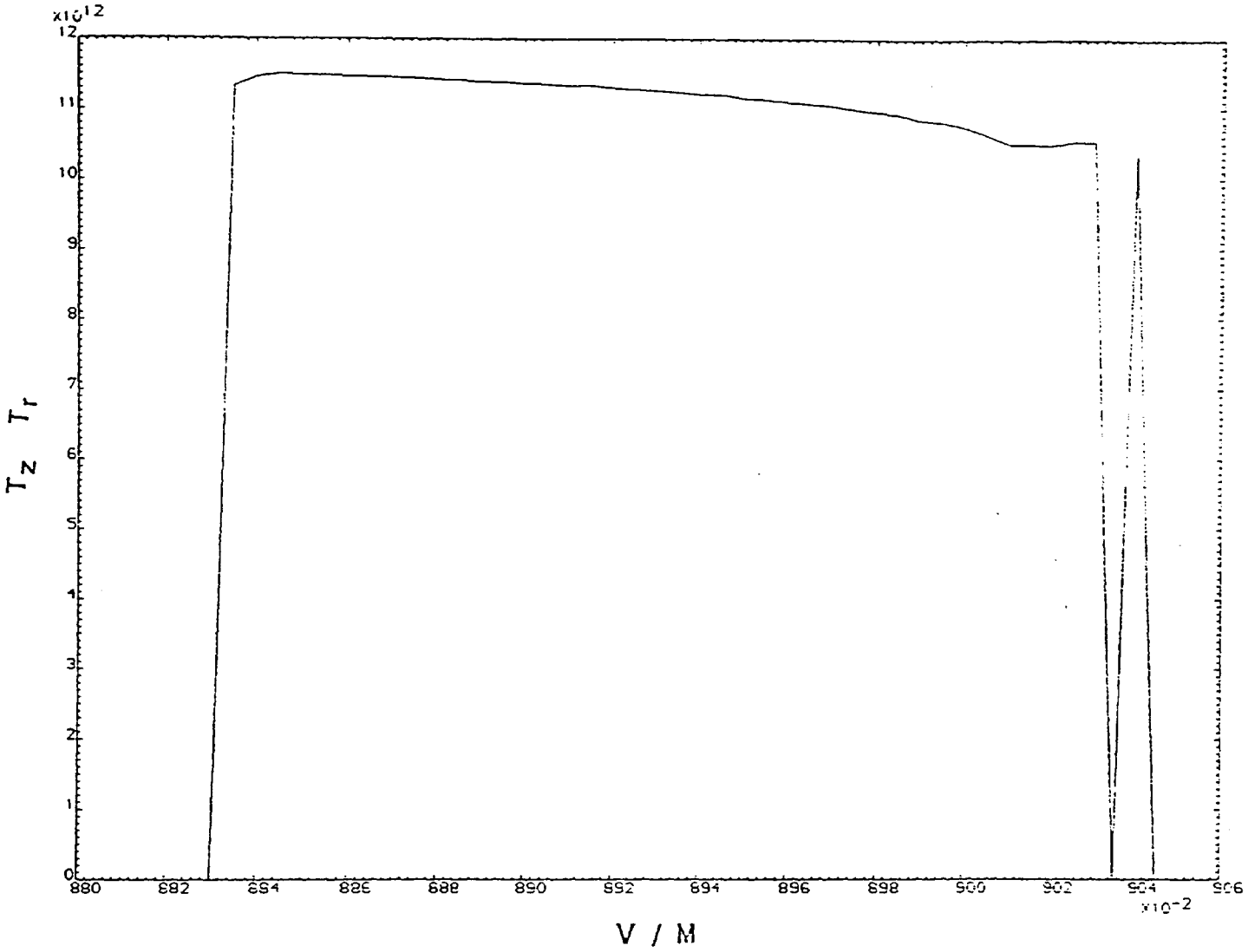

Fig. III.7.21 Trapping efficiency product plot for a Quistor whose electric fields are distorted by the presence of 1 mm holes in the end caps.

Comparing this plot to that for an ideal Quistor (Fig. III.4.1) we see that a number of changes have taken place. The left hand boundary of the plot has moved to the left, from 8.86 to 8.82, while the right hand boundary has moved to the right, from 8.99 to 9.04. This represents effectively a reduction in the DC to RF ratio and is almost certainly related to the penetration of negative potential from the channel plate into the Quistor.

The "dip" in the plot at its right hand boundary is a characteristic effect of distortion in the electric fields in the Quistor, which undoubtedly results from a non - linear resonance line (Ref. 18). It results in a split - peak effect and a reduction in resolution, since the peak width includes both peaks. The resolution here is about 300. This is a considerable loss of resolution compared with about 2000 for an undistorted Quistor.

f) A large hole in each end cap covered by a gauze

The use of a single hole in each end cap, as described above, undoubtedly works. However, in order to minimise the electric field distortion it is necessary to keep the hole small. This means that the sensitivity is low.

If a means could be found of increasing the transparency of the end caps, whilst at the same time keeping the distortion produced low, this would be ideal. The use of a large number of small holes, spread across the end cap surface, would have this effect. This could be arranged either by drilling a large number of small holes in the end cap, for example using a powerful laser, or by placing a preformed, curved, gauze over a large hole in the end caps in order to maintain the integrity of the surface. These two options are regarded as being effectively identical in electrical terms.

Before proceeding any further it is necessary at this point to detail the results of the program which calculates the electric field behaviour of a gauze. The operation of this program has been previously explained.

An analysis of 4 different gauzes was performed, each assumed to consist of a smooth flat conducting layer of 0.13

0.13 mm thickness with square holes upon a square raster. The wire thickness (distance between holes) was 0.13 in each case. The dimensions of the holes were 0.25 mm, 0.5 mm, 0.75 mm and 1.0 mm respectively.

The program assumed that there was a 1 V mm-1 electric field incedent upon one side of the gauze, but that no field was incedent upon the other side. The gauze itself was assumed to be at 0V.

The voltage change of a gauze with arbitrary electric fields incedent upon both sides can thus be found by multiplying the results below, by the difference between the electric field strengths.

The diagrams below are given as an example of the voltage distribution, in this case for the gauze with a 0.5 mm hole.

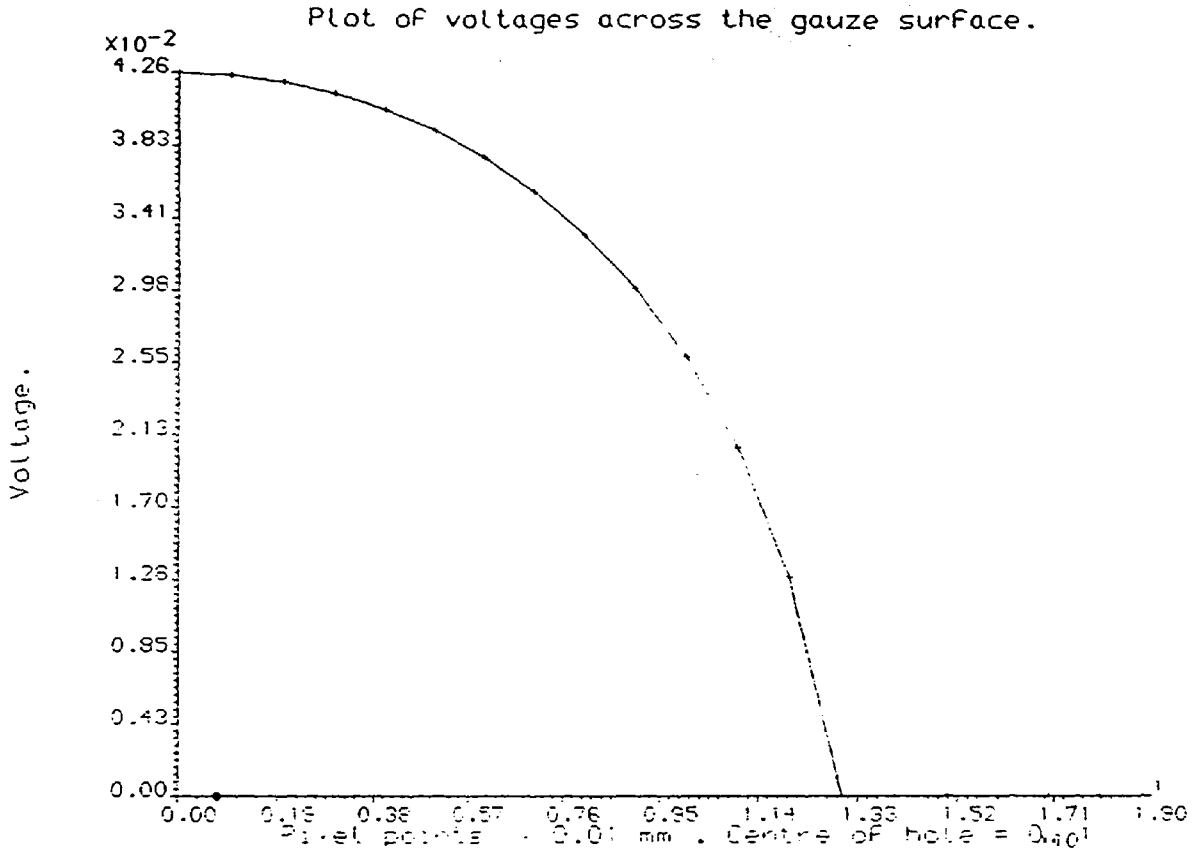

Fig. III.7.22 The voltage distribution plotted horizontally across the gauze surface. The origin is the centre of the hole.

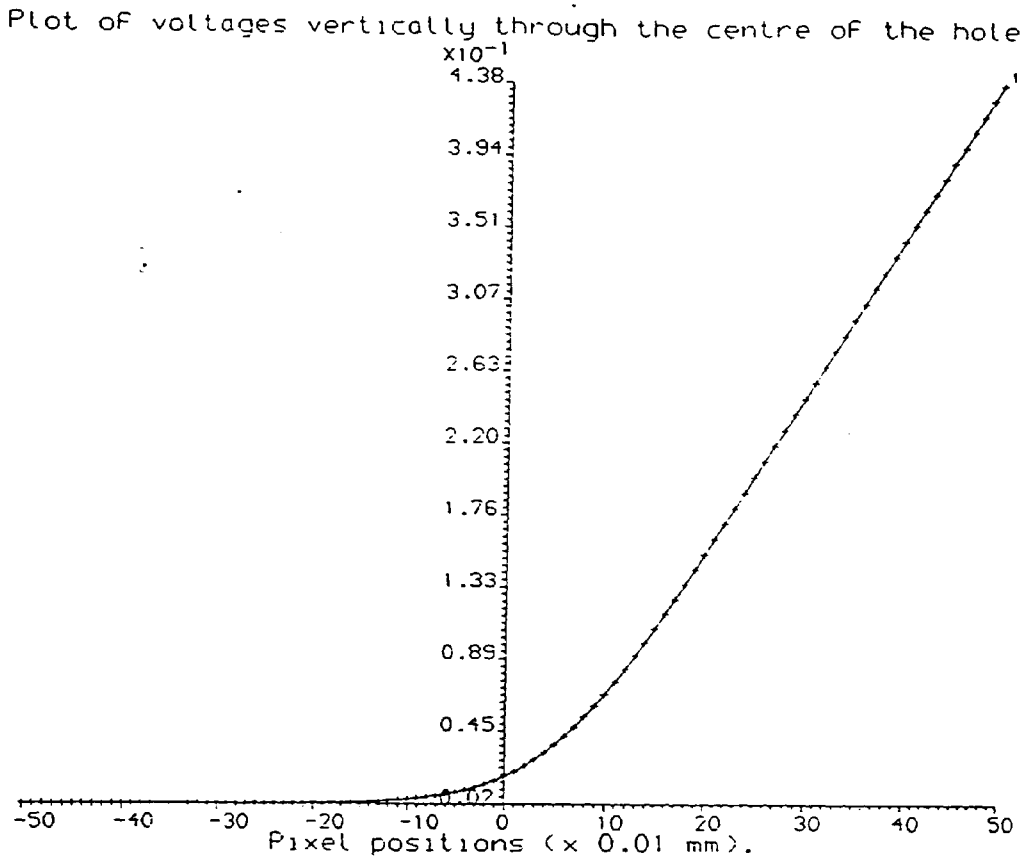

Fig. III.7.23 The voltage distribution plotted vertically through the centre of the hole, normal to the surface.

The result of main interest was the average value (including the wire sections, where the voltage was 0) of the voltage across the gauze surface. This quantity, multiplied by the difference in the electric fields on either side of the gauze, is the average voltage drop which results from the use of a gauze.

The results were :

Hole size (mm)	Average voltage change (mV / (V mm^{-1}))
0.25	10.186
0.50	42.934
0.75	75.405
1.00	112.403

Fig. III.7.24 The average potential across the gauze surface for selected hole sizes.

Not surprisingly, the voltage increases sharply with the hole size. The voltages shown appear to be small, but the electric fields in the Quistor are large and so the result is not trivial.

These values can be entered into the fields program. In the following field distortion plot, there were 8.0 mm holes, covered by a gauze, in each end cap. The end cap voltages were 650 V peak RF and 65 V DC. The channel plate was at -2000 V.

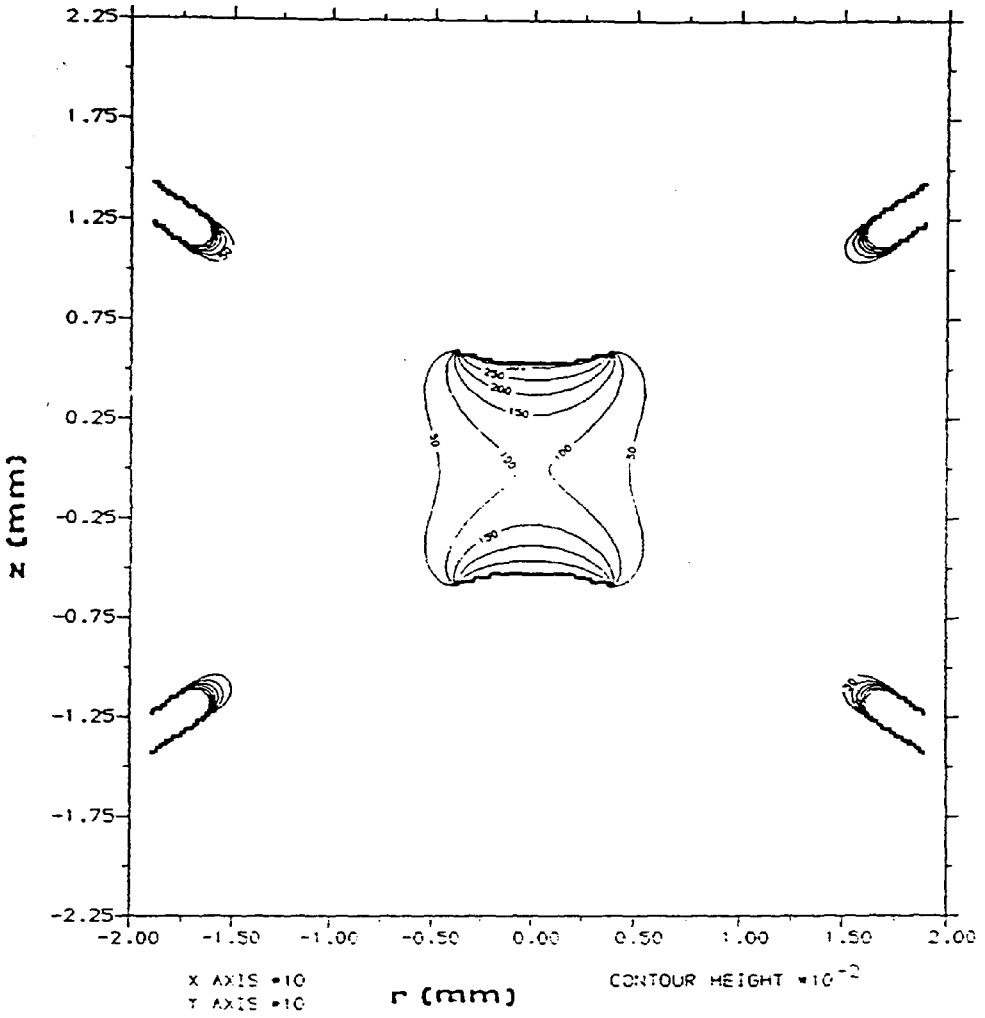

Fig. III.7.25 The electric field distortion due to a single gauze with 0.25 mm holes covering a hole of 8 mm diameter.

Compared with the distortion due to a single hole, as above, the maximum distortion level is much less intense, only about 3.19 V. However the distortion emanates from all points upon the gauze surface. Consequently it is much more evenly spread throughout the main body of the Quistor, and the value at the centre is greater.

The effect of this upon the Quistor's performance is marked. The following trapping efficiency product plot is

for small amplitude ions for a Quistor with the electric field described above. "Small amplitude" is here taken to mean, small compared with the dimensions of the Quistor, so that the ions do not enter the regions close to the holes where the distortions are greatest. The ions therefore experience only a small amount of non - linear electric field. Note that the horizontal scale of the plot is not the same as previous plots.

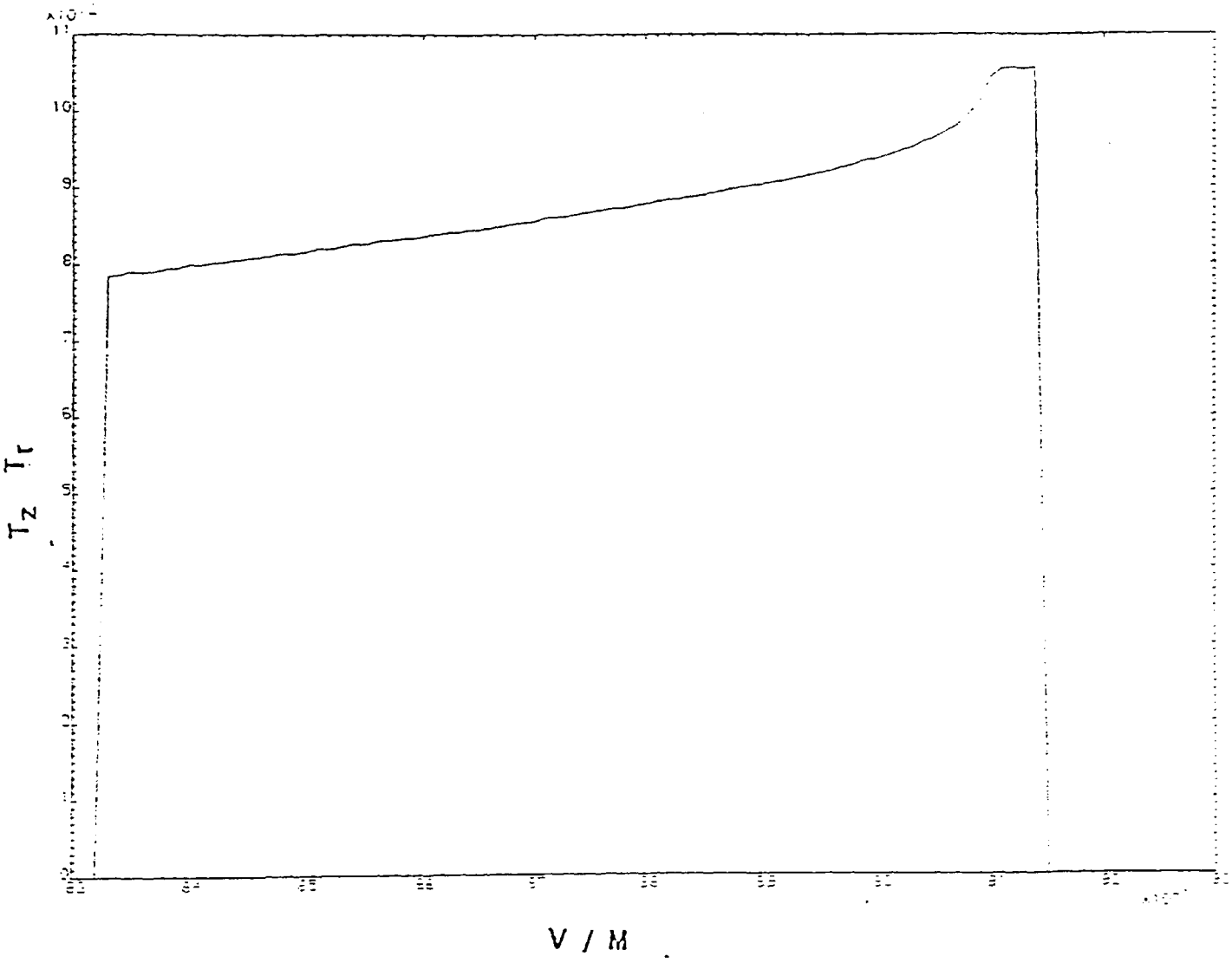

Fig. III.7.26 Small amplitude trapping efficiency product plot for a Quistor whose electric fields are distorted by single gauzes with 0.25 mm holes.

When compared to the trapping efficiency plot for an ideal Quistor, the left hand boundary of the plot has moved to 8.32 V from 8.86 V, and the right hand boundary has moved to 9.15 V form 8.99 V. This is equivalent to a substantial reduction in DC to RF ratio. The trapping efficiency is no longer constant throughout the stable region. Most importantly, the resolution has fallen to about 300.

Emphasis is placed upon the fact that the above plot was for small amplitude ion motion. As the amplitude increases, the ions come closer to the centres of the distortion - the gauzes. Non - linearities in the electric fields increase and the performance drops.

The simulation program was programmed to select automatically an ion amplitude of motion equal to roughly half the Quistor's dimensions. Half the Quistor dimensions was chosen as being the most representative amplitude. The resulting plot is shown below.

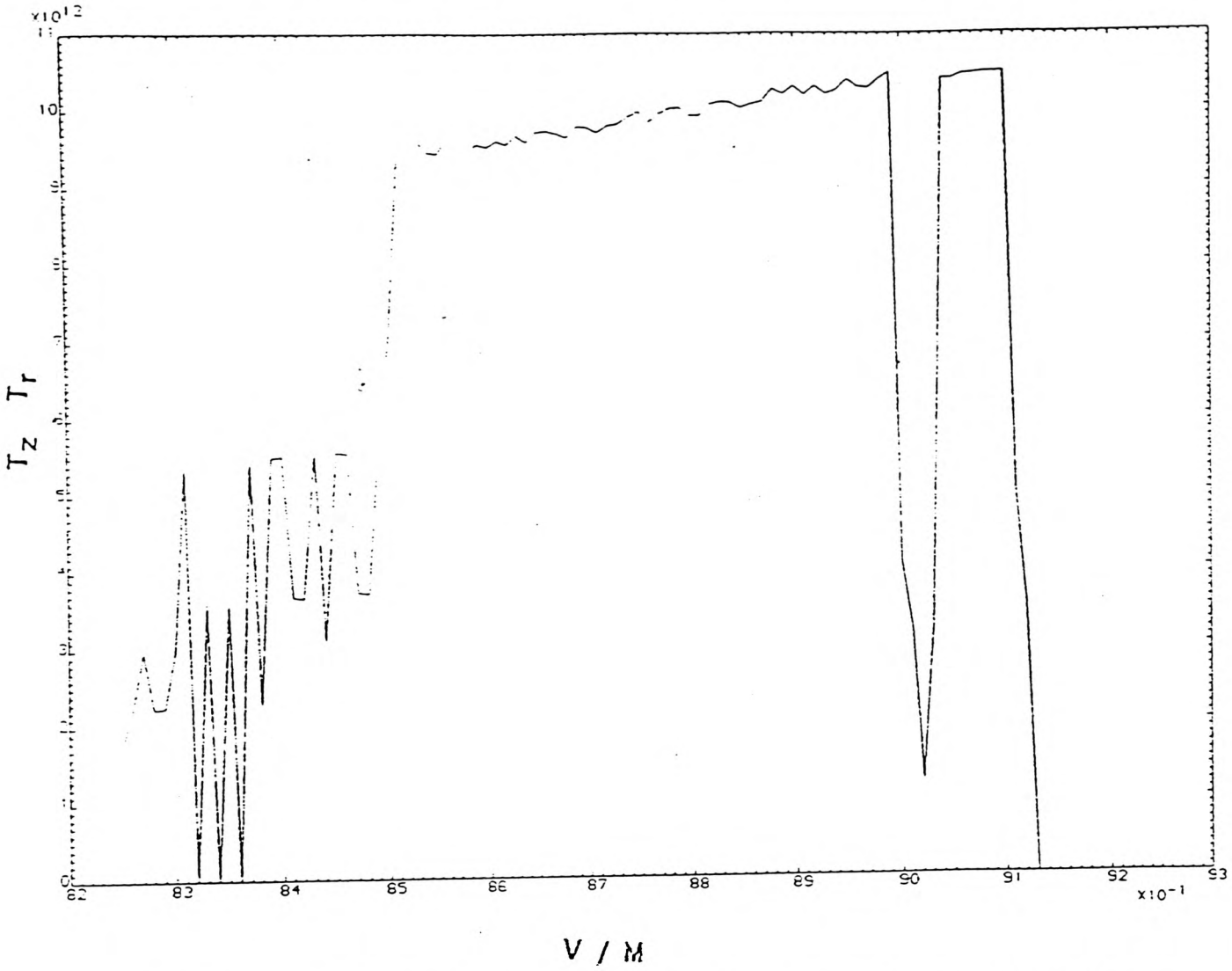

Fig. III.7.27 Large amplitude trapping efficiency product plot for a Quistor whose electic fields are distorted by single gauzes with 0.25 mm holes.

As can be seen, the picture is now further confused. The boundaries of the plot lie at about the same location as those for small ions. The "jaggedness" of the left hand boundary reflects an "indecisiveness" on the part of the ions close to that boundary, on whether they are stable in the r direction, or not. Depending upon their paths, they may, or may not pass through a particular region of distortion - so that they may, or may not be lost from the trap.

The prominent "dip" at the right hand edge of the boundary, is a strong non - linear resonance line. This results in a large split - peak effect and the resolution implied by this plot is poor; only about 50.

The predicted performance for the use of a gauze in this way is therefore discouraging. This was verified experimentally when the first attempt to use end caps with a gauze fitted, produced very poor results. Indeed it proved impossible to produce any meaningful spectrum at all, although ion trapping was demonstrated. The transparency of those end caps was, however, extremely high and so the sensitivity would have been good - if there had been a spectrum to detect.

More detailed data for the use of single gauzes with larger holes has not been produced. However, the level of distortion and consequently the loss of performance will be in proportion to the results of the gauze program above. Ideally one would wish to use a gauze with holes larger than 0.25 mm from a transparency point of view - but the distortion levels introduced with 0.25 mm holes are already too high. Unless this problem can be overcome, the approach of using a gauze would seem to be useless.

g) A gauze shielding the holes in the end caps.

It was felt that the use of a gauze mounted into the rear face of the end caps would help to exclude external fields (such as that due to the channel plate) from entering the Quistor through the holes in the end caps.

Provision was made for this within the fields program. These gauzes were also assumed to be electrically "permeable" in the same way as the curved gauzes in the end caps. They were assumed to have a "permeability" of 0.01 V / (V mm-1). As before, the end cap voltage was 650 V peak RF and 65 V DC, and the channel plate voltage was equal to -2000 V.

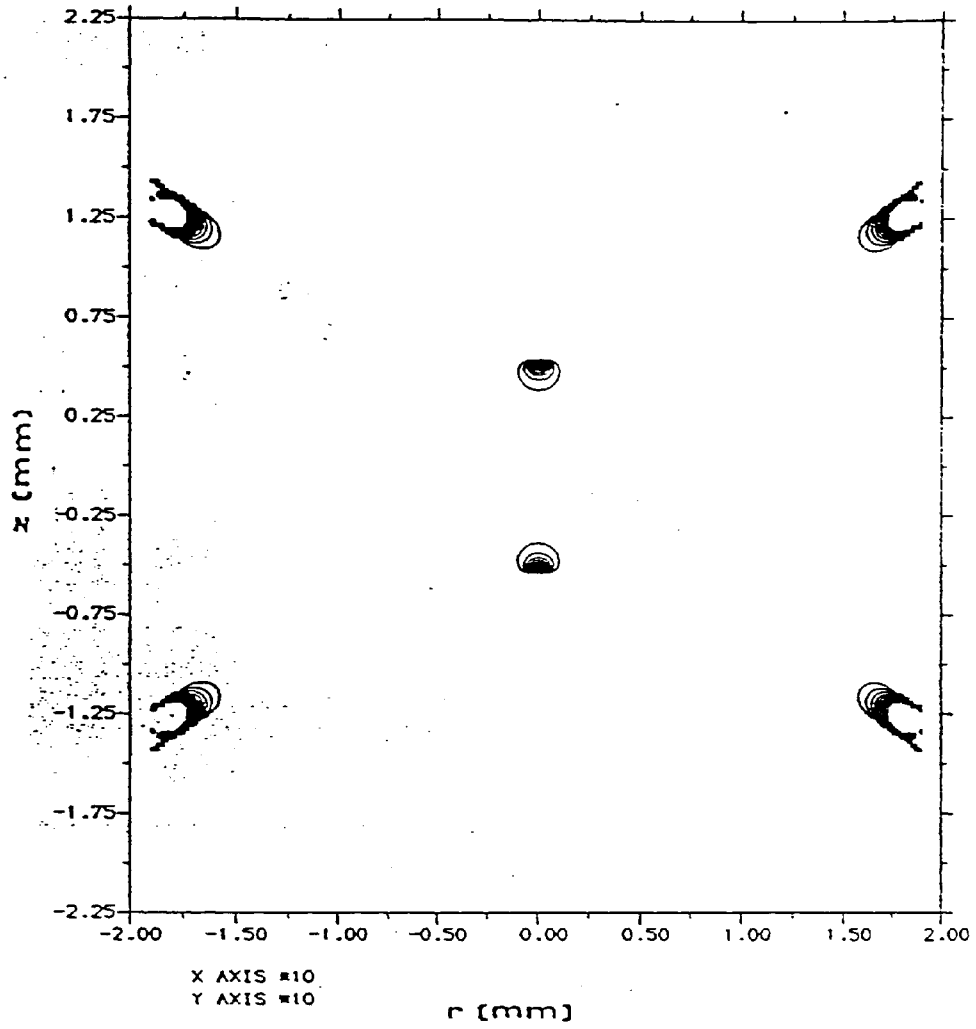

Fig. III.7.28 The electric field distortion due to single holes of 1 mm diameter in each end cap, shielded by a gauze. The contours are at 1V intervals.

At first glance the improvement is disappointing. When compared to Fig. III.7.20 above, the distortion level has fallen slightly from a maximum value of 28.0 V to 27.6 V. The distribution of distortion appears to about the same. It would seem that the use of a gauze in way described is not really justified by these results.

However, when the trapping efficiency is plotted, the improvement appears out of all proportion. The boundaries

of the plot have returned much nearer to their ideal values, there is no "dip" at the right hand edge - and the resolution has improved to about 700.

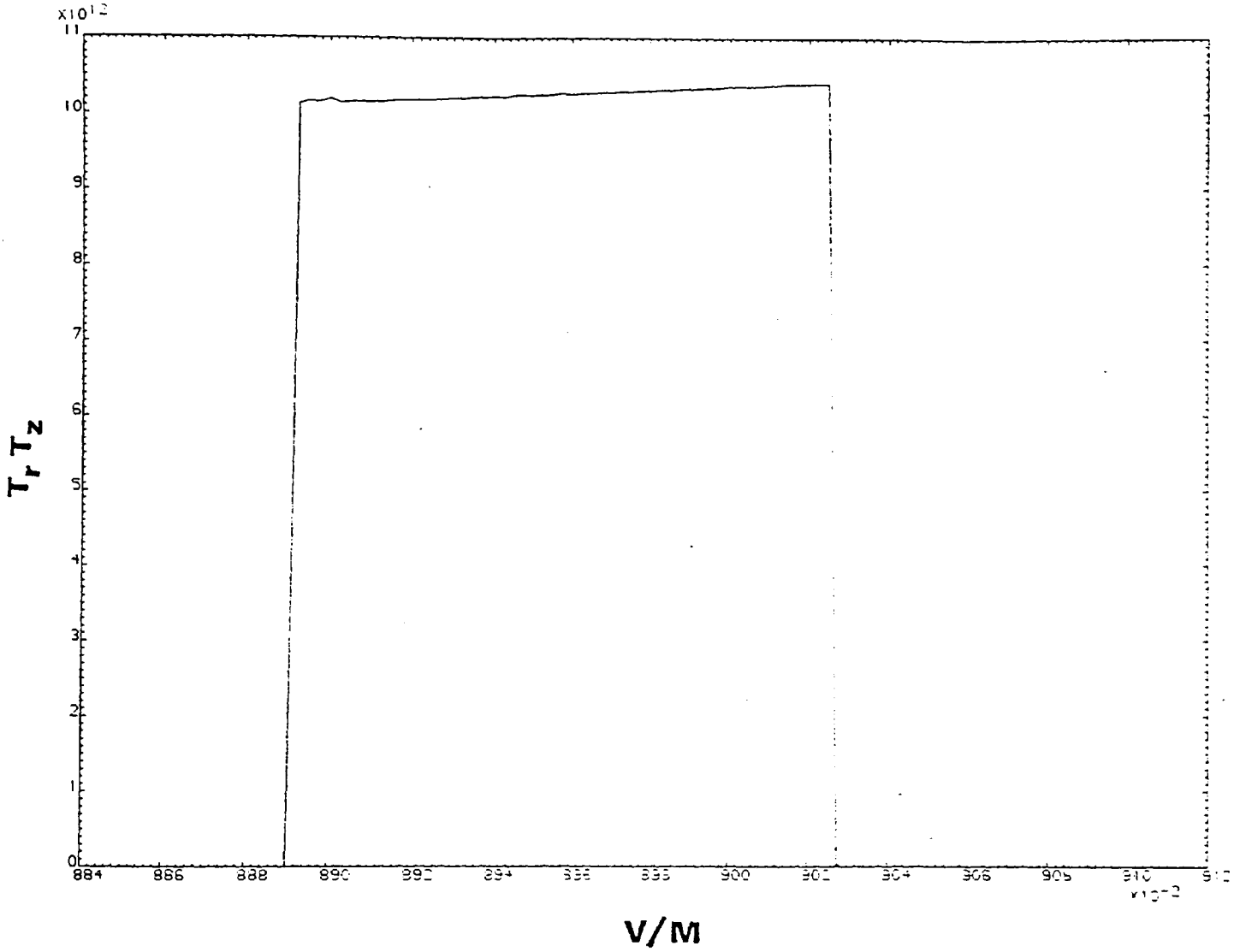

Fig. III.7.29 Trapping efficiency product plot for a Quistor with 1 mm holes in each end cap, shielded by a gauze.

Why the effect of the shielding gauze upon the distortion appears so small - while its effect upon the performance of the Quistor is much greater, is not fully understood. This may be related to the fact that the DC distortion introduced by the channel plate forms only a relatively small part of

the total distortion level, but has a greater effect upon the performance than the rest.

The effect of shielding gauzes fitted into the outer side of endcaps which have large, gauze covered holes has also been investigated. As before, at first glance the improvement is quite limited; the maximum distortion level is reduced slightly from 3.19 V to 3.00 V.

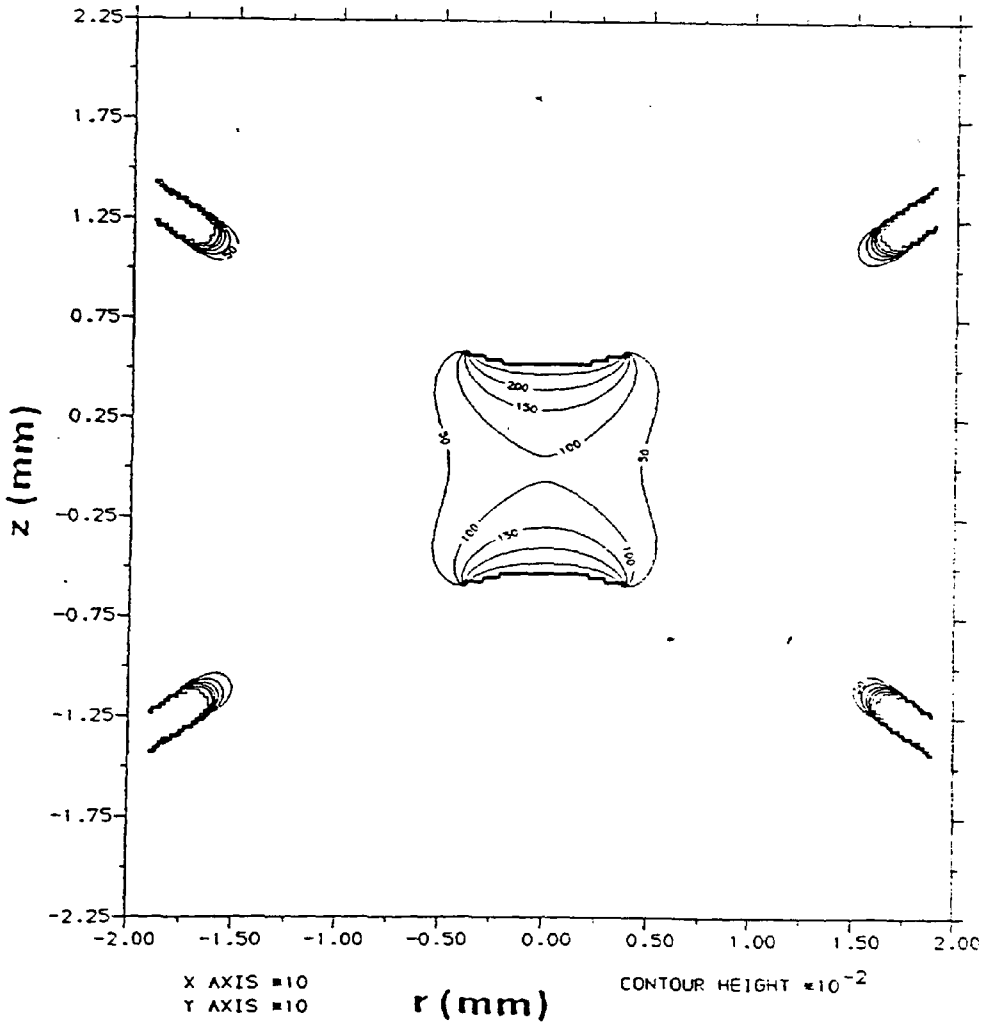

Fig. III.7.30 The electric field distortion due to gauzes with 0.25 mm holes covering holes of 8 mm diameter, shielded by a second gauze.

Again the effect of this upon the predicted performance of the Quistor is out of all proportion to the apparent change in the distortion levels. The plot below is quite close to that for an ideal Quistor - although the boundaries are slightly different. Note that this plot is for small amplitude ions.

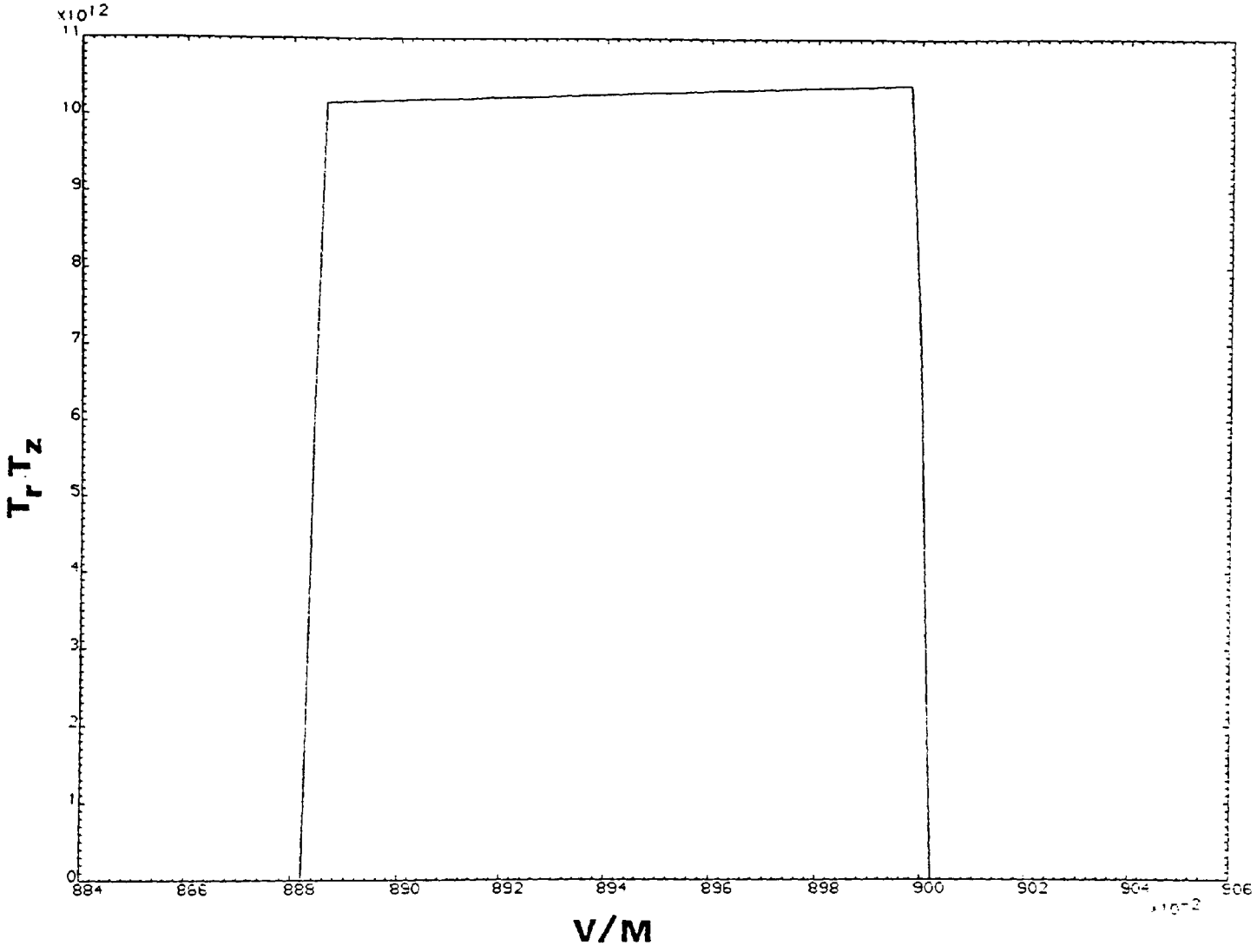

Fig. III.7.31 Trapping efficiency plot for small amplitude ions in a Quistor whose electric fields are distorted by gauzes with 0.25 mm holes covering holes of 8 mm diameter, shielded by a second gauze.

As before, the behaviour depends upon the amplitude

of motion. The plot for ions with an amplitude of about half the Quistor size is shown below.

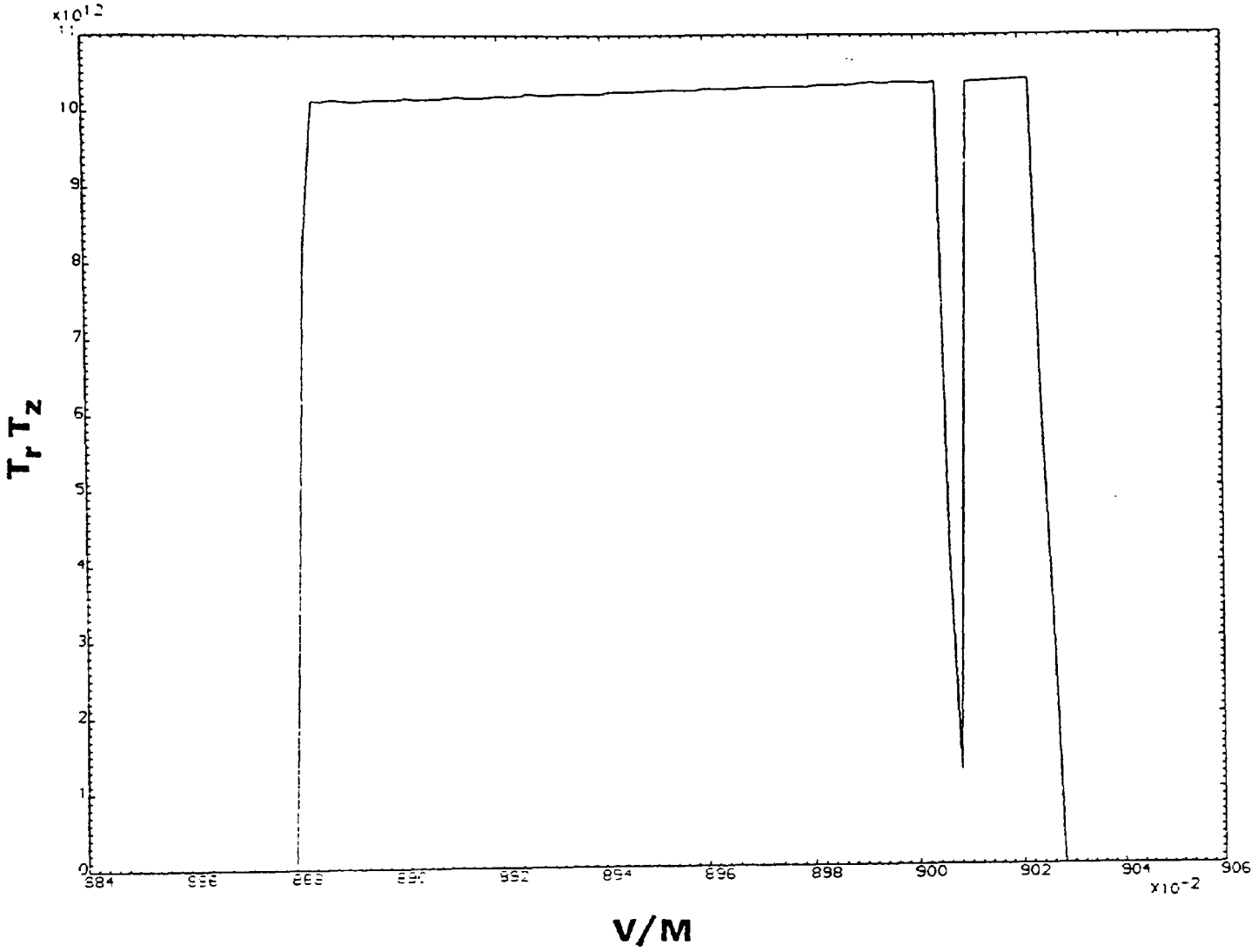

Fig. III.7.32 Trapping efficiency plot for large amplitude ions in a Quistor whose electric fields are distorted by gauzes with 0.25 mm holes covering holes of 8 mm diameter, shielded by a second gauze.

The "dip" at the right hand boundary has returned, leading again to a split peak effect. However, apart from this the plot is well defined and the difference between this and fig. III.7.26 is profound. The resolution at the right hand boundary is about 500, as compared with 50 for the

These surprising predictions were verified experimentally when the single gauze end caps described above were fitted with a second gauze. Quite good spectra were obtained - which had been impossible before. The resolution was limited because the curved gauzes were only crudely shaped and fitted. Later end caps were better.

h) A correction in the position of a gauze to overcome the distortion produced by using it.

The voltage change at the surface of the curved gauze is known by virtue of the "field permeability" data produced by the gauze program described above (and knowing the electric field which is incident upon both sides of the gauze). It follows that if the gauze position is modified so as to place it at the location where the resulting voltage is equal to the ideal Quistor potential, then a return to an undistorted Quistor field is possible in theory.

The fields program was programmed to consider this in detail, and generate the required electrode shape co-ordinates, given the gauze data. It should have been no surprise that the movement of the gauze position required in the z direction (in mm) was roughly equal to the gauze "permeability" data value (in V / (V mm-1)). Thus for a gauze with 0.25 mm holes in it, the required movement was about 10^{-2} mm, although some smooth variation from this value was seen in accordance with variations in the electric fields in the outer sides of the end caps.

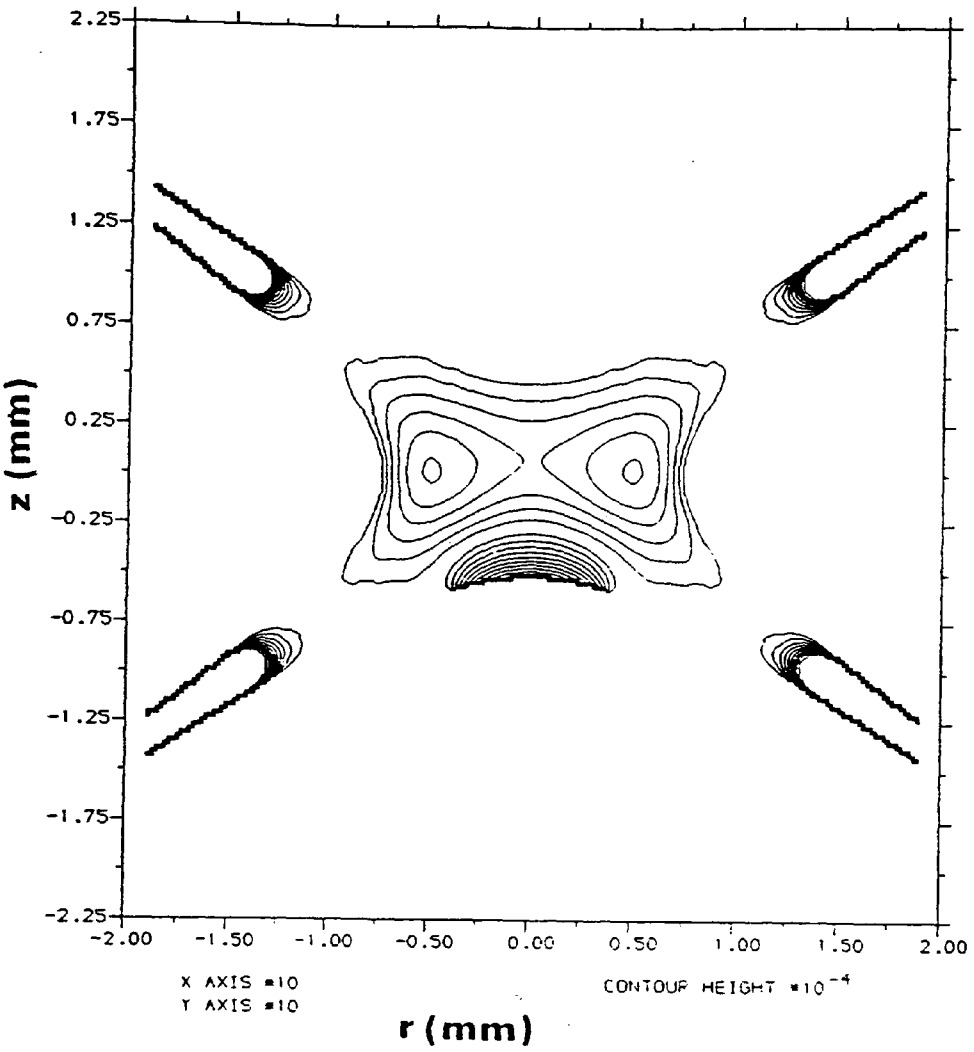

Fig. III.7.33 The electric field distortion due to gauzes with 0.25 mm holes covering holes of 8 mm diameter, shielded by second gauzes and with modified positions.

Some small residual distortion in the overall electric fields in the Quistor is seen. This is because the shielding gauzes were also electrically permeable and so some DC distortion was able to penetrate from the channel plate. Consequently there was a difference between the DC voltage change on the lower gauze, and the RF change. The maximum distortion level here is 0.0129 V.

The program selected a compromise position between the voltage values, so that both were very close to their ideal value, but neither was perfect.

Nonetheless the trapping efficiency plot which results is virtually the same as that that for an ideal Quistor, although the boundaries have moved slightly. The resolution here is about 2000, identical to that for a perfect Quistor. Note that this plot is for ions with an amplitude of half the Quistor dimensions.

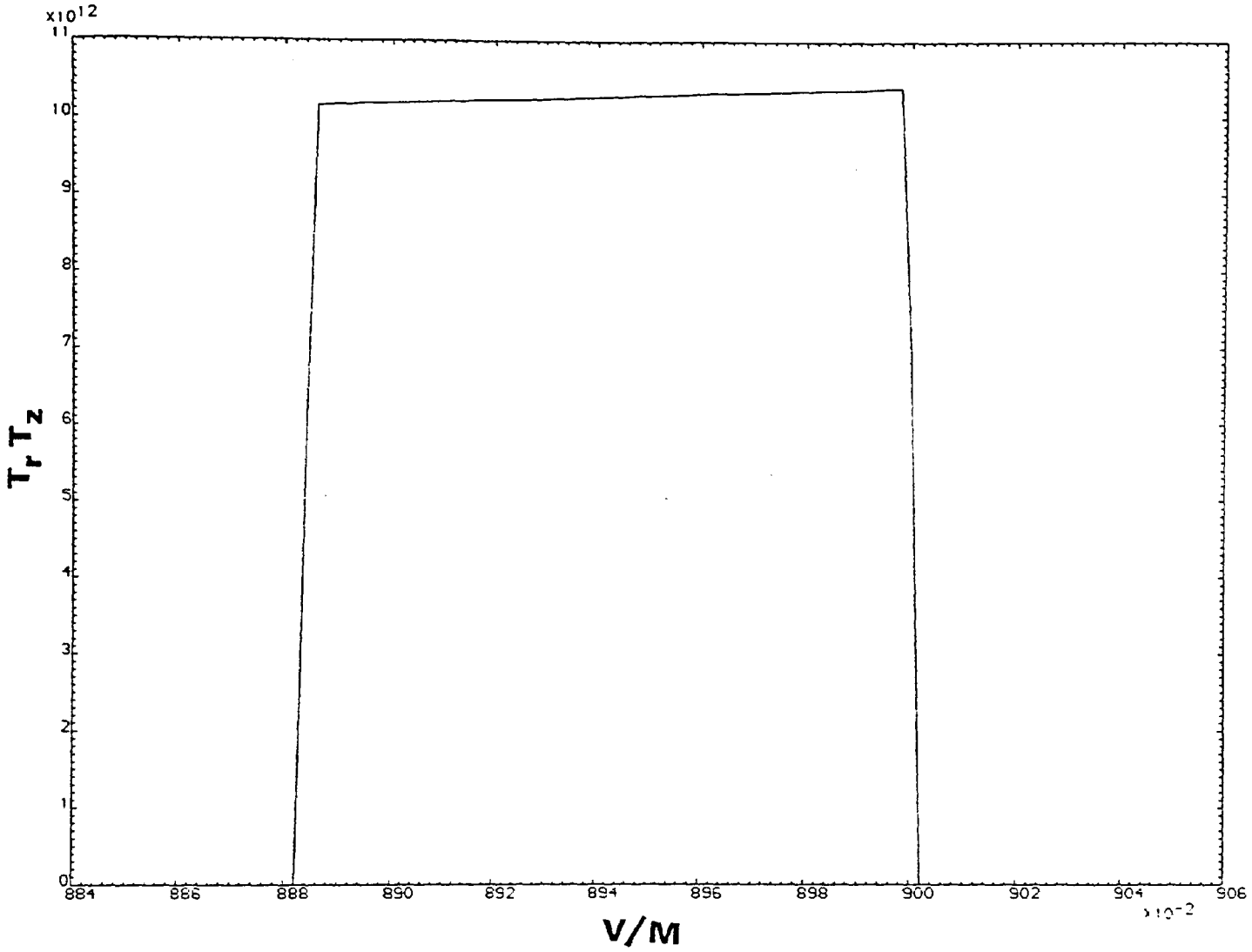

Fig. III.7.34 Trapping efficiency product plot for a Quistor with gauzes with 0.25 mm holes covering holes of 8 mm diameter in each end cap, shielded by second gauzes and with modified positions.

It was found that in practice the 0.25 mm holes were tending to close up when the gauze was formed. This led to relatively low transparency. However, if the size of the holes were increased, then this problem would be of far less importance. Therefore, equivalent data has also been produced for the case of a curved gauze with 0.5 mm holes.

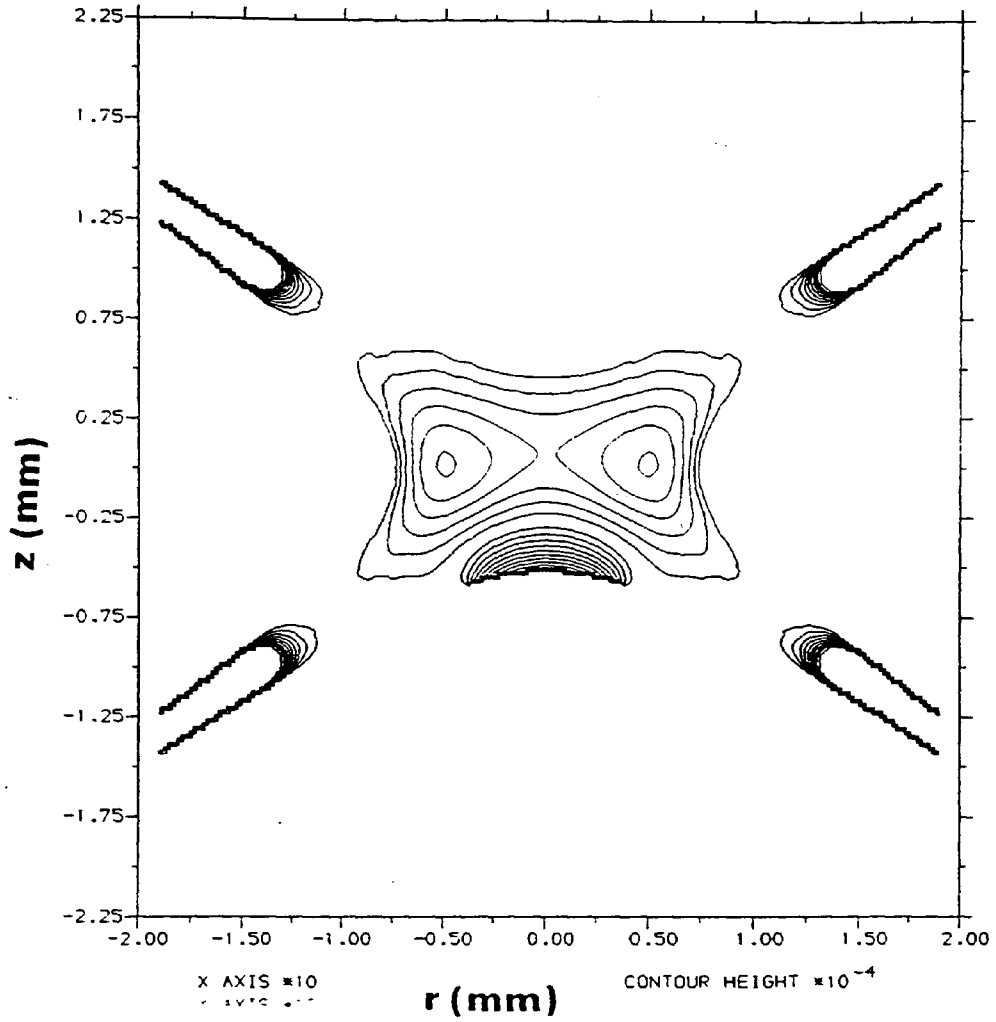

Fig. III.7.35 The electric field distortion due to gauzes with 0.5 mm holes covering holes in the end caps of 8 mm diameter, shielded by second gauzes and with modified positions.

The adjustment has increased to about 0.043 mm as would be expected, and, not surprisingly, the residual distortion has increased; the maximum value here is 0.0207 V.

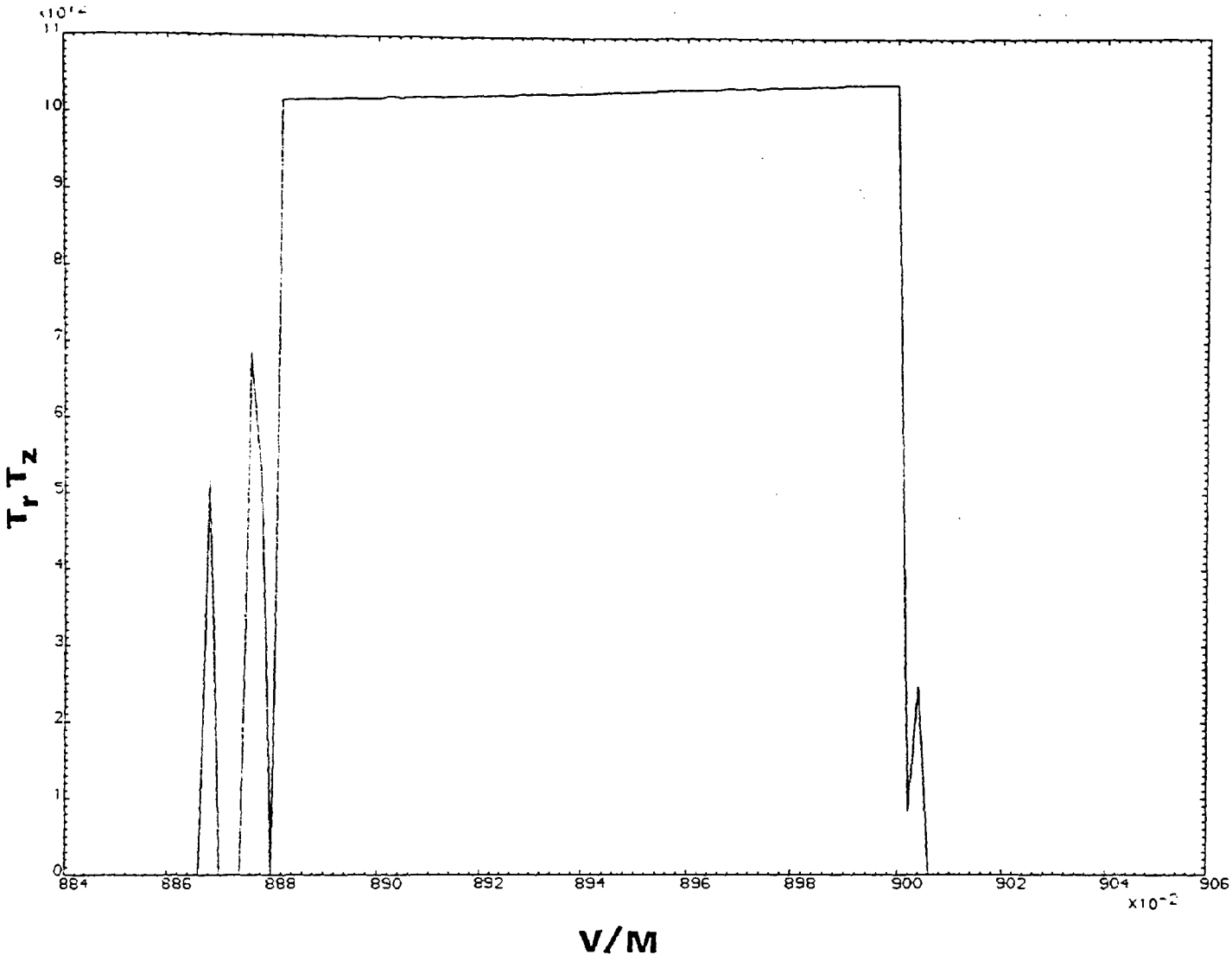

Fig. III.7.36 Trapping efficiency product plot for a Quistor with gauzes with 0.5 mm holes covering holes of 8 mm diameter in each end cap, shielded by second gauzes and with modified positions.

Now some effects of distortion in the plot are visible. Both boundaries show some "zig zag" effects, so some peak splitting could be expected. The size of this effect is quite small however, and the resolution at the right hand boundary has fallen only slightly to about 1800.

Thus the larger hole size in the gauze would lead to a slight theoretical drop in performance, but would certainly

give much greater sensitivity to the Quistor. This seems to be a good trade-off.

It must be said that the precision of manufacture which can be achieved for the end caps, and especially the accuracy of the mounting of the gauze, could probably not be expected to be more than about 0.01 mm. This being about the same as the required adjustment in the gauze position for the 0.25 mm hole size gauzes, the meaning of the adjustment may be limited in that case.

For the gauze with 0.5 mm holes, however, the adjustment becomes much more meaningful, and without making it, it is doubtful whether the gauze with larger holes would lead to good results.

i) The distortion produced by the space charge of trapped ions.

When the Quistor traps ions, those ions will necessarily have charge. As the number of ions trapped increases, the charge of the trapped ion cloud increases. Finally no more ions can be trapped because the net force trapping the ions is equal to the net electrostatic force of the ions which mutually repel each other.

Long before this point is reached, the performance of the Quistor in terms of resolution will be severely affected by the distortion in the Quistor's electric field produced by the charge cloud.

The fields program was modified (see above) in order to generate what was felt to be a typical space charge related electric field. The program also related the maximum space charge density, to the total number of ions trapped. When entered into the simulating program, this field could be

multiplied by the appropriate ratio in order to give the field due to some different number of ions.

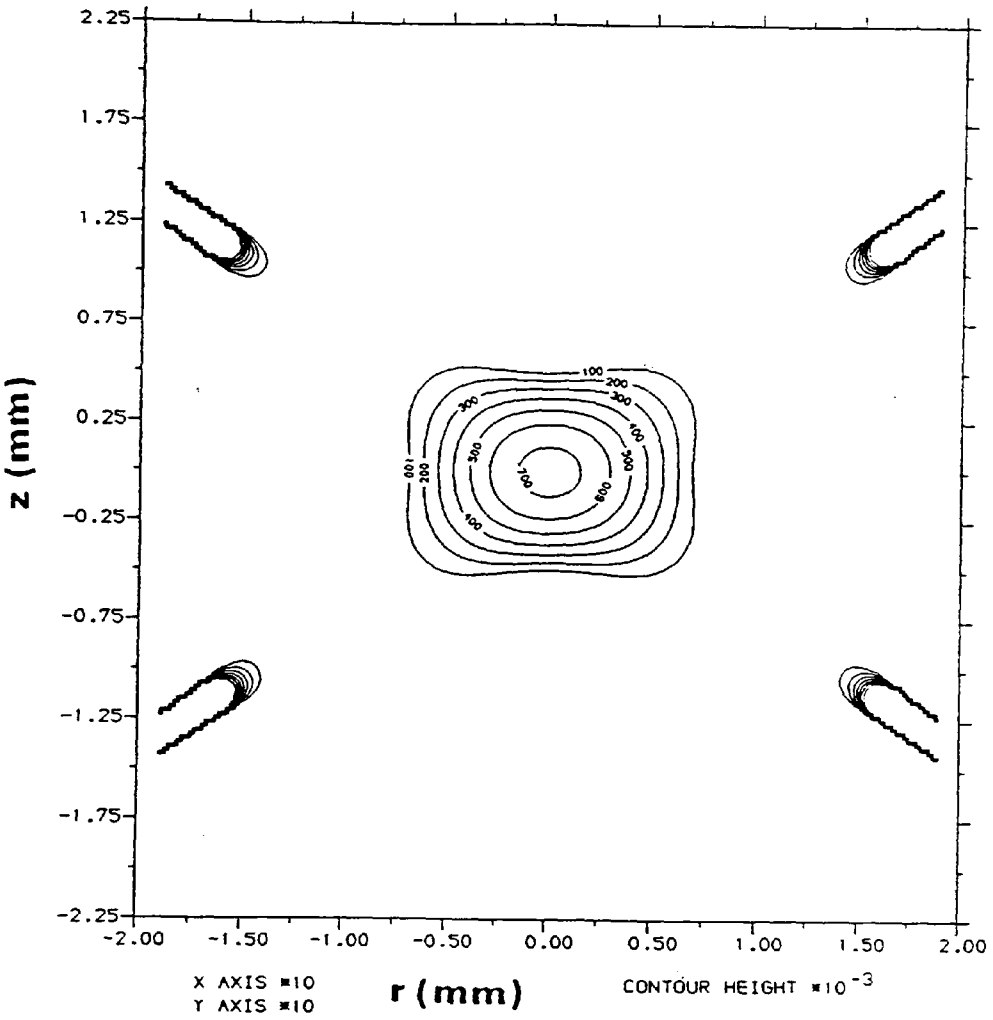

Fig. III.7.37 The electric field due to 4.251 x 10^6 ions trapped in the Quistor. This corresponds to a space charge density at the centre of the trap of 10^{-15} C mm^{-3}

As might be expected, the space charge has produced a potential field with a maximum positive value at the centre of the trap, but with a value of zero at the Quistor electrodes.

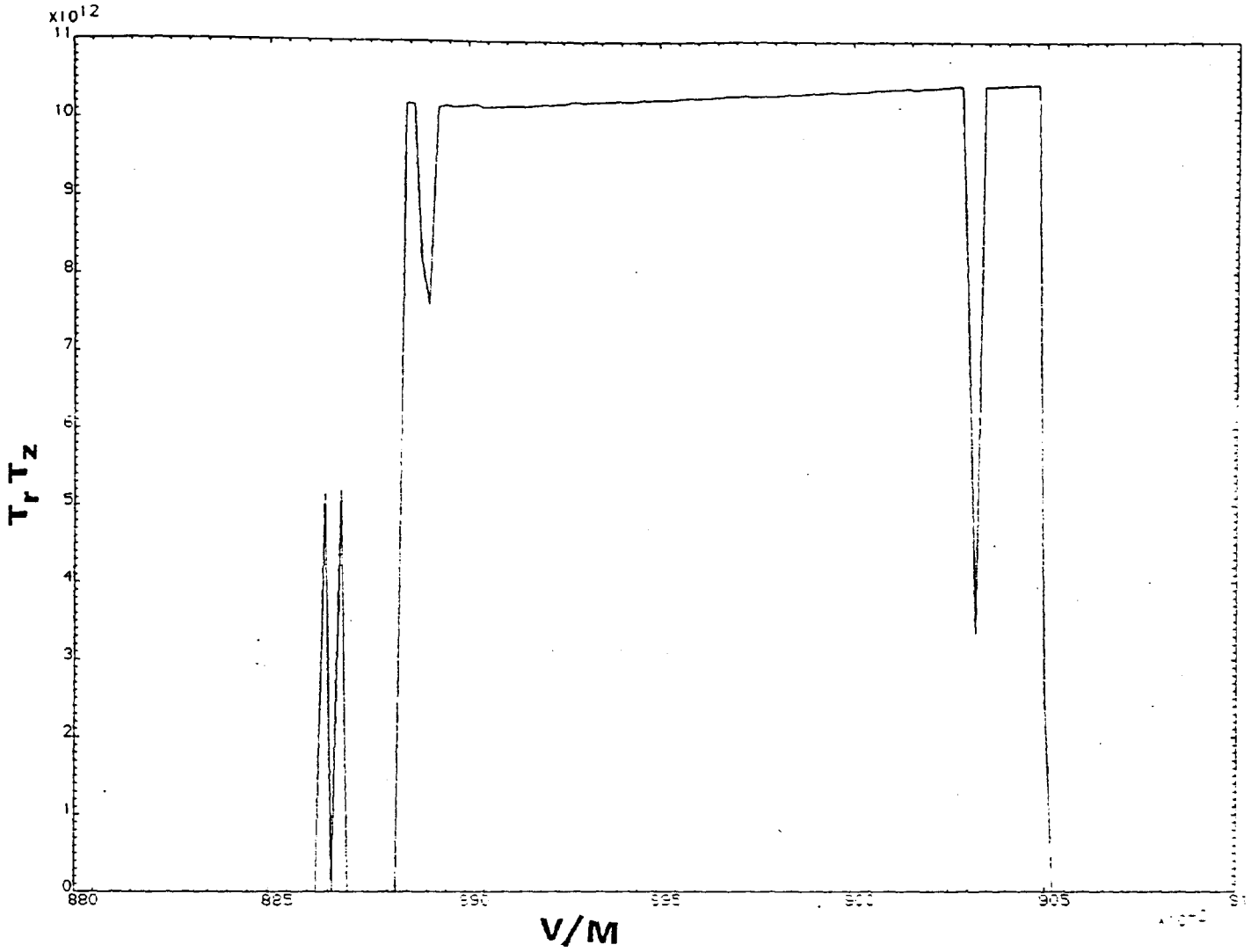

Fig. III.7.38 Trapping efficiency plot for a Quistor whose electric fields are distorted due to the space charge of 10^5 ions.

The space charge has two effects upon the performance. Both boundaries have moved to the right, because the charge has effectively changed the DC to RF ratio. For motion in the r direction, the DC to RF ratio is higher since the ring electrode is negative, while the potential at the centre has become positive. For motion in the z direction, however, the end caps are positive and since the potential at the centre has become positive also, the DC to RF ratio is effectively lower. In accordance with the shape of the

stability diagram, then, both boundaries move to the right.

If the potential distribution was quadratic, this would be the only effect. However, the distribution undoubtedly contains higher (even) order terms, and these result in the "dips" which are visible at the edges (non - linear resonance lines), and consequent peak - splitting and loss of resolution. The resolution here is about 350.

j) Excitation voltages superimposed along the z axis

An excitation voltage superimposed upon the the Quistor's normal field is known (Refs. 44, 75, 93) to be able to improve the resolution of the device in the case where distortion in the Quistor's electric fields, such as that caused by the space charge of trapped ions, has reduced it. This means the application of a small AC voltage at a lower frequency than the main RF frequency, between the two end caps. This voltage has been referred to as a "tickle" voltage.

If the frequency of the exciting voltage matches one of an ions normal oscillation frequencies, (i.e. β_z / 2, 1 - β_z / 2 or 1 + β_z / 2) then the ion is likely to gain energy from the exciting field. In that case, its amplitude of motion will increase and the ion will be lost from the trap. In other words, this effect can be used to eject ions from the trap selectively depending upon their β_z values.

By selecting a frequency which is slightly less than half the RF frequency, ions with β_z values just below 1 are ejected in this way. By so doing, it is possible to increase the resolution of the β_z = 1 boundary, in cases where its resolution has fallen due to the presence of space charge or other distortions. In effect, the

resonance reinforces the boundary.

This is borne out by the following plot.

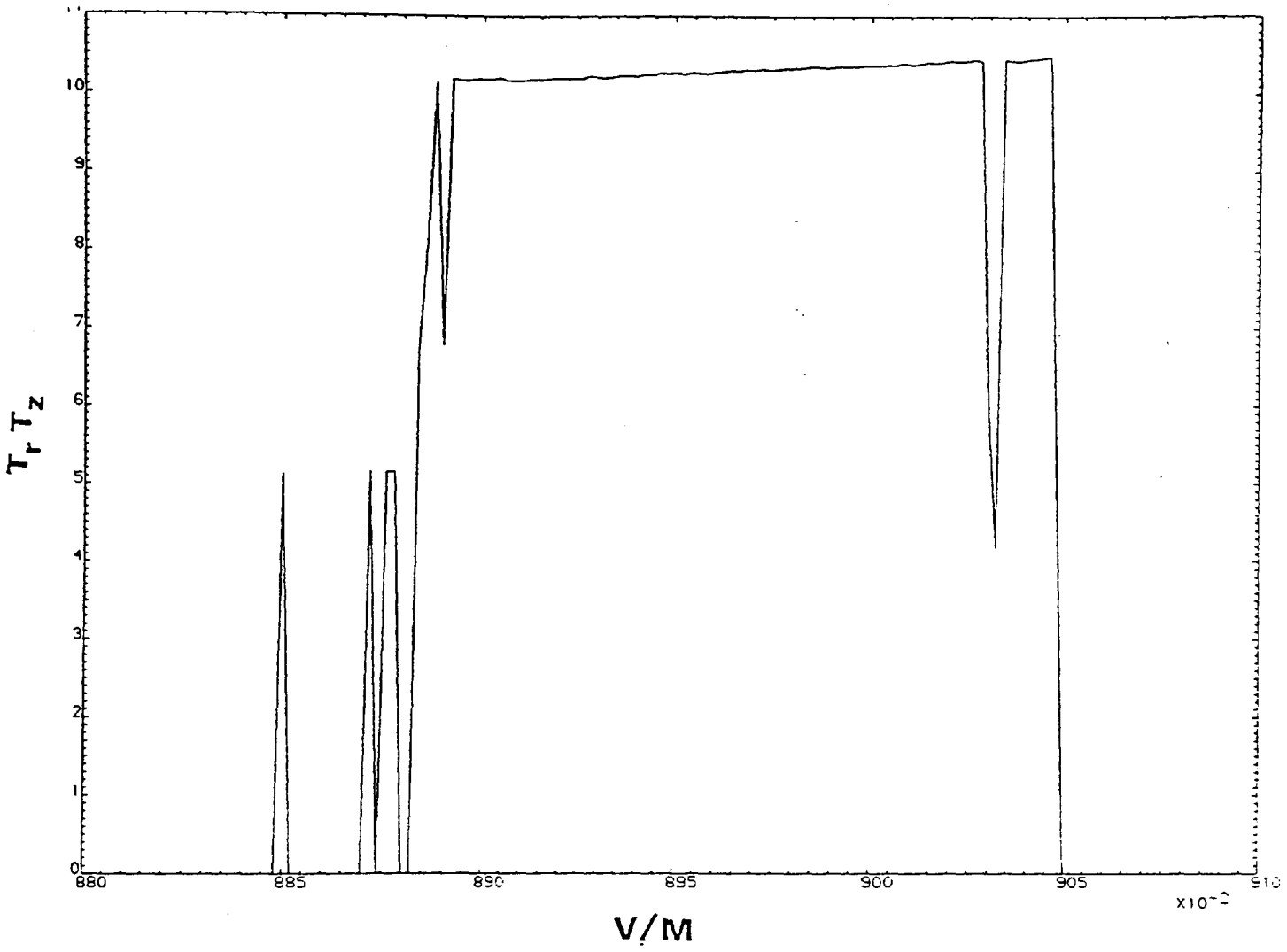

Fig. III.7.39 Trapping efficiency plot for a Quistor whose electric fields are distorted by the presence of 10^5 ions, but with 0.01 V / mm electric field superimposed in the z direction at 0.98 MHz.

The resolution here has improved from about 1/350 to 1/600 as a consequence of the superimposed field. This approach is of great value in the Finnegan Mat Quistor system, where the end cap electrodes are earthed. However,

where (as in the present system) the end caps have RF voltages applied to them, it is not possible add an additional small voltage between the end caps to them.

This effect has also been used in the Finnegan Quistor system operated (Refs. 99, 101) in the total pressure mode, in order to eject selectively from the trap, ions or groups of ions, depending upon their β_z values and, thus, their mass.

The effect is also used (more gently) to increase the kinetic energy of selected ions. The ions then undergo collisions with the buffer gas, resulting in ion fragmentation reactions. This is a very valuable technique in MS - MS experiments.

IV Construction of the prototype Quistor heads

1) The vacuum system.

It is wise at this point to say something about the vacuum system used in all the experimental work which follows. The vacuum system is UHV equipment supplied by Leisk Engineering Ltd. It is fitted with an oil diffusion pump backed by a rotary pump. A liquid nitrogen vapour trap is fitted and when this is in use the system is normally capable of achieving a pressure of about 2×10^{-8} mBar after being pumped for several days. If the system is thoroughly baked for a few days, a pressure of about 6×10^{-9} mBar can be achieved after cooling down again.

The vacuum chamber has a range of ports available, including several FC63 and FC35 ports. The Quistor was fitted into one of the FC63 ports.

The vacuum system is fitted with a Penning UHV pressure gauge sensitive to pressures in the range 10^{-4} to 10^{-10} mBar inside the vacuum chamber. Two Pirani gauges sensitive to pressures down to about 10^{-3} mBar are located in the backing line.

Note that where a pressure has been indicated in this chapter, this is the pressure shown on the Penning gauge. The sensitivity of the gauge to different gases is not the same, mainly because the ionisation cross sections vary. The gauge is calibrated for Nitrogen, but the manufacturer provides data indicating the relative sensitivity of the gauge to several gases. In order to find the true pressure, the measured pressure of a given gas must be divided by the factor shown.

Gas	Factor
Nitrogen	1.000
Helium	0.160
Neon	0.240
Hydrogen	0.480
Argon	1.200
Mercury	4.000

Fig. IV.1.1 Sensitivity of the Penning gauge to selected gases

A needle valve allows a finely controlled flow of gas into the vacuum chamber. Initially the high pressure side of this was open to the atmosphere, but later an evacuateable gas line was added, allowing any selected gas to be bled into the system without impurities.

A Dataquad quadrupole mass filter is also fitted to the vacuum system. This mass spectrometer has a mass range of 100 and can detect partial pressures down to about 10^{-13} mBar. The resolution of the mass filter is claimed to be a peak width of 1 AMU at 10% valley throughout the mass range, although it was found to be frequently poorer.

Some spectra produced by this device are included here, partly for comparison with the spectra produced by the Quistor which follow later in this chapter. Note that each has been produced twice, on different scales, so that both large and small peaks can be made out.

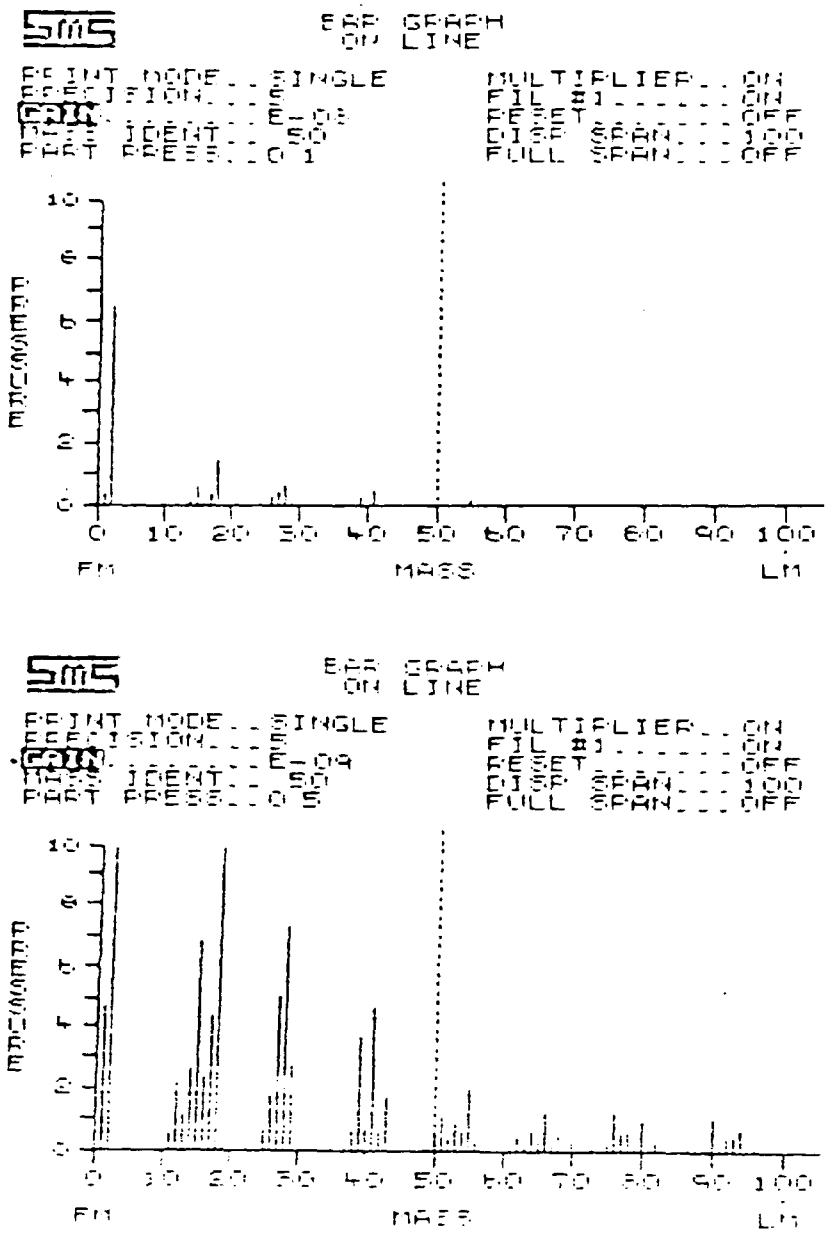

Fig. IV.1.2 Dataquad background spectra at 2 x 10^{-8} mBar with gains of 10^{-8} mBar and 10^{-9} mBar full scale, respectively.

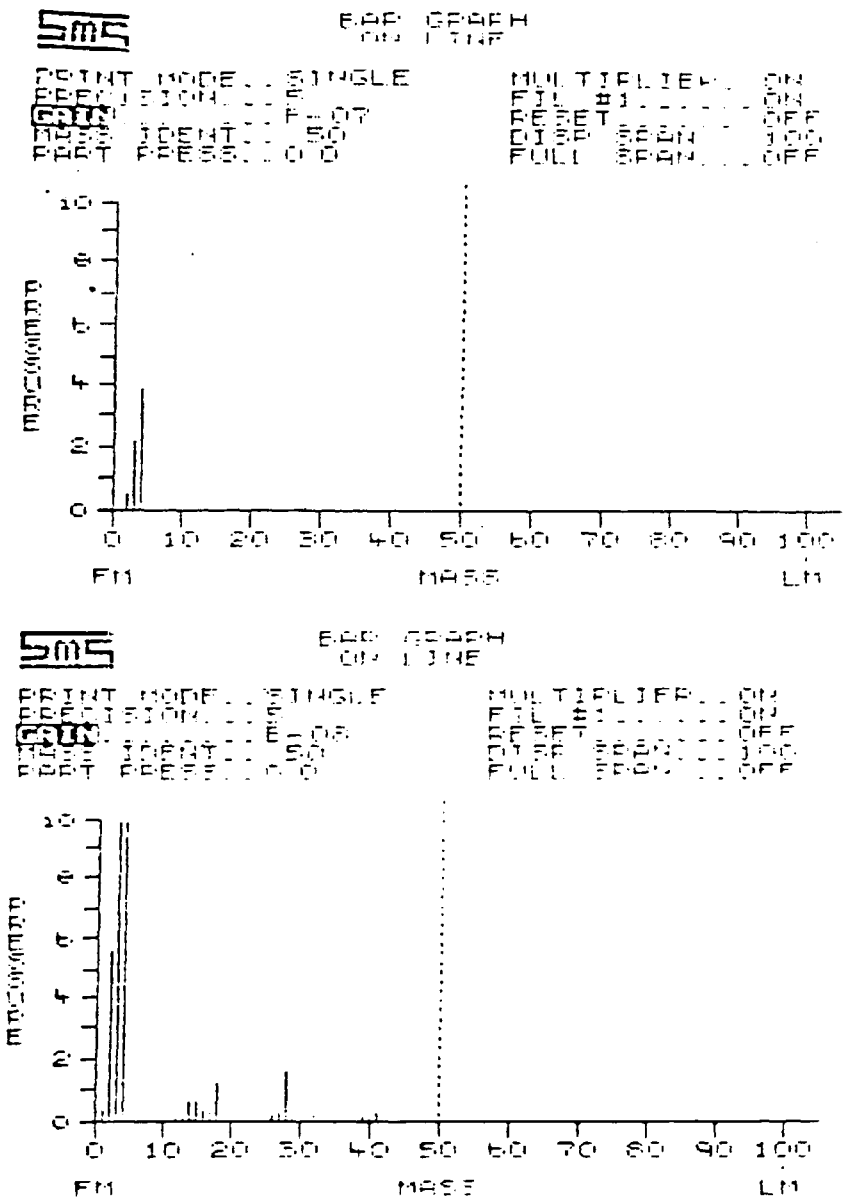

Fig. IV.1.3 Dataquad spectra of Helium at 4.5 x 10^{-7} mBar with gains of 10^{-7} mBar and 10^{-8} mBar full scale, respectively.

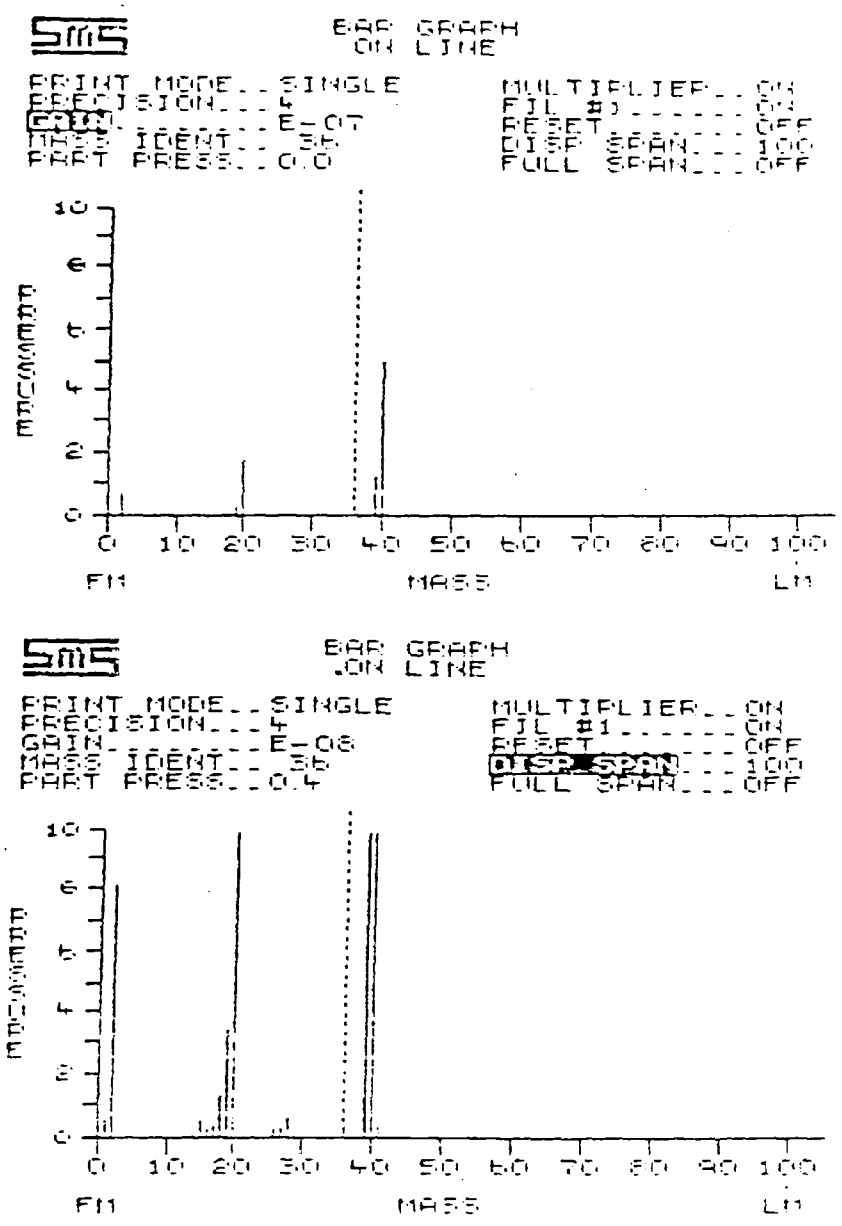

Fig. IV.1.4 Dataquad spectra of Argon at 4 x 10^{-7} mBar with gains of 10^{-7} and 10^{-8} mBar full scale, respectively.

2) The mechanical construction of the first prototype Quistor.

The first prototype Quistor head was constructed of brass. This was because brass is easy to machine and it was convenient for a first attempt. The head consisted of a filament assembly, the Quistor electrodes, and a channel plate assembly. The diagram below is full scale.

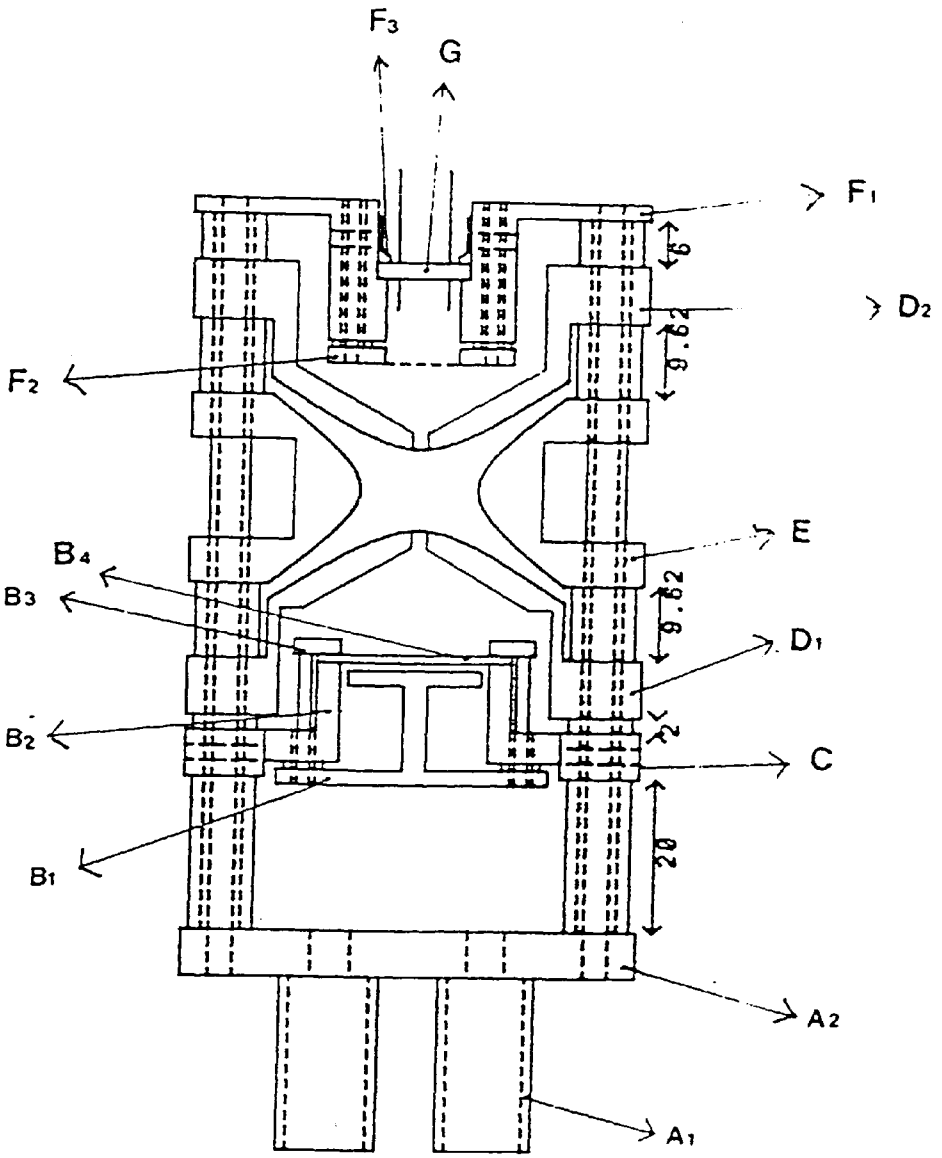

Fig. IV.2.1 The first prototype Quistor, assembled.

The Quistor head was mounted upon an FC63 feedthrough flange which was available because it had been part of a dismantled Quadrupole mass filter system. The flange has 11 feedthroughs; 8 equally spaced in a circular pattern around the side, and 3 equally spaced in a triangle near the centre of the flange. On the inner surface of the flange, holes were tapped into the steel for mounting purposes.

The convention has here been employed that the "top" of the Quistor head is that side furthest from the flange; the "bottom" is nearest to the flange. The above diagram is drawn according to this convention.

The value of r_0, the distance between the centre of the trap and the nearest point on the ring, was 7.5 mm. This means that the value of z_0, the distance between the centre of the trap and the nearest point on both end caps, was about 5.3 mm. The Quistor was designed to have an outer radius of 29 mm, and the Quistor end caps and ring surfaces extended to 19 mm. Between these radii, each electrode was designed to accommodate the ceramics, spacers and studding required to assemble the Quistor, and also most of the electrical connections passed through in this position.

There was a base (A_2) mounted upon the flange upon which the Quistor was assembled. The metal tubes (A_0) were for electrical shielding purposes. The Quistor was assembled upon 3 lengths of M3 studding, which were insulated by 5 mm outer diameter ceramic tubes. These in turn had 5 mm inner diameter, 8 mm outer diameter ceramic washers threaded upon them in order to separate the Quistor's various electrodes. The whole assembly was held together by three nuts at the top of the head.

A channel plate was selected in preference to other forms of electron multiplier detectors because the channel plate is easy to mount and very compact. A single channel plate may be expected to provide a linear gain of up to 1000 or so; it was not clear initially whether this would be sufficient or not, but channel plates may be operated by cascading them in pairs in order to provide for greater gain levels. This is easily accommodated into a design intended for only one plate.

The channel plate (B_4) was mounted into a small separate assembly consisting of 3 electrodes. The topmost electrode (B_3) was in contact with the upper side of the channel plate and the middle electrode (B_2) was in contact with the lower side of the channel plate. The lowest (B_1) was a Faraday plate for collecting the electron current output from the channel plate.

This assembly mounted into the main Quistor head by fitting it into a ring (C) which had locating grub screws fitted into the side. The object of this procedure was that the (delicate) channel plate could first be mounted into the smaller assembly before the entire Quistor was assembled. Unfortunately, it was found that this did not work very well since this proved to be physically awkward in assembly.

The lower Quistor end cap electrode (D_1) was fitted next, followed by the ring electrode (E_1) and the upper end cap electrode (D_2). Each of these electrodes were separated by ceramic spacers. In the case of the ring and end caps, the length of these ceramics was very critical and so they had been ground to length. The diameter of the hole in each end cap through which electrons and ions passed was 2 mm.

The filament consisted of a circular ceramic button (G) in which two small metal pillars were mounted upon which the filament was welded. The button was placed into a holder (F_1), and held in place with a small ring (F_3) which in turn was held in place with some grub screws in the holder. Upon the lower end of the holder was mounted a "gate" or accelerating electrode (F_2), connected electrically and mechanically with the upper side of the filament holder. This completed filament assembly was mounted upon the rest of the Quistor head.

3) Electrical connections made to the electrodes of the first prototype.

Most of the electrical connections made in the Quistor were made by passing wires, insulated by ceramic, along the outside of the Quistor, through holes in each electrode at a radius of 24 mm. In each case, at the appropriate electrode, the wire was bent round and screwed down onto the metal surface.

The channel plate (B_4) and Faraday collector plate (B_1), however, were connected to two of the inner feedthroughs and wires connecting to these passed through the shielding tubes and were connected to the electrodes at a smaller radius from the centre. The channel plate connection was made via M1.6 studding, insulated with ceramic, which passed through the Faraday plate and the channel plate base electrode (B_2), in order to connect to the channel plate HT electrode (B_3).

Externally, the Faraday plate was connected to an amplifier, the base of channel plate to -15V, and the channel plate to -1500V. The base of the channel plate needed to be at -15 V in order to provide a bias to ensure that electrons emitted from it were drawn efficiently to the Faraday plate.

The end caps (D_1 and D_2) were connected together and to one of the RF outputs, the ring (E) to the other RF output.

The filament holder (F_1) was not connected. The filament (G) itself was connected to the filament power supply, which was capable of having its bias potential switched between -80 V and +15 V. The gate electrode (F_2) was switchable in potential between ground and -80 V. This switching was controlled digitally, and the filament and gate potentials

were switched in antiphase.

When the filament was at -80 V, and the gate electrode was at ground, the electron beam was on and ionisation in the Quistor was taking place. When the filament was at +15 V, and the gate electrode at -80 V, the electron beam was disabled. This was necessary so that trapped ion output could be detected without a large random output consisting of untrapped ions obscuring the signal.

4) Results obtained with the first prototype Quistor.

Initially, the Quistor was operated using the RF only scan mode, mode (a) in section I.4. In other words, no DC voltages were applied to the Quistor electrodes. The RF voltages were set at a fairly low initial value for ion trapping while the electron beam was on. Subsequently, the RF voltages were ramped with an 8 bit DAC, in order to successively eject the trapped ion species by making them unstable. This was convenient at the time for the following reasons :

i) It was not necessary to switch the electron beam on and off at a high speed. It could therefore be done within a simple BASIC program using the 10 ms clock built into the BBC computer to get consistent timing.

ii) Since output was produced in one continuous stream, it was a simple matter to display the output upon a digital storage oscilloscope. This was required because the electronics and software required to detect pulses at intervals, between which the electron beam was on and so producing noise, were not yet available. The oscilloscope used was able to output the data to an X-Y plotter for a permanent record.

iii) By ramping quickly, successive data pulses

generated by increments in the RF voltage were superimposed upon each other. Since the resolution of the Quistor was quite poor, each individual pulse would have been very small because only a few of the ions of any one mass would be ejected in one pulse. It was necessary, however, to write the part of the program which caused the DAC to ramp, in assembly language because BASIC was too slow.

The mass range of the spectra produced was roughly from 15 to 40. The spectra depended strongly upon the initial RF voltage selected for ion storage. If a low initial RF voltage was selected, then the sensitivity of peaks, especially those at high mass, was low. On the other hand, if the initial RF voltage was high, then low mass ions would not be trapped in the first place. Tentative identification of ion species was possible and the peak widths were about 1.5 to 2 AMU. The level of background noise was very high.

Some typical scans follow.

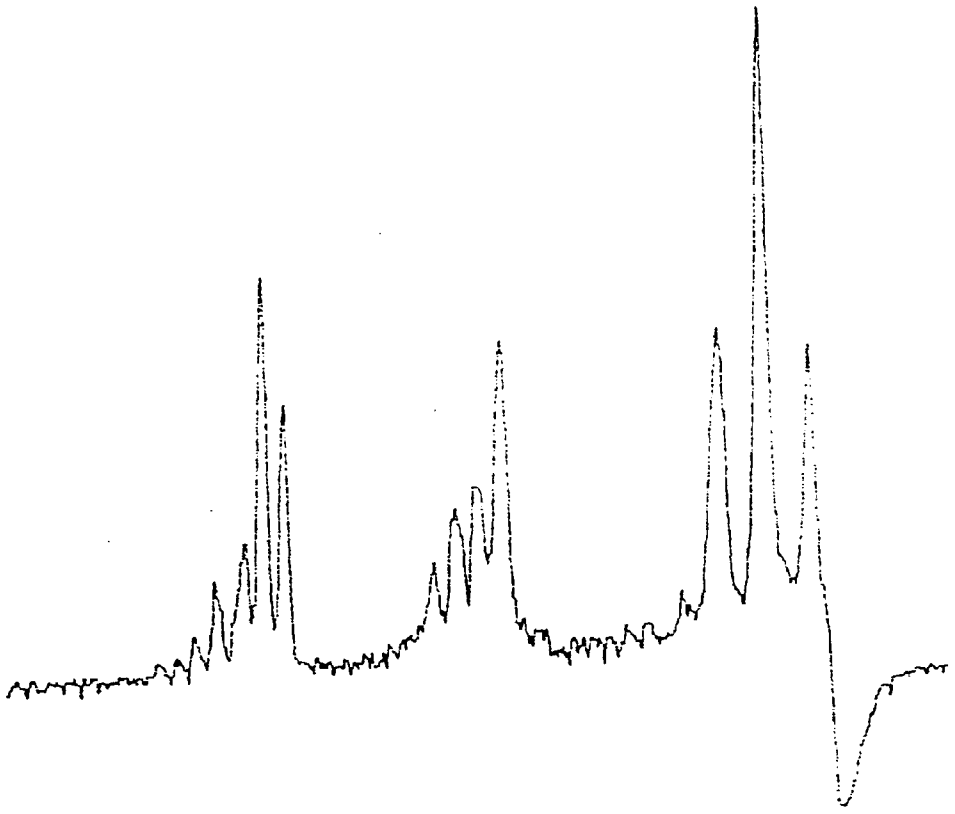

Fig. IV.4.1 Early recorded background scan at 2 x 10^{-7} mBar.

The above scan was recorded using the approach described, but after the results had been optimised by selecting the most appropriate scan speed and ionisation time. Earlier results had been poorer.

The Quadrupole mass spectrometer fitted to the vacuum system was operated at the same time in order to record the conventional spectrum below.

Some air was bled into the vacuum system through the needle valve and the following Quistor mass spectrum was recorded. Note that the vertical scale of the following spectrum had been reduced.

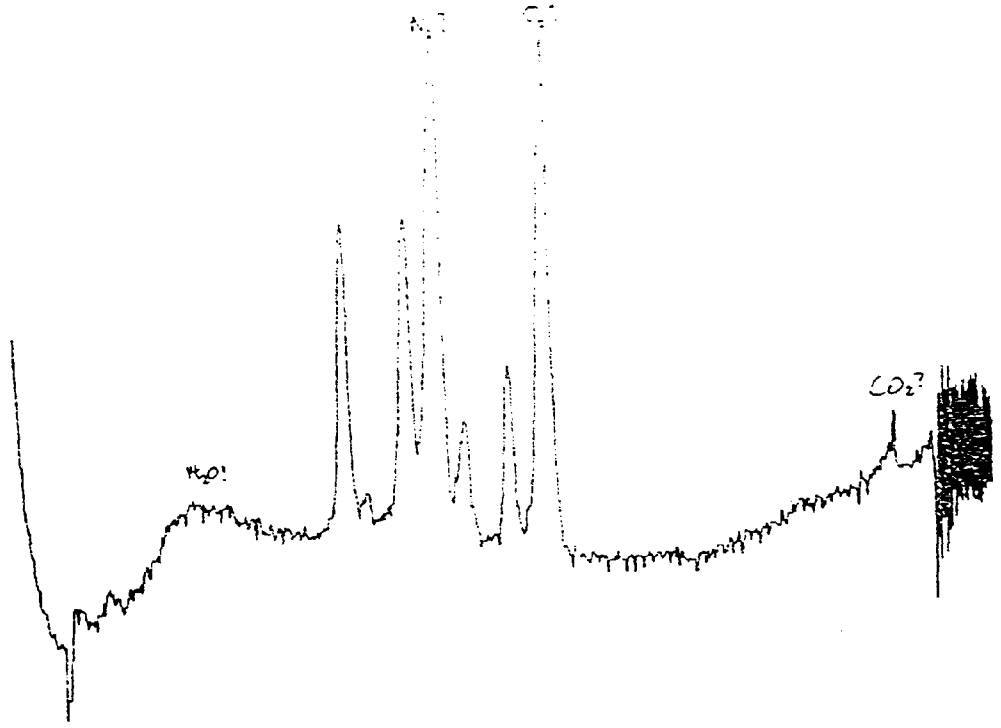

Fig IV.4.2 Early Quistor spectrum of air at 5 x 10^{-6} mBar.

5) Mechanical construction of the second Quistor prototype.

The second prototype Quistor was constructed of stainless steel. This allowed more accurate machining work, was more reliable in use at high temperatures, and was not affected by exposure to the atmosphere or other gasses. While being of essentially a similar design, it incorporated a number of improvements in design on the basis of experience. Consequently it was much more compact, lighter, and easier to assemble (although it is now felt that, especially in the last respect, further improvements are possible). The outer radius of the electrodes was still 29 mm, while the curved surfaces of the electrodes also extended to a radius of 19 mm. The value of r_0, the distance between the centre of the trap and the nearest point of the ring, was still 7.5 mm.

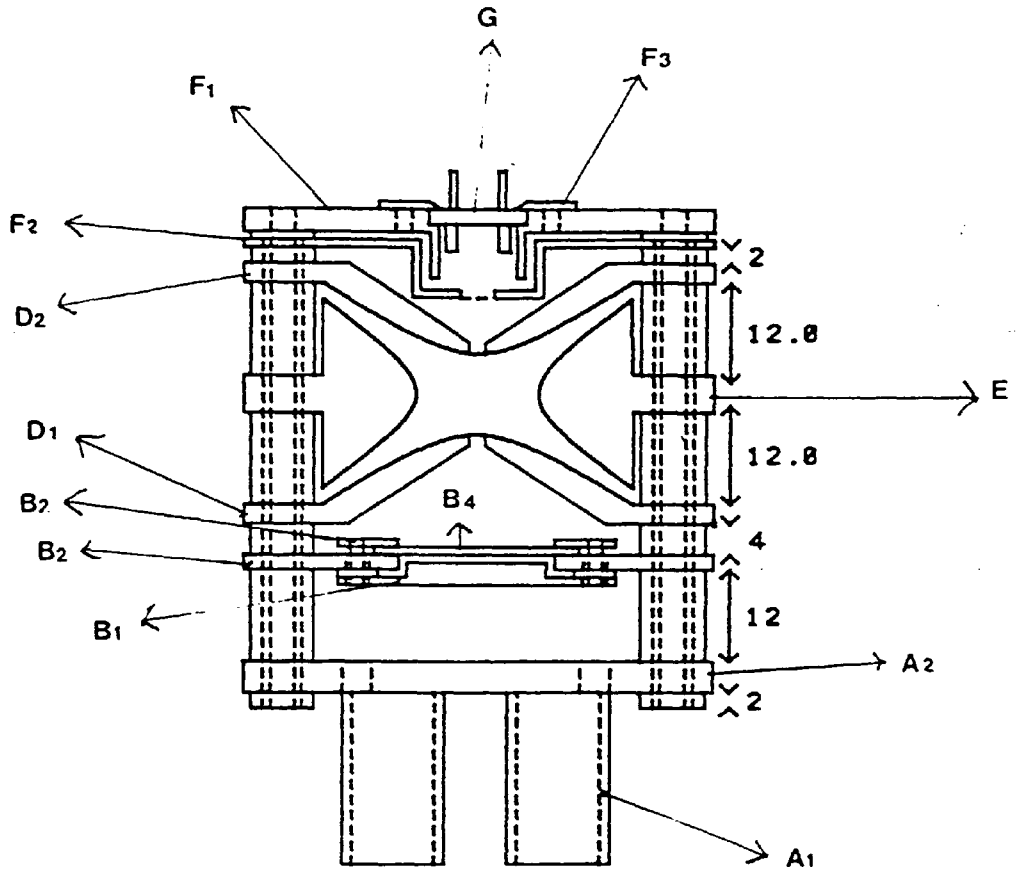

Fig. IV.4.3 The second prototype Quistor, assembled.

As before, the Quistor was mounted upon a base (A_1 and A_2), which was bolted onto the flange. The Quistor assembly was held together in the same way, using M3 studding, and ceramic insulators and spacers. The electrical connections to the electrodes, however, were made using M2 studding instead of wire. The plate to which each contact was made had either a 2 mm hole or an M2 tapped hole through which the studding passed. In the former case, a nut was used to tighten onto the plate in order to make the contact reliable.

The channel plate (B_4) was held in a similar assembly to previously, although it was now much more compact. The electrical connections to the Faraday plate (B_1) and the top of the channel plate (B_2) were made via two of the central feedthroughs on the flange, as before.

The Quistor end caps (D_1 and D_2) and ring electrode (E) were designed more compactly, although they were otherwise broadly similar. The hole in each end cap for ion and electron transmission, had been reduced to 1 mm diameter (although the diagram here shows them as 2 mm) in order to reduce the distortion resulting.

The filament assembly was of a somewhat different design. The gate electrode was mounted onto the Quistor assembly as a separate plate (F_2), followed by the filament holder (F_1). This had a recess at the centre which could accept the filament button (G). The filament was held in place with a small metal plate (F_3) which was screwed down onto it.

The potentials applied to each electrode were the same as in the first prototype.

6) Early results obtained with the second prototype Quistor.

Initially the second Quistor was operated in the the total pressure mode, as had the first, and for the same reasons. The results obtained were better; both the resolution, and the sensitivity had improved. This is mainly attributed to the reduction in electric field distortion caused by the reduction in the size of the holes in the end caps.

The improved electric field meant better resolution and this led to a better level of sensitivity in spite of the fact that the ability of electrons and ions to travel through the end caps had been reduced. This underlines the results of the computer simulation work (see chapter III) which indicates the importance of an accurate electric field for good results in the Quistor, and the adverse effect of the holes in the end caps upon the field.

The scans which follow are a good illustration of the effect described in section (3) above, that in the total pressure mode, scanning quickly improves the output intensity of the data because the ion pulses resulting from each increment are superposed. On the other hand, a consequence of this is that the resolution is poorer. The scans below are recorded at different speeds, the speed being controlled by a delay loop in the machine code. Each unit of the delay therefore corresponds to about 5 μs between voltage increments being applied. Since an 8 - bit scan was used (256 points), the total scan times were therefore about 1.2 ms multiplied by the quoted delay. The electron beam was on for 0.5 seconds and the voltage applied to the channel plate was 1400 V.

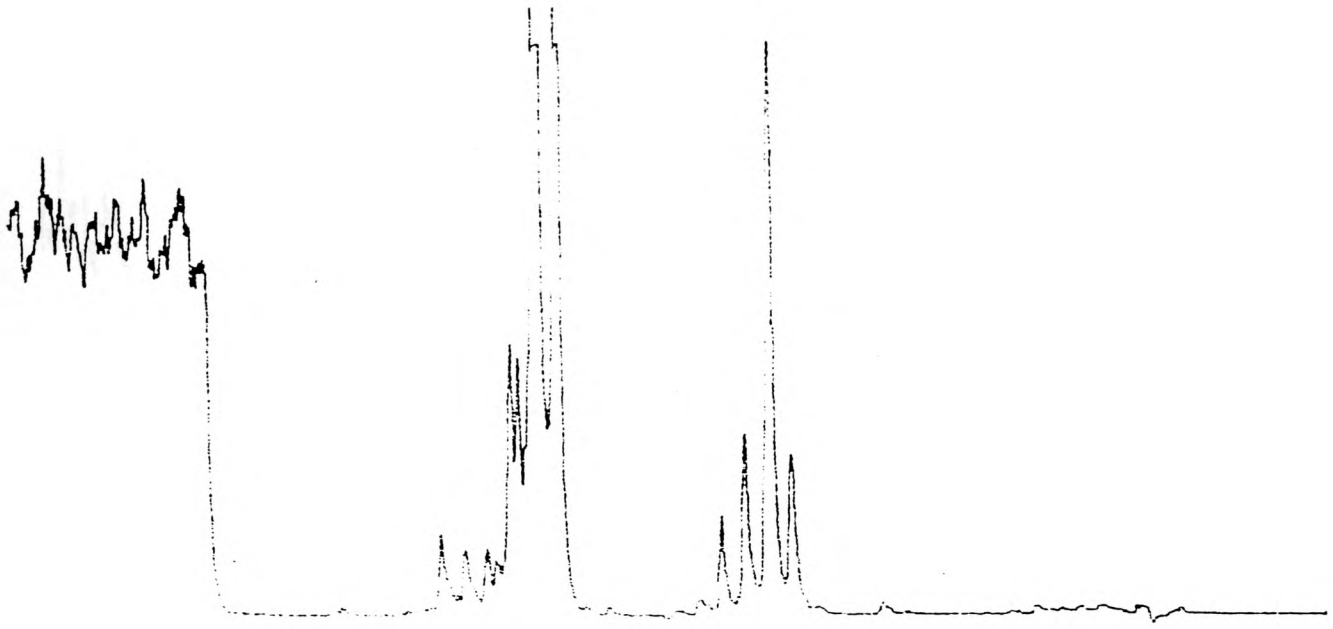

Fig. IV.6.1 Background scan with a delay of 10 between voltage increments (12 ms scan time approximately).

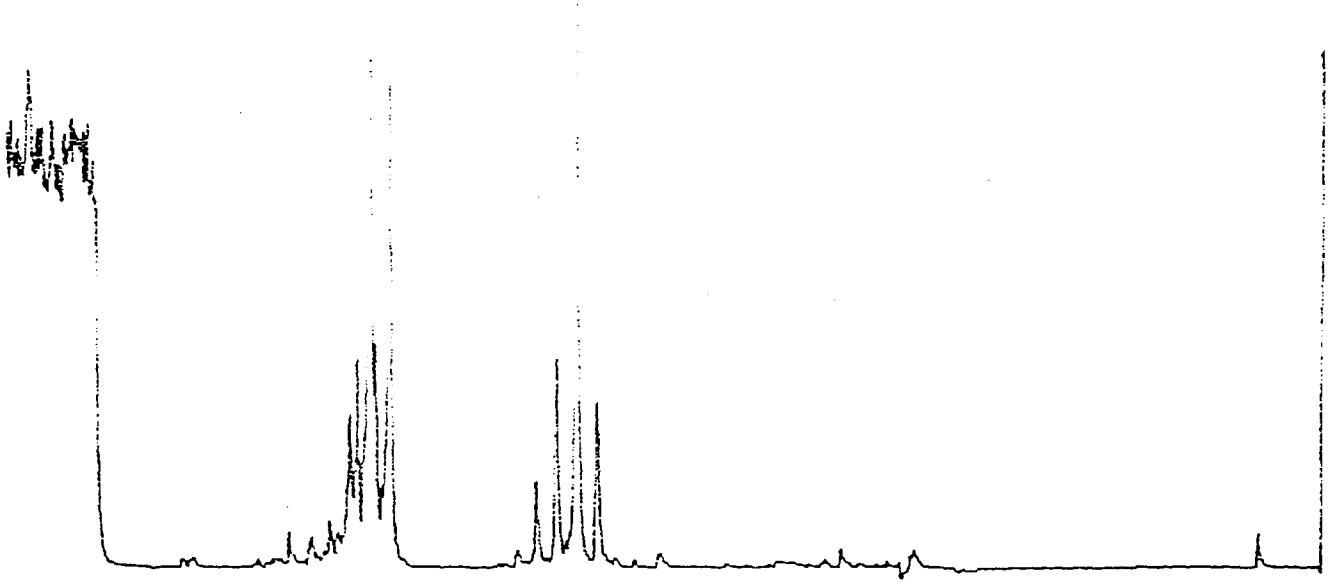

Fig. IV.6.2 Background scan with a delay of 20 between voltage increments (24 ms scan time approximately).

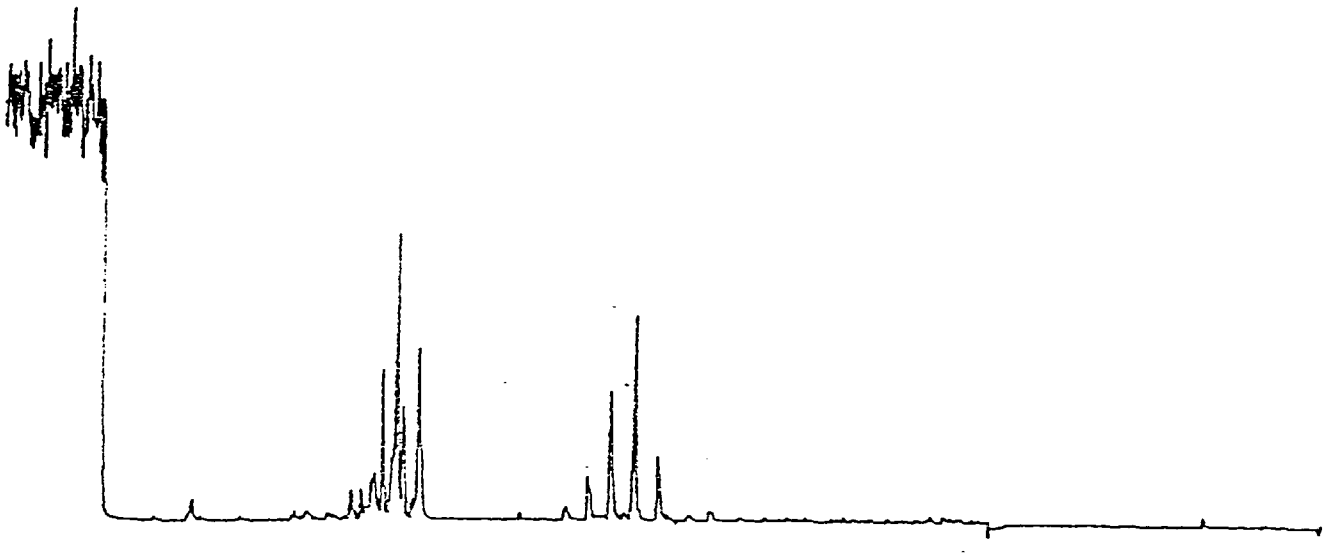

Fig. IV.6.3 Background scan with a delay of 50 between voltage increments (60 ms scan time approximately).

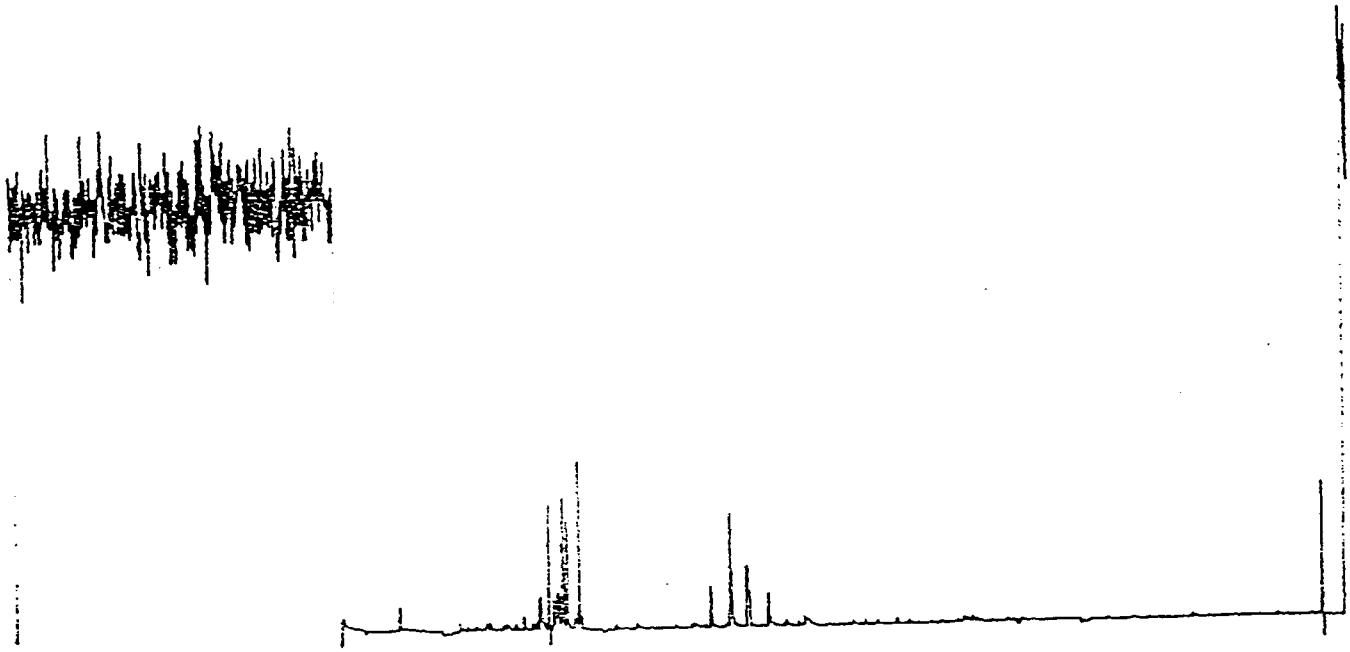

Fig. IV.6.4 Background scan with a delay of 100 between voltage increments (120 ms scan time approximately).

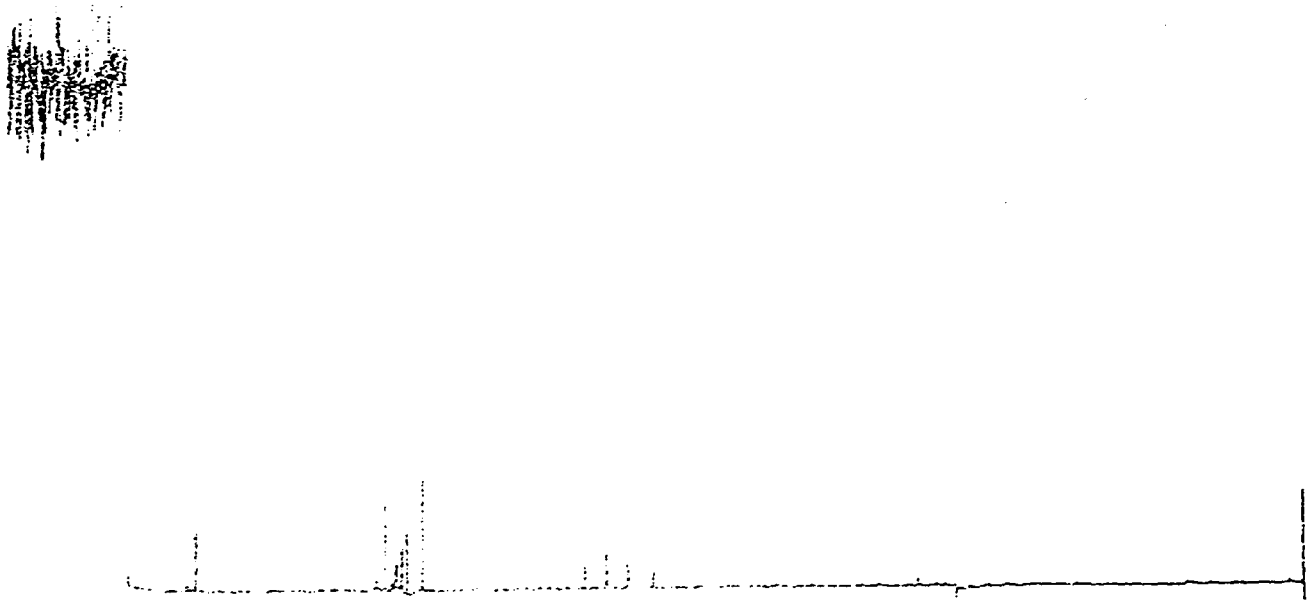

Fig. IV.6.5 Background scan with a delay of 250 between voltage increments (300 ms scan time approximately).

The resolution level in the slower scans is really quite good - a peak width of perhaps 0.25 AMU is achieved at mass 28. The signal to noise ratio has improved a good deal from the first prototype, although a lot of room for improvement remains. The mass range of the scan remains from about 15 to about 40.

On the left hand side of the scans, the untrapped ion current due to the electron beam still being on, is visible. Note that because the scans were obtained at different speeds, the oscilloscope had to be set at a different timebase and the horizontal scales are not the same.

The single channel plate was replaced by a pair in order to increase the gain. The voltage across the combination can thus be increased from a maximum of about 1500 V to about 2500 V, allowing for a gain level in excess of 10^6.

At about the same time as this occurred, the electronics required to interface the BBC microcomputer to the Quistor was produced. This meant that it was possible for pulses to be integrated, discarding the untrapped ion current during the ionisation time. The integrated pulsed were returned by an 8 bit ADC to the computer. The RF voltage was now also controlled by a 12 bit DAC rather than 8, although the resolution of the Quistor was not good enough to allow this to be used in full.

Nonetheless it was now possible to obtain mass spectra using the upper apex scan type (d) intended (see section I.4). Because of the DC:RF voltage ratio was now about 0.09 rather than 0, and because of the shape of the stability diagram, the mass range of the scan had increased to about 60. The peak width in this scan mode was about 0.5 at mass 40. Since the sensitivity of the device in this scan mode depends upon the resolution, the sensitivity was not

initially good. Nonetheless, reliable mass calibration and identification was now possible.

The spectra are displayed using the software written for the BBC which had now become available.

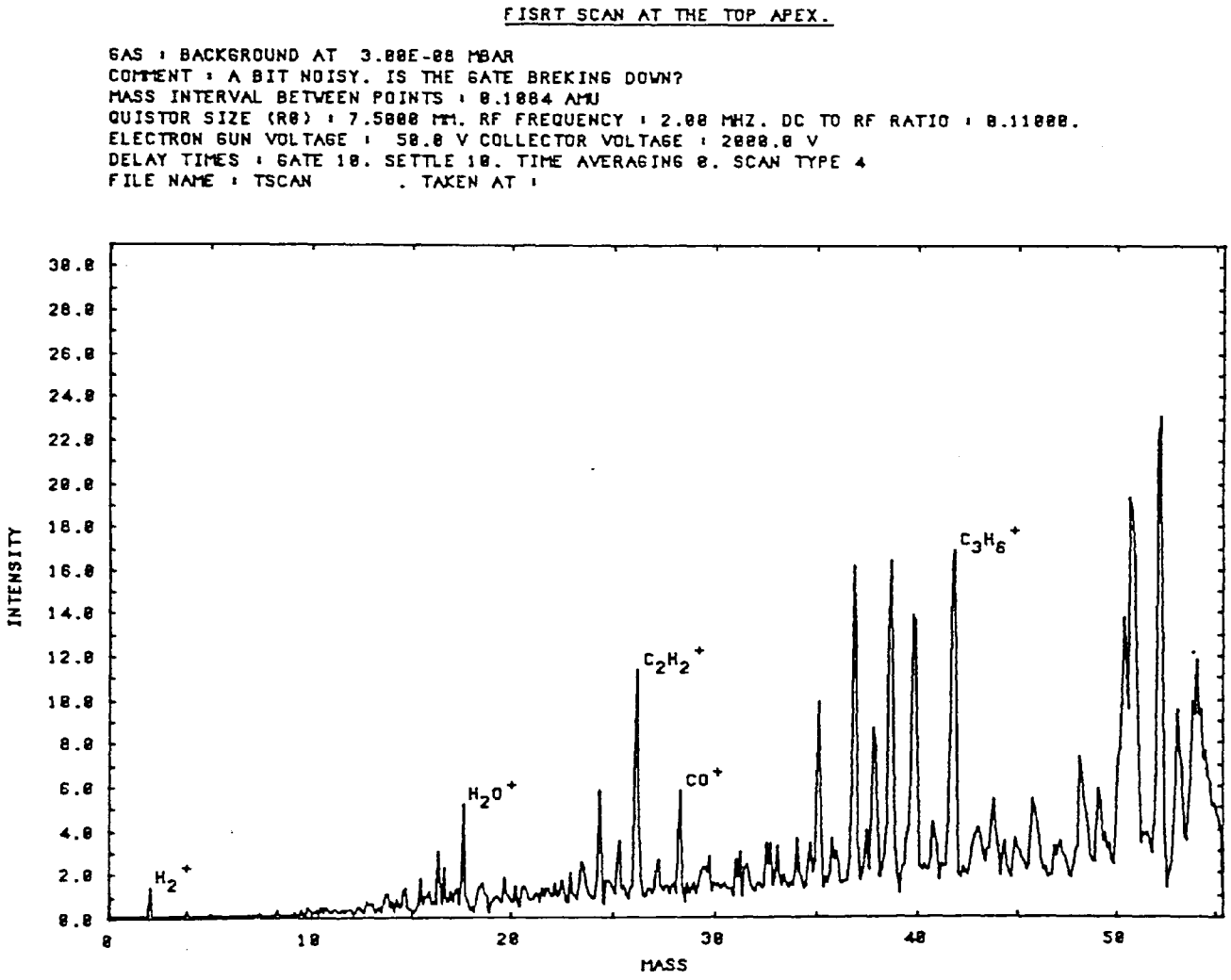

Fig. IV.6.6 The first successful background scan at the top apex.

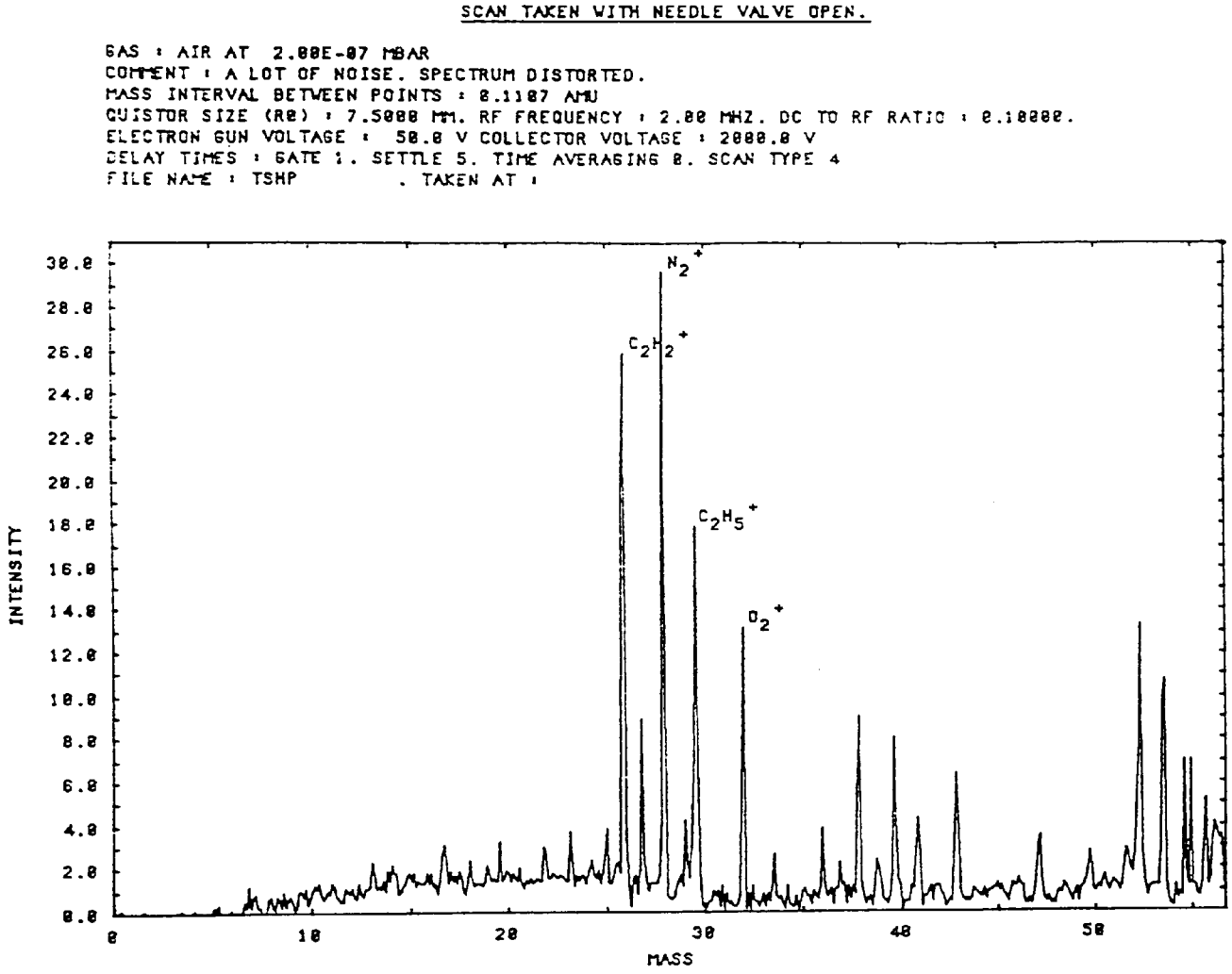

Fig. IV.6.7 An early spectrum of air at 2 x 10^{-7} mBar.

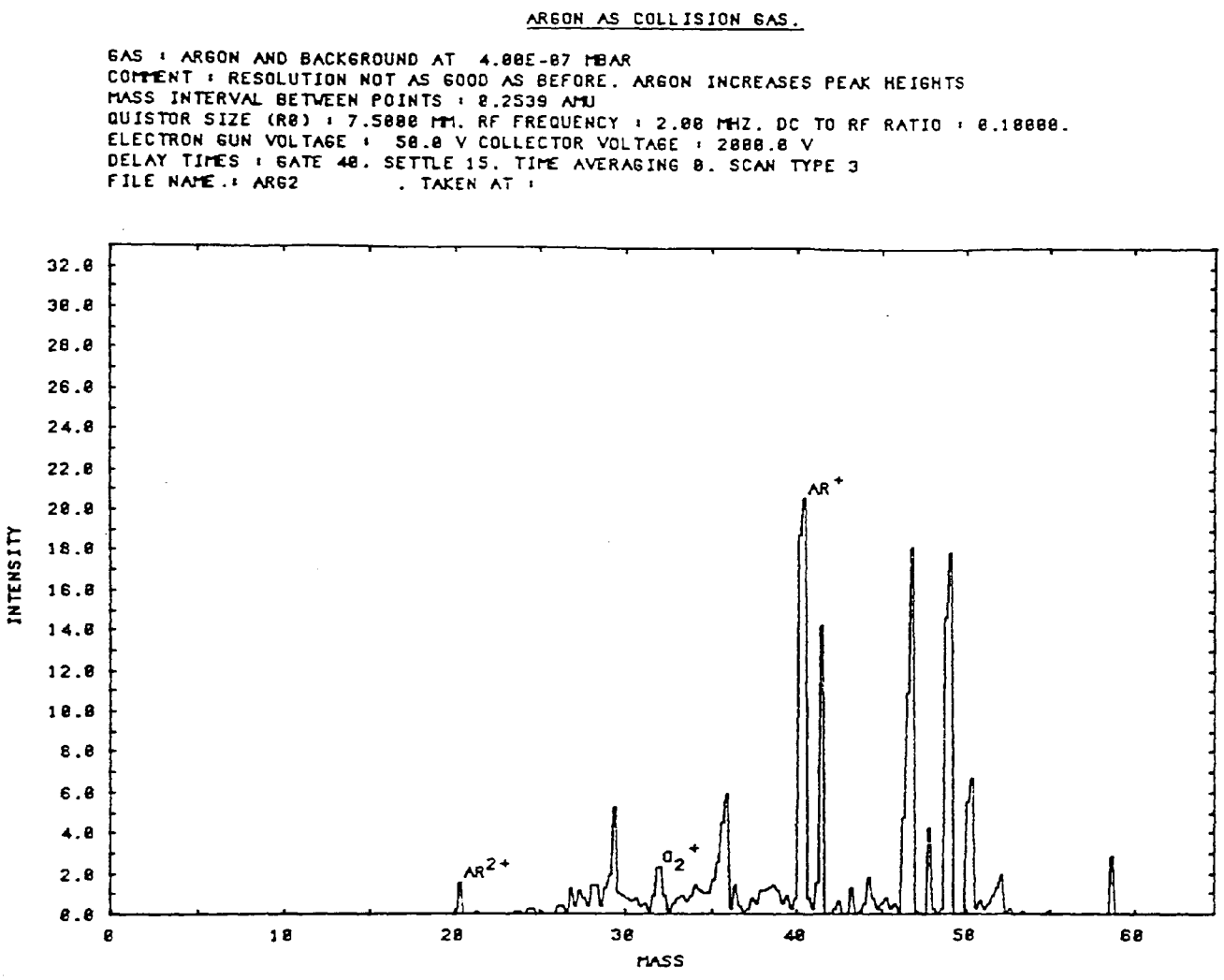

Fig. IV.6.8 An early spectrum of Argon at 4 x 10^{-7} mBar.

The signal to noise ratio was also found to be rather poor. This was found to be mainly because spurious ion output was being detected continuously, and where this output coincided with the output pulse integration, a meaningless background level to the spectrum data resulted. A number of possible causes for the noise were put forward (see section II.6), though it was not clear at the time which of these was or were to blame. This problem was gradually reduced later, as steps were taken to overcome it, but never really disappeared.

Reliable mass calibration and identification of the main peaks was now, however, possible. Some examples of spectra recorded at this time, and displayed using the software which was now available, follow.

The effect of Helium collision gas upon the remainder of the spectrum produced was also investigated. It was found that there was an improvement in resolution and sensitivity, but that the effect was quite small. This is attributed to the fact that a large number of collisions between ions and helium atoms are required in order to have a substantial effect. In order for this to take place within the storage times normally permitted for ions, a pressure of 10^{-3} mBar or so of Helium is required. A pressure such as this would require that the Quistor be differentially pumped since a diffusion pump could not operate directly. This facility is not available on the present system.

Note that the Helium peak in this spectrum has split because of the large level of space charge present in the Quistor.

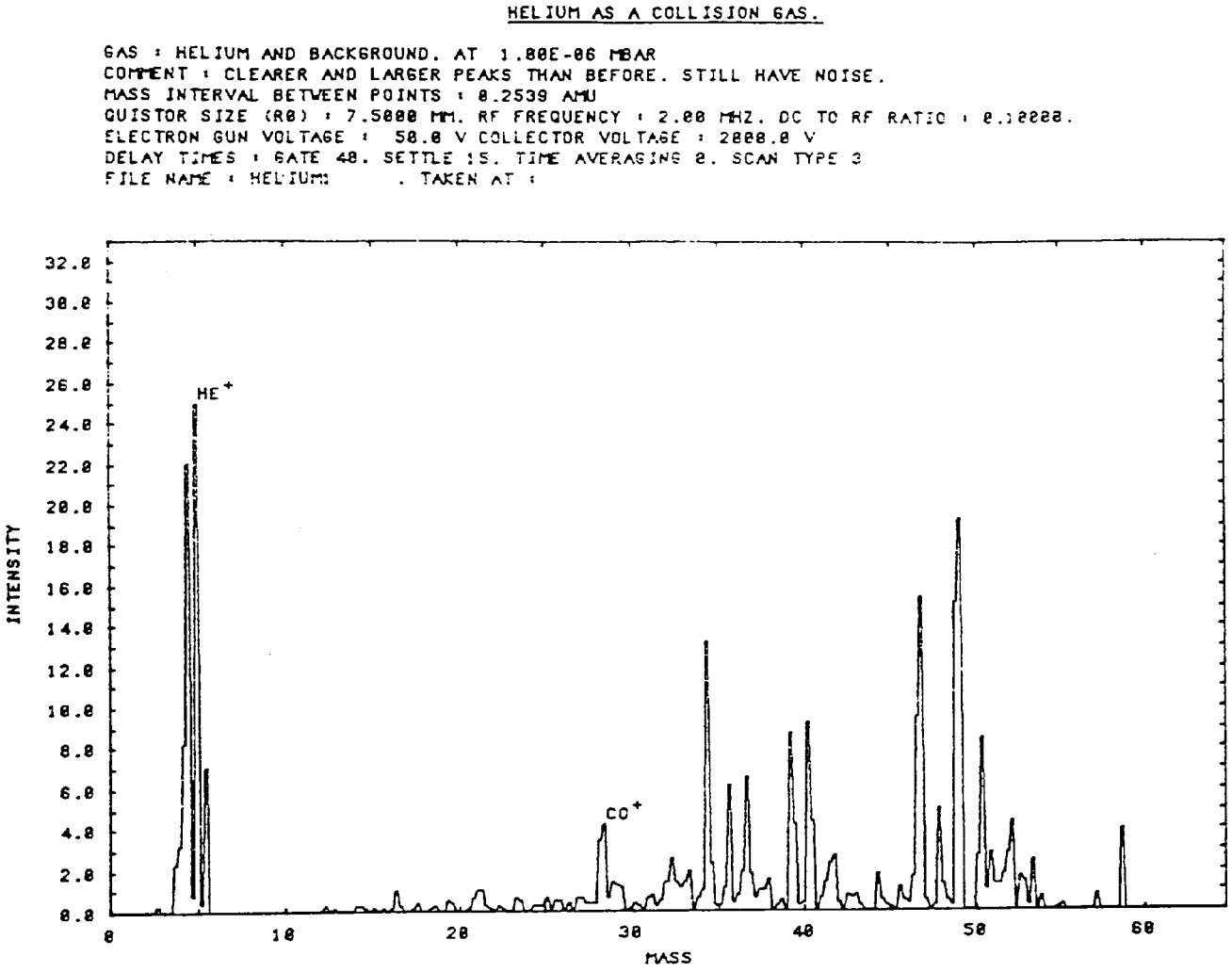

Fig. IV.6.9 Early spectrum with Helium at 1 x 10^{-6} mBar.

Gradually the quality of the spectra improved as the noise problems were reduced. Experience of tuning the RF unit properly, and of using the Quistor at its best, was also gained.

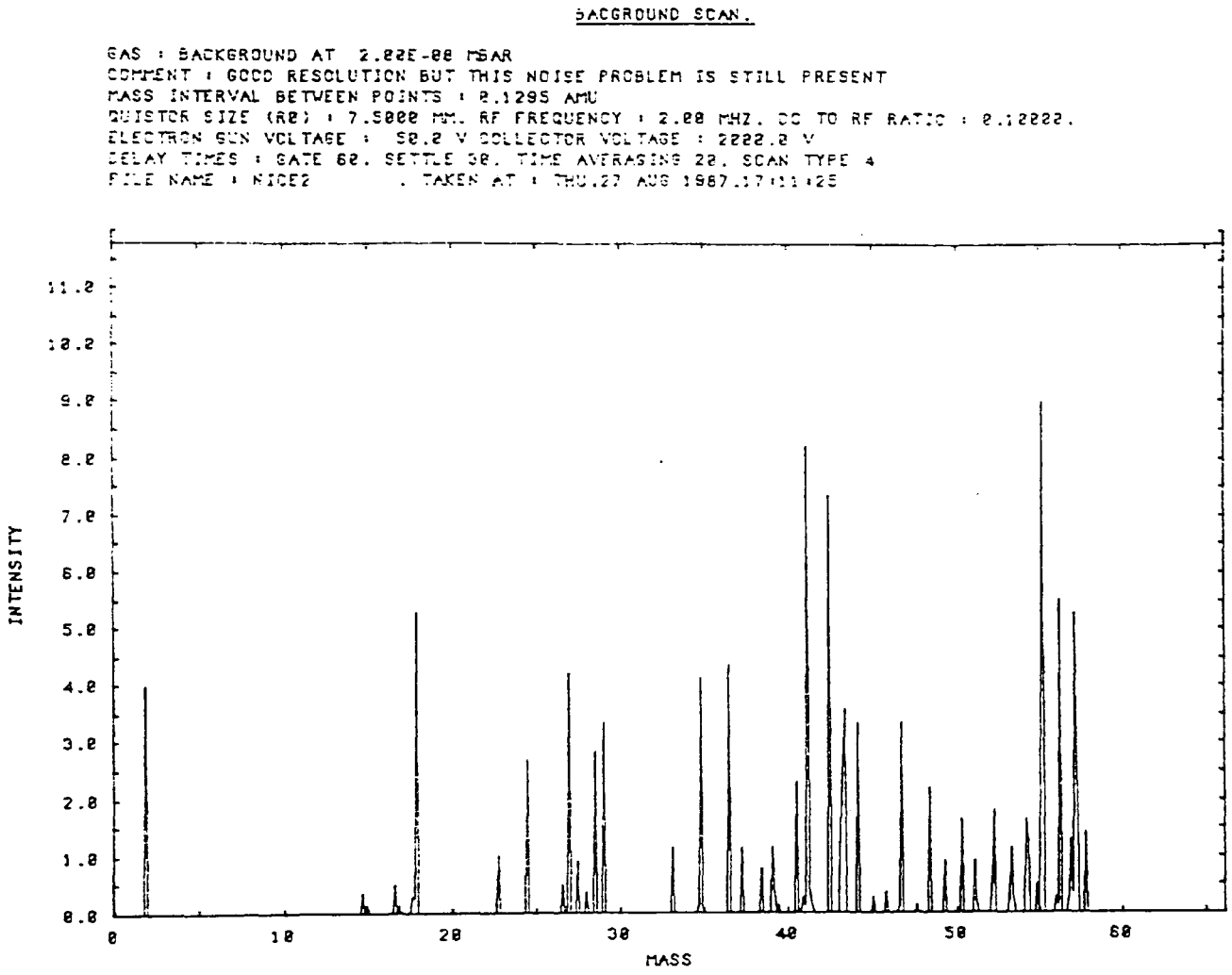

Fig. IV.6.10 Background scan with single hole end caps at 2 x 10^{-8} mBar.

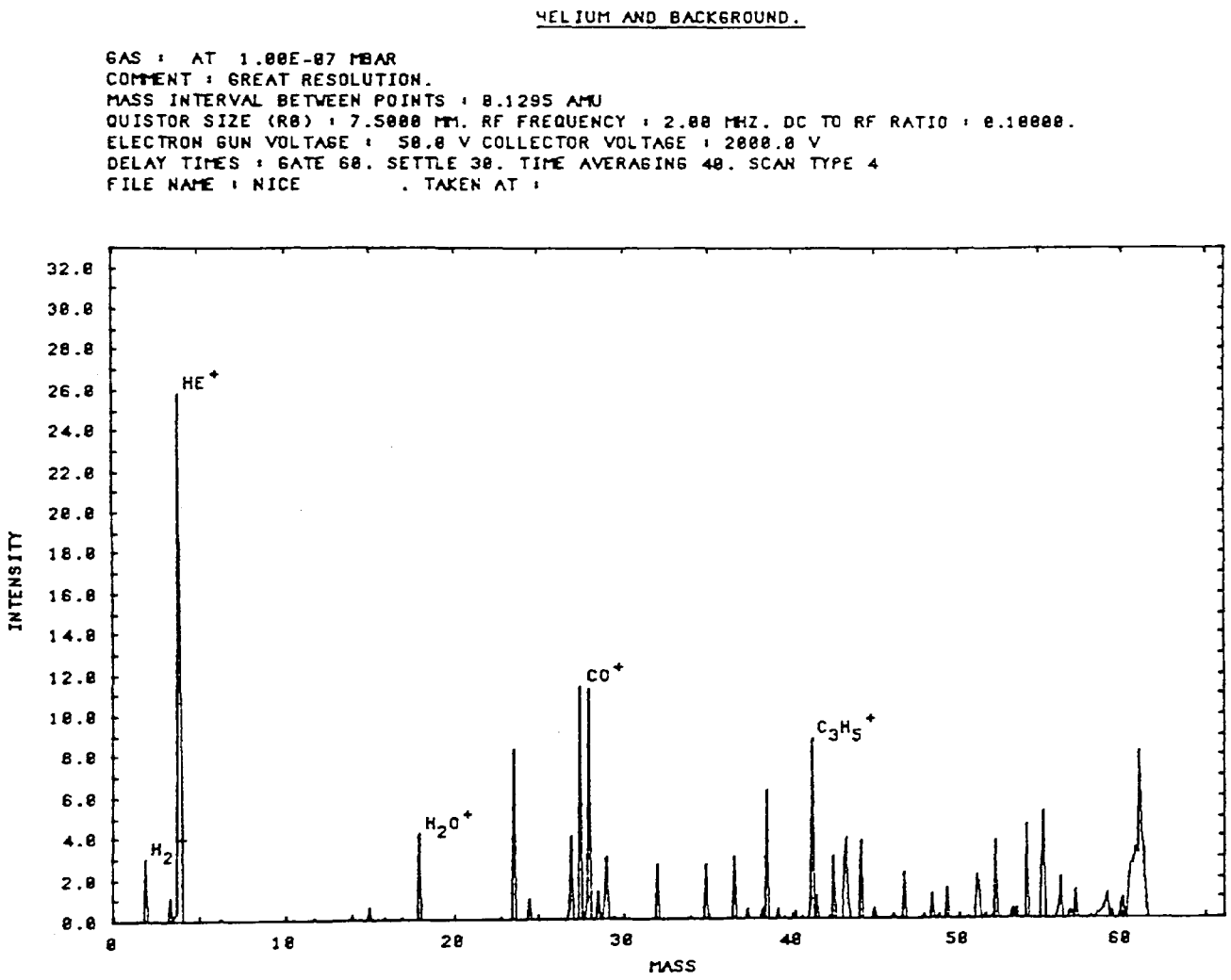

Fig. IV.6.11 Spectrum of Helium at 1 x 10^{-7} mBar using single hole end caps.

The resolution in these spectra is really quite good. At mass 50, the peak width is about 0.25 AMU so that the resolution there is about 200. The signal to noise ratio in these spectra is much better than previously. The sensitivity, however, still leaves much to be desired.

7) Steps taken to reduce the noise level in the spectrum.

It was apparent that the noise level of spectrum data generally increased with the voltages applied to the electrodes. It was felt that the RF voltages on the end caps might be drawing electrons and / or ions into the trap, resulting in the spurious ionic noise observed. Consequently, the Quistor was operated for a time with the end caps earthed, one RF output being unconnected and the RF unit being retuned in order to accommodate the change in capacitance loading.

Inevitably this resulted in a reduction of the mass range by a half, the mass range now being less than 30. The noise level did indeed reduce, but was by no means eliminated.

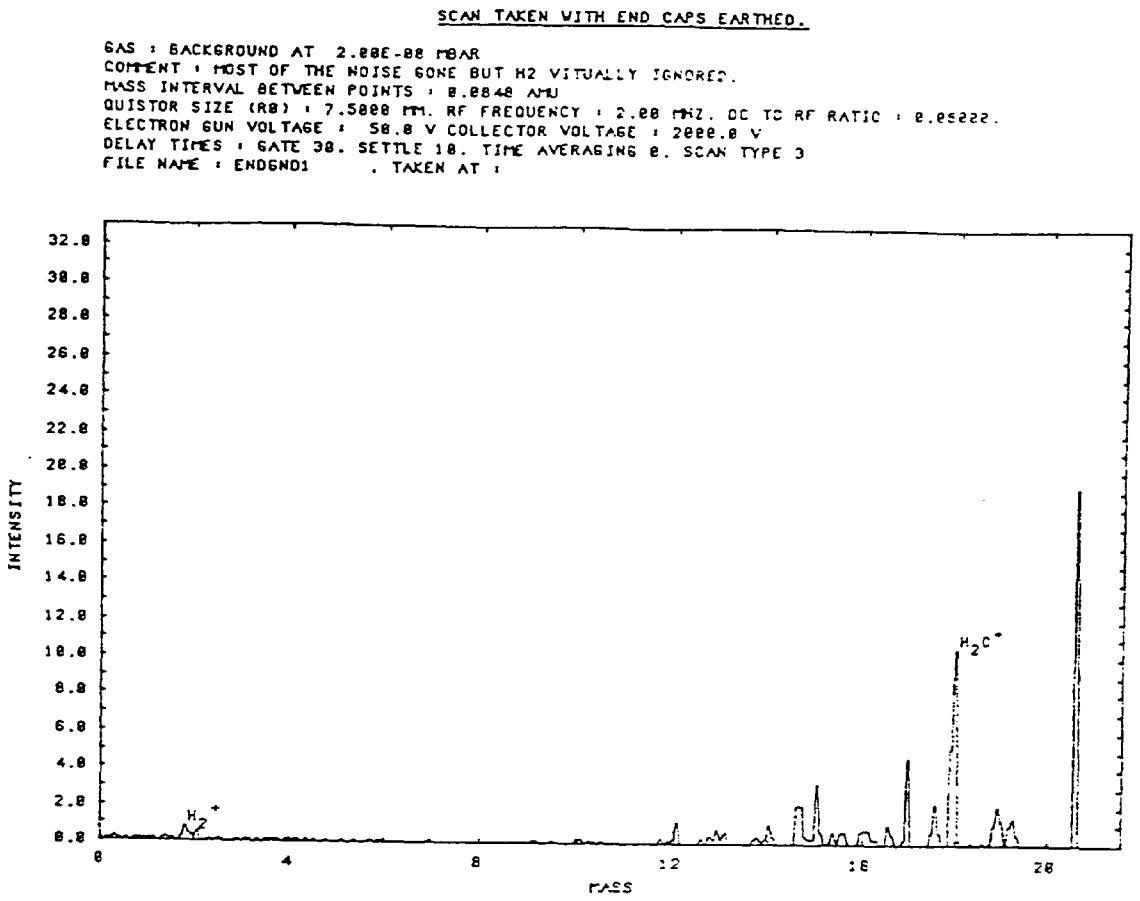

Fig. IV.7.1 Background spectrum recorded with the end caps earthed.

At a later time an earthed metal plate, with a hole covered by a mesh gauze, was placed between the electron gun assembly and the upper end cap electrode. This brought a substantial reduction in the noise level without halving the mass range and was therefore a much better solution.

A great part of the noise is believed to have been caused by the fact that during the period when the electron beam was off, electrons were still being emitted from the hot filament surface but, being unable to pass the repulsive potential of the gate electrode, returned to the filament after a time. During this time ionising collisions between the electrons and gas molecules could, however, take place and the resulting (positive) ions could easily pass the gate

electrode and enter the Quistor. These ions would then almost certainly be quickly ejected so as to be detected as noise.

If the filament during the electron beam off interval is at a negative potential (say, -15 V), and the gate electrode being more negative (say -80 V), the ions will be created in a region which is entirely below ground potential. These ions will therefore not be able to pass an earthed electrode such as either the additional electrode described, or the earthed end caps above. Consequently they cannot enter the trap and thus will not be detected as noise.

It is believed that a great part of the noise remaining is due to the photoelectric effect. The hot, bright filament produces light which can strike the gate electrode or the earthed electrode. Photoelectrons are produced which can enter the trap and produce ions which are ejected and thus detected as noise.

Initially attempts were made to reduce the light emission from the filament by passing the electron beam through a 1 mm diameter hole. This did indeed reduce the noise level, but as it was found to reduce the electron beam current more, the signal to noise ratio was, if anything, worse. That rather defeated the object of the exercise.

Later, Thoriated Tungsten filaments were used instead of simple Tungsten ones, so that a good filament emission could be obtained at a lower filament temperature. Consequently the filament brightness was much lower and far fewer photoelectrons were produced.

This was quite effective at reducing the noise level, although the problem was never completely eliminated. The other approach which was developed in order to reduce its

effects was that the software was able to time - average the data over several scans and so improve the signal to noise ratio in the spectrum. A second software improvement related to this, termed "blip rejection", attempted to differentiate between signal and noise by comparing new data with previously scanned data and rejecting any unexpected "blips" as random noise.

This signal enhancement is, of course, no substitute for good original data. It also means that there is a delay between a change in the gas mixture present in the vacuum system, and that change being fully represented in the displayed spectrum. Nonetheless it is useful in order to help clarify small peaks.

An additional software modification which was added to reduce the effects of ion noise, was to integrate the output voltage twice (for the same time period). The first time is before the voltage increment which generates the output pulse, and the second during the pulse. The average ion noise output should be the same in each case - so that subtracting one from the other in software should help to eliminate the noise. As an additional benefit, the consequences of any offset drift in the preamplifier are removed.

8) Scan types which are available.

A number of different scan types can be used with the Quistor and the operating program can accommodate this. The scan types involved are described below. Note that the "scan type" number shown on the plots corresponds to the numbers given below.

1) 8 bit "Total pressure" mode scan.
2) 12 bit "Total pressure" mode scan.
3) 8 bit upper apex scan.
4) 9 bit upper apex scan.
5) 10 bit upper apex scan.
6) 11 bit upper apex scan.
7) 12 bit upper apex scan.
8) 12 bit upper apex "complex" scan.

Fig. IV.8.1 Table of scan types.

Scan types 1 and 2 consist of switching the DC voltage component off, and selecting a fairly low RF voltage (in this case 25 % of maximum). A large number of ions is stored up, and the RF voltage is ramped upward in order to sweep successive ion species from the trap in order to be detected.

Scan types 3 to 7 consist of the repeated cycle of ionisation, storage, and voltage increment in order to eject ions. The voltage ramping, thus, is the simple staircase formed by digital scanning. A choice of step sizes (and thus the number of points in a scan) is provided.

As explained in chapter III, a proper choice of step size is essential. A large step size (compared with the intrinsic resolution of the Quistor), means that the best possible resolution is not being obtained. A small step size results

in poor sensitivity - while not providing additional resolution. Thus early Quistor spectra (with relatively poor resolution) used only an 8 bit scan. Later spectra were able to use 9 bit scans. Reliable spectra using 10 or more bits have not yet been obtained (although this kind of resolution may yet be achieved).

Scan type 8, referred to as "complex" is a solution to a problem inherent to the Quistor. It is not possible to predict in advance the exact voltage at which a particular ion species will pass the $\beta_z = 1$ boundary. If it so happens, that the ions only just becomes unstable after a given voltage step, then ion ejection is ineffective and the sensitivity is poor. On the other hand if the ions are only just trapped before the step, then only a small number will be trapped, and again the sensitivity is poor. The peak centroid, in fact, would lie at a point midway between.

If more points are taken then the chances of locating the boundary accurately are greater; but then (as explained above), the sensitivity will drop since the step size is too small. Ideally, one would wish to take a large number of points - but still use a sufficiently large step size.

Initially, scan type 8 consisted of the following repeated cycle. Ionisation and storage was followed by a voltage increment of 17 LSD (i.e. an 8 bit increment and a 12 bit increment together) in order to eject the ions. This was followed by a 16 LSD (8 bit) decrement in the voltage so that the net voltage increase was 1 LSD (12 bit) allowing 4096 points.

It was found however that the sensitivity in this scan mode was relatively poor compared with the simple "staircase" scan type 3. This was because ion storage

through two or more cycles of the scan was not effective (see below). Ions which remain in the trap close to the $\beta_z = 1$ boundary after the increment, gain amplitude because of the increment as the trapping efficiency drops. Many are therefore lost. For the ones which remain, when the voltage is decremented, that increased amplitude is retained. The result is a reduction in performance.

Consequently, the scan type was modified. 16 separate 8 bit "staircase" scans, each offset from the previous one by 1 LSD, were produced and superimposed into one 12 bit scan. The composite spectrum has 4096 points, but each voltage increment was an 8 bit one. The peak shapes in the spectrum, and the peak centroids are now clear.

Normally, ions will remain in the trap between scan points. Those ions which are not ejected by passing the $\beta_z = 1$ boundary, remain in the trap and may be ejected on a following voltage increment. Scan types 9 to 14 correspond to scan types 3 to 8, but the RF and DC voltages are dropped to zero after the voltage increment which produces output. In consequence all the remaining trapped ions are lost from the trap. The RF voltage is then returned to its previous value for ion storage. Therefore, all the ions in the trap are new at each point.

It is found the sensitivity of the spectrum produced is about one third of that available in the usual mode (all other factors being the same). This is partly because (for modes 3 to 8) ions which are stored in the trap but not ejected on a particular step, can remain trapped and contribute to the output on a subsequent step. In effect a longer total ionisation time is in use.

In addition, ions which are trapped in the Quistor while they are not close to the stability diagram boundaries, will be trapped more easily. Over a period of time, the ions trapped with large velocities will be lost through ion - molecule collisions. The remaining ions (with lower amplitudes) will remain and these provide good resolution and sensitivity.

The other factor which may affect performance in modes 9 to 14 is that rapid rise and fall of RF voltage puts additional strain upon the RF unit, possibly affecting the quality of the RF outputs.

For these reasons modes 9 to 14 have been used only occasionally. An example follows.

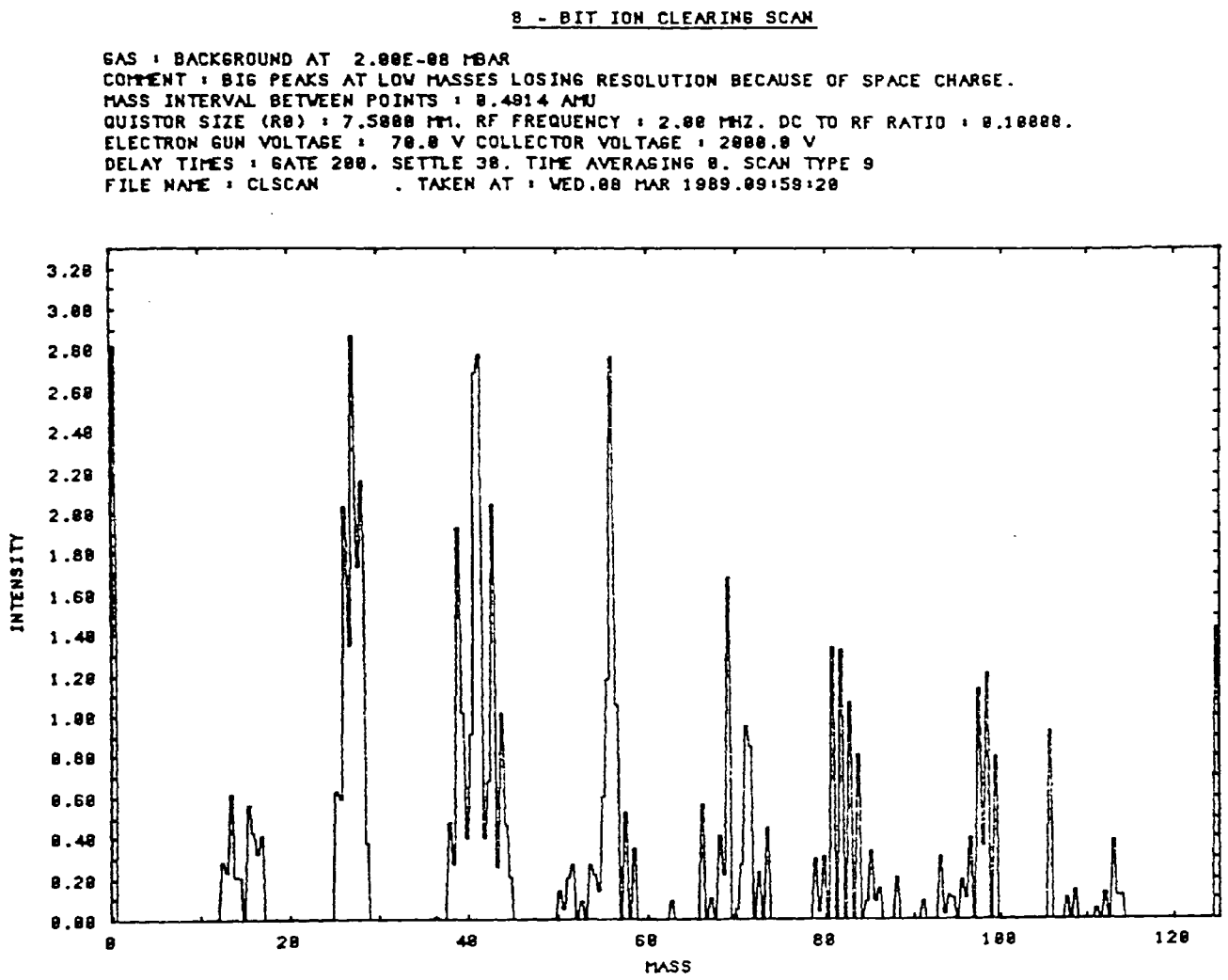

Fig IV.8.2 Ion clearing scan with new RF unit and double gauze end caps.

One additional scan type remains to be explained. By storing ions at the upper apex as usual, but subsequently ramping the RF and DC voltages immediately up to the maximum, all the ions which are stored in the trap are ejected along the z axis.

The ion pulse which is produced in this way way can be integrated so that a spectrum of the ions stored in the trap at any one time is built up. Scan types 15 to 20 correspond to scan types 3 to 8, except for the total ion ejection. Since

the resolution of the scans produced is very low, there has been no point in using more than 256 data points; consequently scan type 15 is the only one which ever been used. This scan type is useful in particular in helping the user to select the most appropriate DC to RF ratio. Ideally some structure between peaks should be visible, but complete separation is not required since the sensitivity will then drop.

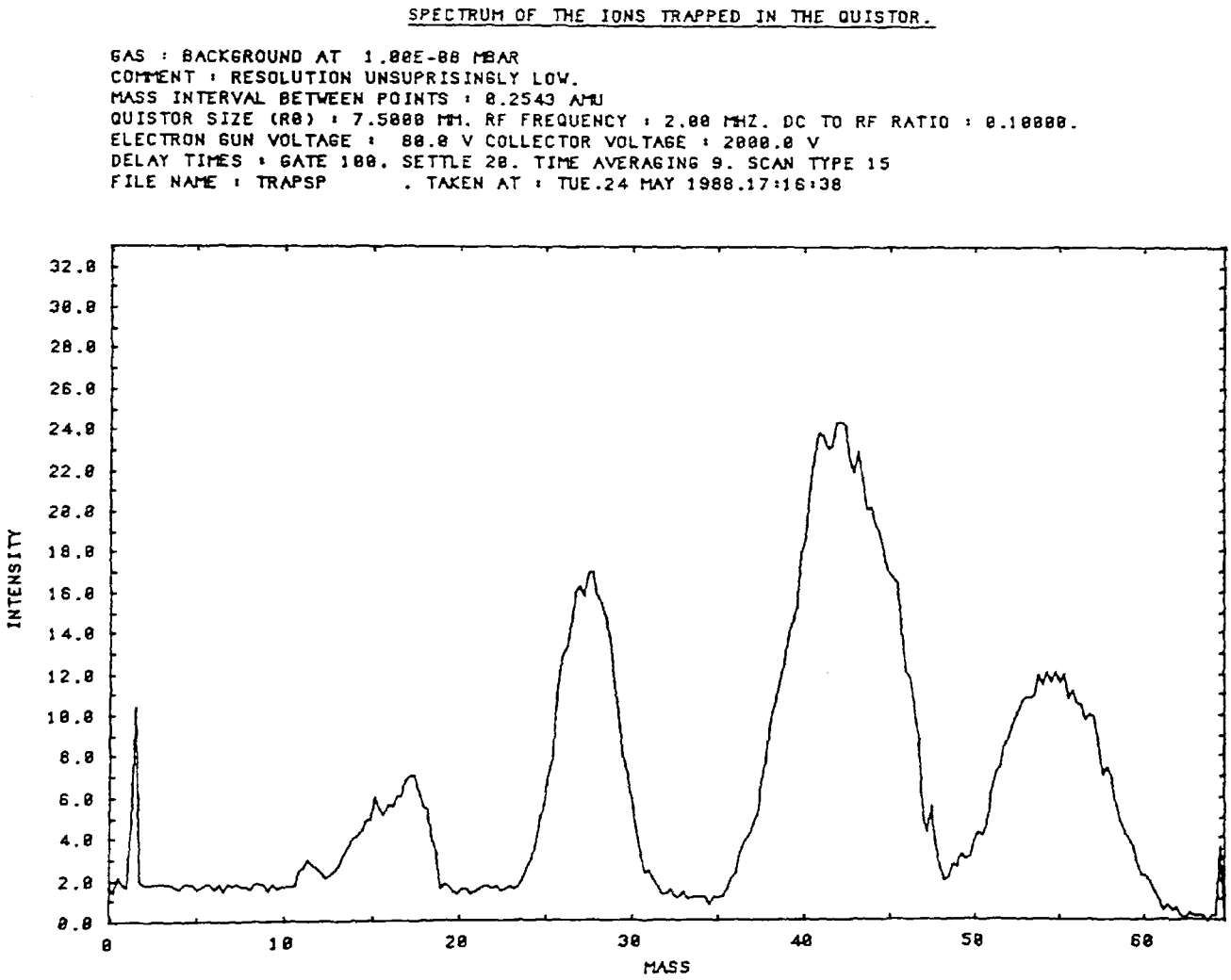

Fig. IV.8.3 Ion trapping scan with mesh end caps. The ratio of DC to RF voltages is quite low.

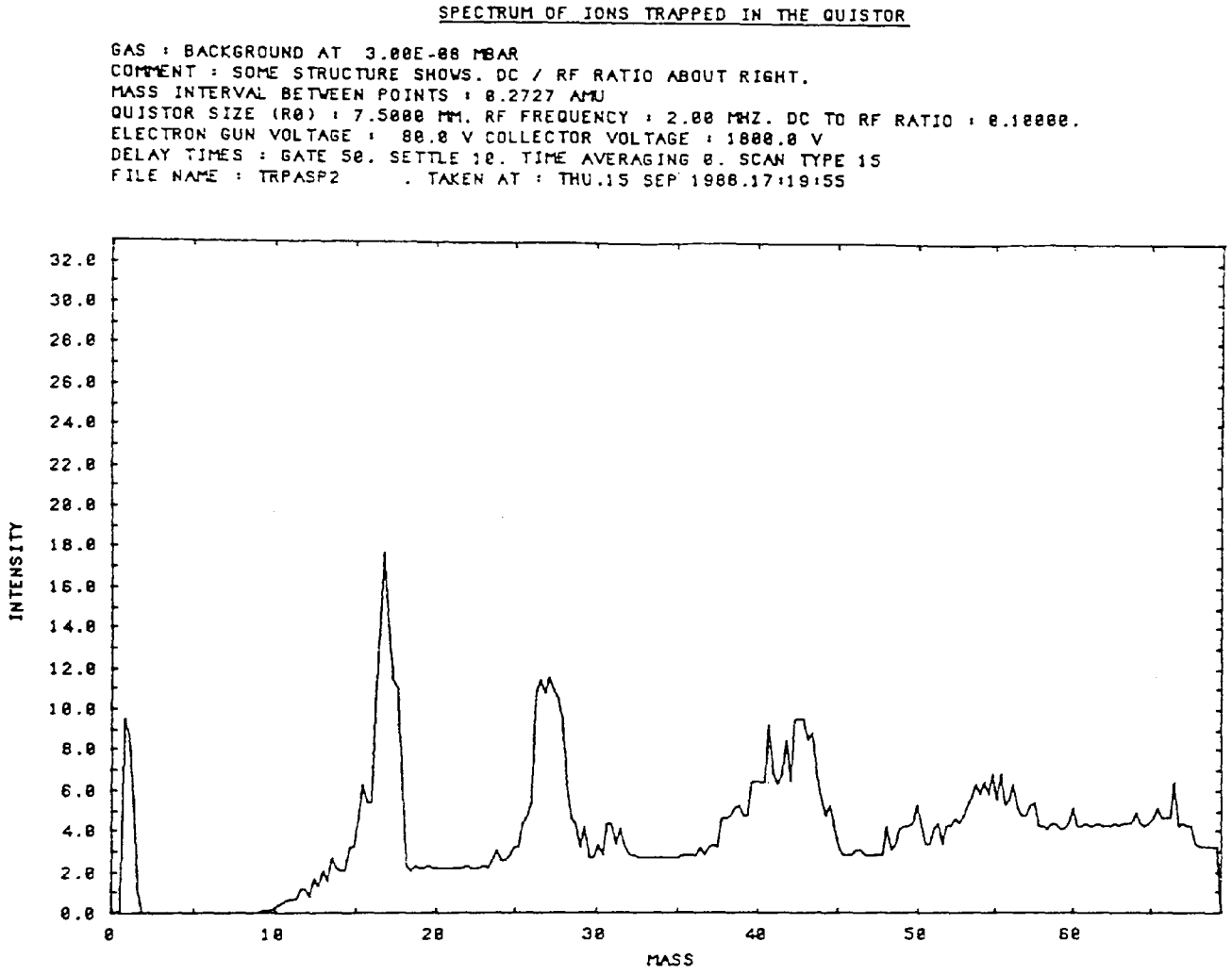

Fig. IV.8.4 Ion trapping scan with mesh end caps. The ratio of DC to RF voltages is greater.

9) Investigation of laser drilled end caps.

It was felt that the overall sensitivity of the Quistor was still unacceptably poor, and that attempts should be made to increase the number of electrons entering the trap, and the proportion of trapped ions leaving it.

In view of what had been found out from the computer work about the distortion produced by the holes in the end caps (see chapter III), it was felt that attempts should be made to produce end caps incorporating a large number of small holes instead of one single large one. This was attempted in two ways; firstly by the use of a powerful industrial laser, a large number of holes were drilled into some end caps; secondly by preforming a gauze into an end cap shaped former and spot welding the gauze over large holes in two other end caps.

The laser drilled end caps were first to be investigated experimentally. The end caps had holes in them arranged in concentric circles. The holes had been drilled with a CO_2 laser. By using a special rotating jig to hold the end caps during laser drilling, the holes had been made perpendicularly to the Quistor electrode surface. This was because computer simulation work had shown that ions would be ejected from the trap along lines normal to the surface. In addition, electrons would probably enter the trap along fairly similar lines. The upper end cap had 55 holes in it, the lower 127. (The difference lay in that the electron beam would enter the trap fairly close to the central axis, while ions could be ejected at quite large r positions.)

Upon inspection, it was found that profile of the holes was considerably tapered, ranging from about 0.1 mm at one end, to about 0.3 mm at the other. Since the holes had been

drilled through from the curved electrode surface, this was the wider end of the holes.

Some electron microscope photographs were taken showing the holes in close detail from both sides. These have been included here.

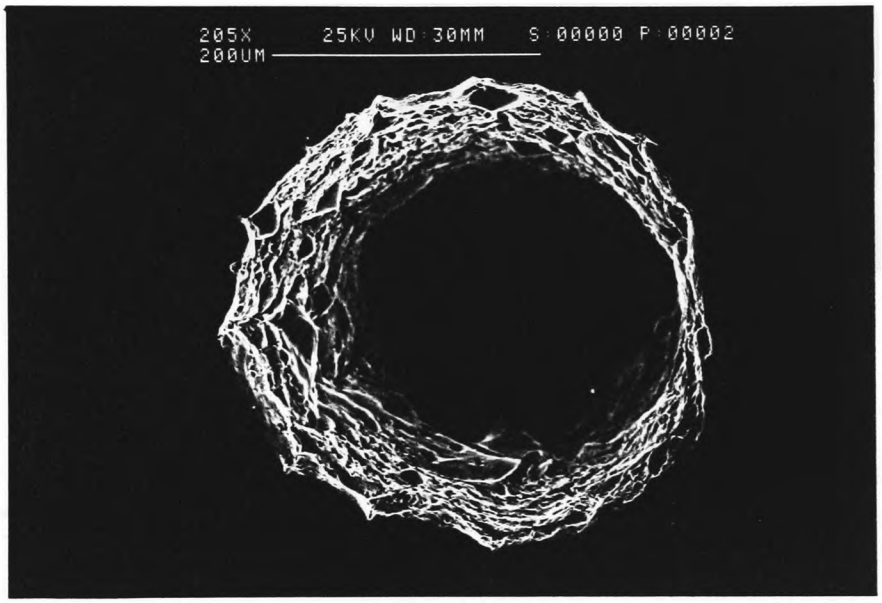

Fig. IV.9.1 Electron micrograph of the wide end of a laser drilled hole.

Fig. IV.9.2 Electron micrograph of the narrow end of a *laser drilled hole.*

This tapering was really rather unfortunate since the distortion produced by the holes would depend largely upon the diameter of the holes at the curved surface (0.3 mm), while the output intensity would depend upon the diameter at the narrowest point (0.1 mm).

It was found that a quite reasonable standard of resolution was obtained using these end caps, but that the output intensity was very poor, largely as a consequence of the small size of the narrow end of the holes.

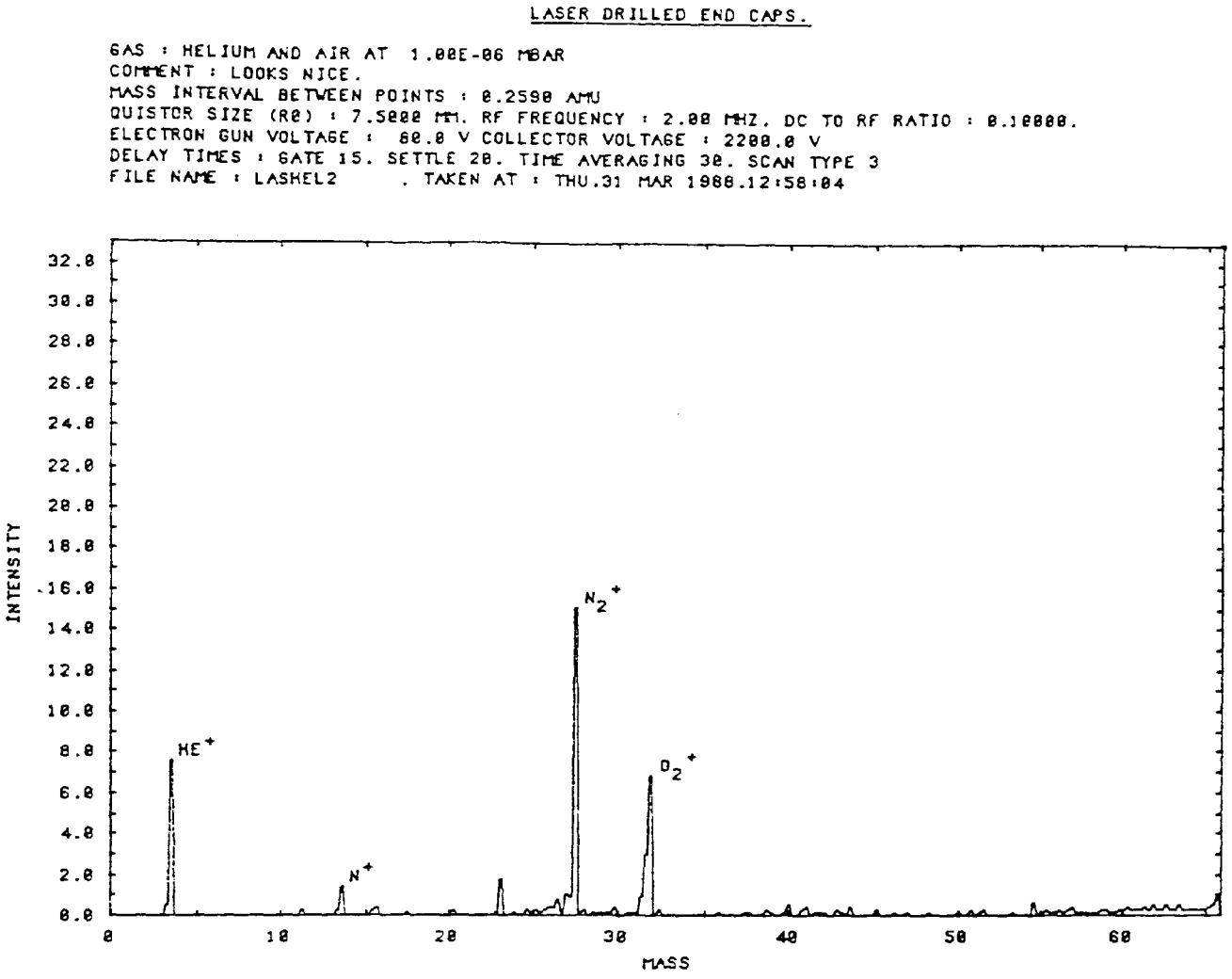

Fig. IV.9.3 Spectrum of a mixture of Helium and air at 1 x 10^{-6} mBar using the laser drilled end caps.

At a later time, these end caps had mesh gauzes fitted into the recess in the outer surface of the end caps, in accordance with the computer simulation results which had indicated that the performance of the Quistor would improve as a result. The interpenetration of electric fields through a long thin tube (as in a laser drilled holes through 2 mm or so of steel) is much less than that through a relatively wide hole through a thin layer. Therefore the improvement was not as great as for the gauze end caps (see below).

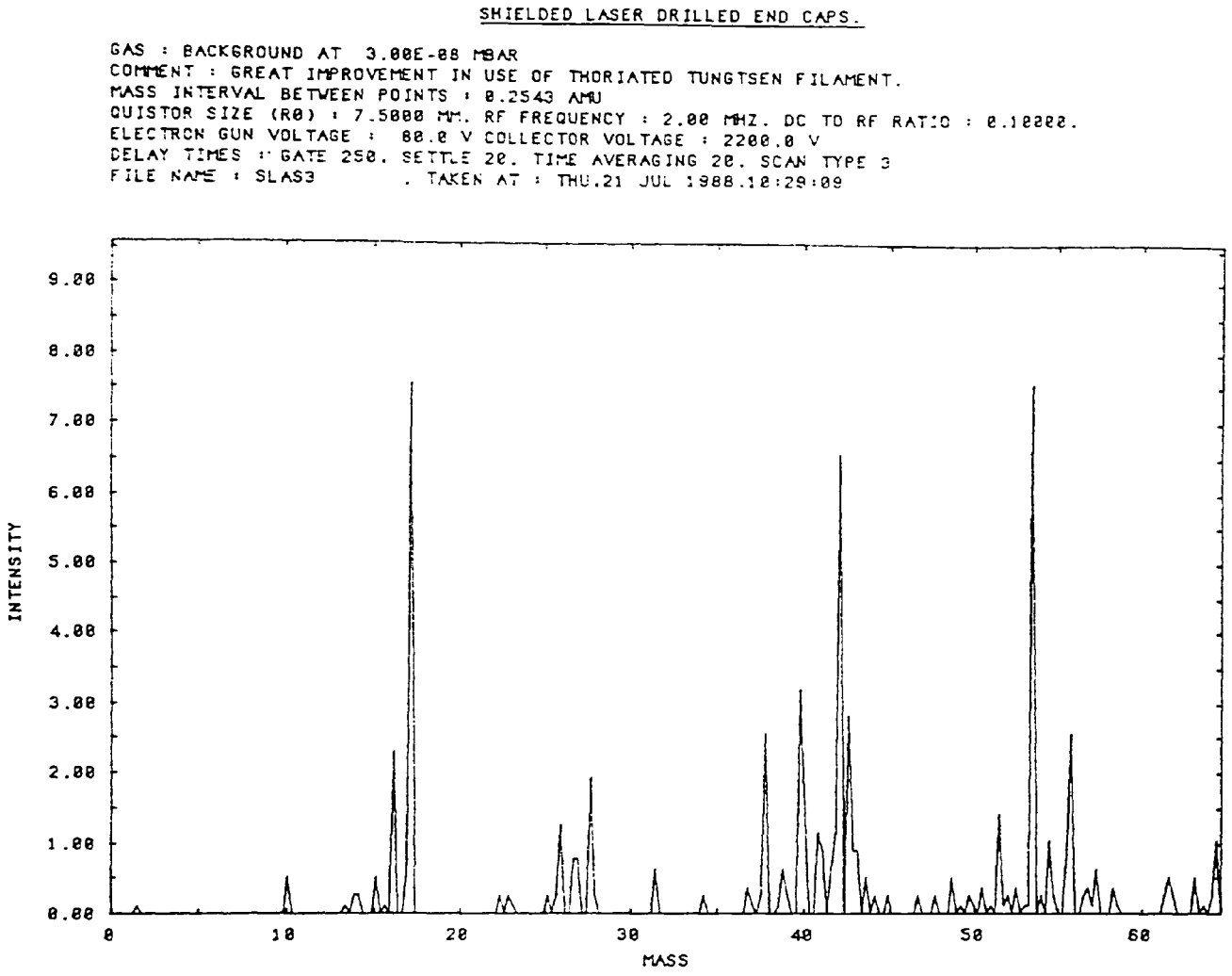

Fig. IV.9.4 Background spectrum recorded with shielded laser drilled end caps.

Some more laser drilled end caps have been produced, which have more holes in both end caps, and for which the holes were drilled through from the other side, so that the narrow end of tapered holes are on the end caps' curved surfaces. A different type of laser was also used which it was felt would lead to less tapering. Unfortunately it has not been possible to date to test these.

10) Investigation of gauze end caps.

The end caps with large holes covered with a mesh gauze were tested next. The first attempt to produce these end caps was made by using some older end caps (the first stainless steel ones, with a single 1 mm holes).

A hole of 5 mm diameter was drilled in the upper end cap, and a hole of 10 mm diameter in the lower. Some of the curved surface of the end cap was removed with a lathe in order to accommodate the thickness of the gauze. This was done, however, in a conical shape, rather than the curved hyperbola of the Quistor. Finally, a fine mesh gauze, preformed into a bowl shaped "female image" of an end cap, was spot welded over the holes.

Initial results obtained using these end caps, were disappointing. The resolution of the Quistor was so poor that it proved to be impossible to produce any sort of meaningful spectrum at all. It was, however, possible to show that ions were being trapped and ejected.

The performance is thought to have been poor for two reasons. Firstly, penetration of external electric fields through the high - transmission gauze, especially the intense field produced by the high negative potential of the channel plate, had distorted the Quistor's electric field to a great degree. Secondly, the fact that the gauze was rather crudely fitted made this problem more severe still.

It was at this time that the computer simulation work (see chapter III) was showing the rather unexpected result that a second gauze fitted into the recess in the end caps outer surface, shielding the end caps from external fields, would lead to a substantial improvement in the Quistor's resolution. Accordingly, this was done, and the modified end

caps were fitted back into the Quistor.

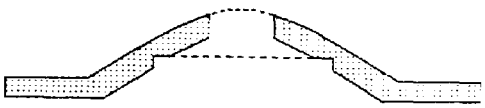

Fig. IV.10.1 Double gauze end cap arrangement

The resulting improvement in the Quistor's performance was dramatic. The resolution of the spectrum produced was still quite poor, because of the crudeness with which the curved gauze had been fitted, with a peak width of, perhaps, 1.5 AMU at mass 40, but good clear spectra could be obtained. The sensitivity of these spectra was greater than any other obtained before that time because of the high transparency of the gauzes used.

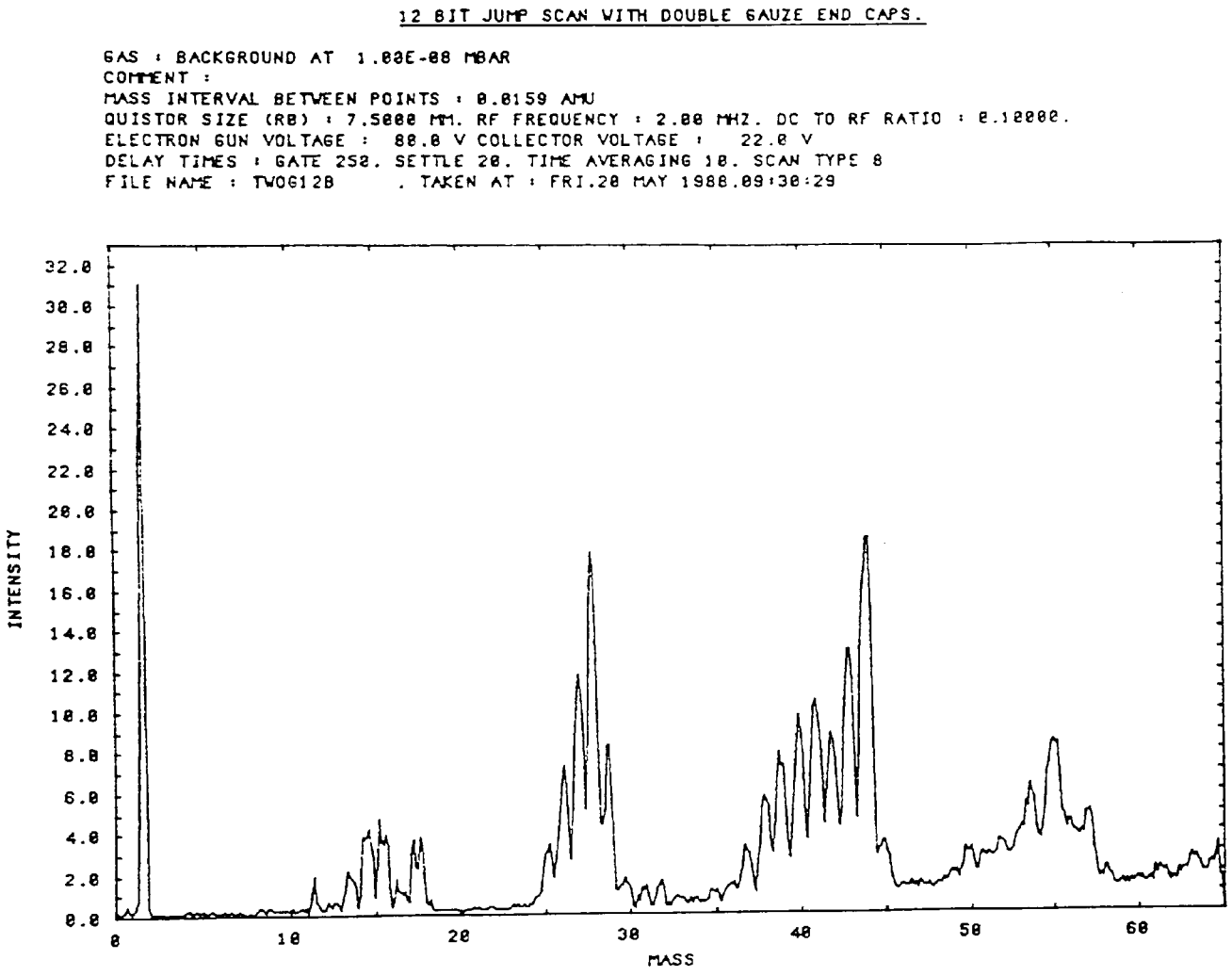

Fig. IV.10.2 Background spectrum obtained with the first double gauze end caps.

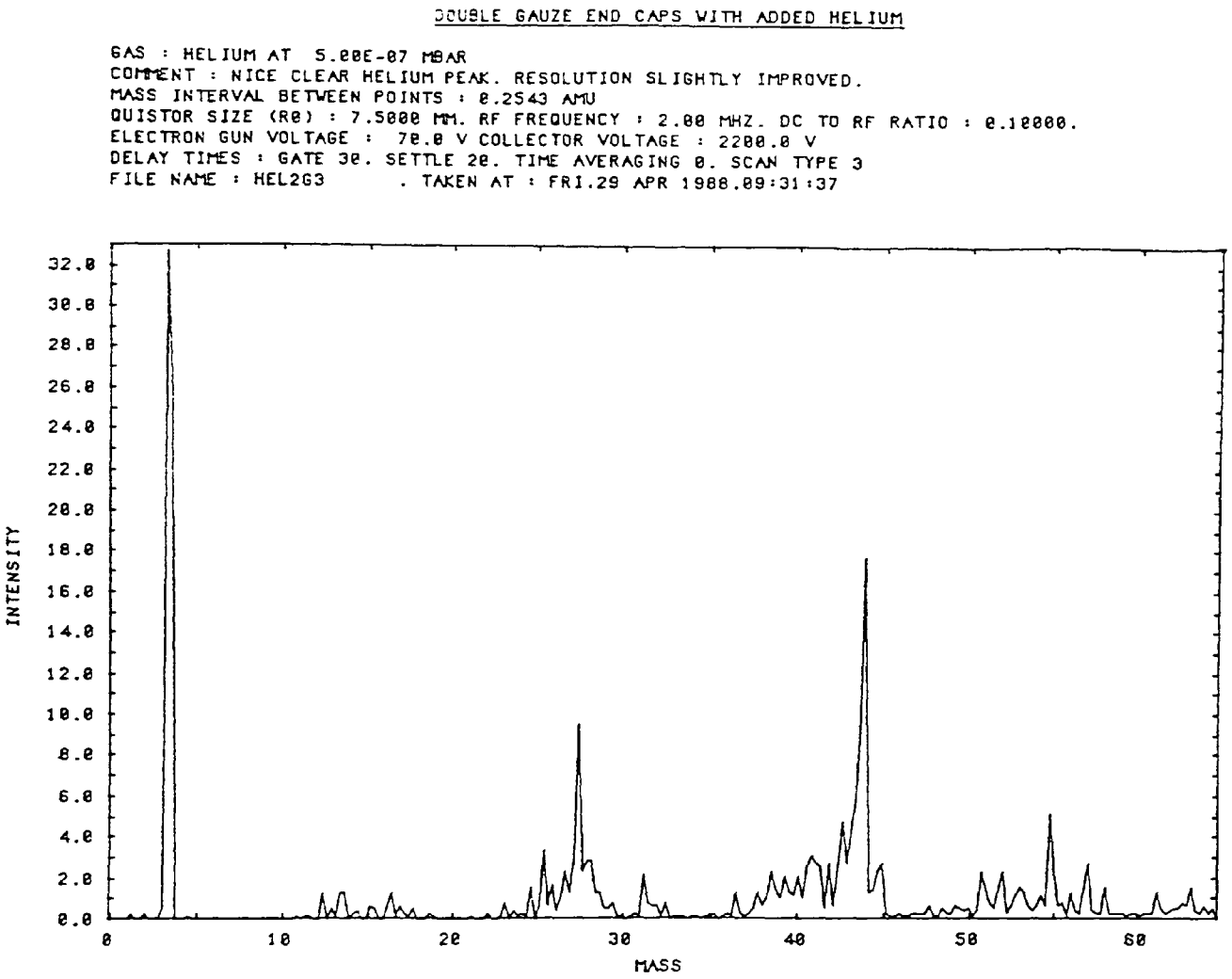

Fig. IV.10.3 Spectrum obtained using the first double gauze end caps with Helium at 5 x 10^{-7} mBar.

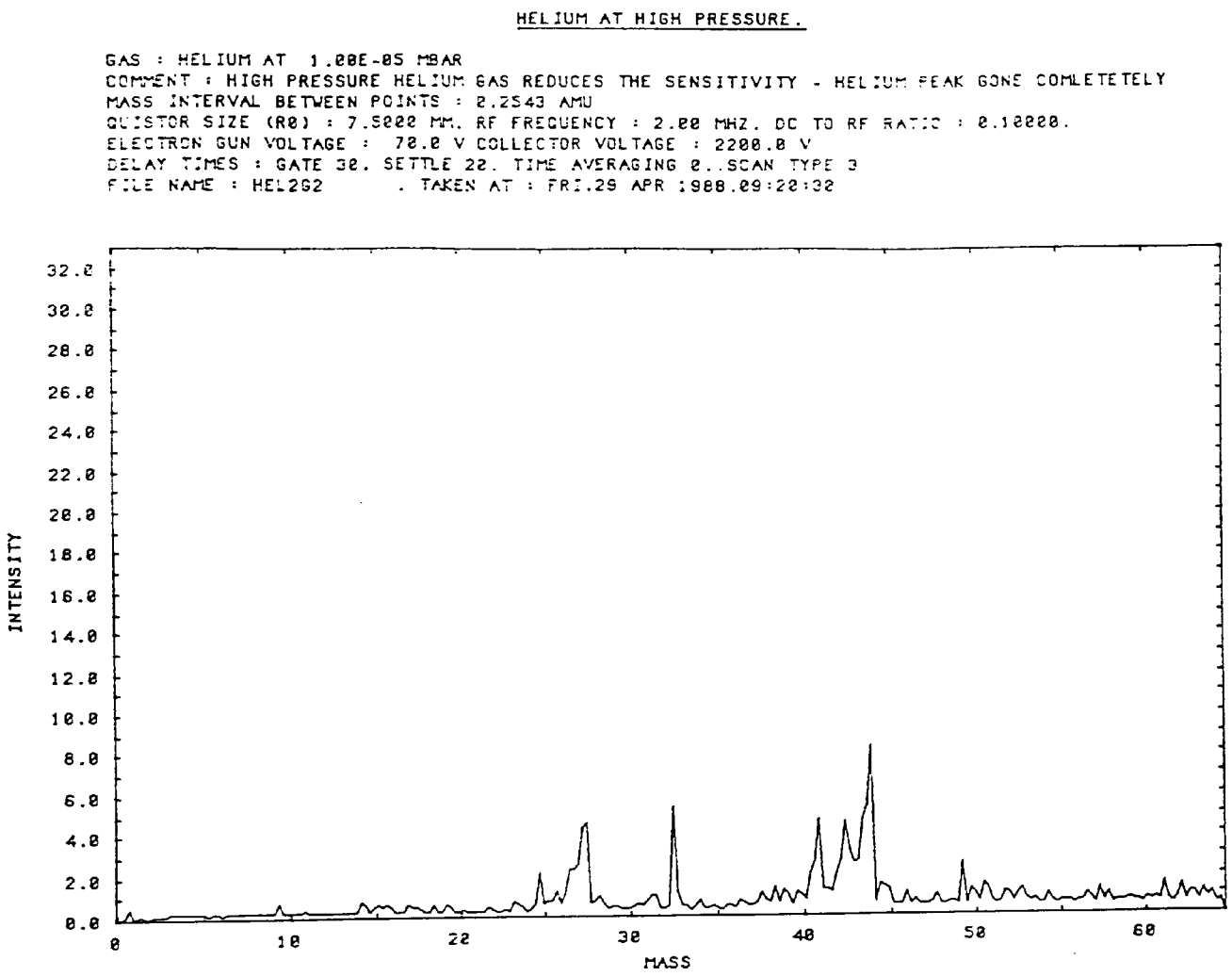

Fig. IV.10.4 Spectrum obtained using the first double gauze end caps with Helium at 1 x 10^{-5} mBar.

In the last spectrum the peaks seem virtually to have disappeared. This is contrary to the expectation that a high pressure of Helium will increase the resolution and sensitivity of the rest of the spectrum (see section III.7.a).

However, the Helium partial pressure is not great enough to have the required effect upon the ion amplitudes. It is also believed that a substantial partial pressure of air had leaked into the gas line which contained the Helium (note that both this spectrum, and the previous one, do show an

Oxygen peak). A high pressure of any other gas than Helium, would reduce the sensitivity and maximum ion storage time.

Based upon the experience gained from these end caps, and the computer work which had indicated that an adjustment in the position of the gauze would help to overcome the remaining distortion produced by the presence of the gauze, some more end caps were manufactured.

These end caps were manufactured according to the data produced by the electric fields program (see chapter III) indicating the adjustment required in the gauze position. The recess into which the gauze would be fitted was machined also according to this data on a CNC lathe.

Instead of using a woven mesh as before, chemically etched stainless steel circular gauzes were produced specially for the Quistor. It was felt the woven mesh with its rough surface was not ideal for the purpose; the chemically etched gauzes had a smoother surface more consistent with obtaining accurate and predictable electric fields.

The transparency of these gauzes was rather lower than that of the woven mesh because the chemical etching process required that the thickness of the wires between holes was at least 0.13 mm. In order to keep the transmission of fields through the gauze to a minimum, it was decided that the square holes in the gauze should have a size of 0.25 mm. This means that the nominal transparency was 43.3 %.

It was, however, found that the holes were smaller than intended, partly because the etching process (like the laser drilling) resulted in a tapering of the holes. This effect was not as severe as with the laser drilling because the gauzes

were much thinner, and because they were etched through from both sides at the same time. In addition it is thought that the forming process, squeezing the gauze as it did, may well have closed the holes up further. The final size of the holes is estimated to be about 0.15 mm so that the transparency was only about 15.6 %.

Because of this, it is now intended to manufacture the Quistor using gauzes with holes of 0.5 mm instead. This should result in a much improved transparency and so much better sensitivity than at present.

This does, however, mean a substantial increase in the adjustment required in the gauze position, to overcome the distortion resulting from the use of a gauze. Previously this had been about 0.011 mm, and since the best obtainable machining precision is estimated to be about this amount, the adjustment was, perhaps, not that meaningful. However, with the increased hole size, the adjustment required is about 0.043 mm which is rather more important. It would probably not be possible to get good results from the Quistor using the larger holes without making this adjustment. This underlines the importance of the computer work to the success of the project.

Second (woven mesh) gauzes were fitted into the recess as before. The new end caps were fitted into the Quistor and tested.

The signal intensity was now very good, since although the transparency of the gauzes was relatively low, the resolution was rather better than that found with the previous gauze end caps. This meant that although the peak areas were rather smaller, the heights were greater. The peak width was about 0.9 AMU at mass 40, although this depended upon the exact conditions selected for scanning.

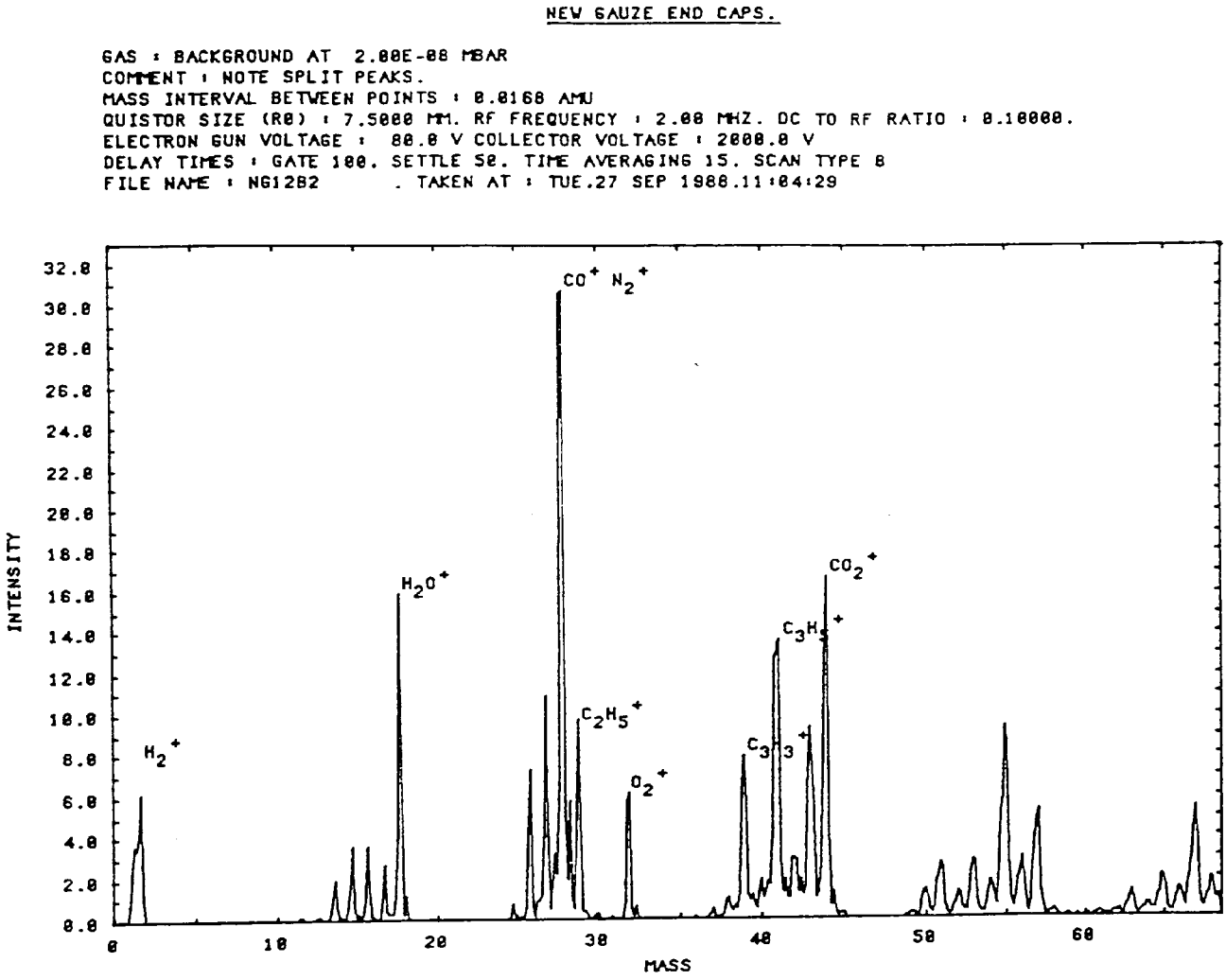

Fig. IV.10.5 Background scan recorded with new double gauze end caps at a pressure of 2 x 10^{-8} mBar.

One effect that is noticeable in this spectrum, as in all spectra produced by the Quistor is that the sensitivity is relatively low at low masses. This is a consequence of the fact that the Quistor can trap more heavy ions than light ones, since the pseudo - potential well is greater.

To some extent this is unavoidable, although adjustment of the DC to RF ratio used does affect the result as far as this is concerned. Increasing this ratio so that the scan

line used is closer to the apex of the stability diagram generally reduces the overall sensitivity - but reduces the sensitivity for high masses more. This is because the effect of space charge is also greatest for low masses - and that effect is to move the apex of the stability diagram upward.

It is, of course, possible to boost the apparent sensitivity for low masses in software in order to make the peak heights more reliable. This may well be required.

Some more spectra produced with these end caps follow.

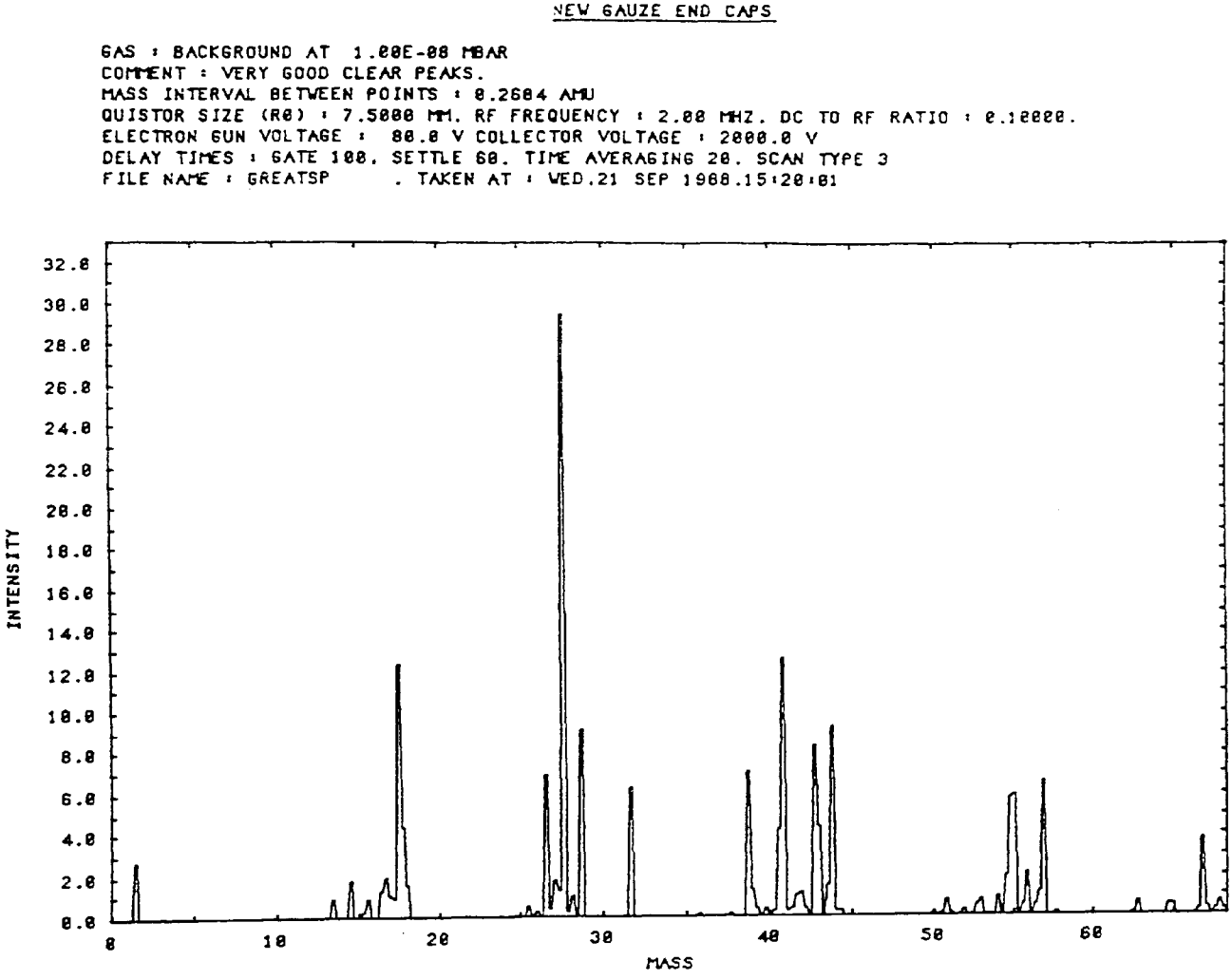

Fig. IV.10.6 Background scan recorded with new double gauze end caps at a pressure of 1 x 10^{-8} mBar after baking.

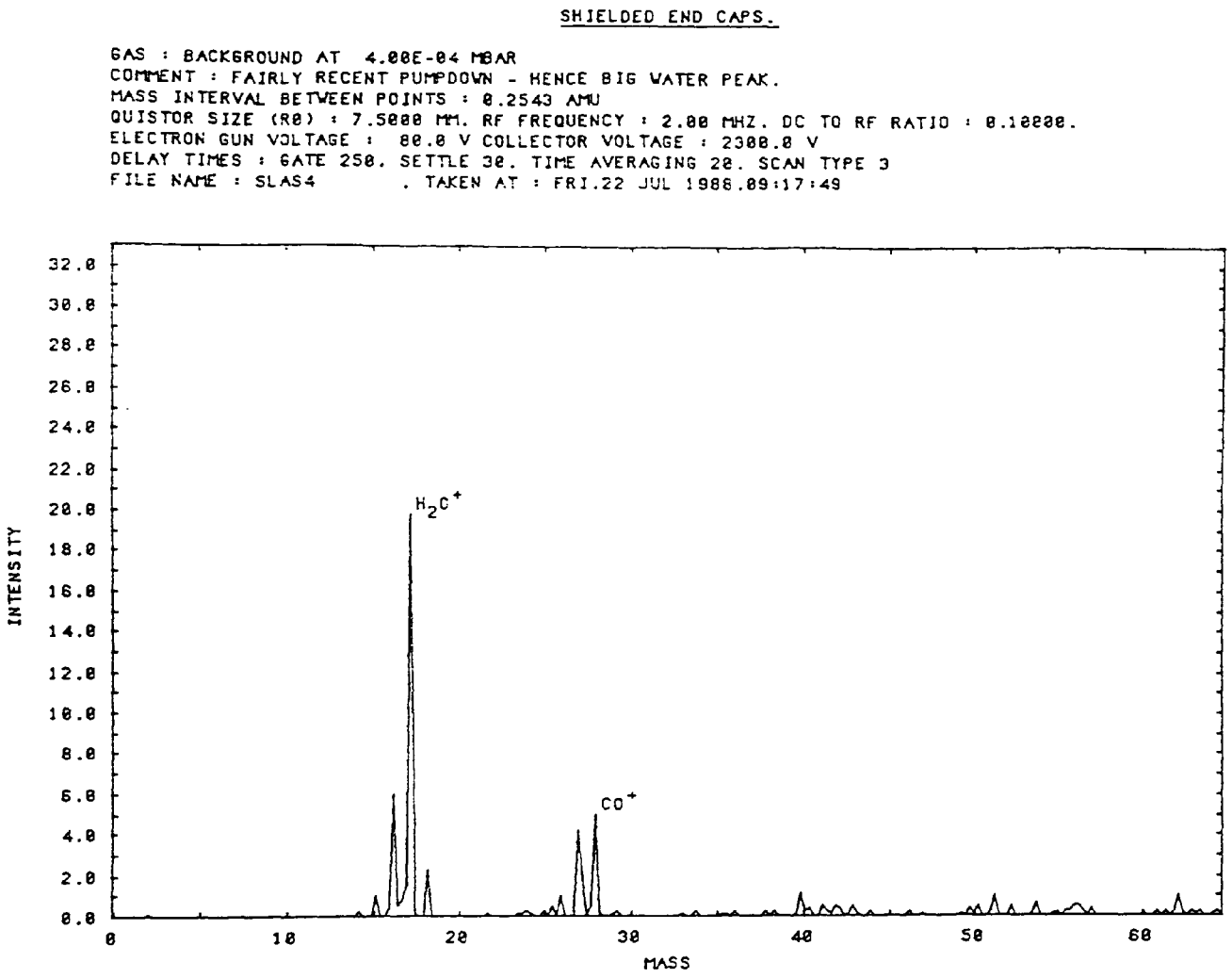

Fig. IV.10.7 Spectrum of air recorded with new double gauze end caps at 4 x 10^{-8} mBar.

The above spectrum shows a ratio of masses 28 to 32 of about 5:2 while the ratio of Nitrogen to Oxygen in air is of course about 4:1.

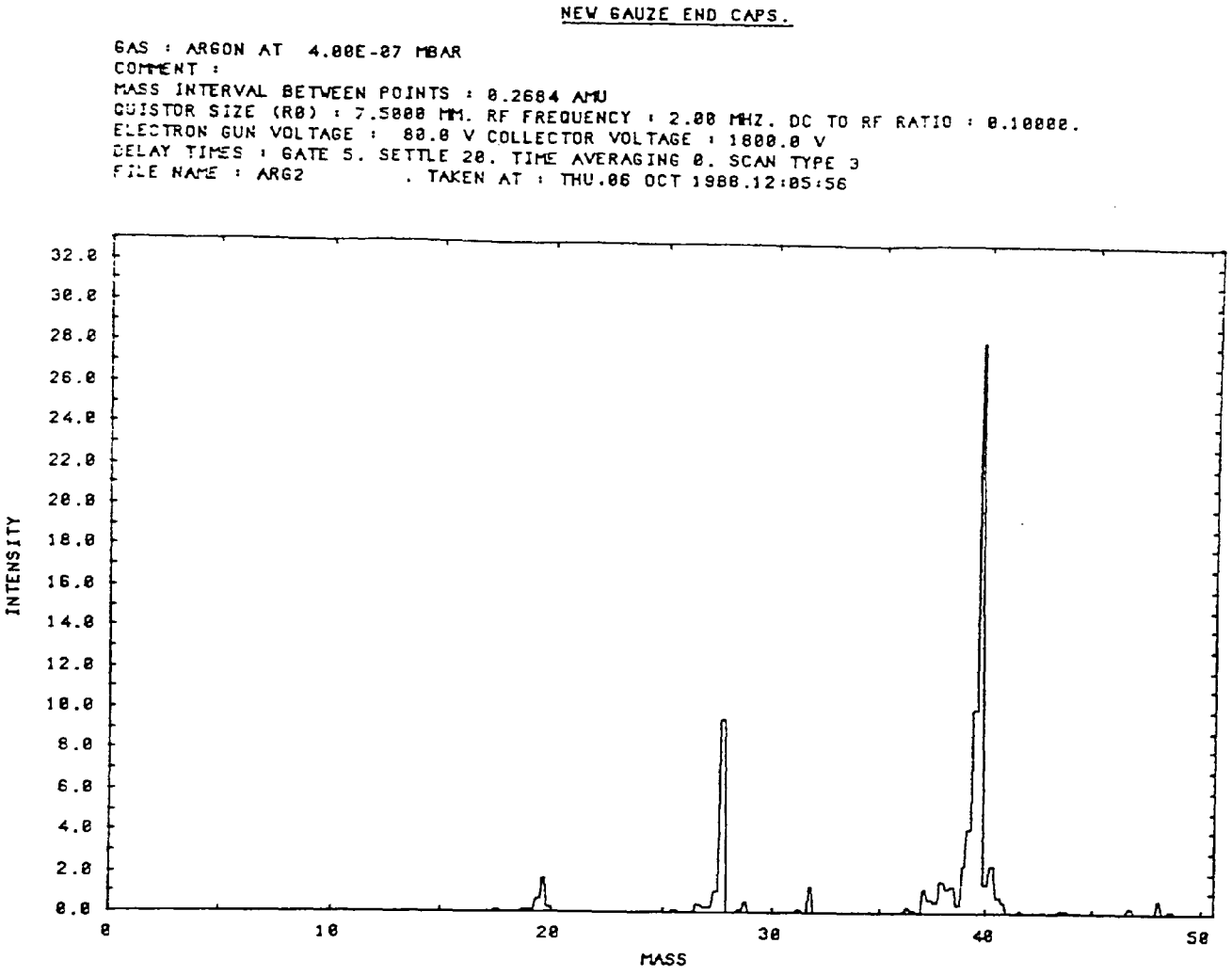

Fig. IV.10.8 Spectrum of Argon at 4 x 10^{-7} mBar recorded with new double gauze end caps.

Peaks at mass 40 (Ar^{+}) and 20 (Ar^{2+}) are clearly seen as may be expected. Peaks at masses 28 and 32 are also clearly seen, suggesting that once again, the Argon bled into the system has been contaminated with air. The argon peak is broadening considerably, perhaps because of the space charge of the Ar^{+} ions.

Two spectra were recorded in an attempt to find out to what extent the presence of a high pressure of a gas affects the other peaks. The scans were recorded under identical

conditions, except for the inclusion of air in one.

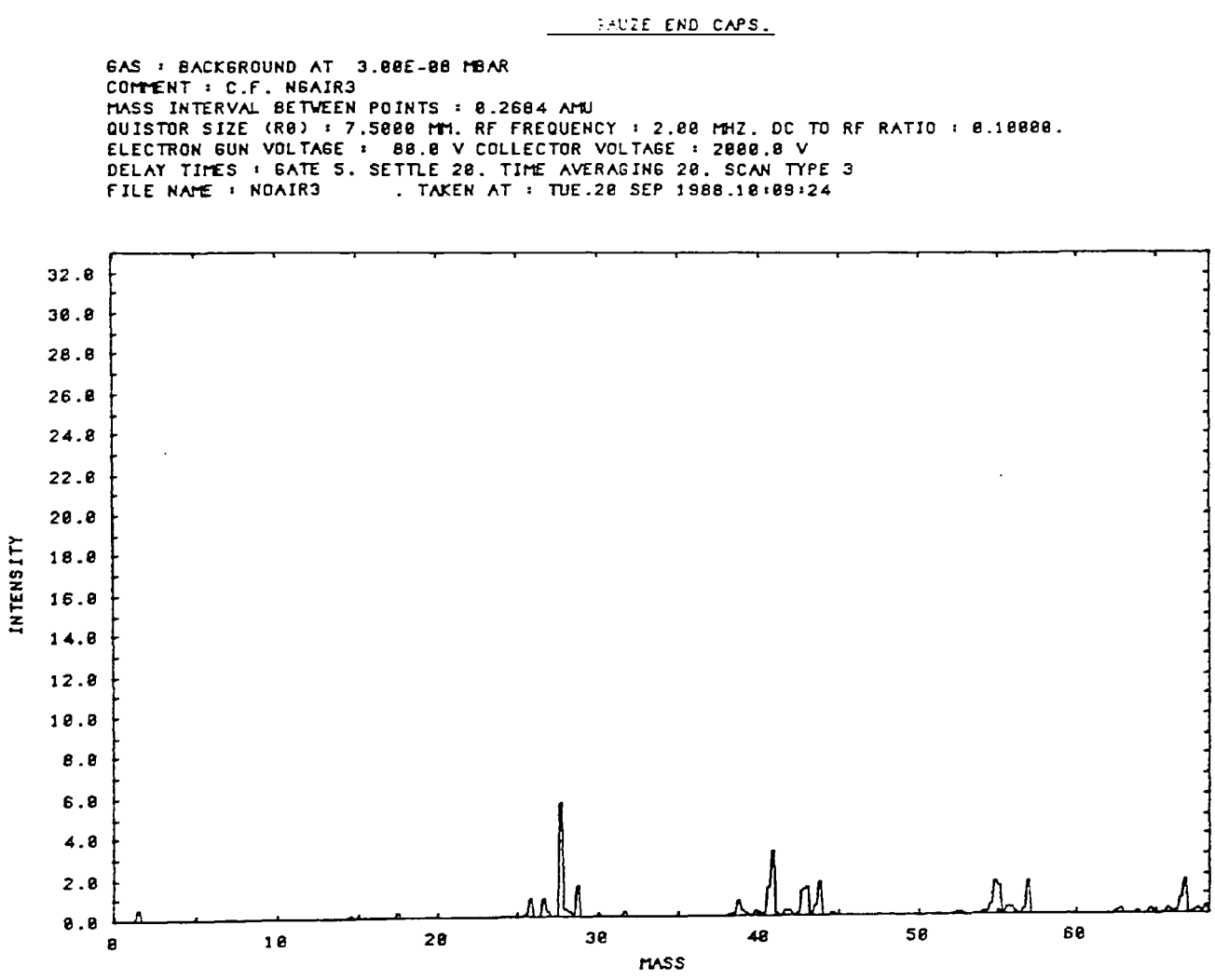

Fig. IV.10.9 Background spectrum with new gauze end caps at 3 x 10^{-8} mBar.

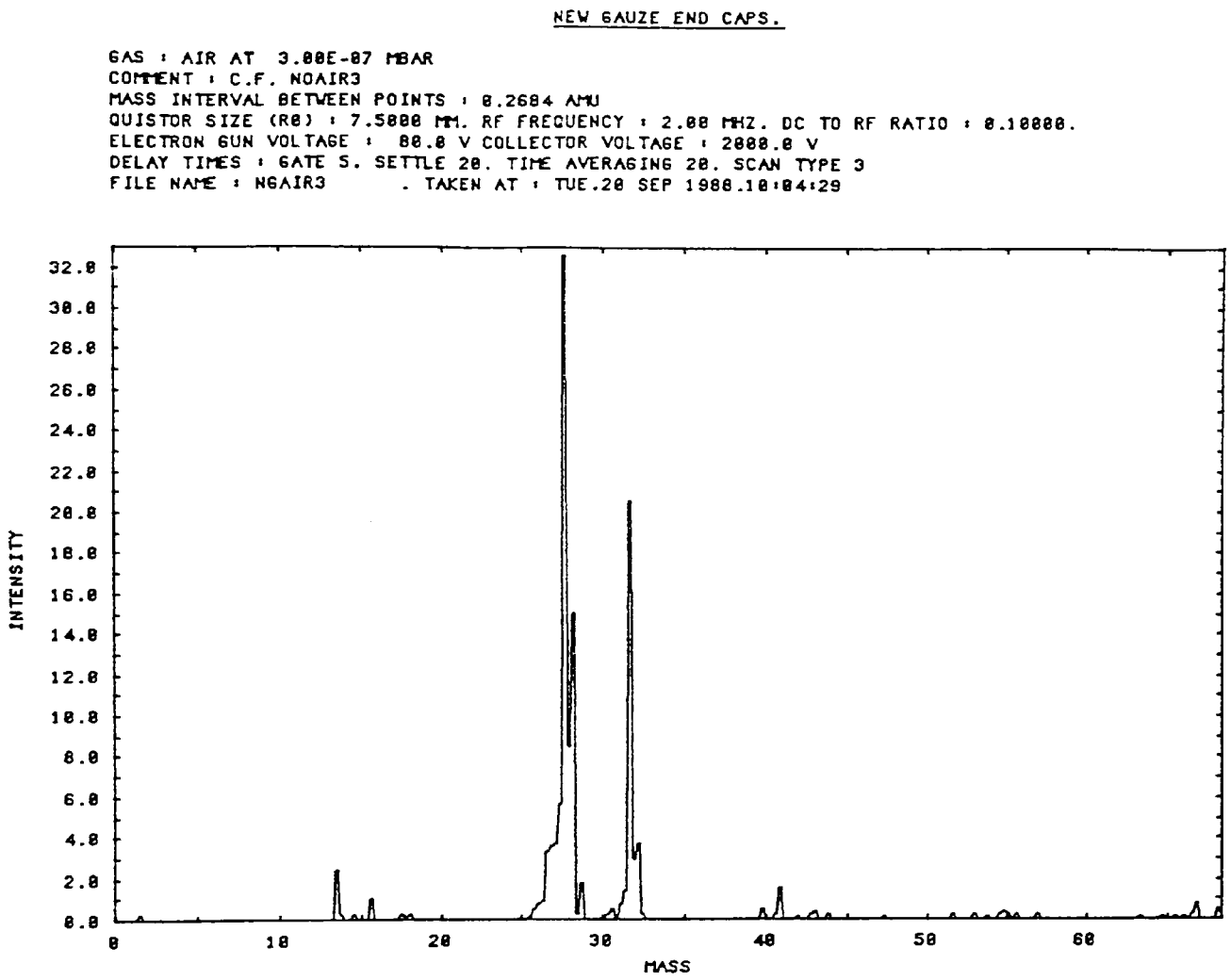

Fig. IV.10.10 Spectrum of air at 3 x 10^{-7} mBar with new gauze end caps.

The sensitivity of the background peaks has been reduced, presumably because of ion - neutral collisions; but the peaks do remain.

Chapter IV : Construction of the prototype Quistor heads.

11) The new RF unit.

The RF unit in use initially produced RF voltages of up to 1350 V peak - peak at 2 Mhz. This unit had been supplied by VG Quadrupoles Ltd., and was intended for operation with a Quadrupole mass filter. The unit suffered from the following drawbacks :

a) The response time constant for a change in the RF and DC voltages was rather long - initially more than 100 μs. This is not ideal for the Quistor since ion ejection depends on a clear voltage increment. This would not affect a Quadrupole.

b) There was no facility for ensuring that the two RF output voltages were equal in amplitude. This depends upon the capacitance loading on each output being correct. The unit originally included a double variable tuning capacitance ganged so that the added capacitance on each output was always the same. That was acceptable for a Quadrupole where the capacitance of the rods themselves was always the same. For the Quistor, the capacitance of the electrodes to ground is not the same and so balancing was required.

The single ganged tuning capacitor was replaced with two separate ones. This allowed correction of the imbalance. However the unit did not include a means of ensuring that the outputs were, in fact, equal. Unequal RF outputs would reduce the mass range which can be achieved, and would severely reduce the resolution obtainable.

c) The output voltage range was quite limited, allowing a mass range of only about 65.

An RF unit, in addition to all the other power

supplies required for the Quistor, was ordered according to the specification required for the Quistor. Unfortunately its delivery was severely delayed, and when it was delivered, its condition was very poor. Nonetheless, (eventually) it could provide about 2200 V peak - peak (approximately equal) at the outputs. The response time constant was about 10 μs.

The unit also incorporated additional power supplies required by the Quistor. These included a filament heater supply, filament biasing, and the -2KV supply to the multiplier.

Once the unit worked properly, better spectra than previously were obtained. The mass range was now about 125 and the resolution, particularly at high masses, was very good. Some examples follow.

An additional feature built into the unit was switchable electronic gain in the output detection circuits. The sensitivity ranges are calibrated in pico - coulombs of charge received from the channel plates. The ranges available are 1.0, 3.3, 10.0, 33.0, 100 and 330 pC.

Previously, where a change in sensitivity was required, this could only be achieved by changing the channel plate voltage. That does not allow for any quantitative calibration so that the switchable gain is very much more convenient.

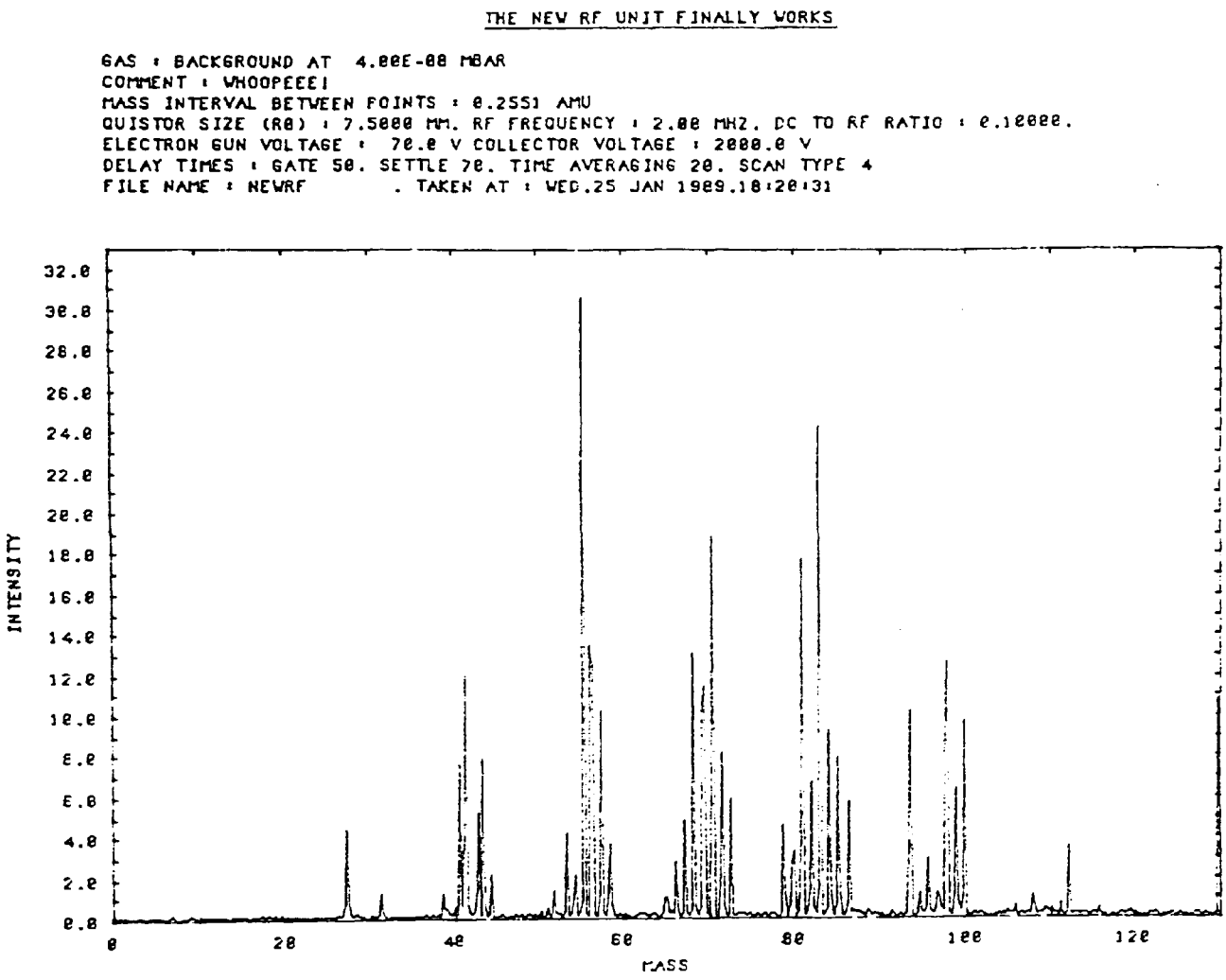

Fig. IV.11.1 Background scan with the new RF unit.

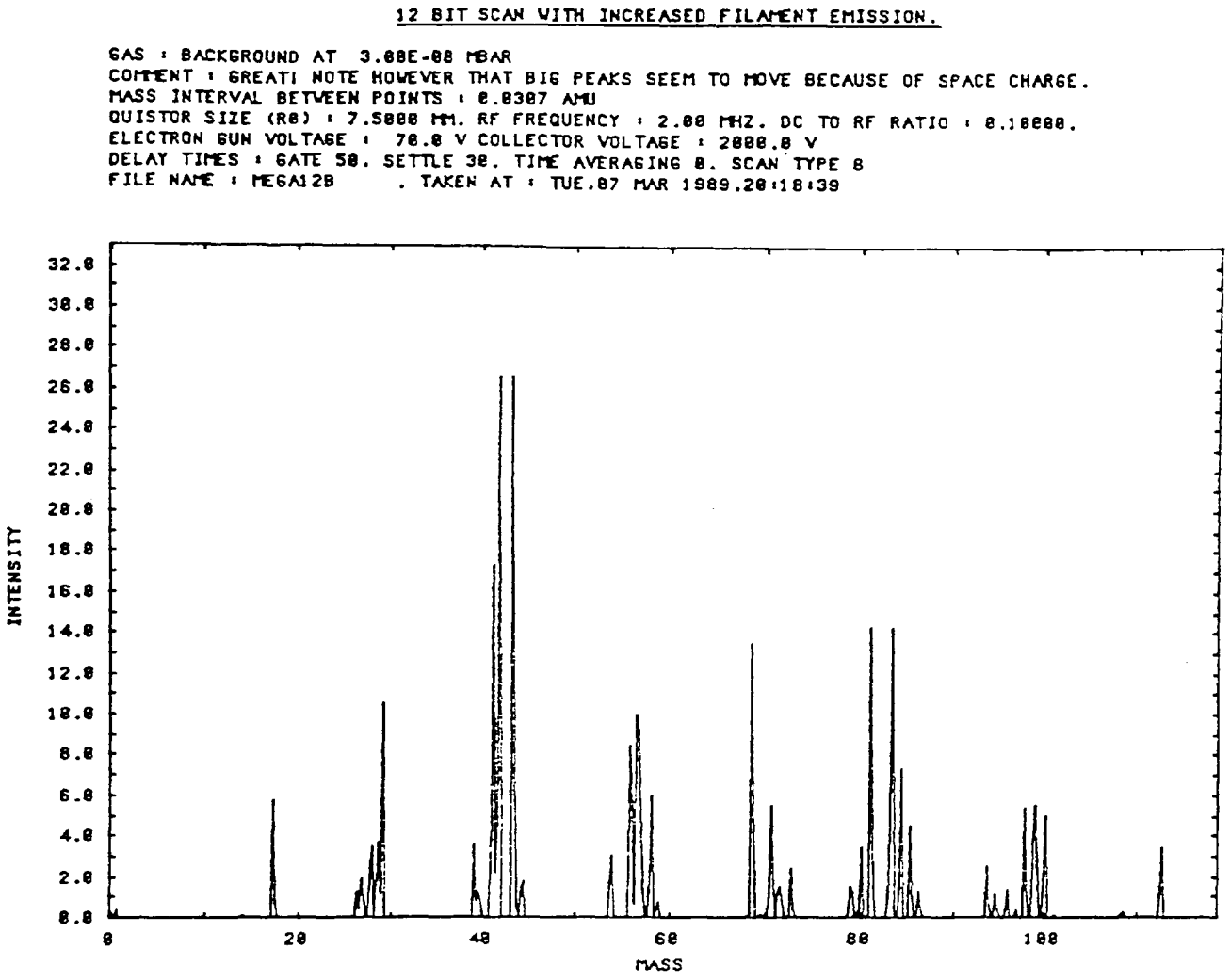

Fig. IV.11.2 12 bit background scan with the new RF unit.

The above scan was recorded using 4096 points (scan type 8, see section IV.8). The filament temperature had been increased in order to increase the filament emission to 0.75 mA. This resulted in better sensitivity, but the larger peaks at low masses show a loss of resolution, and split peak effects, presumably due to the effects of space charge.

This is partly due to a flaw which remains in the RF unit. The feedback which controls the RF output voltage is produced by rectification of a 20 V peak - peak RF signal

proportional to the RF output. The rectifying diodes have a voltage drop (PN junction bias) across them. In consequence, a certain amount of RF must always be produced before the feedback begins to operate.

This results in a constant offset in the RF voltage compared with the DC voltage applied to the electrodes. In consequence the DC to RF ratio is too low at low masses and several ions can be trapped at once so that a lot of space charge is present.

This weakness can easily be overcome by ensuring that a positive bias equal to the PN junction voltage is applied. This has not yet, however, been done.

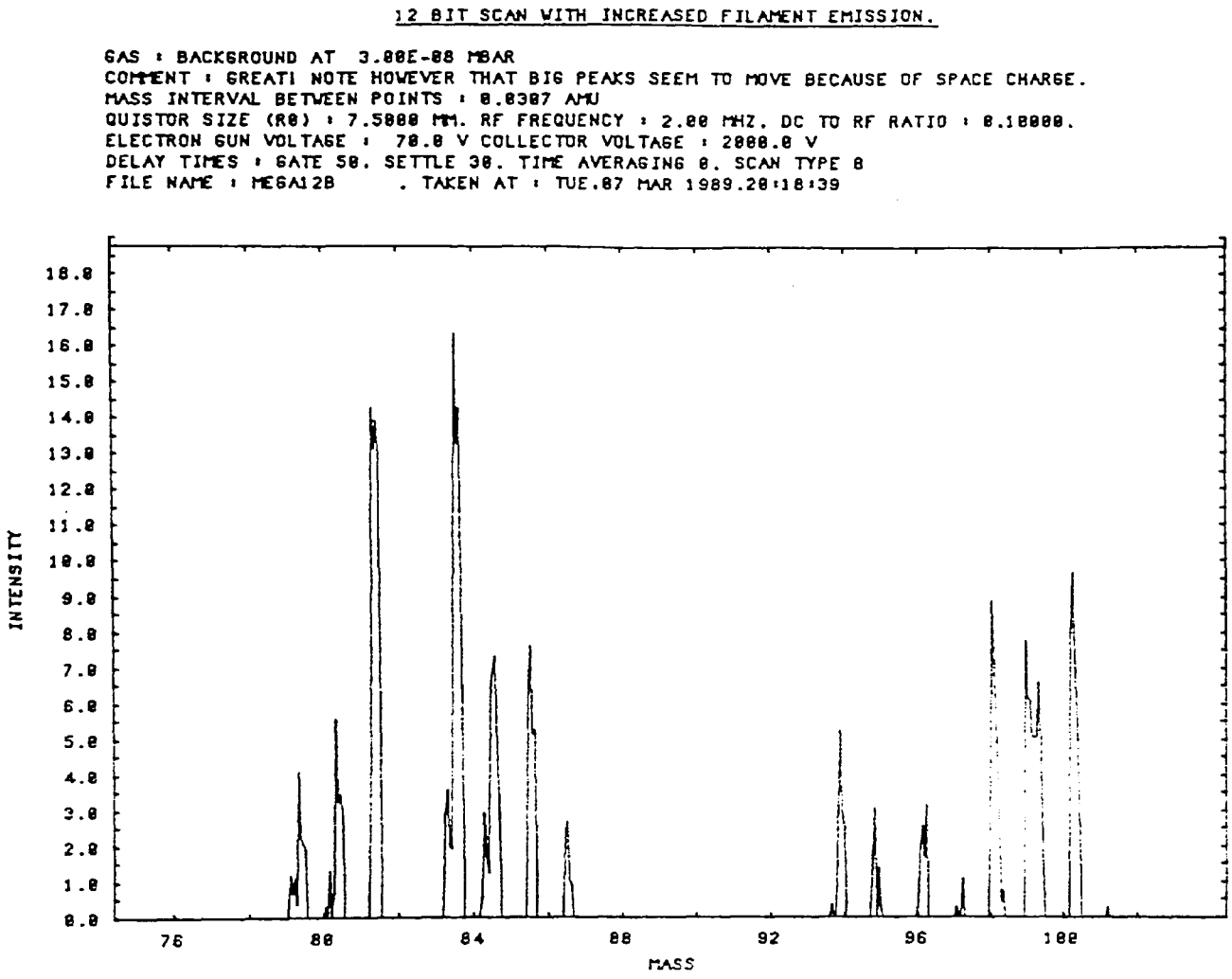

Fig. IV.11.3 Detail of the above spectrum showing the peak shapes.

The resolution shown in this spectrum is about 300 at mass 100, or a peak width of 1/3 of a mass unit. Note though that some degree of peak splitting is still visible.

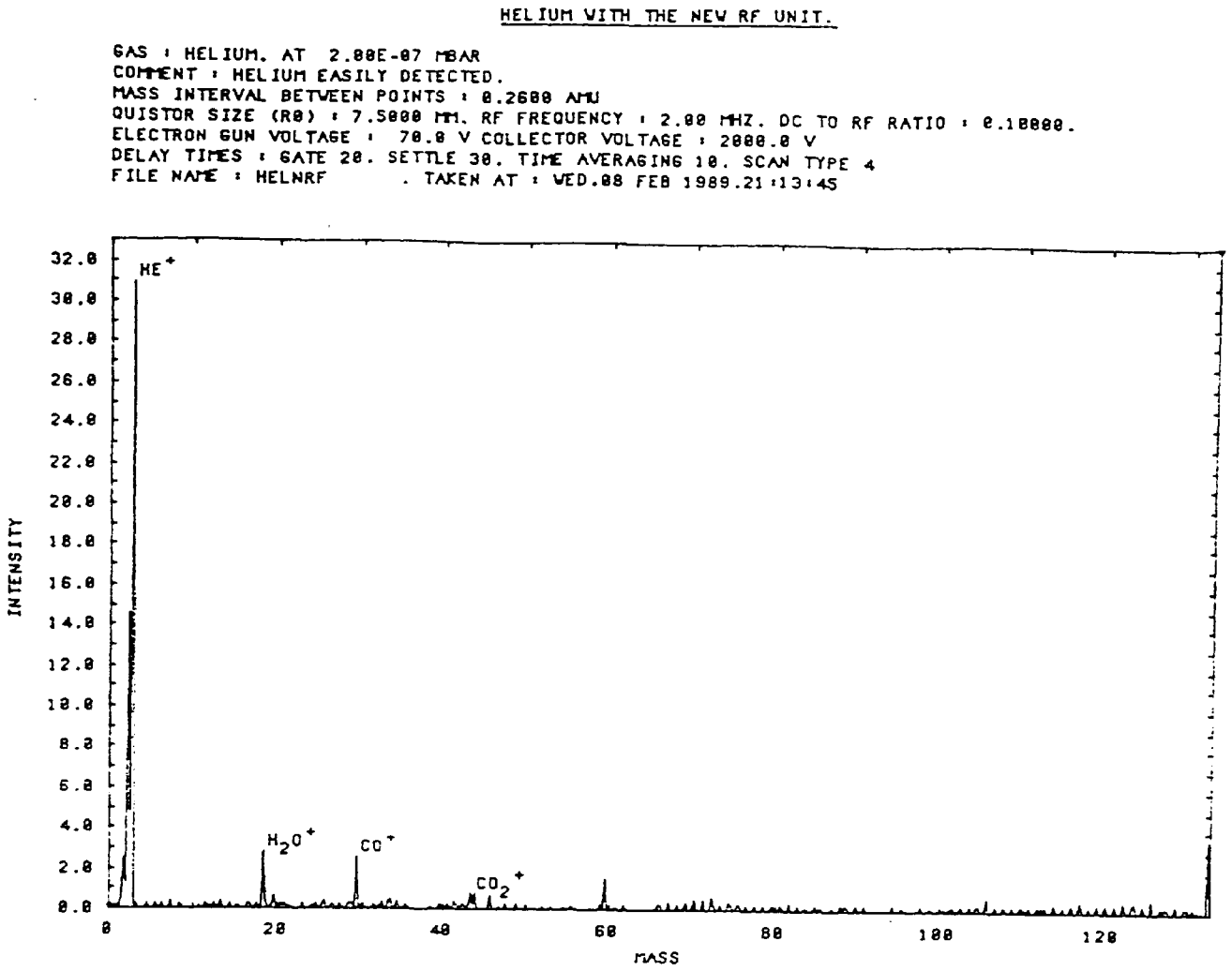

Fig. IV.11.4 Spectrum of Helium at 2 x 10^{-7} mBar with the new RF unit.

Sensitivity of the Quistor to Helium is important because the gas is frequently used for leak detection purposes. Note that the Helium peak has split because of the space charge of the Helium ions.

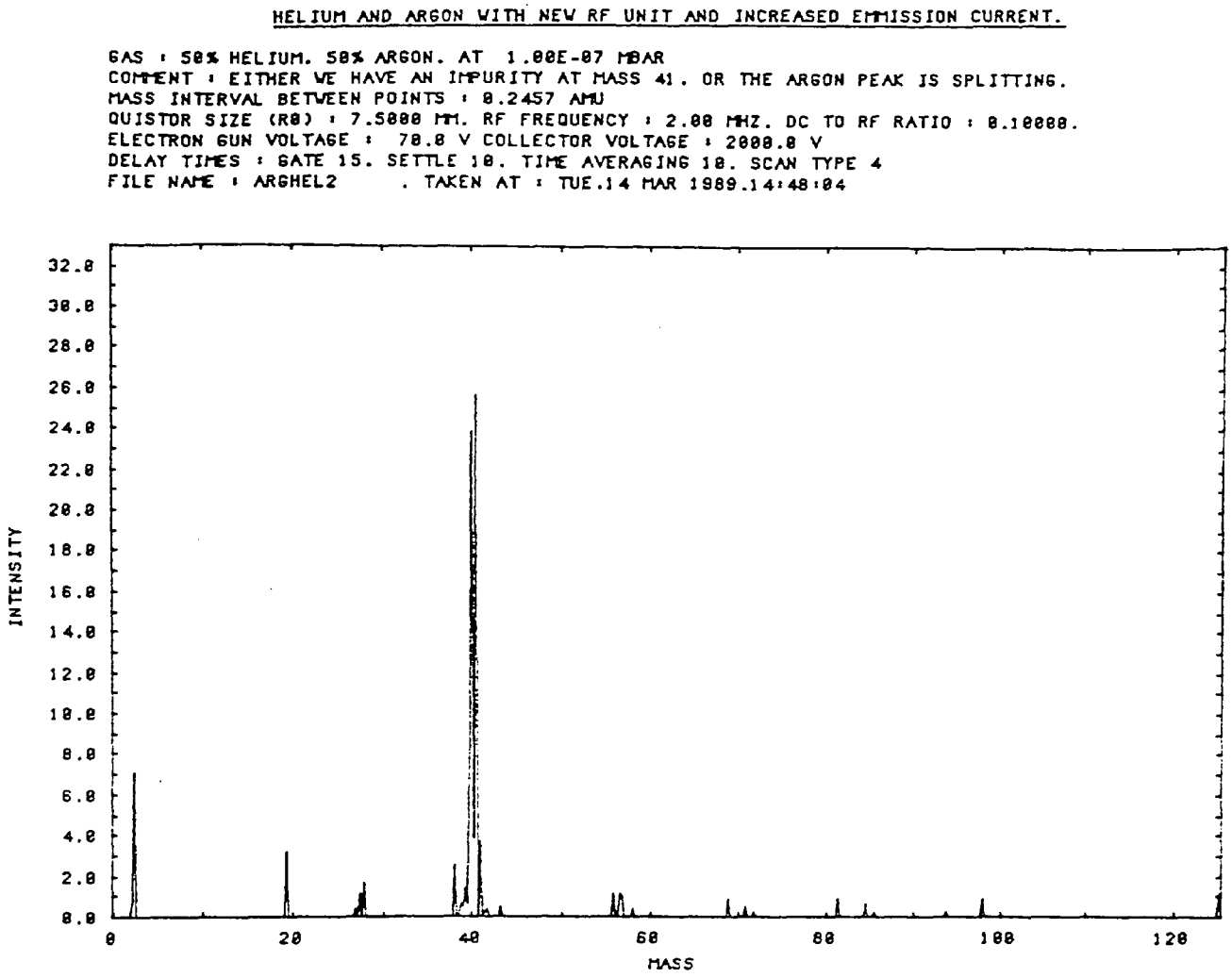

Fig IV.11.5 Spectrum of an equal mixture of Helium and Argon at 1 x 10^{-7} mBar using the new RF unit.

Peaks at masses 4, 20 and 40 are clearly seen. Note that the Argon peak appears to have split due to the space charge of the ions. It is also possible that a contamination of mass 41 or 39 was present in the gas feeding tube, accounting for the apparent double peak in this spectrum.

The Helium peak is much smaller than the Argon peak, probably for three reasons. The Quistor is in any case less sensitive at low masses, and Helium gas is much (about 7.5 times) more difficult to ionise than Argon. Finally it is

likely that some of the Helium may have leaked away from the sample (which was not particularly fresh) as Helium is notoriously good at passing through small leaks.

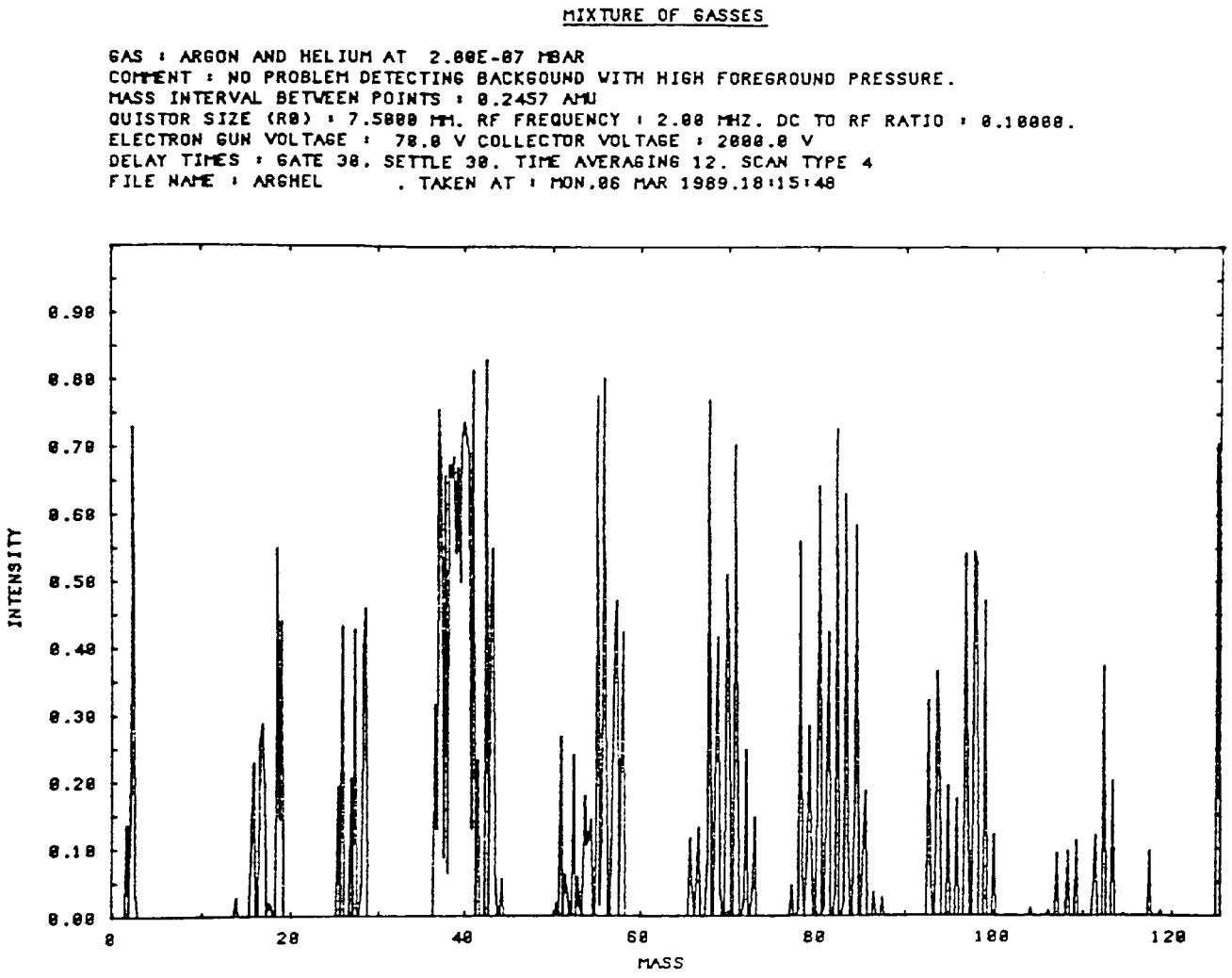

Fig IV.11.6 Spectrum of the background peaks present with 2 x 10^{-7} mBar of an equal mixture of Helium and Argon.

This spectrum was taken with the electronic gain switched up to maximum. It demonstrates that low abundance peaks in the Quistor can still be easily detected in spite of the presence of much more abundant gases. It also demonstrates that the noise level remaining in the spectrum

is now very low, not being visible even at this high gain setting. The abundant Argon peak is substantially spread around mass 40. If the peaks near to this mass were of interest, it would be necessary to reduce the ionisation time in order to increase the resolution of that peak. Naturally this would reduce the sensitivity.

It is also clear that the electronics which amplifies the signal is saturating since the Argon peak in this spectrum should be well off scale. This is a problem which can easily be overcome.

12) Ionisation and ion storage time plots.

In addition to scanning mass spectra, the Quistor operating program allows monitoring of only one, or up to 16 selected ion masses. This is invaluable for, for example, leak detection.

By scanning the programmed ionisation time, or the ion storage time, this feature can also be used to investigate the rate at which ions are built up, and the rate at which they are lost from the trap. This is very useful for selecting the best possible ionisation time and storage time under a given set of conditions.

In addition, this technique can provide very interesting data on, for example, the ion - molecule collision processes involved in the Quistor. (Ref. 103)

The following plots are taken by monitoring the mass 28 peak, and allowing air to enter the vacuum system through the needle valve at a range of pressures. Note that these plots were all taken with the same channel plate and electronic gain.

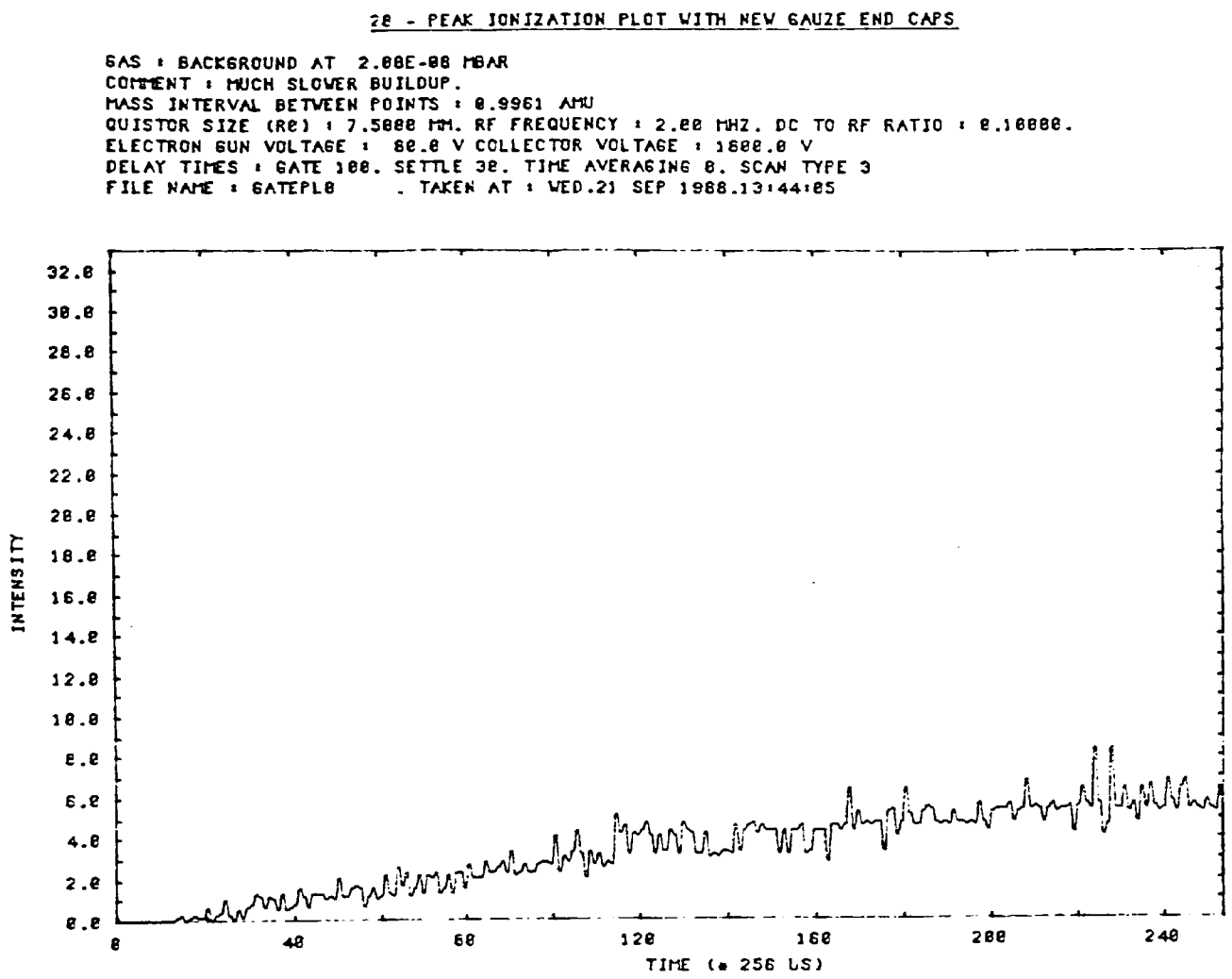

Fig. IV.12.1 Ionisation time plot for mass 28 at 2 x 10^{-8} mBar background pressure.

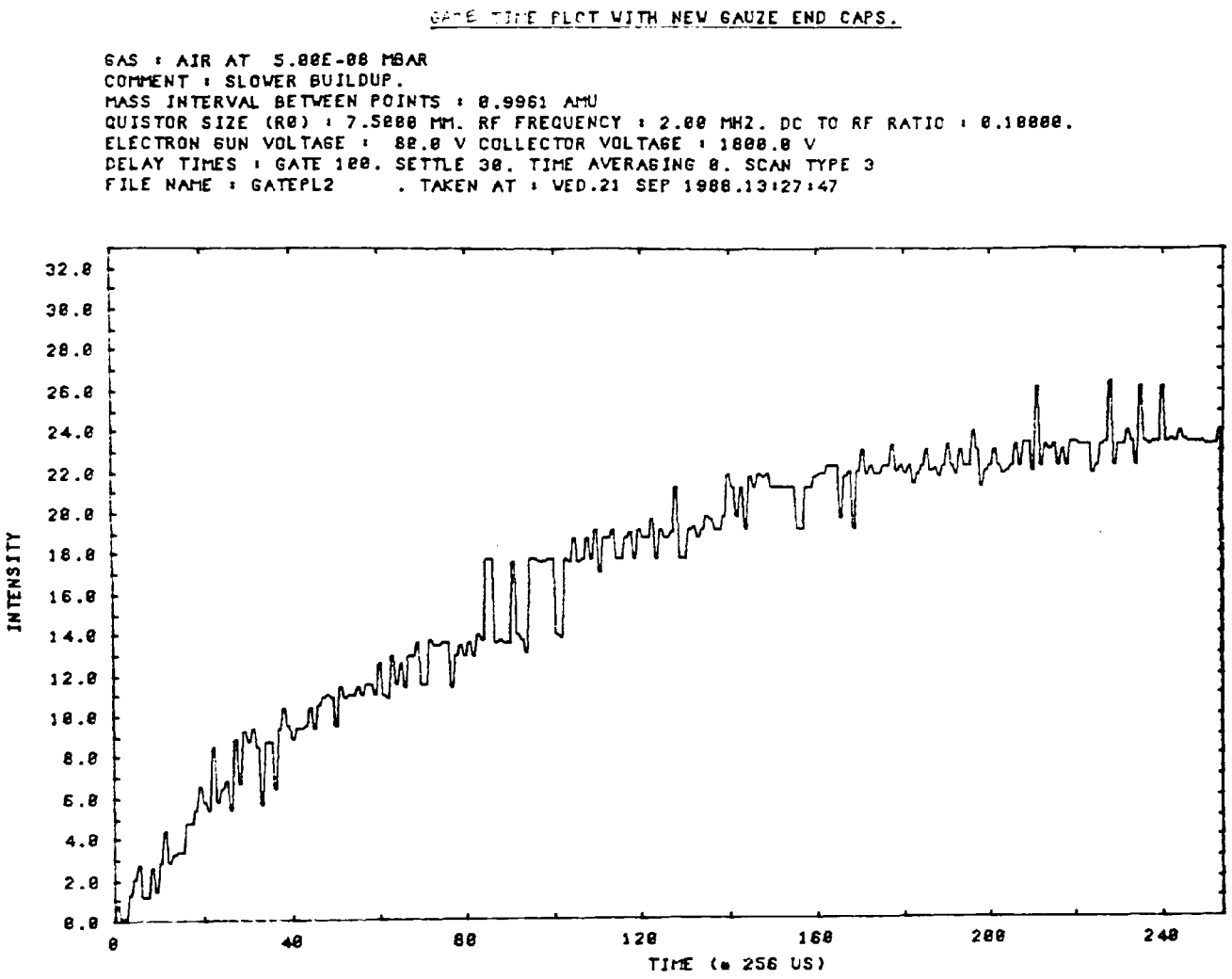

Fig. IV.12.2 Ionisation time plot for mass 28 at 5 x 10^{-8} mBar of air.

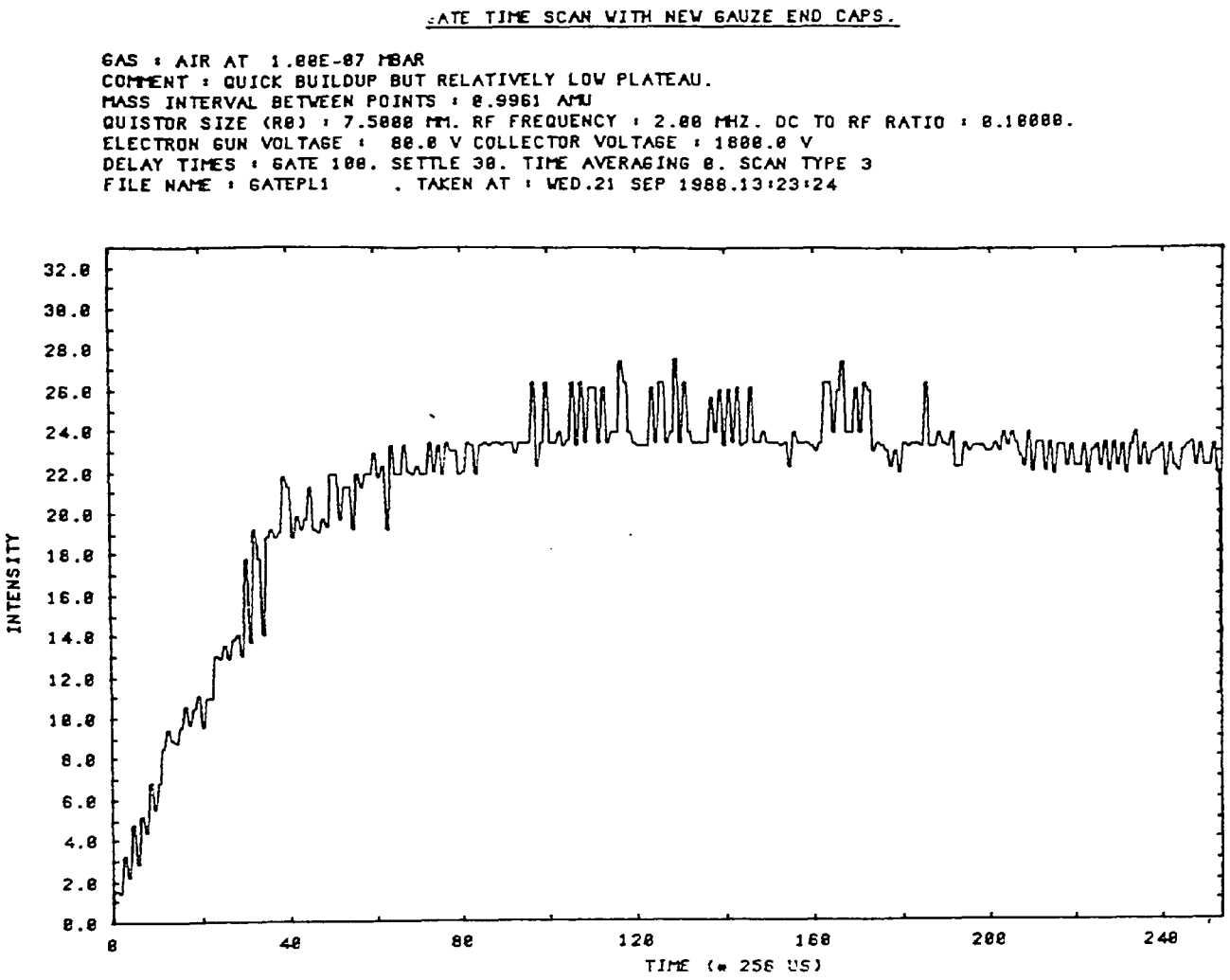

Fig. IV.12.3 Ionisation time plot for mass 28 at 1 x 10^{-7} mBar of air.

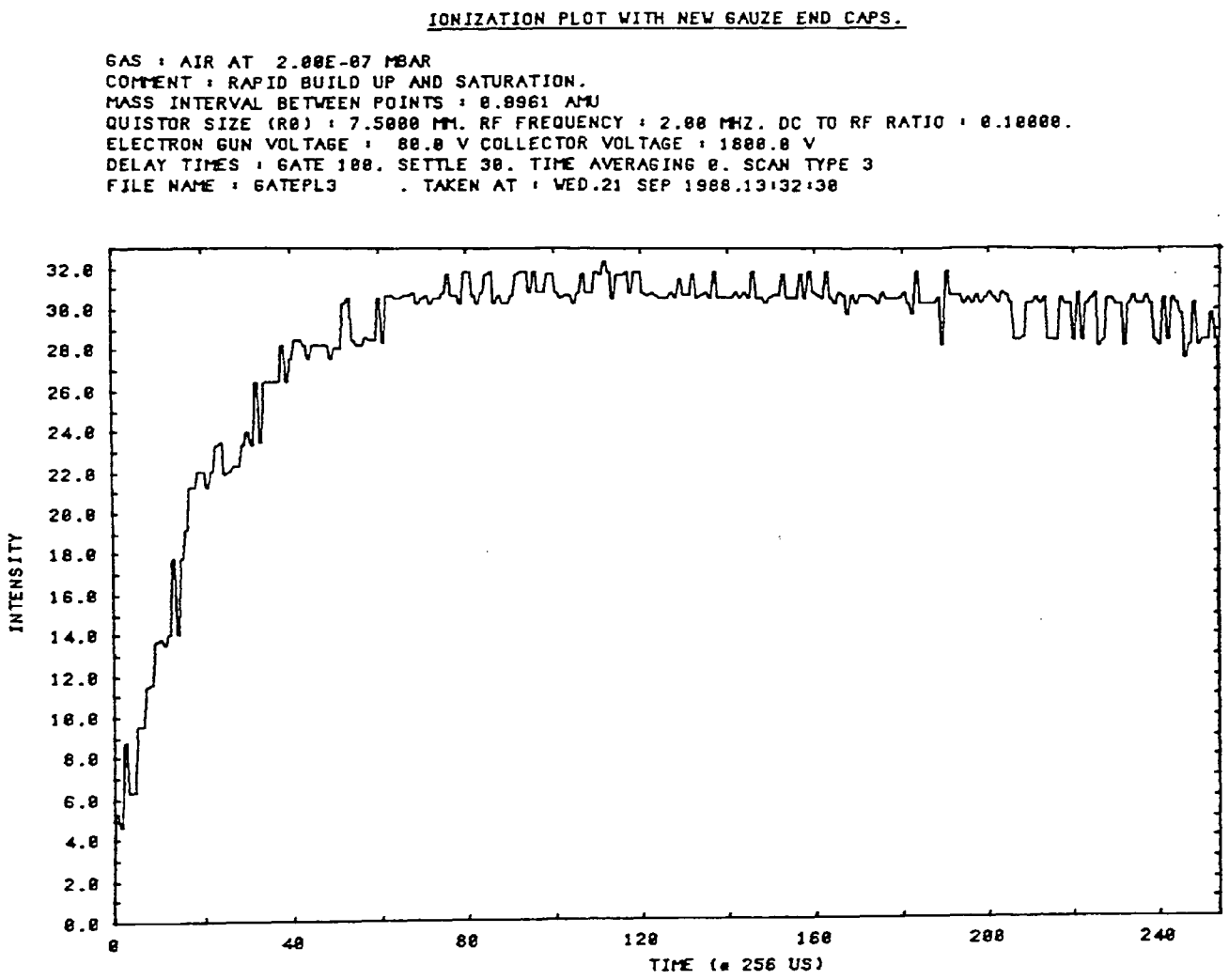

Fig. IV.12.4 Ionisation time plot for mass 28 at 2 x 10^{-7} mBar of air.

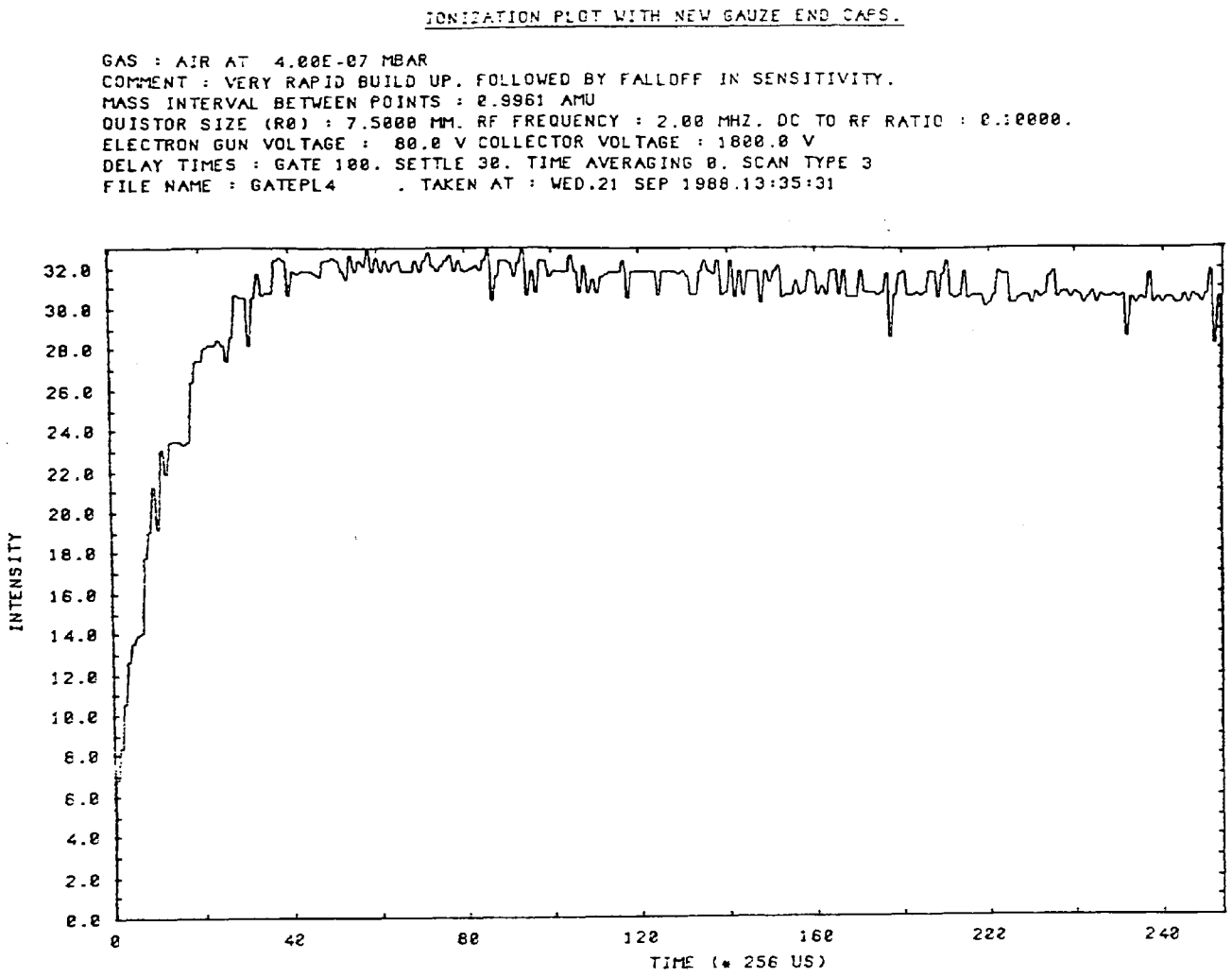

Fig. IV.12.5 Ionisation time plot for mass 28 at 4 x 10^{-7} mBar of air.

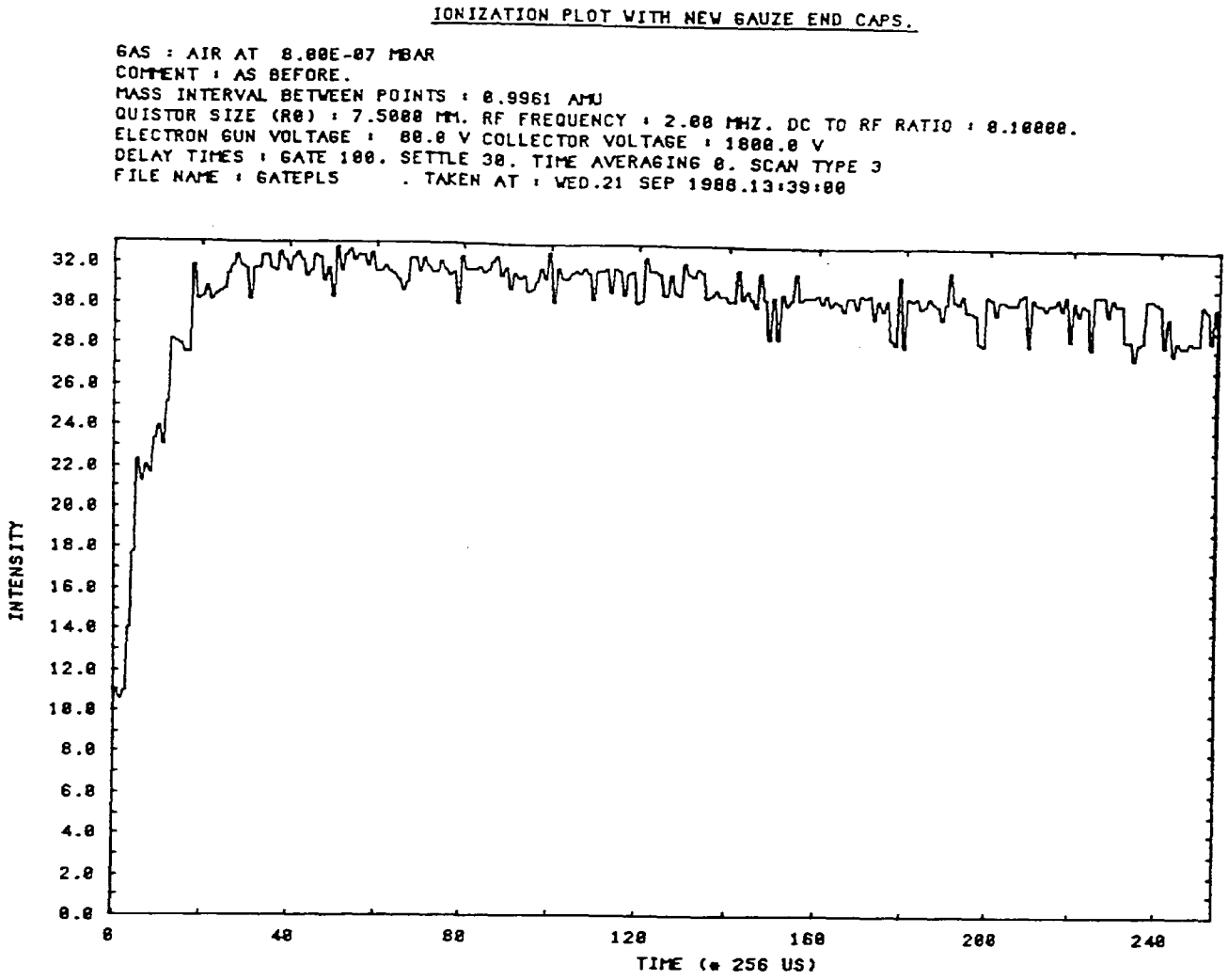

Fig. IV.12.6 Ionisation time plot for mass 28 at 8 x 10^{-7} mBar of air.

The initial rate of ion creation is seen, as expected, to be proportional to the partial pressure of mass 28 in the system. What is clear, however, is that the number of ions in the trap always asymptotically approaches a maximum value. This value depends only upon the ratio of the partial pressure of mass 28, to the total system pressure, and upon the electron beam current entering the trap (This assumes that the space charge limit of the trap's sensitivity is much greater).

Mathematically, the rate of ion build-up can be expressed as :

$$\frac{dN}{dt} = sIp - lPN \qquad (IV.12.1)$$

where

N is the number of ions in the trap,
p is the partial pressure of the selected mass,
I is the electron beam current in the trap,
P is the total system pressure,
s is the electron impact ionisation cross section, and
l is the ion - molecule collision loss cross section.

It follows that the limiting number of ions is given by

$$N_{max} = \frac{sIp}{lP} \qquad (IV.12.2)$$

and that the number of ions at time t is

$$N = \frac{sIp}{lP} (1 - e^{-lPt}).$$

In the plots at very high pressures, the sensitivity actually drops slightly with longer ionisation times. This is attributed to the fact that during the period when the electron beam is off, electrons can still leave the filament and will form a cloud around the filament. As soon as the electron beam is switched on again, these electrons will form a burst of electron beam current which produces a relatively large number of ions at that time. At high pressures, however, these ions will be lost after a fairly short time and so will no longer contribute to the sensitivity.

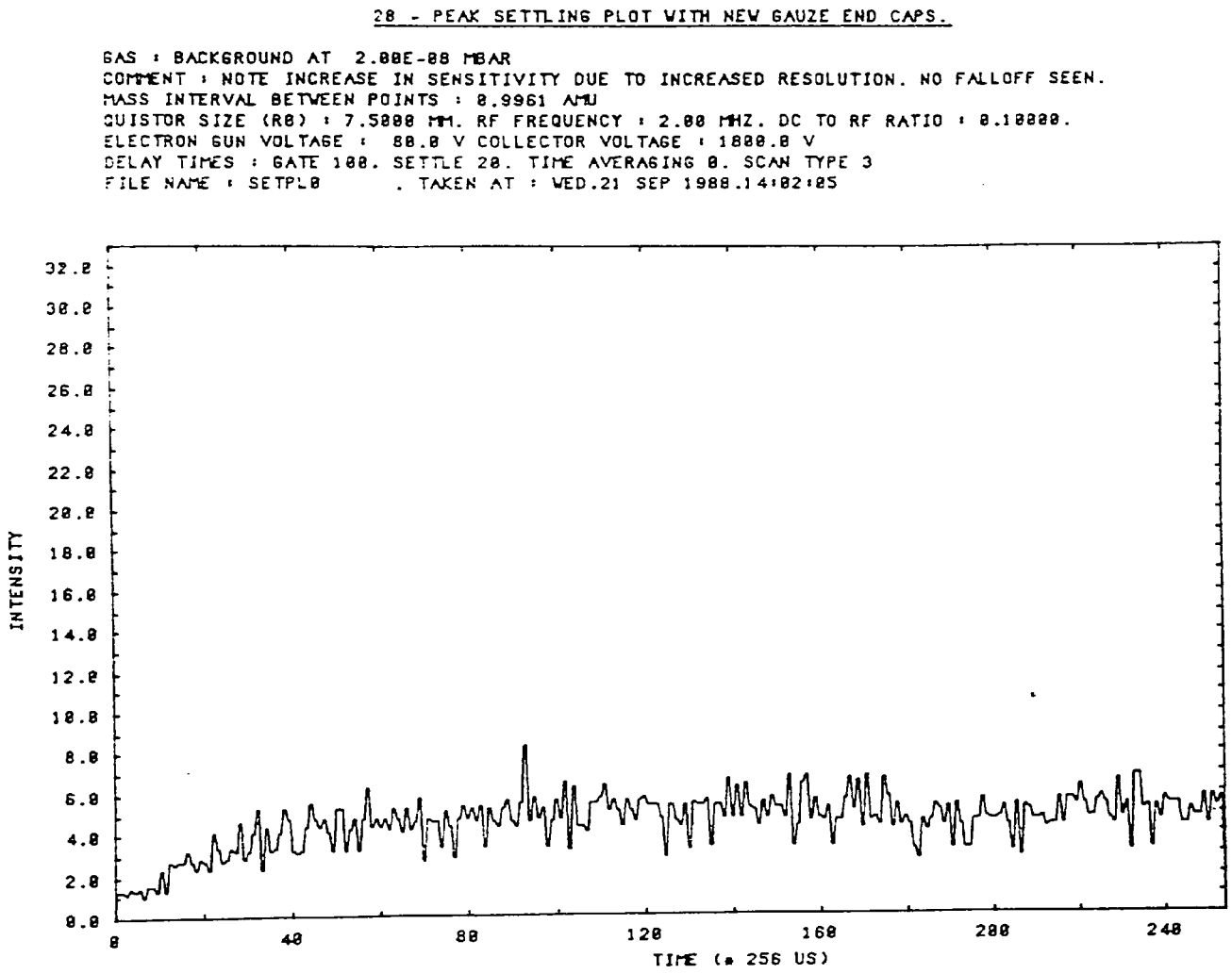

Fig. IV.12.7 Ion storage time plot for mass 28 at a background pressure of 2 x 10^{-8} mBar.

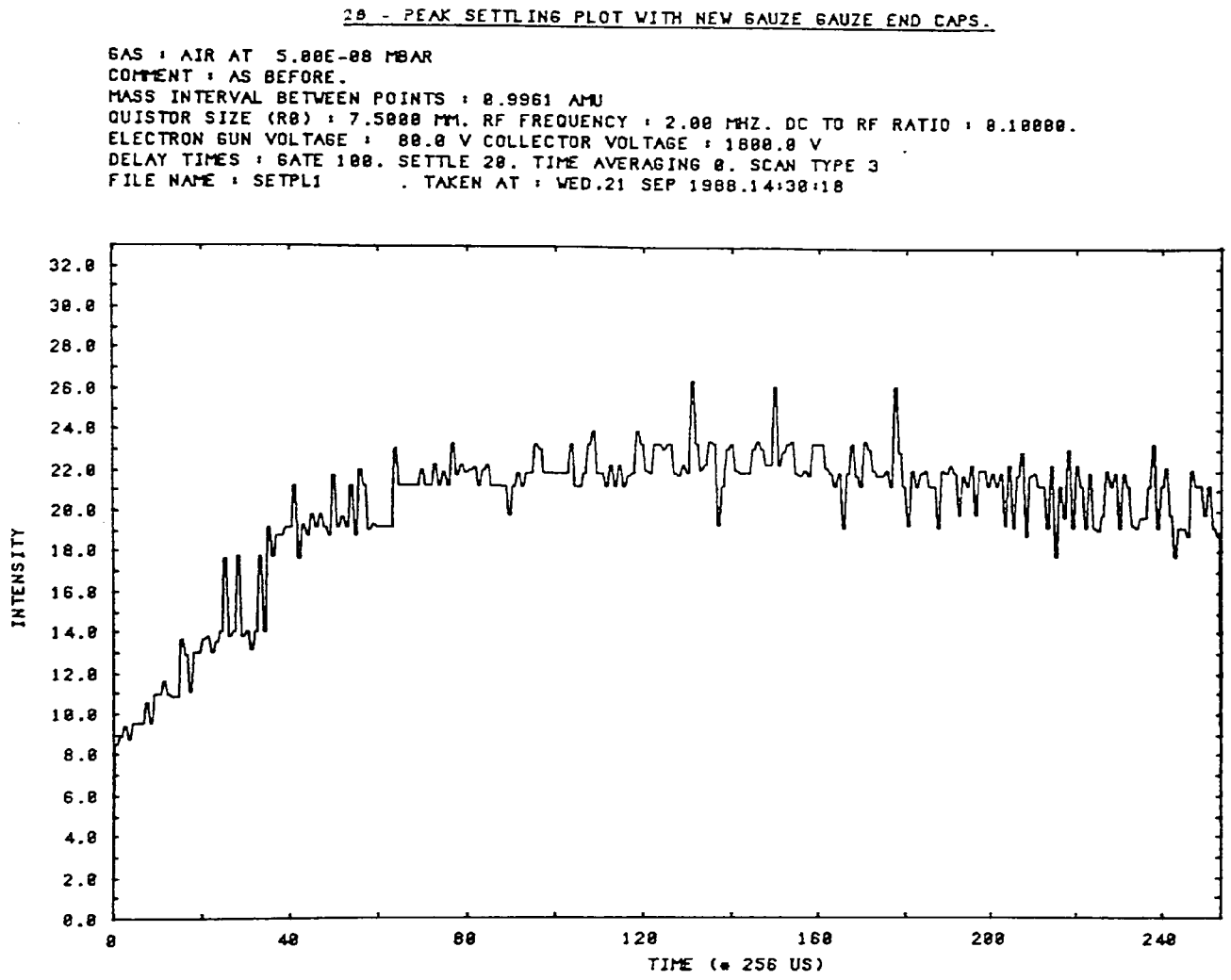

Fig. IV.12.8 Ion storage time plot for mass 28 at a pressure of 5 x 10^{-8} mBar of air.

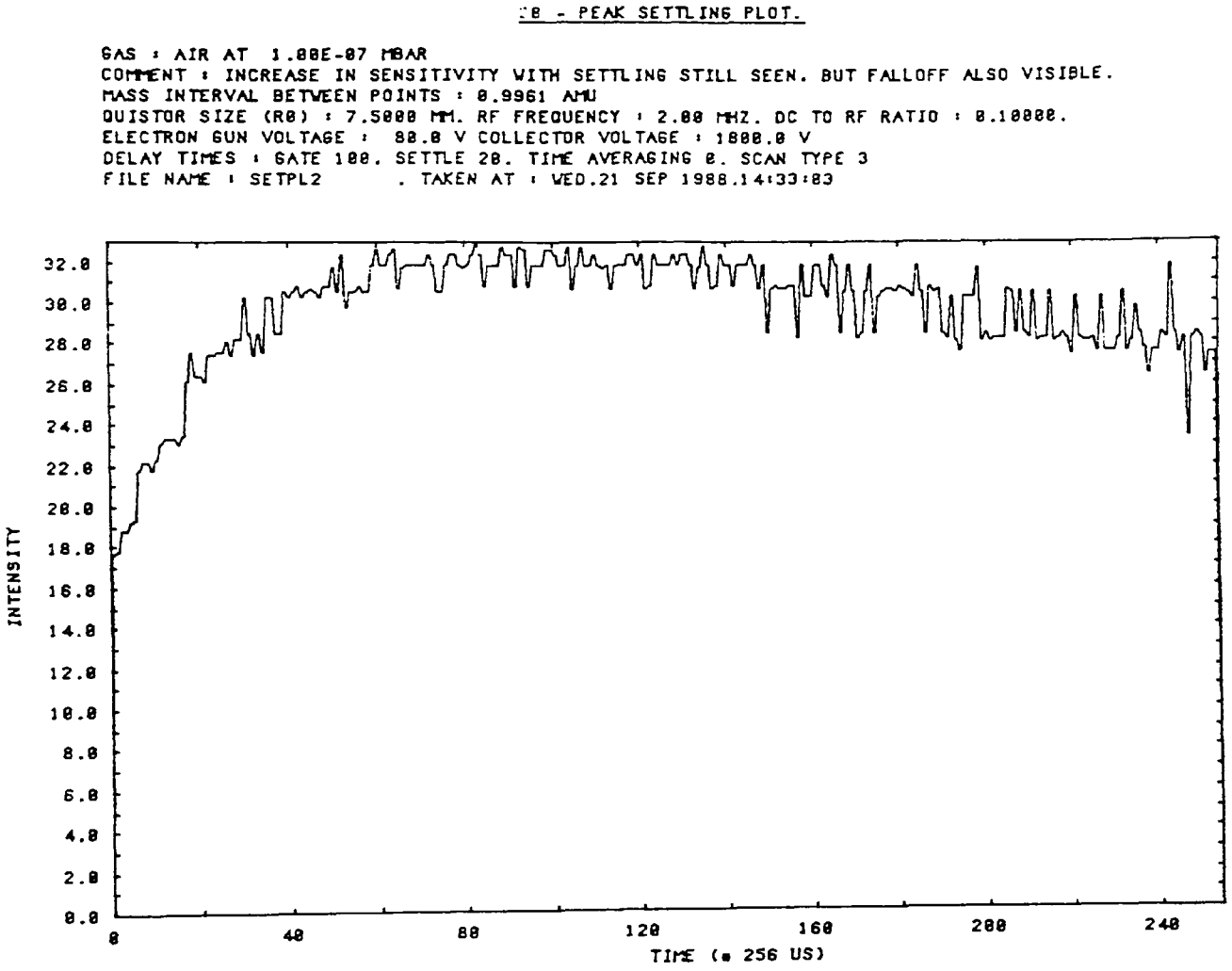

Fig. IV.12.9 Ion storage time plot for mass 28 at a pressure of 1 x 10^{-7} mBar of air.

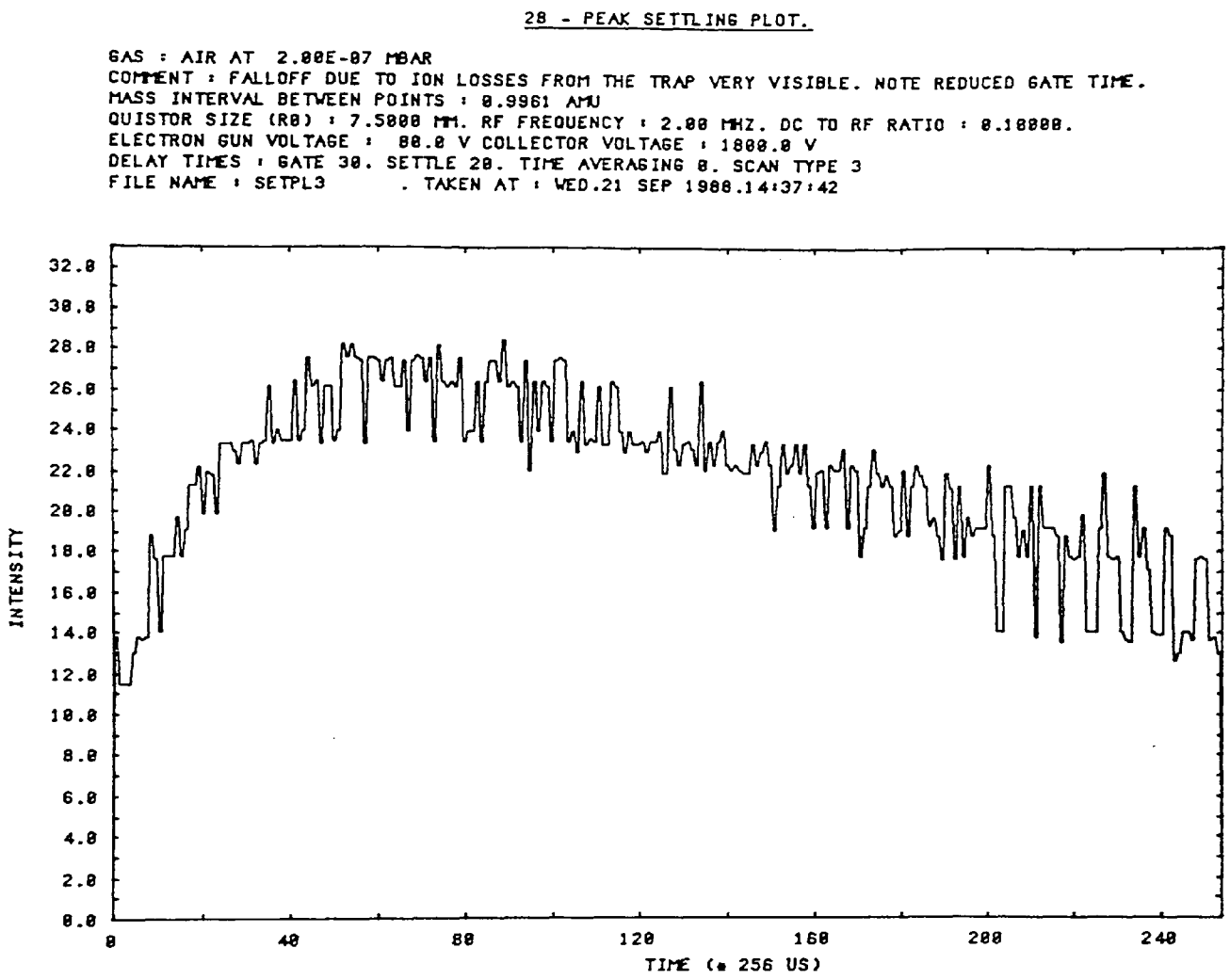

Fig. IV.12.10 Ion storage time plot for mass 28 at a pressure of 2 x 10^{-7} mBar of air.

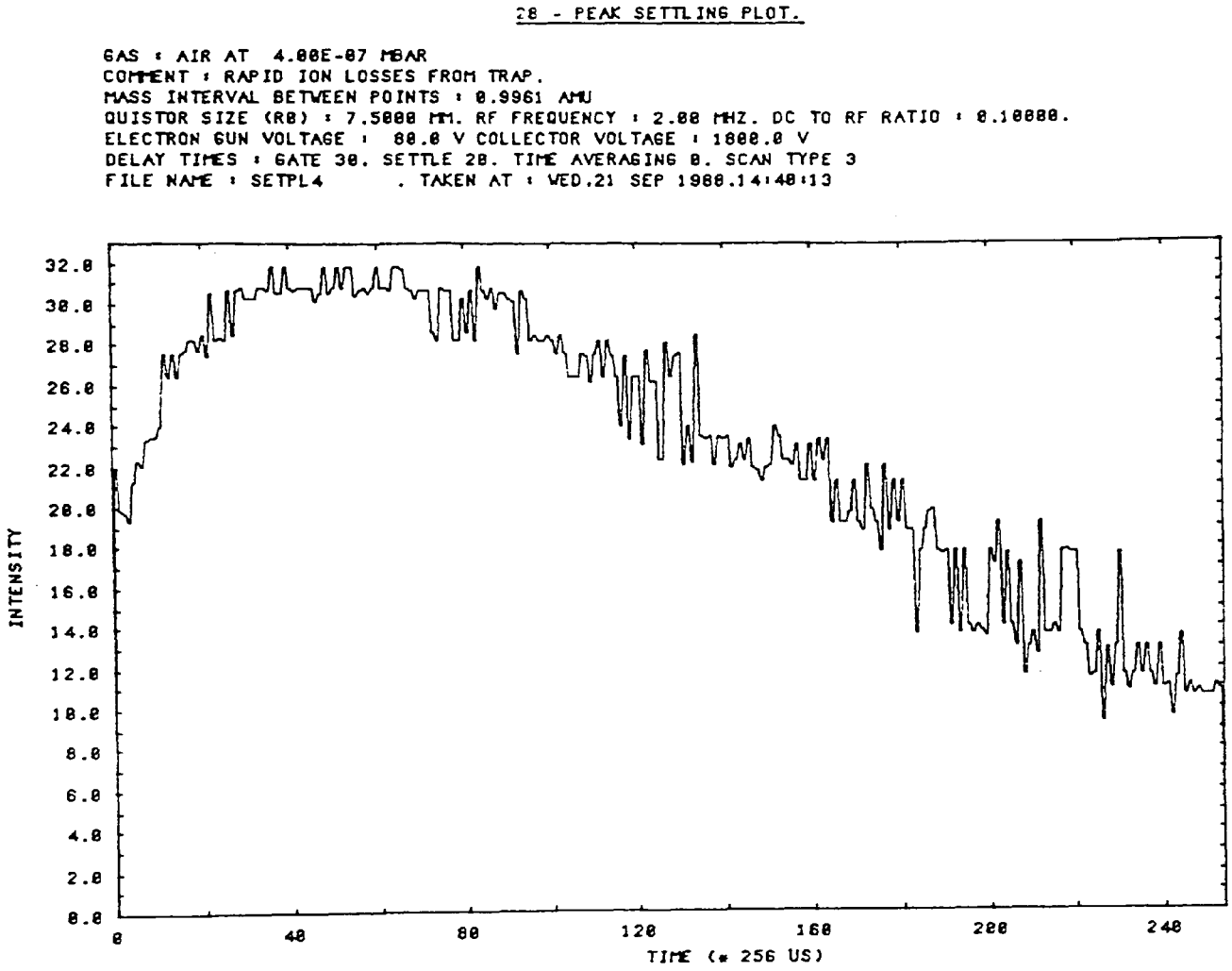

Fig. IV.12.11 Ion storage time plot for mass 28 at a pressure of 4 x 10^{-7} mBar of air.

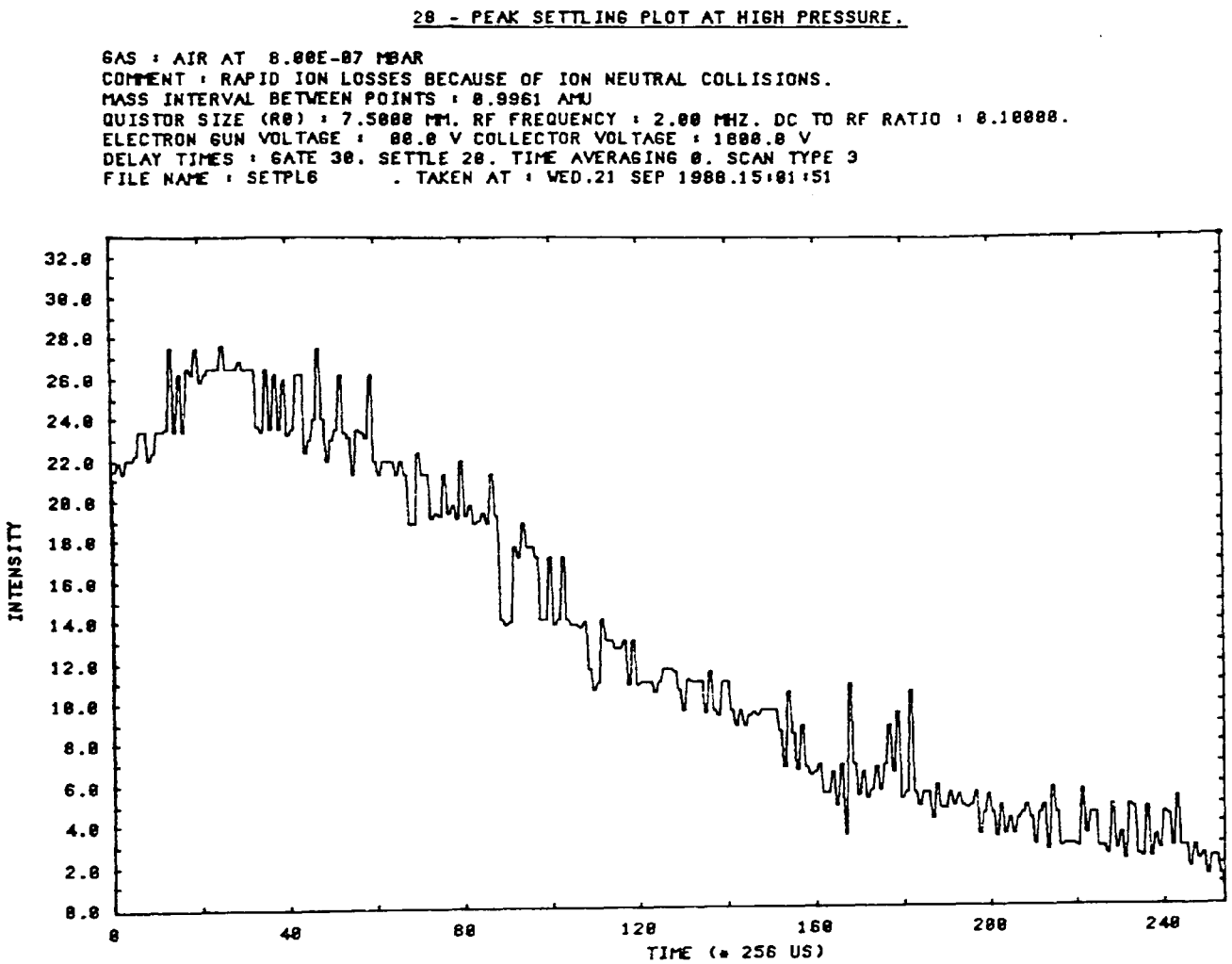

Fig. IV.12.12 Ion storage time plot for mass 28 at a pressure of 8 x 10^{-7} mBar of air.

Two factors are visible in these plots. In each case there is an increase in sensitivity with ion storage time up until a time of about 20 ms. This is because the resolution of the Quistor increases with ion storage time, and in the mode of operation used here, the sensitivity improves with resolution.

The rate of ion loss is also clear, and can be approximately measured from these plots, at any rate at higher pressures. If the loss rate at low pressures needs to

be measured, a longer ion settling time would be required. That is not available on the present system, although planned improvements include more sophisticated control of the ionisation and storage times to allow shorter, and longer times.

The following time constants for 63.2% of the ions (1/e th remain) to be lost are taken from the above plots.

Pressure	Time constant
5×10^{-8}	429.6 ms
1×10^{-7}	236.7 ms
2×10^{-7}	81.2 ms
4×10^{-7}	39.6 ms
8×10^{-7}	20.5 ms

Fig. IV.12.13 Table of ion loss times for mass 28.

Broadly similar results were obtained at a later time for Argon ions in an equal mixture of Argon and Helium.

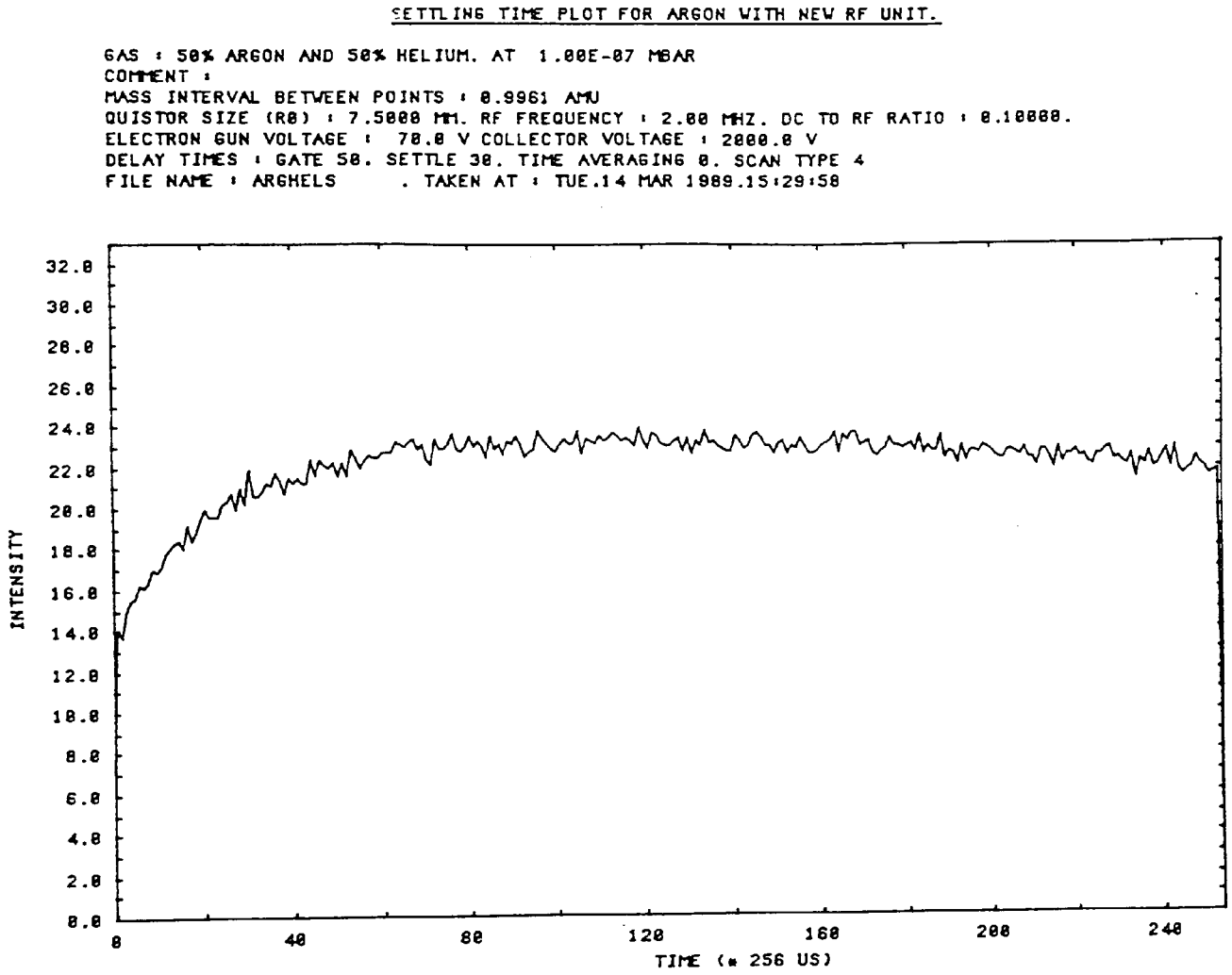

Fig. IV.12.14 Ion storage time plot for Ar^+ ions in an equal mixture of Argon and Helium at 10^{-7} mBar.

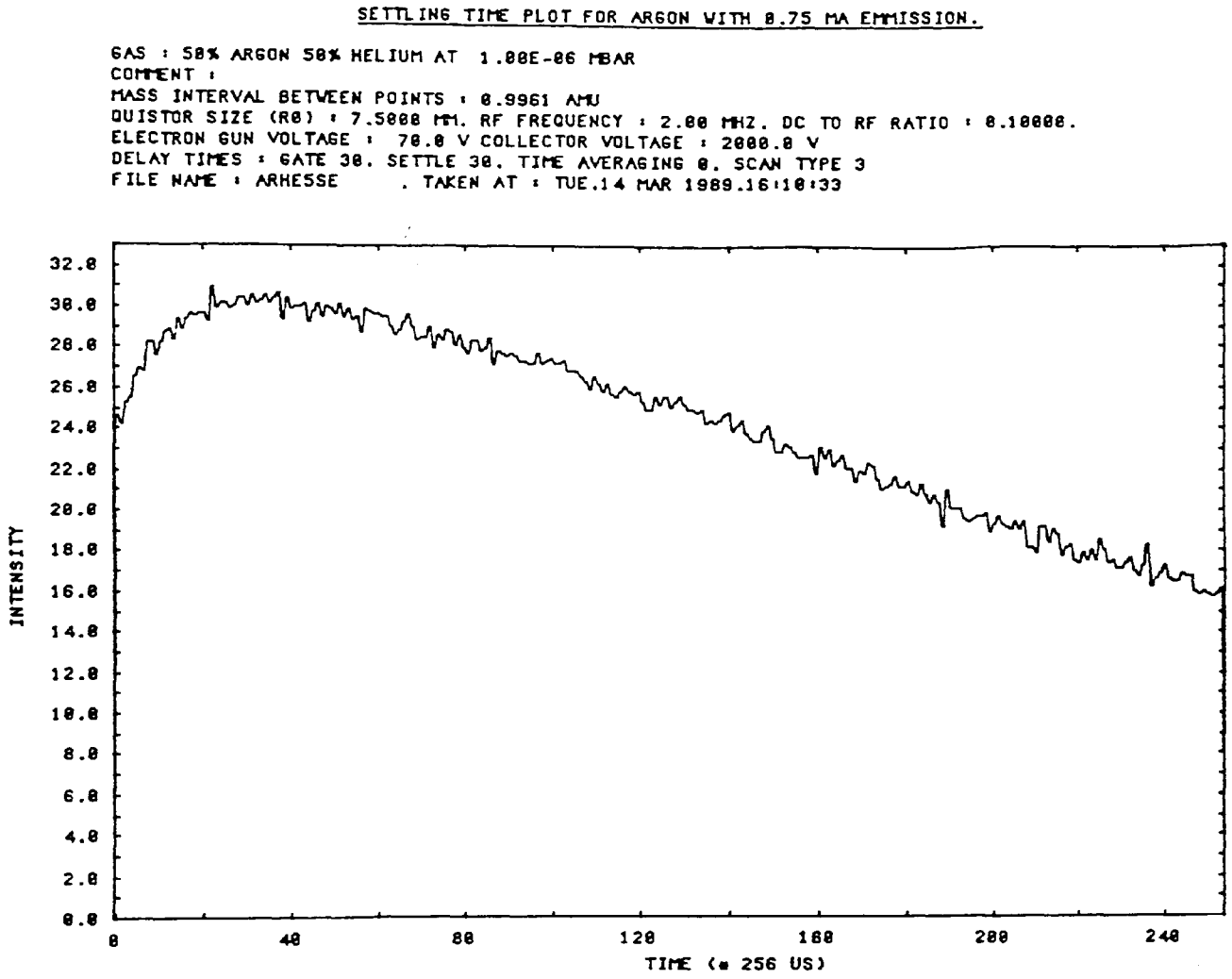

Fig. IV.12.15 Ion storage time plot for Ar^+ ions in an equal mixture of Argon and Helium at 10^{-6} mBar.

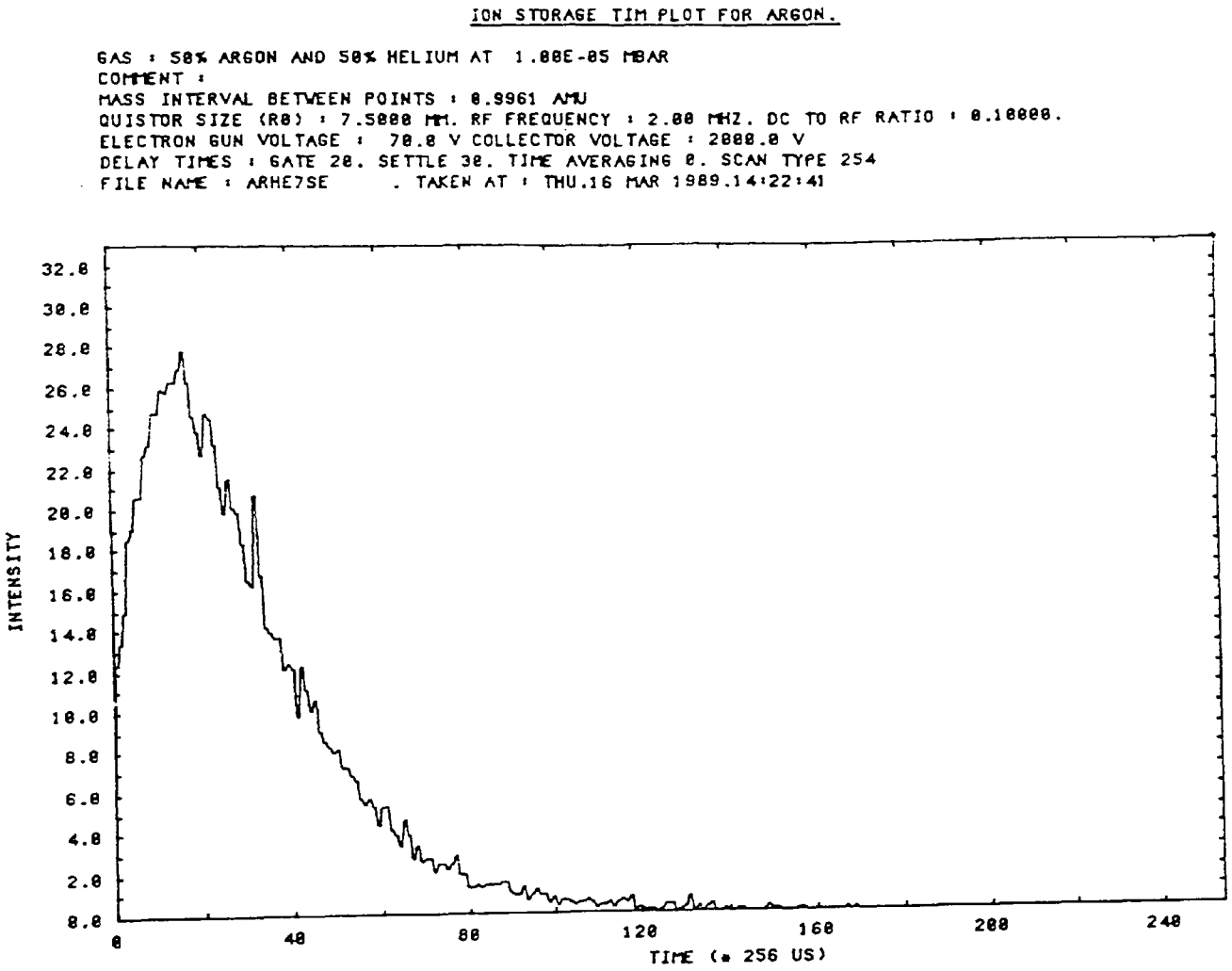

Fig. IV.12.16 Ion storage time plot for Ar^+ ions in an equal mixture of Argon and Helium at 10^{-5} mBar.

In this case the times for 63.2% of ions to be lost times are found to be

Pressure	Time constant
1×10^{-7}	668.7 ms
1×10^{-6}	80.0 ms
1×10^{-5}	6.7 ms

Fig. IV.12.17 Table of ion loss times for Ar^+ ions in an equal mixture of Argon and Helium.

This would seem to indicate that N_2^+ ions are lost about four times more easily then Ar^+ ions. Nitrogen, being a molecule, is larger than Argon (this applies to both the ion and the neutral species) so that the collision cross section must be larger. These results therefore make sense.

Similar results were also obtained by selecting Helium ions from the same gas mixture. The 63.2% ion loss times are given below.

Pressure	Time constant
1×10^{-7}	179.2 ms
1×10^{-6}	82.4 ms
1×10^{-5}	9.2 ms

Fig. IV.12.18 Table of ion loss times for He^+ ions in an equal mixture of Argon and Helium.

These results are broadly similar to those given for Argon ions.

Some rather strange results were obtained with Helium ionisation time plots at 1×10^{-6} mBar of Helium gas. These results were repeatable.

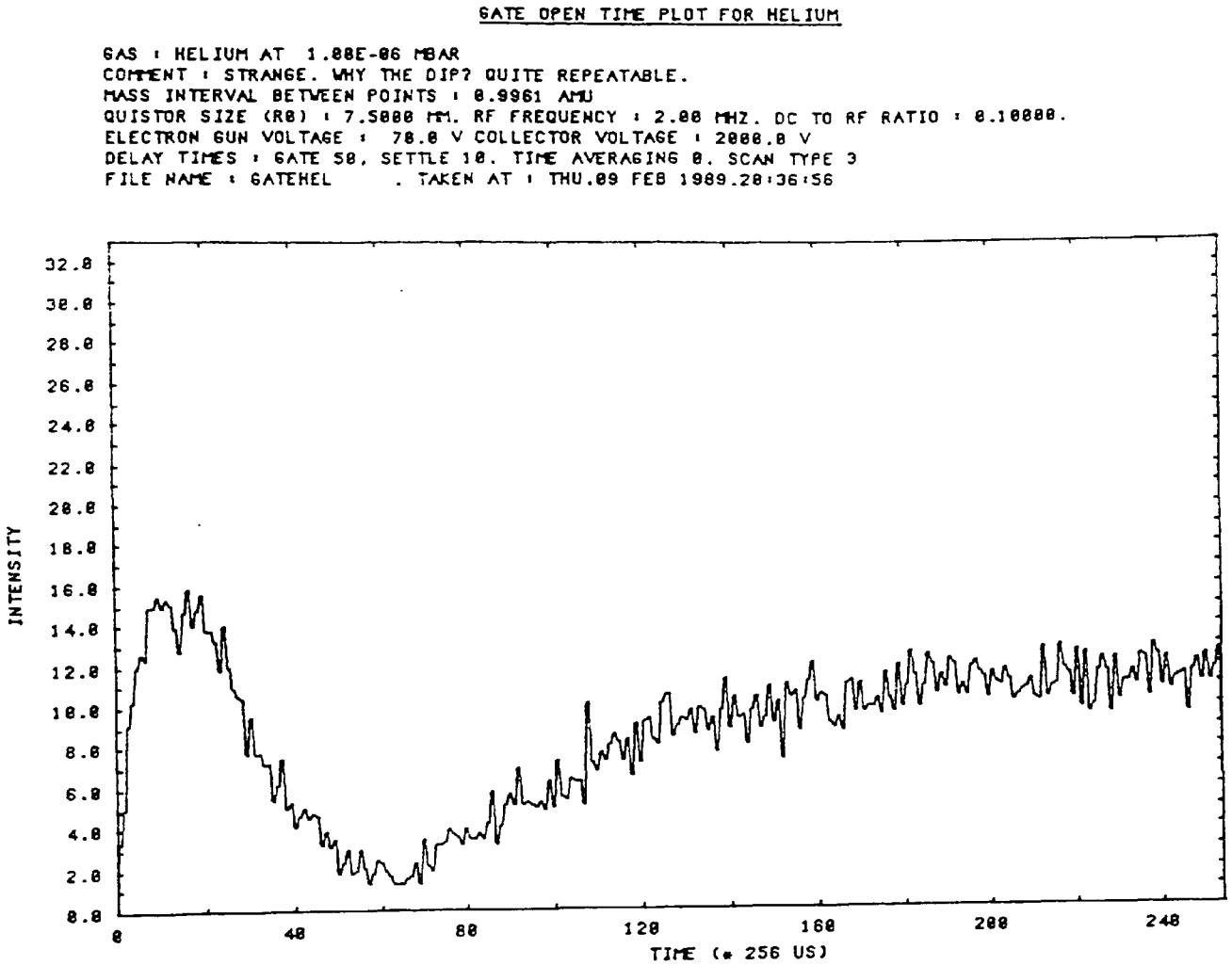

Fig. IV.12.19 Ionisation time plot for He^+ ions at 1 x 10^{-6} mBar of Helium.

The strange "dip" in the plot at between 10 and 20 ms of ionisation time is attributed to the effects of space charge upon the position and width of the Helium peak.

The RF voltage chosen for this scan corresponded to the position of the Helium peak at at moderate ionisation level. As the space charge of Helium ions built up, the peak began to move away to the right from its normal position so that the plot is no longer taken at the peak centroid. This explains the falloff in sensitivity.

At really high levels of space charge, however, the peak begins to broaden considerably as the resolution falls. In consequence, although the centroid continues to move to the right, a part of the peak is now present at the point being scanned, and the sensitivity at that point returns.

ELECTRONIC and ELECTRICAL UNITS WHICH ARE REQUIRED.

1) Preamplifier circuits required to detect the small output current of the channel plate detector.

The output produced by the channel plate consists of a small current which must be preamplified at source. The preamplifier circuit used must convert the current into a voltage, with high gain, and ultra low noise, in order that the output can be measured.

An additional requirement is that a voltage difference of at least 10 V be maintained between the base of the channel plate, and the Faraday plate collector in order to ensure efficient electron collection. This can be done either by connecting the base of the channel plate to -15 V, or by ensuring that the preamplifier input is at +12 V or so.

Also the input voltage should remain roughly constant. If the input voltage becomes negative in response to an electron current input then the bias drawing electrons from the channel plate to the faraday plate falls. This will lead to an unwelome non - linear loss of sensitivity. In other words, a low impedance, or preferably virtual ground, input type amplifier circuit is required.

Finally, since the preamplifier is required to amplify pulses of about 100μs duration, the frequency response of the amplifier should certainly be better than 10 kHz.

Three types of circuit were tested to find out which would be best for the application. Since very small currents are involved, an FET input type (with an input impedance of about 10^{12} Ohms) operational amplifier was used. In each case, during testing, a 3140 FET op-amp was used. It was

decided that a gain of 10^7 V / A was ideal and each circuit had this gain level.

The most obvious circuit type (given the requirements outlined) is to use an inverting amplifier circuit. In order to supply the gain required, a feedback resistor of 10 M Ohm was used, but the input impedance was zero since it was a virtual ground circuit.

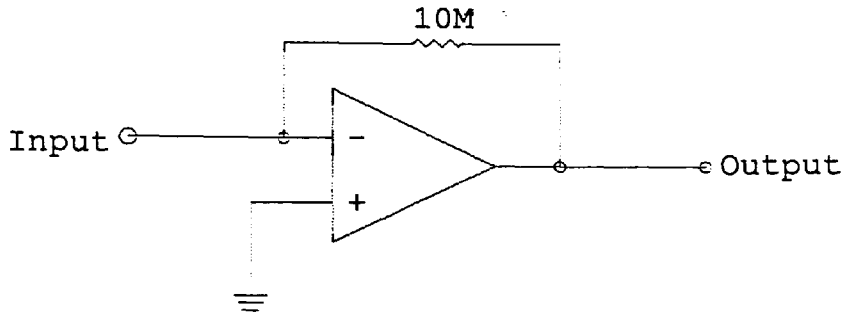

Fig. V.1.1 Inverting op - amp circuit.

A non - inverting op - amp circuit was also built. In this case, the input is not virtual ground and an input impedance as great as 10 MOhm was not permissible. A voltage was developed across a 400 KOhm resistor, but the circuit had an additional voltage gain of 20 in order to produce a total gain of 10^7 V / A.

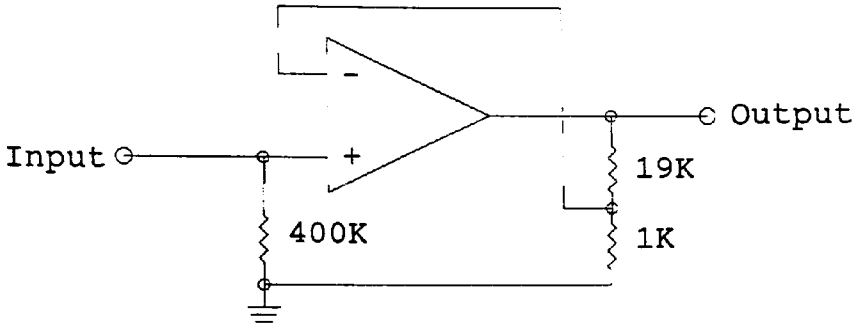

Fig. V.1.2 Non inverting op - amp circuit.

A third circuit, which it was hoped would combine the best features of both inverting and non inverting circuit types, was produced. This circuit, referred to as a hybrid circuit, required a separate, floating power supply. The circuit operates by developing a voltage across the 10 MOhm resistor, between the input, and the power supply. However, the power supply potential changes so as to maintain the non inverting input to the op - amp at ground potential. The output is then taken from the power supply. This means that the circuit is a non inverting one, with a closed loop voltage gain of 1 - but with a virtual ground input.

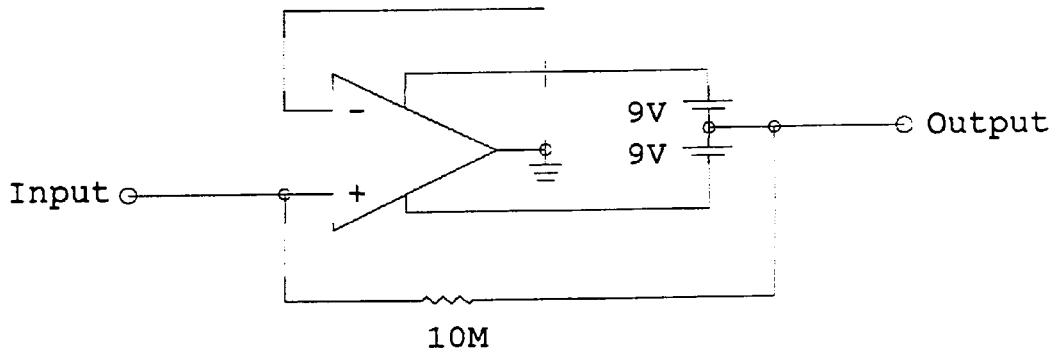

V.1.3 Hybrid op - amp circuit.

There are two factors which limit response of these circuits at high frequencies, the open loop gain falloff of the op - amp, and the input capacitance of the op - amp.

The noise voltage is produced from two sources; the op - amp electronic noise, and the thermal noise in the resistor which converts the current into a voltage. The former is known as pink noise because its frequency distribution is weighted toward low frequencies, and the second is white noise because because its distribution is the same at all frequencies.

The resistor noise voltage can be shown to be proportional to the square root of the resistance value. This means that the noise current is inversely proportional to the resistor value.

The frequency response and approximate peak to peak output noise levels were measured for each circuit, in order to allow selection of the best type.

	Frequency response (Khz)	Noise level (mV)
Inverting	1.2	20
Non inverting	89.4	3
Hybrid	14.9	2

Fig. V.1.4 Frequency response and output noise level of preamplifier circuits.

The inverting circuit is shown to have by far the worst performance, both in terms of frequency response, and noise level. This is because the closed - loop voltage gain in the circuit is very high.

The non - inverting circuit has the best frequency response, but the output noise level is greater than that of the hybrid circuit because the voltage is developed across a smaller resistance. The frequency response of the hybrid circuit was limited by the input capacitance of the op - amp, which is relatively high for the 3140.

Accordingly it was felt that if a high performance FET op - amp was used instead of the 3140, the hybrid circuit would give the best possible performance. An LF157 FET input op - amp was chosen since this combined a low input capacitance (2 pF), a wide bandwidth (5 Mhz) and very low noise (12 nV $Hz^{-0.5}$).

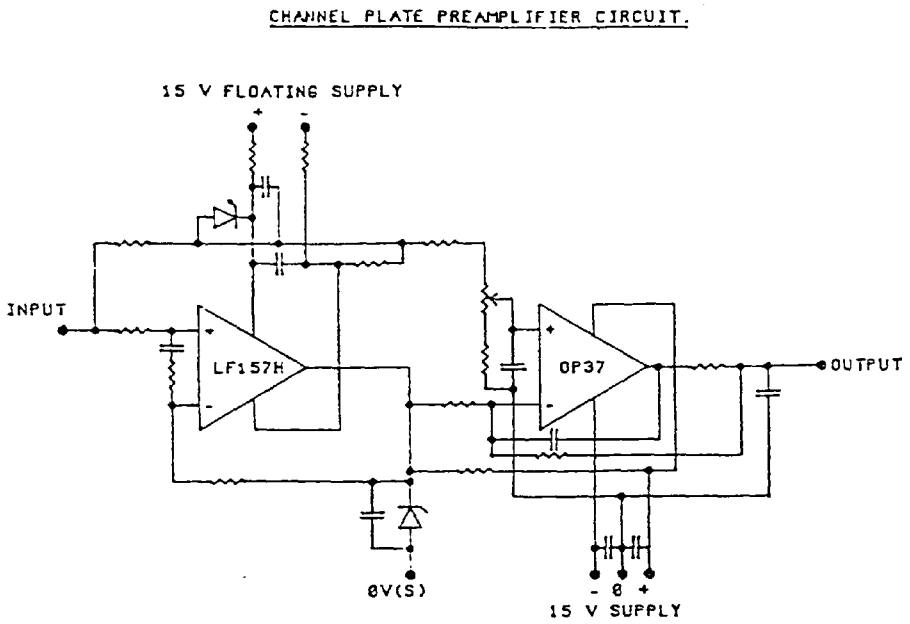

Fig. V.1.5 The preamplifier circuit presently in use.

The circuit which was eventually used combined this performance with two additional features. The input was biased at about +12 V so that the base of the channel plate could be at earth potential (which is more convenient in terms of the Quistor's construction). Also since the OP37 uses a differential amplifier circuit, two separate grounds can be maintained in the circuit. 0V(S) is connected to the vacuum system, while 0V(P) is connected to the power supply mains earth. This is very useful in ensuring good grounding practice.

This circuit has an output noise level equal to about 0.4 mV (thus allowing measurement of currents down to 40 pA), and the bandwidth is about 40 KHz. The circuit fulfils all the requirements.

2) The Control circuits for interfacing between the BBC microcomputer and the Quistor.

The BBC microcomputer is fitted with a 8 - bit parallel digital user port (PB0 - PB7), which has in addition two handshake lines (CB1 and CB2), one of which (CB2) can be programmed as an output.

The Quistor requires the following :

a) A 12 bit digital to analogue converter, to program the RF and DC voltages which are applied to the electrodes.

b) An 8 bit analogue to digital converter, to return the output from the Quistor to the BBC.

c) Digital control of the electron beam.

d) Digital control of the DC voltage applied to the electrodes. If this is switched off, the "total pressure" mode of the Quistor is selected. This is essential for any chemical ionisation, or ms - ms experiments.

e) Digital control of the integrator is required.

f) The analogue to digital converter requires a digital instruction to start a conversion.

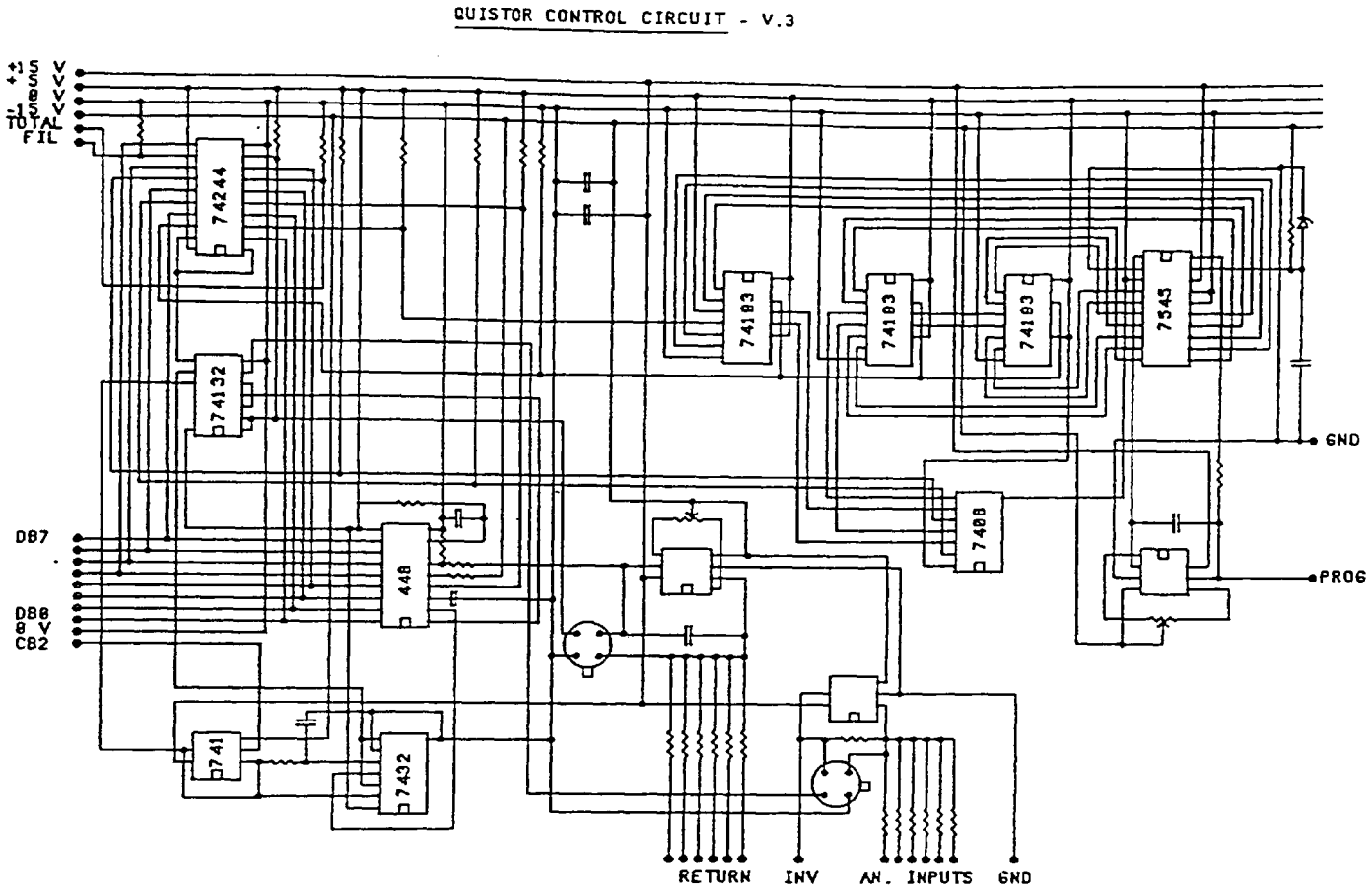

Fig 5.2.1 The BBC microcomputer interface board.

This large number of functions is controlled from the 9 data lines available by multiplexing. The 448 analogue to digital converter has tri - state outputs; the 74244 is a tri - state buffer, and these two chips are controlled in antiphase by CB2. Consequently only one of them is ever connected to the user port at one time.

The 7545 12 bit digital to analogue converter is not directly controlled; the 74244 controls three 74193 4 - bit binary counters, which are connected to the DAC. Therefore, the DAC can only ramp up, or down. This is convenient since

the Quistor is normally controlled by ramping voltages.

Integration of the data pulses is provided, under the control of FET analogue switches, so that integration takes place under software control. The interface also includes a switchable signal amplification scale. The gain ranges available are 1, 3.3, 10, 33, 100, and 330 (pC).

It is anticipated that future development work on the Quistor will be performed using an IBM compatible PC, rather than the BBC microcomputer presently used.

A board allowing interfacing of an IBM compatible PC, fitted with a 48 bit digital parallel I/O card, has already been developed to replace the interface described above.

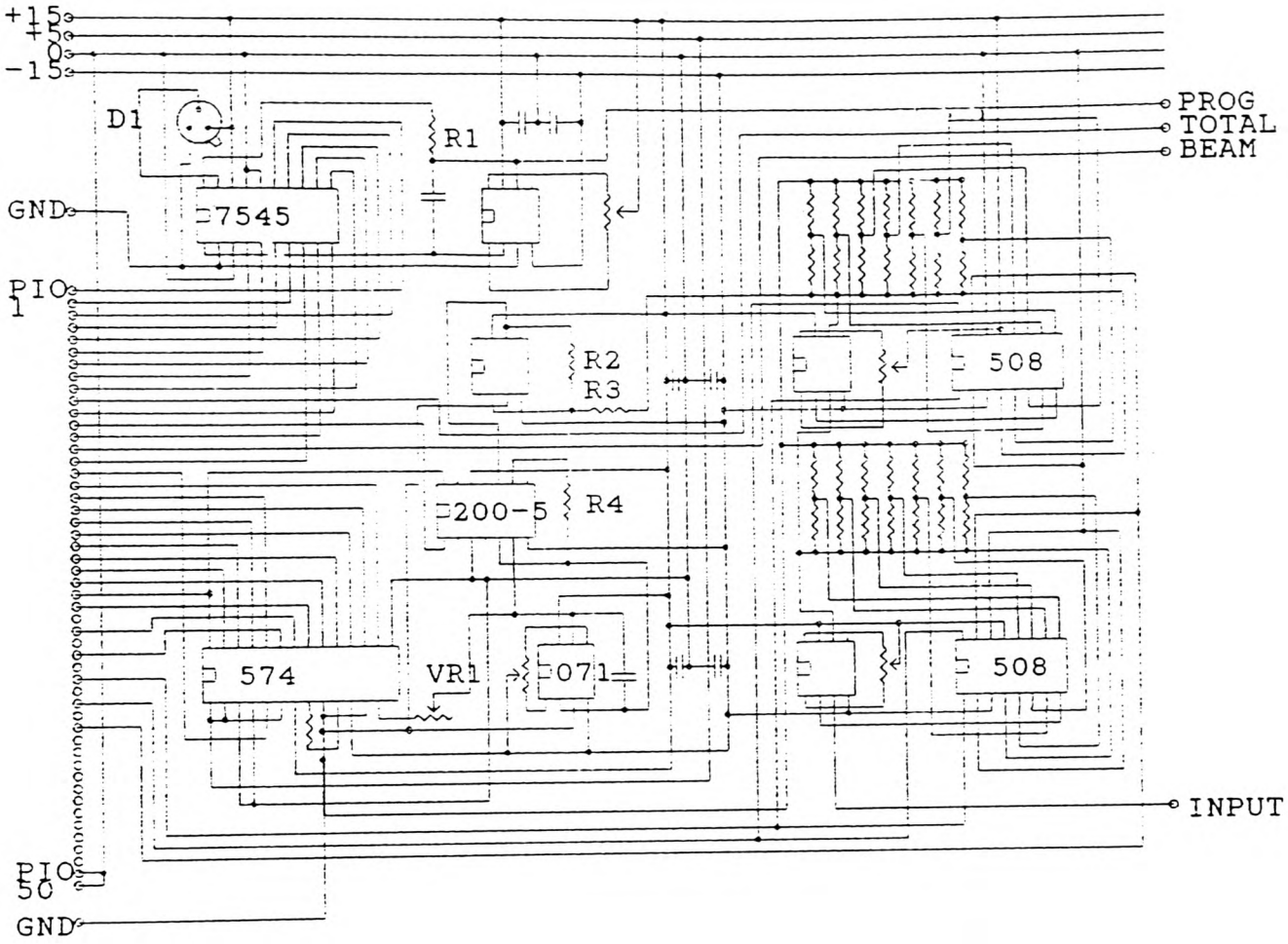

Fig. V.2.2 The IBM PC compatible interface board.

Since a far greater number of lines is available to this interface, multiplexing is not required. Direct connection to a 12 bit digital to analogue converter, and separate direct connection to a 12 bit analogue to digital converter are provided.

In addition to this digitally selectable analogue gain is available under the control of two analogue multiplexer chips. This feature will allow the computer to select the

required signal gain automatically on the basis of its knowledge of previous data.

Apart from these improvements, the function and operation of the board is broadly similar to that used for the BBC microcomputer.

3) Power supplies required for the operation of the Quistor.

The Quistor requires several power supplies for its operation (in addition to those detailed in the following sections). These include :

a) +15 V, -15 V and +5 V DC supplies.

b) A 30 V DC floating power supply for the preamplifier circuit.

c) A +225 V DC, 70 W power supply for the RF unit.

d) A +30 V DC supply for the RF unit. This could have been drawn instead from +15 V and -15 V.

e) +340 V DC and -340 V DC supply (rectified mains) for the DC biasing of the Quistor electrode. The positive supply could have been drawn from (c) above, and the negative supply could be rather lower than it is now.

f) A -2 KV DC supply to the channel plate. This should be current limited to less than 1mA.

g) A -80 V DC power supply for the biasing of the filament and gate electrodes. This could be drawn from the negative power supply in (e) above.

4) The filament power supply and biasing.

The Quistor requires an electron gun with the capacity to switch the electron beam on and off at high speed under digital control. This makes the filament power supply somewhat complex.

The potential of the filament switches between - 70 V and -15 V, while the potential applied to the gate electrode switches between 0 V and -80 V in antiphase.

The filament requires in the region of 2 A at about 2 V, depending on the selected filament temperature and the filament condition, for normal operation. Initially the power supply for the filament was produced by a regulated adjustable constant current circuit. However it was felt that it would be better to ensure regulation of the filament emission current so that any variation in the filament performance would not affect the Quistor's sensitivity.

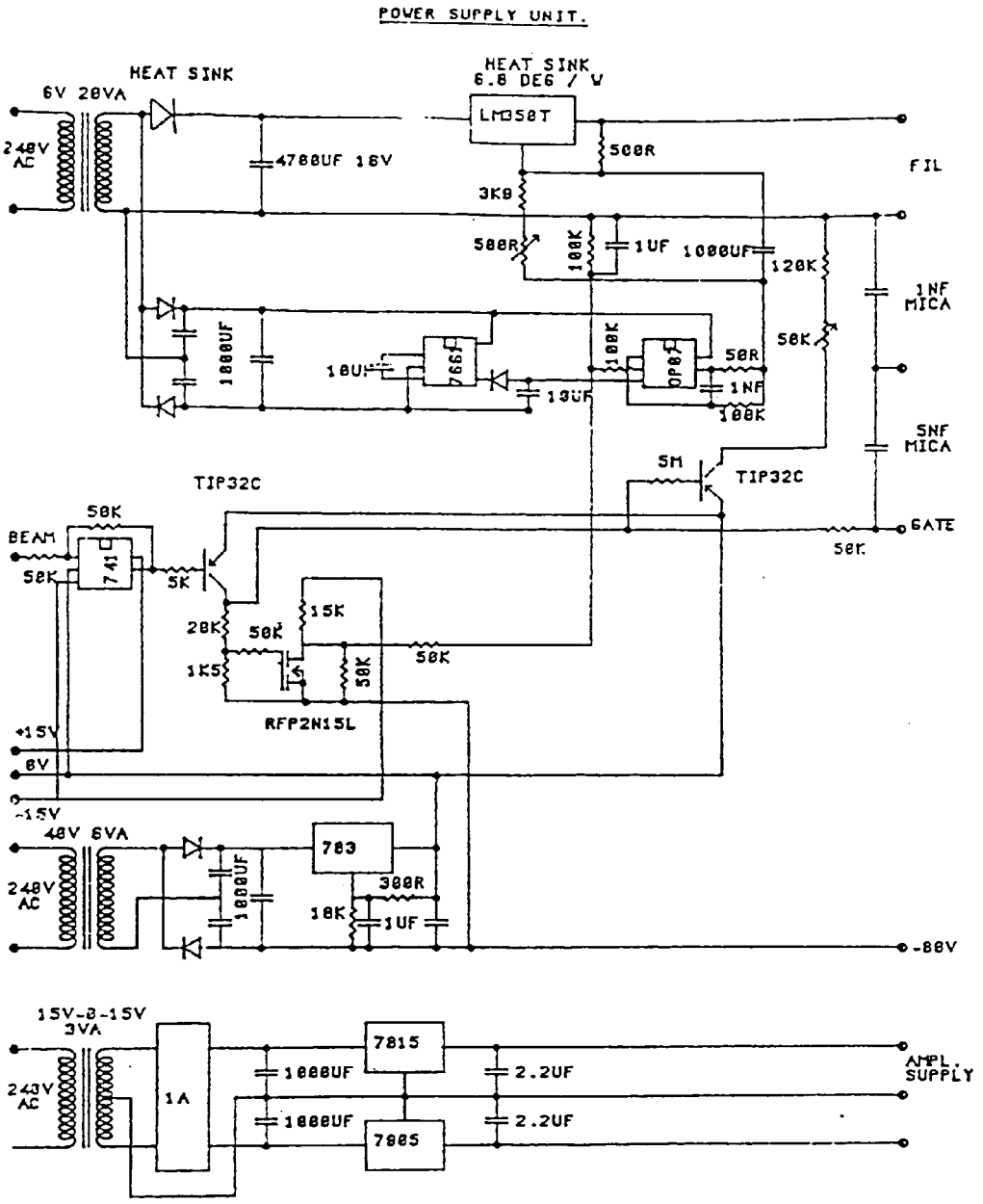

Fig. V.4.1 The filament power supply circuit.

The above circuit supplies the required potentials to the filament and gate electrodes. The filament heater current is regulated by monitoring the filament emission.

During the period when the electron beam is off, regulation in this way is impossible since the emission is zero. A current is drawn (by the rightmost TIP32C) to

simulate the filament emission during this phase so that the regulator does not turn fully on and burn out the filament.

The power supply to the OP07 is drawn entirely from the filament heater power supply. This is because its inputs are switching between high voltages w.r.t. ground, along with the filament supply, and any other connection to this chip would destroy it.

5) The RF unit used to supply the required potentials to the Quistor electrodes.

The RF unit presently in use supplies up to 1000 V peak voltage at 2 MHz in antiphase at both outputs. Superimposed upon these outputs are DC bias voltages of opposite polarity equal to about 10% of the peak voltage. This ratio can be varied by adjusting a potentiometer.

These voltages are all programmable from a 0 to -10 V input voltage. In addition, the DC voltages can be switched off under digital control from the computer to allow operation of the Quistor in the "total pressure" mode.

The earthing arrangements of the RF unit are very important. All RF currents are returned to the vacuum system earth, and not to the power supply ground, or the computer. It is found that any other arrangement results in damage to a wide range of electronic components.

A quartz crystal is used to provide a constant reference frequency. This is amplified under the control of the RF drive feedback described below, and applied to the bases of two transistors. These transistors are powered from the +225 V power supply mentioned in section (3) above, the collectors being connected to a step up auto transformer.

A small portion of the RF voltage is rectified and compared with the programming voltage by an op - amp circuit. The output from this circuit is returned as the RF drive feedback mentioned above in order to provide a feedback loop which ensures output stability.

Conclusion and future developments.

It is clear that the Quistor can easily be developed into a viable commercial instrument. The remaining shortcomings in the present design can be overcome without too much work being required.

It is felt, however, that the Quistor will find a market in specialist applications and research work requiring the use of Chemical Ionisation (CI) and MS - MS techniques rather than general mass spectrometry work. The Quistor is undoubtedly capable of operating as a general purpose mass spectrometer, but that market is already well served by the Quadrupole. It is these special abilities of the Quistor's (which have as yet not been developed upon this system), in addition to its operation as straightforward mass spectrometer, which will allow it to perform a unique service.

It is hoped that these capabilities of the Quistor can be developed as soon as possible, and incorporated into an improved Quistor system. It is hoped to improve upon the present Quistor system by increasing it's mass range by using an RF unit capable of supplying 8000 V peak to peak, as compared with the present 2000 V. This would give the Quistor a mass range of about 400.

Some work which has also not yet been done, but which might be of great value, is to extend the mass range still further by using either a lower frequency of RF, or by using a smaller Quistor (with a smaller value of r_0). Note that both of these options would probably reduce the Quistor's sensitivity. Experimentation with the former, would however be relatively straightforward and would not form a commitment to continue operating at the lower frequency.

In addition, the application of an axial magnetic field to the Quistor has not been studied experimentally (although computer simulation work has been done in this area). The application of a constant electromagnetic, or permanent, magnetic field along the axis of the Quistor should, however, be a reasonably simple matter, and it is hoped that this can be done quite soon.

As mentioned in section V.2 above, it is intended that future development work on the Quistor will be performed using an IBM PC compatible computer, rather than the BBC computer presently used. The IBM PC, and compatibles, are much more powerful computers, with much more memory, and much faster processors, thus allowing far more sophisticated programming as will be required for a commercial system. The IBM PC is, of course, also more generally acceptable as an industry standard than the BBC computer.

Finally, a commercial Quistor system will require a dual filament (so that if the user burns out a filament, the Quistor can continue to operate without immediately replacing it), and a facility for measuring the channel plate gain. These features, in addition to numerous refinements in the Quistor system's design, will be added before the Quistor is placed on the market.

REFERENCES

1 An Exact Solution of the Motion in Three Dimensional Quadrupole Ion Traps. Baril M. and Todd J. F. J. International Journal of Mass Spectrometry and Ion Physics, Vol. 46, P. 67-70, 1983.

2 Ion Storage in a Cylindrical Ion Trap by a RF Electric Field. (French) Benilan M-N., Avdoin C. International Journal of Mass Spectroscopy and Ion Physics, Vol. 11, P421-432, 1973.

3 A Model of the Dynamics of Ions stored in a Paul Trap (German). Blatt R., Zoeller P., Holtzmuller G., Verhandlungen Deutshes Physik Gesellschaft, V. 21, N. 4, P. 388-389, 1986.

4 A Novel Trapped - Ion Mass Spectrometer for the Study of Ion Molecule Reactions. Miasek P. G., Beuchamp J. L. International Journal of Mass Spectrometry and Ion Physics, Vol. 15, No. 1, P. 49-66, 1974.

5 Ion-Molecule reaction studies with a quadrupole ion trap. Bonner R. F., Lawson G., Todd J. F. J. International Journal of Mass Spectrometry and Ion Physics, Vol. 10 No. 2 P.197-203, 1972.

6 The Quadrupole Ion Store as a Novel Source for a Mass Spectrometer. Bonner R. F., Lawson G., Todd J. F. J. Journal of Scientific Instrumentation, Series 2, Vol. 6, No. 4, P. 357-362, 1973.

7 Ion Storage Mass Spectroscopy. Applications in the Study of Ionic Processes and Chemical Ionisation Reactions. Bonner R. F., Lawson G., Todd J. F. J. Proceedings of the 6th International Mass Spectrometry Conference, Edinburgh, 1973. Abstract No. 20, P. 29.

8 Theoretical and Experimental Studies with the Quadrupole Ion Storage Trap ('QUISTOR'). Bonner R. F., Lawson G., Todd J. F. J. Dynamic Mass Spectroscopy, Vol. 4. (Book, Editors D. Price and J. F. J. Todd, Heydon and Son Ltd., London, 1975), Chapter 4, P. 39-81.

9 Derivations of the Field Equations and Stability Parameters for 3 operating modes of the Three Dimensional Quadrupole. Bonner R. F. International Journal of Mass Spectrometry and Ion Physics, Vol. 23, No. 4, P. 249-257, 1977.

10 The Cylindrical Ion Trap. Part I : General Introduction. Bonner R. F, Fulford J. E., March R. E., Hamilton G. F. International Journal of Mass Spectrometry and Ion Physics, Vol. 24, No. 3, P. 255-269, 1977.

References

11 Thermal Energy Ion Molecule Reactions. Bowers M. T., Su T. (Book, Advances in Electronics and Electron Physics, editor Marton L., Academic Press, New York, USA, 1973. P. 223-279)

12 The Ion Trap : a New Detector for Gas Chromatography. Cambell C., McLure C. R., Le Munyon F. Proceedings of the 26th Rocky Mountain Conference, Denver, Colorado, USA, 1984. Abstract No. 41.

13 Recent advances in Quadrupole Mass Spectrometry. Carrico J. P. Proceedings of the Pittsburgh Conference on Analytical Chemistry and Applied Spectroscopy, Cleveland, Ohio, USA, 1972.

14 Applications of Inhomogeneous Oscillating Electric Fields in Ion Physics. Carrico J. P. (Book) Dynamic Mass Spectroscopy, V. 3, P. 1-65, Heydon, 1972

15 Ordered Structures of Ions Stored in an R. F. Trap. Casdorff R., Blatt R., Toschek P. E. Ser. Opt. Sci. V. 55, P. 73-74, 1987. (Proceedings of the 8'th International Conference on Laser Spectroscopy, Are, Sweden, 22-26 June 1987)

16 Ion Storage in Three-Dimensional, Rotationally Symmetrical Quadrupole Fields, I. Theoretical Treatment. Dawson P. H. and Whetton N. R.. The Journal of Vacuum Science and Technology, Vol. 5, No. 1, P. 1-10, 1968.

17 Ion Storage in Three-Dimensional, Rotationally Symmetric, Quadrupole Fields, II. A Sensitive Mass Spectrometer. Dawson P. H. and Whetton N. R. The Journal of Vacuum Science and Technology, Vol. 5, No. 1, P. 11-18, 1968.

18 Non - Linear Resonances in Quadrupole Mass Spectrometers due to Imperfect Fields I. The Quadrupole Ion Trap. Dawson P. H., Whetton N R. International Journal of Mass Spectrometry and Ion Physics, Vol. 2, P. 45-59, 1969.

19 Mass Spectroscopy Using RF Quadrupole Fields. Dawson P. H. and Whetton N. R. (Book, Advances in Electronics and Electron Physics, Volume 27, 1969, Editor Marton L., Academic Press) P. 60-182.

20 Quadrupole Mass Spectrometry. Dawson P. H., Whetton N. R. Dynamic Mass Spectroscopy, Vol. 2. (Book, Editor D. Price, Heydon and Son Ltd., London, 1972)

21 High Pressure Characteristics of the Quadrupole Ion

Trap. Dawson P. H., Lambert C. Journal of Vacuum Science and Technology. Vol. 12, No. 4, P. 941-942, 1975.

22 The Effects of Collisions on Ion Motion in Quadrupole Fields. Dawson P. H., International Journal of Mass Spectrometry and Ion Physics, Vol. 24, No. 4, P. 447-451, 1977.

23 Radio Frequency Mass Spectrometers. Dawson P. H. Advances in Electronics and Electron Physics, No. 13B, P. 173-256, 1980.

24 Photo Dissociation of Trapped Ions. Dunbar R. C. Bulletin of the American Physical Society, Vol. 24, No. 9, P. 1325, 1981.

25 The Use of Quadrupole and Ion Trap Mass Spectrometers for the Identification of Air and Water Pollutants. Evans S., Smith R. D., Welby J. K. International Journal of Mass Spectrometry and Ion Processes, Vol. 60, P. 189- 199, 1984.

26 Use of a Quadrupole Ion Trap in Mass Analysis. Fies W. J., Kelley P. E. Reynolds W. E., Stafford G. C., Syka J. E. P. US Patent US4656999, Finnegan Corporation, USA, 1987.

27 (Title not known) Fisher. (German) Zeitschrift fur Physik, 156, 26, 1959.

28 Ion Molecule Reactions. Friedman L. Annual Review of Physical Chemistry. Vol. 19, P. 273-300, 1968.

29 A New Mode of Operation for the Three Dimensional Quadrupole Ion Store (QUISTOR). The Selective Ion Reactor. Fulford J. E., March R. E. International Journal of Mass Spectrometry and Ion Physics, Vol. 26, No. 2, P. 155-162, 1978.

30 Ion Withdrawal Studies of the Quadrupole Ion Storage Trap (QUISTOR). Part 1 : Characterisation of the Magnitude of the Ion Trapping Potential Well and the Location of the Extractable Ions. Fulford J. E. and March R. E. International Journal of Mass Spectrometry and Ion Physics, Vol. 30, No. 1, P. 38-55, 1979.

31 Radio Frequency Mass Selective Excitation and Resonant Ejection of Ions in a Three - Dimensional Quadrupole Ion Trap. Fulford J. E., Hoa D. N., Hughes D. J., March R. E. Bonner R. F. and Wong G. J. Journal of Vacuum Science and Technology, Vol. 17, No. 4, P. 829-835, 1980.

32 The Cylindrical Ion trap : A Theoretical and

Experimental Study. Fulford J. E., March R. E., Mather R. E., Todd J. F. J. and Waldren R. M. The Canadian Journal of Mass Spectroscopy, Vol. 25, No. 4, 1980

33 Absolute measurement of the Total Number of Ions Stored in an RF Quadrupole Trap. Gaboriava M. N., Desaintfuscien M and Major F. G. International Journal of Mass Spectrometry and Ion Physics, Vol. 41, No. 1-2, P109-123, 1981.

34 Ion Path Lengths in a Three Dimensional RF Quadrupole trap. Ghosh P. K., Arora A. S., Narayan L. International Journal of Mass Spectrometry and Ion Physics, Vol. 23, No. 3, P. 237-240, 1977.

35 Chemical Physics with QUISTORs. Ghosh P. K. Journal of the Indian Chemistry Society, V. 63, N. 1, P. 64-68, 1986.

36 Proposal for the Design, construction and testing of a Quadrupole Ion Trap. Griffiths I. W., The Polytechnic of Wales. Discussion document, 1984.

37 Apparatus and Method for the Control and / or analysis of Charged Particles. Griffiths I. W. British Patent Nr. 2202080/A. National Resource Development Corporation, UK, 1987.

38 New Techniques for Quistor Mass Spectrometry. I. W. Griffiths I. W., Heesterman P. J. L. Advances in Mass Spectrometry V. 11A, (Proceedings of the 11'th International Mass Spectrometry Conference, Bordeaux, France, 29 Aug. - 2 Sept., 1988), P. 150- 151, 1989

39 Rate Constants and Cross Sections. Henchman M. (Book, Ion Molecule Reactions, Editor Franklin J. L., Butterworths, London, England. Chapter 5, P. 101-259, 1972)

40 Near Thermal Stored Ion Charge Capture Studies. Holzscheiter H. M. and Church D. A. Bulletin of the American Physical Society, Vol. 24, No. 9, P. 1178, 1979.

41 Laser Spectroscopic studies of cold, trapped ions. Itana W. M., Bulletin of the American Physical Society, Vol. 29, No. 4, P 816, 1984.

42 Theory of Laser Cooling of Stored Ions. Itana W. M., Wineland D. A. Bulletin of the American Physical Society, Vol. 25, No. 9, P. 1127, 1980.

43 Application of the Quadrupole Ion Storage Trap (QUISTOR) to the Study of Gas Phase Ion / Molecule

Reactions. Kamar A. A. E-E., Dissertation Abstracts International, Section B. V. 47, N. 7, P. 2934, 1987.

44 New Advances in the Operation of the Ion Trap Mass Spectrometer, Kelley P. E., Stafford G. C., Syka J. E. P., Reynolds W. E. Lores J. N., Amy J. W., Todd J. F. J., Proceedings of the 33'rd Annual Conference on Mass Spectrometry and Allied Topics, San Diego, California, USA, 26-31 May 1985, P. 707- 708, 1985.

45 Operation and Application of an Advanced Ion Trap MS / MS Spectrometer. Kelley P. E., Stafford G. E., Syka J. E. P., Evans S. Proceedings of th 16'th Meeting of the British Mass Spectrometry Society, York, UK, 6-9 Sept. 1987, P. 103, 1988.

46 High Sensitivity MS / MS with an Ion Trap Mass Spectrometer. Kelley P. E., Weber-Grabau M., Cambell C. S., Yost R. A., Johnson J. V. Proceedings of the 39'th Pittsburgh Conference on Analytical Chemistry and Applied Spectroscopy, New Orleans, USA, 22-26 February 1988, Abstract N. 901, 1988.

47 Mass Range Extension in a Quadrupole Ion Trap Mass Spectrometer. Kaiser R. E., Cooks R. G., Moss J. Hemberger P. H. Rapid Communications in Mass Spectrometry, V. 2, N. 2, P. 50-53, 1989.

48 Effective Potential of an R.F. Cylindrical Trap. Lagadec H., Meis C., Jardin M. International Journal of Mass Spectrometry and Ion Processes, V. 85, N. 3, P. 287-299, 1988.

49 Trapped Negative Ions. Larson D. Bulletin of the American Physical Society, Vol. 27, No. 7, P. 789, 1982.

50 Radiofrequency Quadrupole Mass Spectrometers. Lawson G., Todd J. F. J. Chemistry in Britain. Vol. 8, No. 9, P. 373-380, 1972.

51 Quadrupole Ion Store (QUISTOR). Part I. Ion molecule reactions in Methane, Water, and Ammonia. Lawson G., Bonner R. F, Mather R. E., Todd J. F. J, March R. E. Journal of the Chemistry Society, Vol. 72, No. 3, P. 547-557, 1976.

52 Time Dependent Mass Spectra and Breakdown Graphs I. 1, 5 Hexadiyne. Lifshitz C. and Weiss M. International Journal of Mass Spectrometry and Ion Physics, Vol. 35, No. 1-2, P. 73-81, 1980.

53 Fundamentals of Laser Interactions : Dynamics of the laser cooling of a trapped ion. Lindberg M. (Book) Lecture Notes on Physics Nr. 229, Spring - Verlag,

P231-248, 1985.

54 Method of Operating a Quadrupole Ion Trap for Chemical Ionisation Mass Spectrometry. Louris J. N., Syka J. E. P., Kelley P. E. European Patent Application EP215615, Finnegan Corporation, USA, 1988.

55 Further Characterisation of Mass Selectivity in the Quadrupole Ion Storage Trap (QUISTOR). March R. E., Young A. B., Hughes R. J., Kamar A., Baril M. Spectroscopy International Journal, Vol. 3, No. 1, P. 17-32, 1984.

56 The Quadrupole Ion Store (QUISTOR). A simple model for the ion ejection process. Mather R. E. and Todd J. F. J. International Journal of Mass Spectrometry and Ion Physics, Vol. 31, No. 1-2, P. 1-13, 1979.

57 The Quadrupole Ion Store (QUISTOR) Part VII. Simultaneous Positive / Negative Ion Mass Spectrometry. Mather R. E. and Todd J. F. J. International Journal of Mass Spectrometry and Ion Physics, Vol. 33, No. 2, P. 159-165, 1980.

58 Some operation characteristics of a Quadrupole Ion Store Mass Spectrometer having Cylindrical Geometry. Mather R. E., Waldren R. M., Todd J. F. J. and March R. E. International Journal of Mass Spectrometry and Ion Physics, Vol. 33, No. 3, P. 201-320, 1980.

59 Theory and Application of Mathieu Functions. McLachlan N. W., Dover, New York, 1964.

60 Collision - Activated Dissociation of Negative Ions in an Ion Trap Mass Spectrometer. McLuckey S. A., Glish G. L., Kelley P. E. Analytical Chemistry V. 52, N. 13, P. 1670-1674, 1987.

61 Microchannel Plates. Mullard Technical Publication M81-0151, Mullard.

62 Confinement of Ions Created Externally in a Quadrupole Ion Trap operated in the Combined RF and Penning Mode. O C-S. and Schussler H. A. Journal of Applied Physics, Vol. 52, No. 4, P. 2601-2607, 1981.

63 Infrared Absorption Spectroscopy of Gaseous Ions by the Ion Trapping Technique. Okumura M., Yeh L. I. Lee Y. T. Abstracts of the 191'st American Chemical Society National Meeting, New York, USA, 13-18 Apr. 1986).

64 Verfahren zur Trennung bzw. zum gretrennten Nachweis von Ionen verschiedener spezifischer Ladung. Paul W.

and Steinweidel H. West German Patent Nr. 944900, 1956.

65 Automated GC / MS Drug Screening Confirmation Using an Ion Trap Detector. Patkin A. J. Proceedings of the 39'th Pittsburgh Conference on Analytical Chemistry and applied Spectroscopy, New Orleans, LA, USA. Abstract Nr. 868, 1988.

66 (Title not known) (German) Rettinghaus G. Zeitscrift fuer Angewante Physik, 22, 231, 1967.

67 Waveform Parameter Tolerances for the Quadrupole Mass Filter with Rectangular Excitation. Richards J. A., Huey R. M. and Hillier J. International Journal of Mass Spectrometry and Ion Physics, Vol. 15, P. 417-428, 1974.

68 Ion Storage in a Trap with Semi - Spherical Electrodes. Schussler C. S. O. and Schussler H. A. Bulletin of the American Physical Society, Vol. 24, No. 9, P. 1203, 1979.

69 Generation and Confinement of Multiply Charged Ions in an R.F. Quadrupole Ion Trap. (French). Schwebel C., Muller P. A. Revue de Physique Applicee. Vol. 10, No. 4, P. 227-239, 1975.

70 Shape of the Mass Peak in the Three Dimensional Quadrupole Mass Spectrometer. Sheretov E. P., Zenkin V. A. Soviet Physics. Technical Physics. Vol. 17, No. 1 P. 160-162, 1972. (Translation)

71 Three Dimensional Quadrupole Mass Spectrometer with Sweep of the Mass Spectrum by Variation of the Frequency of the Supply Signal. Sheretov E. P., Zenkin V. A., Samodurov V. F., Veselkin N. D. Instruments and Experimental Techniques, Vol. 16, No. 1, P. 163-165, 1973. (Translation)

72 Effect of Space Charge on a Three Dimensional Quadrupole Mass Spectrometer. Sheretov E. P., Zenkin V. A., Samodorov V. F. Soviet Physics. Technical Physics, Vol. 18, No. 2, P262-265, 1973. (Translation)

73 The Medium Range Kinetic Energy of Stored Ion Clouds in a Paul Trap. (German) Siemens I., Sauter T., Bialas J., Neuhauser W., Blatt R. Verhandlungen Deutshes Physik Gesellshaft, V. 21, N. 4, P389.

74 Dynamics of Ion Clouds in Paul Traps. Siemers I., Blatt R., Sauter T., Neuhauser W. P. Physical Revue, Section A, V. 38, N 10, P5121-5128, 1988.

75 Recent improvements in ion trap technology. Stafford G. C., Kelley P. E., Reynolds W. E., Syka J. E. P. Proceedings of the 31st Annual Conference

on Mass Spectrometry and Allied Topics, Boston, Mass., USA, 1983.

76 Method of Mass Analysing a Sample by Use of a Quadrupole Ion Trap. Stafford G. C. Kelley P., Stephens D. R., US Patent Nr. US4540884. Finnegan Corporation, USA, 1987.

77 Advanced Ion Trap Technology in an Economical Detector for GC. Stafford G. C., Kelley P. E. and Bradford D. C. Int. Lab., Vol. 13, No. 7, P. 84-92, 1983.

78 Ion Trap Chemical Ionisation Mass Spectrometry : RF / DC for Isolating Unique Reactant Ions. Strike R. J., Keller P. R. Organic Mass Spectrometry, V. 24, N. 3, P. 201-204, 1989.

79 The Finnegan MAT Ion Trap Mass Spectrometer (ITMS™) - A New Development in Ion Trap Technology. Syka J. E. P., Kelley P. E. and Stafford G. C., Finnegan MAT, San Jose, California and Louris J. N,, Dept. Of Chemistry, Purdue University, West Laffayette, Indiana, USA. Finnegan MAT technical publication, 1985.

80 Direct Coupling of a Gas Chromatograph to an Ion Trap Detector. Tiebach R., Blass W. Journal of Chromatography V. 454, P. 372-381, 1988.

81 First Trap Your Atom. Thompson R. New Scientist, 3 September 1987.

82 Experiments on Magnesium Ions Confined in a Penning Trap. Thompson R. C., Barwood G. P., Gill P., Europhysics Conference Abstracts V.9B (2'nd European Conference on Atomic and Molecular Physics, Amsterdam, Netherlands 15-19 Apr. 1985).

83 The Quadrupole Ion Store (QUISTOR) part VIII. The Theoretical Estimation of Ion Kinetic Energies; a Comparative Study of the Field. Todd J. F. J., Waldren R. M., Mather R. E. International Journal of Mass Spectrometry and Ion Physics, Vol. 34, No. 1-2, P. 17-36, 1980.

84 The Quadrupole Ion Store (QUISTOR) part IX. Space Charge and Ion Stability; a Theoretical Background and Experimental Results. Todd J. F. J., Waldren R. M., Mather R. E. International Journal of Mass Spectrometry and Ion Physics, Vol. 34, No. 3-4, P. 325-349, 1980.

85 The Quadrupole Ion Store (QUISTOR) Part X. Space Charge and Ion stability B. On the Theoretical Distribution and Density of Stored Charge in RF

Quadrupole Fields. Todd J. F. J., Waldren R. M., Freer D. A. and Turner R. B. International Journal of Mass Spectrometry and Ion Physics, Vol. 35, No. 1-2, P. 107-150, 1980.

86 The Quadrupole Ion Store (QUISTOR) part XI. The Model of Ion Motion in a Pseudo - Potential Well; an Appraisal in terms of Phase Space Dynamics. Todd J. F. J., Freer D. A. and Waldren D. M. International Journal of Mass Spectrometry and Ion Physics, Vol. 36, No. 2, P. 185-203, 1980.

87 The Quadrupole Ion Store (QUISTOR) part XII. The Trapping of Ions Injected From an External Source; a Description in Terms of Phase Space Dynamics. Todd J. F. J., Freer D. A. and Waldren D. M. International Journal of Mass Spectrometry and Ion Physics, Vol. 36, No. 3, P. 371-386, 1980.

88 Quadrupoles and Related Devices, Todd J. F. J. (Book, Dynamic Mass Spectroscopy, V. 3) P. 11-23, 1975.

89 A Survey of the Current State of Quadrupole Mass Spectrometry. Todd J. F. J. Chapter 1 (Book, Dynamic Mass Spectroscopy, Vol. 6, Price D. and Todd J. F. J., editors, Heydon and Sons Limited, London), P. 1-13, 1981.

90 Recent Developments in the Theory and Application of the Quadrupole Ion Storage Trap (QUISTOR). Todd J. F. J. Chapter 4 (Book, Dynamic Mass Spectroscopy, Vol. 6, Price D. and Todd J. F. J., editors, Heydon and Sons Limited, London), P. 44- 70, 1981.

91 A theoretical model for mass selective instability and high pressure operation of the ion trap. Todd J. F. J., Bexon J. J., Kelling P. E., Stafford G. C., Fies W. J., Syka J. E. P., McIver R. T., Hunter R. C. Proceedings of the 14th Meeting of the British Mass Spectrometry Society, Edinburgh, UK, 1984. Abstract Nr. 41.

92 A Survey of the Current State of Quadrupole Mass Spectrometry. Todd J. F. J. International Journal of Mass Spectrometry and Ion Processes. Vol. 60, P. 61-81, 1984.

93 Continuing Developments in Ion Trap Mass Spectrometry. Todd J. F. J., Stafford G. C., Kelley P. E., Louris J. N., Smith R. D. Proceedings of the 15'th Meeting of the British Mass Spectrometry Society, Brighton, UK, 14-17'th Sept. 1986, P. 46- 47, 1987.

94 Ion Trajectory Modelling for the Ion Trap Mass

Spectrometer. Todd J. F. J., Bexon J. J. Smith R. D. Proceedings of the 16'th Meeting of the British Mass Spectrometry Society, York, UK, 6-9 Sept., 1987, P. 127-131, 1988.

95 Some Recent Extensions of Ion Trap Operation. Todd J. F. J., Bexon J. J. Smith R. D., Weber-Grabau M., Kelley P. E., Syka J. E. P., Stafford G. C., Bradshaw S. C. Proceedings of the 16'th Meeting of the British Mass Spectrometry Society, York, UK, 6- 9 September 1987, P. 206-209, 1988.

96 New Trends in Atomic Physics, Vol. 1 : Atomic Particles in traps, Toscheck P. E., (Book) North Holland Physics Publications, (38'th Les Houches Summerschool, Les Houches, France 28'th Jul. 1982), P381 - 450, 1984.

97 Computation for Ions Stored in a Quadrupole RF Trap Cooled by a Buffer Gas. Influence of Working Conditions on Space Charge Effects. Vedel F., Andre J. International Journal of Mass Spectrometry and Ion Processes, Vol. 65, No. 1-2, P. 1-22, 1985.

98 Direct Evidence of the Instantaneous Mean Kinetic Energy of Ions Stored in a RF Quadrupole Trap. Vedel F., Vedel M., Advances in Mass Spectrometry, V. 11A (Proceedings of the 11'th Mass Spectrometry Conference, Bordeaux, 29 Aug. - 2 Sept. 1988), P. 242 - 245, 1989.

99 The Quadrupole Ion Store (QUISTOR). Studies on Phase Synchronised Ion Ejection; the Effects of Ejection Pulse Amplitude. Waldren R. M. and Todd J. F. J. International Journal of Mass Spectrometry and Ion Physics, Vol. 31, No. 1-2, P. 15-29, 1979.

100 Storing Ions for Collision Studies. Walls F. L., Dunn G. H. Physics Today, Vol. 27, No. 8, P. 30-35, 1974.

101 Recent Developments in Ion Trap Technology. Weber-Grabau M., Kelley P., Bradshaw S., Hoekman D., Tucker D., Evans S., Bishop P. (Finnegan MAT). New Advances in Mass Spectrometry, V. 11A (Proceedings of the 11'th Mass Spectrometry Conference, Bordeaux, 29 Aug. - 2 Sept., 1988), P 152-153, 1989.

102 Macroscopic Particle Motion in Quadrupole fields. Whetton N. R. Journal of Vacuum Science and Technology, Vol. 9, No. 1, P. 486, 1972.

103 Measurement of Storage times of N_2 ions trapped in an R.F. trap. Yoda J., Sugiyama K. Japanese Journal of Applied Physics Part 2, V. 26, N. 11, P. L1780- L1783, 1987.

References

104 Ion Molecule Reactions - Summary of Abstracts. No Author, Proceedings of the 35'th ASMS Conference on Mass Spectrometry and Allied Topics. Denver, Colorado, USA, 24-29 May 1987, P. 331-346, 1987.

105 Ion Traps : Instrumentation - Summary of Abstracts. No Author, Proceedings of the 35'th ASMS Conference on Mass Spectrometry and Allied Topics. Denver, Colorado, USA, 24-29 May 1987, P. 767-790, 1987.

106 Ion Trapping : Methods and Applications - Summary of Abstracts. No Author, Proceedings of the 36'th ASMS Conference on Mass Spectrometry and Allied Topics, San Francisco, California, USA, 5-10 June 1988, P. 1302-1307, 1988.